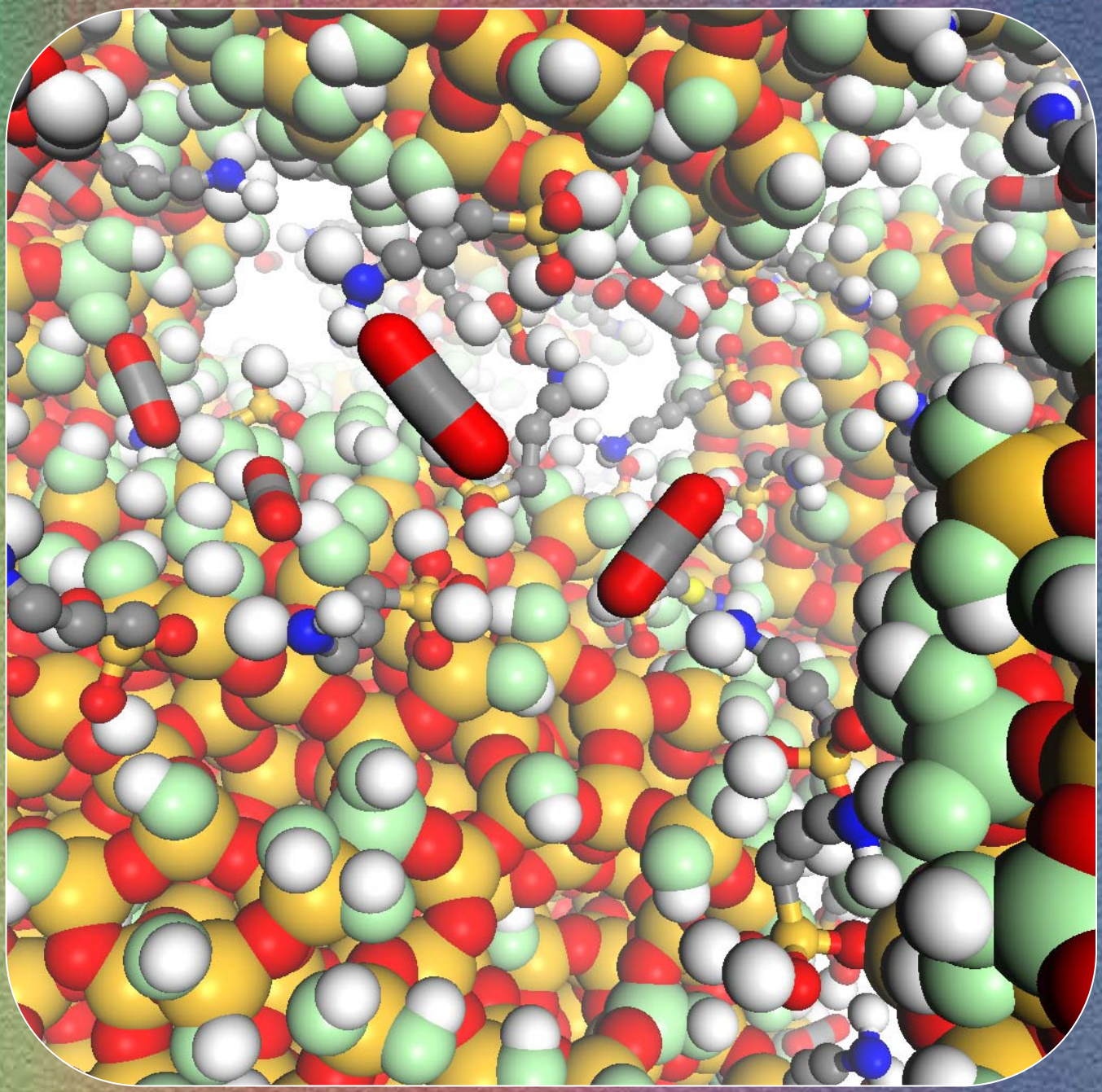

Understanding the behavior of materials for capture of greenhouse gases by molecular simulations

Understanding the behavior of materials for capture of greenhouse gases by molecular simulations

A dissertation submitted in partial fulfillment of the requirements for the degree of
DOCTOR OF PHILOSOPHY

In the Department of Physics at the
UNIVERSITAT AUTONOMA DE BARCELONA

By
Santiago Builes Toro

Supervisor: Dr. Lourdes F. Vega

Bellaterra, January 2012

Understanding the behavior of materials for capture of greenhouse gases by molecular simulations

Thesis committee:

President: Edward Maginn

Secretary: Concepción Domingo Pascual

Vocal 1: Tina Düren

Substitutes:

Francisco Medina Cabello

Roberta Pacciani

Declaration

The work reported in this Doctoral Thesis was carried out at the Molecular Simulation Group of MATGAS 2000 AIE. No part of this thesis has been submitted elsewhere for any other degree or qualification and it is all my own work unless referenced to the contrary in the text.

January 2012

_____

Santiago Builes Toro

PhD candidate

_____

Lourdes F. Vega

Supervisor

Acknowledgments

Completing this dissertation would not have been possible without the mentorship and support I received from many people. More specifically, I would like to express my gratitude and thanks to:

- To the Spanish Government (projects CEN2008-1027 CENIT SOST-CO2 and CTQ2008-05370/PPQ), the Catalan Government (project 2009SGR-666) for the economic support for this work. I am grateful to the Catalan Government and MATGAS (through a Talent grant from the Commission for Universities and Research of the Generalitat de Catalunya) and to Carburos Metálicos (for a grant through the Fundació Empresa i Ciencia) for financial support during this thesis. The computational time provided by CESCA, the supercomputer Center of Catalonia was deeply appreciated.

- To my supervisor Lourdes Vega, for her support, encouragement and guidance during these years. My academic pursuit would have been much harder without the guidance and plenty of freedom Lourdes gave me.

- To Thomas Roussel for his valuable science discussions, supervision and for reading some chapters of this thesis and giving his critical comments about them. To Pedro Lopez and Concepción Domingo for numerous fruitful discussions and their well substantiated help.

- To Montse Salas, Helena Lundvist and Montse Poveda for being great and efficient secretaries. Thanks to Montse Poveda for helping me in the printing stages of this manuscript. And thanks to the people in MATGAS and ICMAB that I have had the pleasure to met and whose contribution, one way or another, has helped me in the making of this thesis.

- To Aurelio, Jordi, Thomas, Felix, Abel, Pedro, Gabriel, Alicia, Aida, Toni, Oscar, Roberta, Falk, Edoardo, Almudena and Mariana for being not only excellent colleagues but also very good friends.

- To my family, who deserves special mention for their inseparable support, prayers and for teaching me that the most important thing in life is to be happy. And special thanks to Adriana for being an important part of my life and for helping and supporting me all these years.

Table of Contents

List of Figures

List of Tables

List of Acronyms

APTES:	3-aminopropyltriethoxysilane
APTMS:	3-aminopropyltrimethoxysilane
CDCB:	Coupled Decoupled Configurational Bias
CHA:	Chabazite zeolite framework
COF:	Covalent-Organic Framework
DDR:	Deca-dodecasil 3R zeolite framework
DEA:	Diethanolamine
DFT:	Density Functional Theory
EMT:	EMC-2 (Elf Mulhouse Chimie - 2) zeolite framework
EMT-ZTC:	EMT zeolite templated carbon
EoS:	Equation of State
ERI:	Erionite zeolite framework
FAU:	Faujasite zeolite framework
FAU-ZTC:	FAU-Y zeolite templated carbon
FTIR:	Fourier Transform Infrared Spectroscopy
GCMC:	Grand Canonical Monte Carlo
GHG:	Greenhouse Gas

LCP:	Local Curvature Parameter
LJ:	Lennard Jones
LTA:	Linde type A zeolite framework
MC:	Monte Carlo
MD:	Molecular Dynamics
MDEA:	Methyldiethanolamine
MFI:	ZSM-5 (Zeolite Socony Mobil – 5) zeolite framework
MOF:	Metal-Organic Framework
MOP:	Microporous Organic Polymers
PBC:	Periodic Boundary Conditions
TEA:	Triethanolamine
VLE:	Vapor liquid equilibrium
ZIF:	Zeolite Imidazolate Frameworks
ZTC:	Zeolite Templated Carbon

Summary

The establishment of a global limit on the emissions of greenhouse gases has been hindered by the complexity to prove the effects of manmade greenhouse gases on a global scale. This is highlighted by carbon dioxide the most abundant manmade greenhouse gas, which is naturally abundant in the environment, plays an important role in many ecosystems, and is a by-product of the combustion of fossil fuels. Nonetheless, in order to achieve a sustainable development it is important to limit, and when possible to eliminate, emissions of industrial greenhouse gases to the atmosphere. In this context, adsorption has been established as one of the best cost-effective means of reducing emissions of greenhouse gases in the short-term. In this thesis, the main objective is to study at a molecular level the adsorption of greenhouse gases to get a better insight into the capture processes for their optimization.

First, the use of molecular simulations to find the optimal conditions for the separation by adsorption of sulfur hexafluoride from a gaseous mixture with nitrogen is presented. Sulfur hexafluoride is typically emitted in small quantities, but because it is a potent greenhouse gas and possesses extremely long lifetimes, there is a pressing need for a strict control of its emissions. The mixture of sulfur hexafluoride and nitrogen is of key interest in electrical applications where sulfur hexafluoride is used as insulating gas. The effect of pore size, pressure, and mixture compositions on the selective adsorption of SF6 was investigated using simple fluid models adsorbed on a cylindrical pore model. Next, simulations using two atomistic models of zeolite templated carbons were performed. The average pore sizes of these materials are close to the optimal size predicted using the cylindrical pore model. The separation selectivities were calculated and compared to the materials previously reported for the separation of this mixture.

Moreover, the potential use of these two templated carbon materials to capture CO_2 at room temperature is reported. Their high-pressure CO_2 adsorption isotherms are among

the highest carbon capture capacity for carbonaceous materials and are comparable to the best CO_2 adsorbing materials. The importance of these results is discussed in light of CO_2 emissions mitigation. In addition, the simulated adsorption isotherms were used to obtain new insights into the adsorption process of the templated carbons.

Hybrid organic-inorganic adsorbents were also studied. These materials consist of a solid matrix functionalized by the grafting of organic moities. In particular for CO_2 capture solid adsorbents are functionalized with amino groups largely increasing their adsorption capabilities. However, the underlying mechanism of the adsorption process in the functionalized materials is not fully understood, limiting the possibility of designing optimal adsorbent materials for different applications. The availability of complementary methods to advance in this field is of great interest. The adsorption of CO_2 in amine-functionalized silica materials was studied using Monte Carlo molecular simulations. A simulation methodology for the design of post-synthesis functionalized silica materials was proposed, in which realistic model adsorbents were generated using an energy-bias selection scheme for the possible grafting sites. The methodology can be applied to different materials. The methodology was evaluated using models of silica gel and MCM-41 functionalized with different organic groups, comparing the resulting adsorption isotherms and grafting density to available experimental data. Furthermore, a new methodology that allows accounting for the chemisorbed CO_2 on the adsorption isotherms is presented. It is shown how molecular simulations can serve as a guide to quantify the CO_2 amount that can be easily desorbed for carbon capture applications.

Overall conclusions and future research lines are proposed in the final chapter. In summary, this PhD thesis highlights different possibilities for the capture and separation of greenhouse gases and provides new tools for evaluating and optimizing capture systems. Finally, this dissertation shows the use of basic research in Materials Science as an established tool for evaluating and optimizing thermodynamics of engineering processes.

Chapter I

Introduction

"We operate with nothing but things which do not exist, with lines, planes, bodies, atoms, divisible time, divisible space -- how should explanation even be possible when we first make everything into an image, into our own image!"

Friedrich Nietzsche (Twilight of the Idols)

It is important prior to start with the discussion of this dissertation to reflect on the physical laws from an epistemological perspective and not from their results as they will be addressed in the rest of this work. These laws constitute the principles of science and suppose the existence in nature of ideal topological objects like points or straight lines. All different kinds of phenomena can be explained by creating theories and models based on these laws.

The real elements in an object of study are represented by expressions; however, this representation is purely formal, that is, there is no strict requirement level between the phenomenon and the mathematical term that represents it. Hence, the models might include simplifications and be considered as an idealization of the situations they represent. The idealization present in the models comes from neglecting or assuming constant, in the equations, some terms believed to be of less relevance. The validity of the idealized models is evaluated by their prediction of real phenomena and/or their consistency with other well-established theories or models.

The ideal nature of the model provides two great benefits: the comprehension is easier and the resolution of the mathematical process is simpler than the complex phenomena that it represents. This dissertation deals with both of these aspects (i) the construction of models that simplify the understanding of a physical system and (ii) the use and development of mathematical tools for their resolution.

Furthermore, in certain scientific fields, such as thermodynamics, the results of the ideal models constitute limiting behaviors, which might be employed as standards for the systems under study.

The scientific work in this dissertation has a dual nature. On the one hand, the development of a mathematical model and of the tools to solve them is a deductive process that does not resort to experimentation, although the parameters used in the models or the models themselves proceed from experimental observations. This is a formal procedure intended to set the relationships between the objects of study. On the other hand, the process of comparing these results to other data whose results have been validated previously is an empirical process. This test, from which the rigor of the model as a representation of reality is verified, is a method of factual validation.

New models and predictions have to be not only coherent with scientifically accepted theories, but also their results have to be similar to the findings on the real phenomena. Both conditions ensure a rough correspondence between the object of study and the abstraction represented by the model and the extent that this similarity increases the greater the usefulness of the proposed models. This principle of rationality and possibility of verification of concepts will be followed during the discussions presented in the following chapters.

First, chapter 2 reviews the established methodologies and the physical and mathematical descriptions used in the dissertation for studying adsorption of greenhouse gases. An introduction to the different molecular models and their degrees of detail is presented. Moreover, the basis of molecular modeling and the different techniques for solving the potential energy equations represented by the models are presented in this chapter. Also, the application of molecular modeling to adsorption processes is introduced.

Then, in chapter 3 a discussion of the problematic and the need for capturing greenhouse gases is presented along with the state of the art in the capture of carbon dioxide using solid adsorbents at room temperature.

In chapters 4 to 6 the simulation techniques are used in different systems involving the adsorption of greenhouse gases. Chapter 4 is devoted to finding the optimal pore size of an adsorbent for separating a mixture of a potent greenhouse gas (sulfur hexafluoride) diluted with nitrogen. Models of different degrees of complexity are presented in the study, starting from very simple models up to atomistic structures. The simpler models, which require less computational power, allow an initial screening of the range of conditions to be used in the more complex models.

In chapter 5 atomistic models of carbon adsorbents are compared to experimental data for the adsorption of CO_2, the ideality of the models is considered and conclusions about the synthesis procedure and internal structure of the material are drawn.

In chapter 6 new methodologies for functionalizing silica materials and considering chemical reactions in molecular simulations are presented. The results are validated by comparing with experimental data.

The dissertation concludes in chapter 7 with general conclusions and an outline for future work.

Chapter II

Molecular Simulation Applied to Adsorption

"Would you tell me, please, which way I ought to go from here?" "That depends a good deal on where you want to get to," said the Cat. "I don't much care where---" said Alice. "Then it doesn't matter which way you go," said the Cat. "-- so long as I get somewhere," Alice added as an explanation. "Oh you're sure to do that," said the Cat, "if you only walk long enough."

Lewis Carroll (Alice in Wonderland)

In some cases, it is necessary to separate a component or group of components of a gas stream. This might occur for a variety of reasons, for instance: separating the pollutants in flue gases before being released to the atmosphere or concentrating a product present in a gas for its use on other process. Adsorption is one of the most commonly used processes for separating a component or group of components of a gas stream. The separation is possible due to the attraction between the atoms of the fluid and a surface. Adsorption is an equilibrium process between the adsorbent in contact with the bulk phase and an interfacial layer. This layer is composed of two regions: (i) the gas attracted by the solid surface and (ii) the surface layer of the solid. Adsorption takes place when the bonding of the adsorption sites is sufficiently strong to prevent displacement of the adsorbed molecules along the surface.

Adsorption can be either chemical (chemisorption) or physical (physisorption). Physisorption is a reversible process that occurs at a temperature lower or close to the critical temperature of

an adsorbed substance, and its nature can be liken to the condensation process of the adsorptive. Physisorption is an exothermic process, because of a decrease in free energy and entropy of the adsorption system. Chemisorption occurs usually at temperatures much higher than the critical temperature and is a specific process, meaning that it can only take place on some solid surfaces for a given gas [1].

The surface onto which the molecules adhere is called adsorbent. They are commonly solid materials with high surface area; adsorbents are usually employed in separation processes. Therefore, the most important parameters for selecting an adsorbent for a specific application are selectivity and capacity [2].

Selectivity is the preference of a substance to adsorb over others; this property depends on the fluid-surface interactions, although it can also be the result of molecular sieving effects. The molecular sieving is due to one adsorbate being able to reach regions of the pore network that are inaccessible to another adsorbate because of their molecular size and/or shape.

The capacity is the maximum amount of fluid that can be taken up by the adsorbent; it is determined by fitting macroscopic adsorption data [3]. Its value is usually high in porous adsorbents, because of their large specific surface. This property assesses the feasibility of using a material as an industrial adsorbent.

The IUPAC classifies pores in three different groups according to their width [4]: (i) those of less than 2nm are called micropores, (ii) mesopores are pores between 2 and 50 nm and (iii) macropores represent pores greater than 50 nm. The size of micropores is comparable with those of the adsorbed molecule, therefore in a micropore all adsorbed molecules can interact with the surface. Hence, adsorption in micropores is essentially a pore filling process in which the void volume is the main controlling factor [1]. For mesopores the basic parameters for their characterization are: specific surface, pore volume and pore size. Whereas in macropores, the action of adsorption forces takes place only at close distance from the surface and not through the entire void volume.

In meso and macro pores, more than one layer of adsorbed molecules can be fitted in the pore interface, forming first a monolayer. Then, the molecules start to adsorb more distant from

the surface forming successive layers. In mesopores, after the formation of multilayers a process called capillary condensation occurs. Capillary condensation is the equivalent of condensation for confined fluids. In the former, the liquefaction of physisorbed vapors can occur at pressures below the saturation pressure.

When a fluid is confined in a pore, bulk phase transitions are generally shifted to different bulk pressures and temperatures. The magnitude of this change depends on the pore size, geometry and the nature of the fluid-surface interaction. In addition, some surface transitions, such as pre-wetting, do not have a bulk counterpart [5]. The phase transitions are sensitive to the nature of both fluid-fluid and fluid-surface interactions.

The fundamental concept in adsorption science is the adsorption isotherm. It is a graphical representation of the equilibrium relationship between the amount of adsorbed material and the pressure or concentration in the bulk fluid phase at constant temperature. Isotherms are used as the main source of information about adsorption and its mechanisms; they are characteristic of a given adsorption system and all information derived from an adsorption isotherm deals only with a concrete adsorbent and adsorbate.

The information commonly extracted directly from adsorption isotherms is: (i) the capacity of the adsorbent at a given temperature; (ii) the method of sorbent regeneration, whether a pressure or a temperature swing; and (iii) the product purities [6].

The characteristics of an adsorbent such as surface and pore size distribution, are usually calculated by fitting different parameters of isotherm equations. These equations attempt to encode all relevant phenomena with few fitted parameters; consequently, they have limited insight and restricted confidence [5].

Adsorption isotherms can also be generated using molecular simulations. The main advantage of using molecular simulations is that the information behind the isotherm is kept; therefore, the relevant information about the characteristics of the adsorption system is not limited in insight. Bearing in mind their limitations, simulations are an ideal tool to study small-scale materials phenomena.

Molecular simulation methods can be used to study complex systems with a level of detail hard to achieve by conventional experiments. Molecular modeling allows recognizing and retrieving useful or even predictive information about the simulated system. Its predictive capabilities are used in adsorption science for designing and testing of adsorbent materials. Simulations allow calculating a large number of material properties prior to their synthesis. In some complex systems, experimental studies have been preceded by theoretical ones [1]. Nowadays simulation plays a critical role in understanding, characterizing and developing adsorption systems [2]. In the field of adsorption science the main applications of molecular simulations are: (i) advance theory and discover new physical phenomena and (ii) augment and explain experiments.

In adsorption studies, a range of different computational methods is used. Monte Carlo simulations are commonly used to obtain adsorption isotherms and heats of adsorption. Quantum mechanical density functional theory (DFT) is employed for calculations of binding energies and finding specific sites of adsorption.

2.1. BASIC CONCEPTS OF MOLECULAR SIMULATIONS

Molecular simulation consists on emulating the behavior of systems and physical processes within the atomic scale. The results obtained from simulations allow the user to calculate some thermodynamic, transport, and structural properties of the simulated system. Microscopic properties hard, or even impossible, to see experimentally can be analyzed by molecular simulations.

The collective behavior of the atoms in a system has a different effect on how a material undergoes deformation, phase changes, or other phenomena, providing links between the atomic scale to meso/macro phenomena. A macroscopic system is composed of particles that move in different directions and with different momentum. Macroscopic properties are the result of the interaction of a large number of particles in a system. Thus, these properties can be determined as functions of the particle's coordinates and momentum. The conversion of this microscopic information to macroscopic observables such as pressure, stress tensor, strain tensor, energy, heat capacities, etc., requires theories and strategies developed in the realm of

statistical mechanics. Statistical mechanics provides the theoretical connection between the microscopic description of matter (e.g. positions and velocities of molecules) and the macroscopic description, which uses observables such as pressure, density, and temperature.

Since molecules interact among themselves, statistical averaging if their individual (not interacting) properties does not provide any meaningful quantity descriptive of a macroscopic system. Only for ideal gases, statistical averaging of the individual energies of a molecule allows calculating the internal energy of the system. The solution to this problem is to deal with a large number of identical systems known as an ensemble. An ensemble is a number of replicas of the system, each of them with its own distribution of allowable states and subject to the macroscopic thermodynamic constraints imposed on the original N-particle system of interest. The states of all replicas define the probability distribution. Given that it is impossible to generate all members of the ensemble, ensemble averages will always be subject to statistical uncertainties even if there are no systematic errors. The required length of a simulation will depend upon the magnitude of fluctuations in a quantity of interest and the associated level of statistical error that is considered satisfactory [7].

Ensembles are classified according to the way in which their members interact with outside systems. A microcanonical ensemble (fixed N, V, E) has no interaction at all, in a canonical ensemble (fixed N, V, T) its members interact thermally and/or mechanically with an outside system and a grand canonical ensemble (fixed μ, V, T) interacts thermally, mechanically, and diffusively with the environment [8].

Statistical mechanics postulates that the energy on the microscopic scale is made up of quanta or discrete units. Thus, the energy of a system at any instant is the sum of these discrete energy levels. The partition function is a state function, which severs as the bridge between the quantum mechanical energy states of a macroscopic system and its thermodynamic properties. For instance the Hemholtz free energy (A) in terms of the partition function is given by Equation 2.1.

$$A = -\beta \ \ln(Q) \tag{2.1}$$

Where Q is the partition function at constant molecules (N), volume (V) and temperature (T) and can be defined as a function of the energy states (E_j) of an N-body system; β is the thermodynamic beta ($\beta = 1/(k_b T)$, k_b is the Boltzmann constant)

$$Q = \sum_j \exp\left(-\beta E_j\right) \tag{2.2}$$

The main problem for determining the thermodynamic properties lies in being able to determine the energy states for an N-body system. One possible solution is to approximate the system using classical mechanics. In classical mechanics, the molecules are represented as inert rigid masses, disregarding the variations in the electron cloud. The discrete sets of energy E_j in Equation 2.2 disappears in the classical treatment because the position and momentum of a particle can vary continuously. Hence, the partition function becomes an integral over all coordinates (r) and momenta (p).

$$Q_{classical} = \frac{1}{h^{3N} N!} \int \exp\left(-\beta \left(\frac{\sum p_i^{\,2}}{2m_i} + U\left(r^N\right) \right) \right) dp^N dr^N \tag{2.3}$$

Where h is Planck's constant, N the number of particles and m_i is the mass of the particle i.

The integral in Equation 2.3 has several constraints to be evaluated numerically because most of the phase space does not contribute significantly to the system, therefore numerical integration is time-consuming because it attempts to evaluate all the points in the phase space. A workaround is to start the system in one of the states that contributes to the integral and propagate it through either time or ensemble space in such a way that the fraction of time it spends in any particular state is given by a probability distribution. There are two different ways to sample a system according to the probability distribution in such a way that the average value of the property can be calculated without wasting computer time on unimportant states. Those two different ways of moving from one state to the next are called Molecular Dynamics (MD) and Monte Carlo (MC) and they form the two branches of classical molecular simulations. While they are different approaches, because the ergodicity postulate they are equivalent from the viewpoint of statistical mechanics.

2.2. MONTE CARLO SIMULATIONS

We will focus on the description of the MC simulation technique, because this is the main method used in this thesis. Monte Carlo simulations, in a broad sense, are methods that generate a large set of random configurations and measure the average of some quantity in the system. They are named after the famous gambling location due to the random numbers used to generate trial moves. In the field of molecular simulation, MC samples the relevant states of a system in accordance with the laws of equilibrium statistical mechanics (ie: the Boltzmann distribution) [7, 9]. In the context of this thesis, the term Monte Carlo or MC refers only to this particular application of the MC technique.

MC is based on the Metropolis algorithm [10], which allows the calculation of averages of system properties defined in configurational space. These averages represent the properties in thermodynamic equilibrium. Since MC does not follow a natural time evolution, trajectory-dependent properties, such as transport properties, cannot be computed. However, this means that processes that take a long physical time can be studied using MC. In addition, certain ensembles specifically designed for computing phase equilibrium, which are very difficult to simulate using molecular dynamics, can be used in MC.

MC works around the problem of determining the partition function by using the probability that a system at temperature T will be found at an energy state i. Then, it is possible to compute the thermal average of some observable M.

$$\langle M \rangle = \frac{\int \exp\left(-\beta\left(\frac{\sum p_i^{\,2}}{2m_i} + U_i\left(r^N\right)\right)\right) M \; dp^N dr^N}{\int \exp\left(-\beta\left(\frac{\sum p_j^{\,2}}{2m_j} + U_j\left(r^N\right)\right)\right) dp^N dr^N} \tag{2.4}$$

This equation can be related to the following expression:

$$\langle M \rangle \approx \sum_i n\left(r_i^N\right) M\left(r_i^N\right) \tag{2.5}$$

Where $n(r_i^N)$ is the probability density of finding the system in a configuration around r^N.

The calculation of the integral in the denominator of the Equation 2.4 is not required because as shown in Equation 2.5 it only involves the ratio of the probability densities. The importance sampling algorithm [10] considers the function in the denominator as a weight function and can estimate the ratio of the two integrals that define property M by generating random values of r^N uniformly distributed.

The main algorithmic challenge of designing a MC simulation lies in devising ways to sample adequately and efficiently the equilibrium distribution in the correct statistical-mechanical ensemble. Metropolis et al[10] showed that one can sample such a distribution by treating the problem as if it were a Markov chain. A Markov chain is a collection of states where the probability of moving from one state to another depends only upon the current state, independently of how the system got into that state. The trick is to select the probabilities of moving from one state to another in such a way that the system converges to a stationary distribution with the probabilities given in Equation 2.4.

Calculating a thermal average by means of a Markov chain is the central idea in the Metropolis algorithm. In a Markov chain, the transition from one state point (r^N_{old}) to the next (r^N_{new}) only depends on the relative probabilities of the two state points involved. Millions of states are sampled starting from an arbitrary equilibrium configuration (i.e. one with a non-vanishing Boltzmann factor). The Markov chain starts from this configuration and proceeds to sample only the parts of configurational space accessible to the system (without sampling not significant points). It does so performing a small series of moves of the particles in the system. The aim is to construct the Markov chain in such a way that the configurations visited by it are distributed according to the probability density.

Since Markov chains describe stochastic processes "without memory", setting up a translational move only requires a rule on how to generate the next point from the last point already generated. For the points on the Markov chain to obey the probability density each configuration has to be visited by the chain according to its statistical weight. This means that for a Markov chain sampling equilibrium states, for any two states *i* and *j*, the probability of reaching state *j* from *i* should be equal to that of the reverse move. [9]

$$n(i)\ prob(i \rightarrow j)\ acc(i \rightarrow j) = n(j)\ prob(j \rightarrow i)\ acc(j \rightarrow i) \tag{2.6}$$

Equation 2.6 is known as detailed balance. In the Metropolis algorithm, the transition from one state to another is split into two steps: first, the new configuration is generated in a "trial move" as a random perturbation of the old state, with a probability described by a matrix *prob(i → j)*. Then, the generated trial move is accepted with probability *acc(j → j)* or else rejected. If the move is rejected, the Markov chain stays in its old state.

If no bias is used during the sampling, then *prob(i → j) = prob(j → i)* and the acceptance rules are simplified. The use of bias will be discussed in later sections, for now we will assume that no bias is included. Therefore, the acceptance probabilities are simplified to:

$$\frac{acc(i \rightarrow j)}{acc(j \rightarrow i)} = \frac{n(j)}{n(i)} \tag{2.7}$$

The ratio of acceptance probabilities for a move from *i* to *j* and its reverse move is therefore equal to the ratio of the statistical weights of their probabilities densities.

Adsorption studies employ mainly MC simulations over MD because: (i) adsorption systems allow the number of particles in the system to fluctuate connecting the adsorbent to a gas reservoir. In Monte Carlo Grand Canonical (GCMC) ensemble, the number of particles can fluctuate without being explicitly necessary to simulate the gas reservoir. (ii) Due to the slow diffusion of gases in real microporous adsorbents, the equilibration time for gas adsorption is typically in the range of minutes to hours, which is currently not possible to simulate with MD.

2.3. GRAND CANONICAL MONTE CARLO

In the present thesis, GCMC is used to simulate adsorption systems. This ensemble fixes the simulation volume, the temperature of the system and the chemical potential. Hence representing the variables fixed in experiments, because most experiments use an isothermal system, at constant volume with heat and mass interactions. Although the experimentalists usually fix the pressure of the gas phase, there is a pressure gradient due to the wall itself and

the quantity that remains fixed between the bulk and the adsorbed phase is the chemical potential.

There are two main kinds of movements in GCMC: (i) intrabox translations and (ii) insertion/deletion of molecules. The former corresponds to the system in thermal equilibrium, and the latter to the diffusive equilibrium. The acceptance probabilities of each move are different, because intrabox moves do not have a change in the number of molecules in the simulation system they actually correspond to the canonical ensemble.

The probability distribution for the canonical ensemble is given by the Boltzmann factor. Therefore the acceptance rule for changes in the position of the molecules is given by:

$$\frac{acc(i \to f)}{acc(f \to i)} = \frac{n(f)}{n(i)} = \exp(-\beta \cdot [U(f) - U(i)]) \tag{2.8}$$

$$acc(i \to f) = \min(1, \exp(-\beta \cdot [U(f) - U(i)])) \tag{2.9}$$

The acceptance rules for the intrabox movements are handled by the Metropolis method. The energies of the particle at the initial, *U(i)*, and final sites, *U(f)*, are the main criteria for this type of move. Thus, in order to compute a translational move the energies of the state before the move (*i*) and after the move (*f*) have to be calculated. If the energy change is negative the probability of the new state is greater than that of the old state, then the move is accepted. However, if the energy change is positive, then the move is accepted with probability *exp(-β [U(f) - U(i)])*. This is done by computing a random number uniformly distributed over the interval *(0,1)*. The move is accepted if the random number is less than *exp(-β [U(f) - U(i)])*. If a move is accepted, the new location is counted in the averaging, otherwise the molecule is returned to its original location, and the old configuration is counted again in the averaging.

The translation moves or intrabox moves are common to all MC ensembles that have fixed temperature. The movements with a fluctuating number of particles in the system have a probability density specific to the grand canonical ensemble.

$$n(r^N) \propto \frac{\exp(\beta\mu N) V^N \exp(-\beta \cdot U(r^N))}{\Lambda^{3N} N!} \tag{2.10}$$

where μ is the chemical potential and Λ is the thermal de Broglie wavelength.

Since experimentally, the pressure of a gas reservoir is imposed on the adsorption system, we need an explicit relation between the pressure (or the fugacity) of the bulk phase and the chemical potential for a direct comparison of the simulation results with experiments. For the gas in the reservoir chemical potential (per molecule) can be calculated as the sum of the chemical potential of the ideal gas (μ^{id}) and the excess one (μ^{ex}).

$$\mu = \mu^{id} + \mu^{ex} \tag{2.11}$$

The chemical potential for the ideal gas is defined in terms of the thermal de Broglie wavelength, and the excess chemical potential is defined in terms of the fugacity.

$$\mu = \frac{1}{\beta} \cdot Ln\left(\beta P \Lambda^3\right) + \frac{1}{\beta} \cdot Ln\left(\frac{f}{P}\right) \tag{2.12}$$

Then, multiplying by βN and taking the exponential of both sides of the equation.

$$\exp(\beta \mu N) = \left(\Lambda^{3N}\right)\left(\beta f^{N}\right) \tag{2.13}$$

where μ^{id}: chemical potential of the ideal gas, μ^{ex}: excess chemical potential, P: pressure of the bulk phase and f is the fugacity of the bulk gas

Then the Equation 2.10 becomes:

$$n\left(r^N\right) \propto \frac{\beta\ f^N V^N \exp\left(-\beta \cdot U\left(r^N\right)\right)}{N!} \tag{2.14}$$

The acceptance rules for the insertion and destruction steps depend of the change in energy due to the insertion/destruction of the molecule. The acceptance rules for these movements in terms of the fugacity for a simulation box of size V are:

$$\frac{acc(N \to N+1)}{acc(N+1 \to N)} = \frac{V \beta\ f}{N+1} \cdot \exp\left(-\beta \cdot \left[U\left(r^{N+1}\right) - U\left(r^N\right)\right]\right) \tag{2.15}$$

$$\frac{acc(N \to N-1)}{acc(N-1 \to N)} = \frac{N}{V\,\beta\,f} \cdot \exp\left(\beta \cdot \left[U\left(r^{N-1}\right) - U\left(r^{N}\right)\right]\right) \tag{2.16}$$

The energy before the insertion/destruction attempt is $U(r^N)$, the energy of the configuration after the particle insertion attempt is $U(r^{N+1})$, and $U(r^{N-1})$ is the energy after the particle destruction attempt. Therefore, as for Equation 2.8, the acceptance criteria become:

$$acc(N \to N+1) = \min\left(1, \frac{V \cdot \beta \cdot f}{N+1} \cdot \exp\left(-\beta \cdot \left[U\left(r^{N+1}\right) - U\left(r^{N}\right)\right]\right)\right) \tag{2.17}$$

$$acc(N \to N-1) = \min\left(1, \frac{N}{V \cdot \beta \cdot f} \cdot \exp\left(\beta \cdot \left[U\left(r^{N-1}\right) - U\left(r^{N}\right)\right]\right)\right) \tag{2.18}$$

Thus, to compute the acceptance of insertion and/or depletion of molecules, the energy associated to the creation and/or removal of the particle has to be calculated.

In summary, in a GCMC simulation, it is necessary to sample a large number of states starting from an arbitrary equilibrium configuration and each step in the Markov chain is generated by randomly selecting one of the following trial moves:

- Intrabox displacement of a randomly selected particle and acceptance or rejection of the move according to Equation 2.9.

- Insertion of a particle at a random position within the accessible volume in the simulation box and acceptance of the move according to Equation 2.17.

- Deletion of a randomly selected particle and acceptance of the move according to Equation 2.18.

The number of steps in the Markov chain has to be predefined and it depends on the particular system being studied. During a MC simulation the properties of interest, the number of particles and the energy, are calculated and stored at periodic intervals. The first part of the simulation results are discarded, because they depend on the initial conditions. The saved portion of the data corresponds to equilibrium conditions, because the detailed balance imposed on generating a MC system guarantees that once the system is in equilibrium it will

stay in it. The equilibration phase needs to be at least long enough for the data to stop drifting and to start fluctuating around the equilibrium values, which can be seen by looking at the variance of block average.

In order to satisfy microscopic reversibility, the probabilities for selecting a particle insertion or deletion trial move must be equal. The relative probabilities of translation, rotation and particle exchange trial moves can be chosen freely, and are normally adapted to each system studied to ensure an efficient sampling of the phase space accessible to the system. It has been seen that for GCMC if the creation, addition, and removal moves are chosen with equal probabilities, the system converges faster.[7]

Computing power limits the number of particles that can be studied in molecular simulations to a few thousands. To enable such relatively small system to mimic a macroscopic system requires the use of periodic boundary conditions (PBCs), in which particles are simulated inside a small box that is assumed to replicate infinite times in the space. If the system is sufficiently large, the PBCs will not affect the results. In addition, the molecular interactions are truncated at a suitable distance to limit the computational cost. A very popular yet simple method is the minimum image convention. Only the nearest image of a particle j relative to particle i is used to calculate the interaction energy.

Thus, the calculation of macroscopic thermodynamic properties by statistical mechanics requires determining the energy of the system. The energy of a system is the sum of the kinetic energy and the potential energy. At the atomic level, the kinetic energy corresponds movement of the atoms without considering their interactions; hence, this quantity is the resultant of the ideal gas calculation. Furthermore, the potential energy is calculated as the result of the interactions among atoms.

In the simulations, a molecule is described as a series of charged points that can be interconnected. In general, the charged points can represent an atom, or group of atoms, and the interconnections emulate the intramolecular bonds. The combination of the charged points and the intramolecular bonds allow the calculation of the potential energy, which is then used for determining the acceptance criteria for the MC moves.

2.4. MOLECULAR INTERACTION POTENTIALS

The two main kinds of classical molecular simulation techniques are MD and MC. From the statistical mechanics point of view, they are equivalent methods, but each of them has different strengths and weaknesses. Whereas, molecular dynamics solves the equations of motion defining the classical trajectory in phase space, Monte Carlo samples states from phase space, using random numbers, by constructing a stochastic Markov chain.

Both simulation methods, MD and MC, use interaction potentials for the calculation of the energy. An interaction potential is the mathematical description of the interactions of the different atoms in a system. The particular expression for a potential depends on the model used to represent the atoms in the system. The potential energy of a molecule can be expressed as:

$$E = E_{valence} + E_{non-bond} \tag{2.19}$$

Where $E_{valence}$ is the energy due to intramolecular interactions, which is usually expressed as a sum of contributions of bond angle and torsion angle energies; and $E_{non\text{-}bond}$ is the result of the van der Wals interactions, coulombic countributions and hydrogen bonds.

There are many different forcefields available in the literature. They differ in (i) the functional forms used to describe the interaction and (ii) the parameters used to describe the functional forms. Therefore, the accuracy of a model depends on (i) the type of functional forms, (ii) the quality of the parameters and (iii) the system of interest and the system for which the parameters were derived.

Usually the expressions are distance dependent equations with parameters to model the behavior of the specific interaction between pairs of atoms. Obtaining adequate values for the parameters of these equations can be achieved by two different means. Whereas, the first is derived by adjusting the parameter by to experimental data such as liquid and vapor densities, heats of adsorption, dipole moment, or heat of vaporization; the second method consists in using parameters derived by quantum mechanical studies fitted to different conformations of a structure.[11]

Usually for computation of non-bonded potentials, a cut-off distance is defined; the effect of atom *j* on the force perceived by atom *i* vanishes, or starts to vanish with a predefined behavior, when the separation is larger than that cut-off distance.

The van der Wals interactions is the sum of repulsive and an attractive forces, which are usually calculated according to Lennard Jones (LJ) potential.[9]

$$E_{vdW} = 4 \cdot \varepsilon_{ff} \left(\left(\frac{\sigma_{sf}}{r} \right)^{12} - \left(\frac{\sigma_{sf}}{r} \right)^{6} \right) \tag{2.20}$$

where r is the distance between the interacting LJ spheres, ε_{ff} is the potential well depth and σ_{ff} the collision diameter.

Electrostatic interactions arise from interactions due to the unequal charge distribution over the atoms of a molecule. A common way of representing this charge distribution is by placing partial charges on the centers of the atoms. The electrostatic interaction between two partial charges is calculated according to Coulomb's law.[7, 9] For particles with a charge q_i in a cube box with diameter L and n numbers of periodic images the electrostatic energy is given by:

$$E_{electrostatic} = \frac{1}{2} \sum_{i=1}^{N} \sum_{j \neq i}^{N} \frac{q_i \cdot q_j}{\left| r_{ij} + nL \right|} \tag{2.21}$$

Valence potentials represent atoms bonded to each other directly or atoms in the same molecule that are separated by a maximum of three bonds in series. There are three main components of intramolecular interactions: angle bending, is the interaction of two atoms which are bonded to a common atom; bond stretching, describes a bond between two atoms; and dihedral angle, describes the interaction arising from torsional forces in molecules.

$$E = \left(E_{\text{angle-bending}} + E_{\text{bond-stretching}} + E_{\text{dihedral-angle}} \right) + \left(E_{\text{short-range}} + E_{\text{long-range}} \right) \tag{2.22}$$

The expression in Equation 2.22 is the general calculation that has to be performed after every MC movement. However, depending on the particular model used in the simulations, additional terms may appear in Equation 2.22. Solving this equation allows evaluating the

acceptance criteria provided by the different ensembles. Each change in the configuration of the molecules requires a new calculation of this term. In the next section, it is shown how to use GCMC and the potential energy calculations for the generation of adsorption isotherms.

2.5. MONTE CARLO SIMULATIONS OF ADSORPTION

Simulations of adsorption systems resort to GCMC simulations due to their simplicity of representing this kind of systems. The intensive variables of the grand canonical ensemble represent phase equilibria and since adsorption is an equilibrium process, the temperature and the chemical potential are equal in both the gas phase and the adsorbed form. Besides reproducing the equilibrium conditions that exist during adsorption, the advantage of GCMC simulations for adsorption systems is that the bulk gas phase does not have to be explicitly simulated. Moreover, since MC simulations do not follow natural time evolution, the equilibration of the system is not hindered by slow diffusion of the fluid molecules in the adsorbent.

Simulations of adsorption employing GCMC are widely used in research. Several works on adsorption using GCMC have focused on the comparison of the results of the simulation with the experimental data and on the additional insight obtained by simulation. [12-15]. Simulations have been used to simulate adsorption of a large number of fluids on different adsorbents, such as: zeolites [16-18], carbons [2, 19] and metal organic frameworks [20, 21]. Moreover, simulations have been used to study theoretically the influence of different variables on the adsorption isotherms by using ideal pore models, such as slit and cylindrical pores. [22-25]

Simulations of adsorption using GCMC simulate only the adsorbed phase. Therefore, in addition to an interaction potential model for the fluid molecules, the simulation of the adsorbed phase has to reproduce the solid interactions with the fluid. This can be achieved in several ways: (i) using an effective potential, such as Steele's[26] or Tjatjopoulos' [27] for slit or cylindrical pores respectively, or (ii) using an atomistic potential, where the different atoms in the solid are represented with a explicit potential.

In general, the calculation of an adsorption isotherm using GCMC abides to the following procedure:

1) Fix the temperature, the size of the simulation cell and the PBCs.

2) Define and set-up the interaction potential for the adsorbent inside the simulation cell, it can consist of an expression of the energy in terms of the position inside the simulation cell (i.e. an effective potential) or locating the explicit interaction points in a solid framework that interacts via equations such as those in equations 3.20 and 3.21.

3) Define the interaction potential of the fluid molecules.

4) Fix the fugacity of the bulk gas phase, for comparison with experimental data the fugacity can be converted to pressure using either simulations or an equation of state (EoS).

5) Set up a starting position for the molecules, ideally the starting position should be set up with a density close to the equilibrium value, however a cell with no fluid molecules can be used as starting point by using a longer equilibration steps.

6) Make a trial attempt to insert, remove or displace a molecule inside the simulation cell, calculate the change in the energy and, using the corresponding expression from Equations 2.9, 2.17 and 2.18, determine if the move is accepted.

7) Repeat step 5 for a predefined (large) number of steps. The number of steps should be divided in two sections; the first section is the equilibration, and this should not be used to gain information about the system. The second section is the production part, from this point on the values are used to determine the average in the properties of interest during the simulation, such as the number of molecules.

8) Repeat steps 3-6 changing the fugacity. The plot of the average number of fluid molecules as a function of the fugacity represents the adsorption isotherm of the system.

This algorithm shows the basic calculation of an adsorption isotherm. However, it does not go into detail on how the calculation of the energy is performed or how to sample properly the phase space. In some systems, techniques such as the Ewalds summation and configurational

bias are introduced in the calculations to improve their results. The next section introduces these concepts, as they will be used during this thesis.

2.6. ADVANCED TECHNIQUES

2.6.1. Ewald summation

The expression for the Coulomb contribution to the energy is a conditionally convergent sum. The problem arises from the fact that the electrostatic energy of an elementary charge with another charge is infinite when periodic boundary conditions are applied. Different techniques, such as the Ewald summation, are used in order to improve the convergence of the sum. The Ewald method makes two amendments to the Coulomb potential. First, each ion is effectively neutralized by superposition of a spherical Gaussian cloud of opposite charge centered on the ion. The second part is to nullify the effect of the Gaussians superposing a second set of Gaussian charges, but this time with the same charge as the original ions. Thus, the Ewald summation splits the lattice summation into a short-range and a long-range part, where the long-range is evaluated in a fast converging Fourier representation. In the short range, which works in real space, are calculated particle-particle interactions originating from the Gaussian charge distribution, and are corrected the calculation of the electrostatic interactions of the ion to itself due in the reciprocal space part. Furthermore, molecular systems need additional modifications to correct the intramolecular coulombic interactions; this is achieved by adding a term that corresponds to the potential energy of an ion due to the Gaussian charge on a neighboring charge [28]. The expression for the long-range potential is calculated according to the following formula:

$$E_{electrostatic} = \frac{1}{2V}\sum_{k=0}^{k_{max}} \frac{4\pi}{k^2}\left|\rho(\underline{k})\right|^2 \exp\left(-k^2/4\alpha^2\right) - \left(\alpha/\sqrt{\pi}\right)\sum_{i=1}^{N_m N_a} q_i + \frac{1}{2}\sum_{i\neq j}^{N_m N_a}\frac{q_i q_j erfc\left(\alpha\, r_{ij}\right)}{r_{ij}} - \sum_{n=1}^{Nm}\sum_{k=1}^{Na}\sum_{\lambda=k+1}^{Na} q_{nk}\cdot q_{n\alpha}\frac{erf\left(\alpha|r_{k\alpha}|\right)}{r_{k\alpha}} \tag{2.23}$$

$$\rho(\underline{k}) = \sum_{i=1}^{N_m N_a} q_i\left(\cos(\underline{k}\cdot\underline{r}_i) + i\sin(\underline{k}\cdot\underline{r}_i)\right) \tag{2.24}$$

The factor $1/(4\pi\varepsilon_0)$ is omitted for simplicity (ε_0 is the permittivity of vacuum); $erf(x)$ and $erfc(x)$ are the error function and the complementary error function respectively; the width of the Gaussian charge distribution is $(2/\alpha)^{1/2}$ is the parameter that characterizes the shape of the Gaussian charge distribution; N_a is the number of charged points per molecule; N_m is the number of molecules; k is the reciprocal lattice vector $2\pi <l_x/L_x, l_y/L_y, l_z/L_z>$; L_x is the length in the x direction.

The charge density, Equation 2.24, depends on all the charges in the system, hence for any change in the system the full energy for the reciprocal space section has to be calculated. In contrast, the energy for the real space, as well as the expression for the van der Wals energy, is the sum of the contribution for each charge. In the implementation of the Ewald sum used in this thesis, Equation 2.24 is stored in arrays. That way, only changes in the charge density are calculated, avoiding doing them for all the atoms in the system for each step of the simulation.

2.6.2 Configurational bias Monte Carlo

In some systems, the Metropolis sampling algorithm is not enough to properly sample the phase space in a reasonable time. For instance, in dense fluids or systems with large molecules most insertion attempts are rejected.

It is possible to use the knowledge of the system to bias the sampling. When biasing the sampling it is necessary that the new move is reversible, i.e. there is not a zero probability of generating any conformation that might actually occur. Any change during the generation of the trials means that the probabilities in Equation 2.6 are no longer equal and the acceptance rules for the different moves change depending on the bias used.

One of the alternative sampling methods most commonly used is the configurational-bias Monte Carlo (CBMC).[29] This algorithm addresses in particular the case of long linear or branched molecules that can adopt numerous conformations. The basic concept is that molecules are grown atom by atom into a dense fluid in such a way that the local space for each new atom is sampled and the lower energy positions are more likely to be chosen to continue the growth of the molecule.

The probability of choosing a molecule generated using this algorithm depends on the number of points (k) used to sample the local phase space of each atom. The selection of one trial for the bead a depends on the sum of the Boltzmann factor for all the trials (Rosenbluth factor, w_a).

$$P_a = \frac{\exp(-\beta \cdot U(r_i))}{w_a} = \frac{\exp(-\beta \cdot U_a(r_i))}{\sum_j^k \exp(-\beta \cdot U_a(r_j))} \tag{2.25}$$

where P_a is the probability of selecting the trial i for bead a. Equation 2.25 depends on the energy of the bead a and not on the energy of the whole system, because computationally is easier to calculate the energy of one molecule than the potential energy for all the atoms in each MC move.

This biased selection accumulates a bias that has to be removed in the acceptance rules. For example, during the generation of a new molecule the acceptance probability becomes:

$$\frac{acc(N \to N+1)}{acc(N+1 \to N)} = \frac{n(N+1)}{n(N)} \frac{prob(N+1 \to N)}{prob(N \to N+1)} \tag{2.26}$$

Where $n(N+1)/n(N)$ is equal to the solution of the case with no bias, see Equation 2.15.

$$\frac{acc(N \to N+1)}{acc(N+1 \to N)} = \frac{V \beta f}{N+1} \cdot \exp(-\beta \cdot [U(r^{N+1}) - U(r^N)]) \frac{prob(N+1 \to N)}{prob(N \to N+1)} \tag{2.27}$$

The probabilities in this case are different. Whereas from N to $N+1$ the probability is given by Equation 2.25, the reverse move has a homogeneous probability of being chosen of $1/k$.

$$\frac{acc(N \to N+1)}{acc(N+1 \to N)} = \frac{V \beta f \exp(-\beta \cdot [U(r^{N+1}) - U(r^N)])}{N+1} \frac{1/k}{\exp(-\beta \cdot U_{N+1})/w_{N+1}} \tag{2.28}$$

Since the move in $N+1$ consists on creating a new molecule, the energy $U(r^{N+1})$ can be decomposed in $U(r^N)+U_{N+1}$, it is possible to simplify the expression and obtain the acceptance rules.

$$\frac{acc(N \rightarrow N+1)}{acc(N+1 \rightarrow N)} = \frac{V \beta f}{(N+1)} \frac{w_{N+1}}{k} \tag{2.29}$$

Then the acceptance criterion becomes:

$$acc(N \rightarrow N+1) = \min\left(1, \frac{V \beta f}{N+1} \cdot \frac{w_{N+1}}{k}\right) \tag{2.30}$$

Equation 2.30 is the general expression for the acceptance of a bias move for one atom in the CBMC for insertion of molecules. The second term of the equation is the consequence of the bias and can be decomposed in different beads and/or energy components, as the product of exponentials, if a sequential biased generation is used. The other two acceptance rules for GCMC are modified in a similar way to include the bias.

For the removal of an atom:

$$acc(N \rightarrow N-1) = \min\left(1, \frac{N}{V \beta f} \cdot \frac{k}{w_N}\right) \tag{2.31}$$

And for intrabox movements it becomes:

$$acc(i \rightarrow j) = \min\left(1, \cdot \frac{w_i}{w_j}\right) \tag{2.32}$$

In short, biases are a way to sample more efficiently the phase space. They avoid expending most of the simulation time in configurations with negligible probability density. Any bias introduced during the generation of the movements has to be removed in the acceptance rules, and it has to satisfy the detailed balance.

2.7. CONCLUSIONS

The application of the different MC techniques for simulation of adsorption of a gas in a solid surface can be applied to gain insight at a molecular level of the interactions of the different molecules inside the solid material. Different types of approaches can be used depending on

the complexity of the system under study; all the analysis of the outcome has to consider the limitations and simplifications used in the models. In the following chapters, these MC simulation techniques are applied to different problems involving the adsorption of greenhouse gases on solid materials. It is shown how different simulation techniques can be applied depending on the particular problem at hand. The MC simulations are used in this thesis as a tool to gain insight and make predictions about particular adsorption systems.

REFERENCES

1. Dabrowski A. *"Adsorption - from theory to practice"*. Adv Colloid Interface Sci. **2001**;93 (1-3).135-224.

2. Tenney CM, Lastoskie CM. *"Molecular simulation of carbon dioxide adsorption chemically and structurally heterogeneous porous carbons"*. Environ Prog. **2006**;25 (4).343-54.

3. Bhatia SK, Tran K, Nguyen TX, Nicholson D. *"High-pressure adsorption capacity and structure of CO2 in carbon slit pores: Theory and simulation"*. Langmuir. **2004**;20 (22).9612-20.

4. Everett DH. *"Manual of Symbols and Terminology for Physicochemical Quantities and Units: Appendix II: Definitions, terminology and symbols in colloid and surface chemistry - part 1: Colloid and surface chemistry."*. International Union of Pure and Applied Chemistry. **1972**;31 579-638.

5. Sweatman MB, Quirke N. *"Modelling gas mixture adsorption in active carbons"*. Mol Simul. **2005**;31 (9).667-81.

6. Ralph TY. *"Sorbent Selection: Equilibrium Isotherms, Diffusion, Cyclic Processes, and Sorbent Selection Criteria"*. Adsorbents: Fundamentals and Applications; **2003**. p. 17-53.

7. Allen MP, Tildesley DJ. *"Computer Simulation of Liquids"*: Clarendon Press; **1987**.

8. Stowe K. *"Introduction to Statistical Mechanics and Thermodynamics"*. 1 ed. New York: Wiley; **1983**.

9. Frenkel D, Smit B. *"Understanding molecular simulation: from algorithms to applications"*. San Diego: Academic Press; **2002**.

10. Metropolis N, Rosenbluth AW, Rosenbluth MN, Teller AH, Teller E. *"Equation of State Calculations by Fast Computing Machines"*. J Chem Phys. **1953**;21 (6).1087-92.

11. Truhlar DG, Brown FB, Schwenke DW, Steckler R, Garrett BC. *"Dynamics Calculations Based on Ab Initio Potential Energy Surfaces"*. In: Bartlett RJ, editor. Comparison of Ab Initio Quantum Chemistry with Experiment for Small Molecules. Dordrecht, Holland: Reidel Publishing Company; **1985**. p. 95-139.

12. Myers AL, Calles JA, Calleja G. *"Comparison of molecular simulation of adsorption with experiment"*. Adsorption. **1997**;3 (2).107-15.

13. Davies GM, Seaton NA. *"The effect of the choice of pore model on the characterization of the internal structure of microporous carbons using pore size distributions"*. Carbon. **1998**;36 (10).1473-90.

14. Wongkoblap A, Do DD, Nicholson D. *"Explanation of the unusual peak of calorimetric heat in the adsorption of nitrogen, argon and methane on graphitized thermal carbon black"*. Phys Chem Chem Phys. **2008**;10 (8).1106-13.

15. Do DD, Do HD. *"GCMC-surface area of carbonaceous materials with N2 and Ar adsorption as an alternative to the classical BET method"*. Carbon. **2005**;43 (10).2112-21.

16. Lachet V, Boutin A, Tavitian B, H. Fuchs A. *"Grand canonical Monte Carlo simulations of adsorption of mixtures of xylene molecules in faujasite zeolites"*. Faraday Discuss. **1997**;106 307-23.

17. Goj A, Sholl DS, Akten ED, Kohen D. *"Atomistic Simulations of CO2 and N2 Adsorption in Silica Zeolites: The Impact of Pore Size and Shape"*. J Phys Chem B. **2002**;106 (33).8367-75.

18. Fuchs AH, Cheetham AK. *"Adsorption of Guest Molecules in Zeolitic Materials: Computational Aspects"*. J Phys Chem B. **2001**;105 (31).7375-83.

19. Palmer JC, Brennan JK, Hurley MM, Balboa A, Gubbins KE. *"Detailed structural models for activated carbons from molecular simulation"*. Carbon. **2009**;47 (12).2904-13.

20. Fairen-Jimenez D, Moggach SA, Wharmby MT, Wright PA, Parsons S, Düren T. *"Opening the Gate: Framework Flexibility in ZIF-8 Explored by Experiments and Simulations"*. J Am Chem Soc. **2011**;133 (23).8900-2.

21. Rossin A, Fairen-Jimenez D, Düren T, Giambastiani G, Peruzzini M, Vitillo JG. *"Hydrogen Uptake by {H[Mg(HCOO)3]⊃NHMe2}∞ and Determination of Its H2 Adsorption Sites through Monte Carlo Simulations"*. Langmuir. **2011**;27 (16).10124-31.

22. Sweatman MB, Quirke N. *"Modelling Gas Adsorption in Slit-Pores Using Monte Carlo Simulation"*. Mol Simul. **2001**;27 (5-6).295-321.

23. Do DD, Nicholson D, Fan C. *"Development of Equations for Differential and Integral Enthalpy Change of Adsorption for Simulation Studies"*. Langmuir. **2011**;27 (23).14290-9.

24. Nguyen PTM, Do DD, Nicholson D. *"On The Cavitation and Pore Blocking in Cylindrical Pores with Simple Connectivity"*. J Phys Chem B. **2011**;115 (42).12160-72.

25. Do DD, Nicholson D, Do HD. *"Effects of Adsorbent Deformation on the Adsorption of Gases in Slitlike Graphitic Pores: A Computer Simulation Study"*. J Phys Chem C. **2008**;112 (36).14075-89.

26. Steele W. *"Molecular interactions for physical adsorption"*. Chem Rev. **1993**;93 (7).2355-78.

27. Tjatjopoulos GJ, Feke DL, Mann JA. *"Molecule-micropore interaction potentials"*. J Phys Chem. **1988**;92 (13).4006-7.

28. Pantatosaki E, Papaioannou A, Stubos AK, Papadopoulos GK. *"Atomistic simulation of sorption in model pores with reduced spatial periodicity"*. Appl Surf Sci. **2007**;253 (13).5606-9.

29. Frenkel D, Mooij GCAM, Smit B. *"Novel scheme to study structural and thermal properties of continuously deformable molecules"*. J Phys: Condens Matter. **1992**;4 (12).3053.

Chapter III

Materials for capture of carbon dioxide

"No sensible decision can be made any longer without taking into account not only the world as it is, but the world as it will be."

Isaac Asimov (Asimov on Science Fiction)

Our lives and comfort greatly depend on the energy generated by the combustion of organic materials. During combustion, oxygen and organic compounds react and produce heat, water, and carbon dioxide. At first glance, the combustion process seems like a clean process with no harmful effects on the earth. Heat can be transformed to electricity, water is an important component of organic processes, and CO_2 is a non-toxic gas, which is also the product of cellular respiration.

Historically, the main problems with combustion of fuels have been the presence of substances different from hydrocarbons or other organic compounds on the fuels, or the presence of gases other than oxygen (such as nitrogen). The presence of such compounds may produce some toxic or environmentally harmful compounds, such as sulfur dioxide, or partially oxidized compounds such as carbon monoxide.

It has been possible to successfully, in most cases, separate these compounds or use catalysts to improve the combustion. The environmental problem nowadays is that our energetic needs have grown and we rely heavily on combustion to produce electricity. This is a problem

because such growth has increased the concentration of carbon dioxide in the atmosphere. This small change in the concentration does not have a direct effect on life, other than increasing the number of autotrophic organisms. However, there is some scientific evidence that such rise of carbon dioxide has increased the natural greenhouse effect. [1] The belief is that CO_2 along other industrial gases are increasing their content on the earth atmosphere; this increased concentration is reducing the heat loss of the earth's atmosphere onto the space, hence increasing the global temperatures.

The gases that reduce the heat loss of earth's atmoshphere are called greenhouse gases (GHGs). According to the Intergovernmental Panel on Climate Change the GHGs are: carbon dioxide, water vapor, methane, nitrous oxide, ozone, chlorofluorocarbons and sulfur hexafluoride. It has been difficult to establish global limits on the emissions of GHGs, due to the complexity to prove their effects on a global scale and to the fact that the main greenhouse gas, CO_2, is naturally abundant in the environment, plays an important role in many ecosystems and it is a by-product of the energy production. The economic needs that tie economic growth and generation of GHGs have hindered an agreement on specific goals for limiting GHGs. Nonetheless, it is imperative that GHG emissions are dramatically reduced; it is important first to limit and possibly eliminate emissions of industrial GHGs to the atmosphere.

The reduction of emissions of GHGs without changing our current industrial production methods requires their capture before being emitted to the atmosphere. Many technological process allow the separation and concentration of gases; among them are: absorption, adsorption, membrane separation, cryogenic distillation and biotechnology. In addition, within each of those processes different materials and schemes can be employed to target the separation of a specific gas. The optimum capture process can be determined by analyzing its costs in the context of power generation. Besides, depending on the source of the GHGs, i.e. the temperature, the pressure and the composition, a different kind of technology and/or materials might be more appropriate for the separation.

The objective of this chapter is to review the available literature on separation and capture of GHGs at room temperature and provide the context for the work presented in the following

chapters. Most of the literature is focused on CO_2, because it is the main GHG and is produced at large single sources. Likewise, the review presented on this chapter is focused on CO_2 capture. Given that most current research is focused on CO_2, alternative materials developed for CO_2 are likely to produce good candidate materials for adsorption of other GHGs. Moreover, in chapter 4 of this dissertation a review specific to adsorbents for a potent GHG (SF_6) is presented.

The review in this chapter is focused on the theoretical and experimental work for CO_2 capture performed in adsorbent materials at room temperature. High temperature adsorbents such as calcium [2, 3] and lithium oxides [4, 5], and hydrotalcites [6-8] are not included in this review.

Numerous materials have been studied for the separation and storage of GHGs. The principle for the separation materials is to use their chemical affinity and/or their network geometry to concentrate one of the species. We present next the review of different families of substances that have been used for adsorption of CO_2 at room temperature. The basic requirements for an adsorbent to be considered as viable material for CO_2 capture are: large CO_2 adsorption/desorption capacity, high affinity towards CO_2 and low energy requirements to perform a cycle of adsorption/desorption.

3.1. AQUEOUS AMINES

Amines are chemicals that can be described as derivatives of ammonia, in which one or more of the hydrogen atoms has been replaced by an alkyl or aryl group. They are classified as primary, secondary and tertiary depending on whether one, two, or three of the hydrogen atoms of ammonia have been replaced by organic functional groups.

This family of substances is included in this review even though they do not use adsorption for the separation of CO_2. They are included because amines, specially monoethanolamine (MEA), are currently the benchmark technology for CO_2 capture. Commercially carbon dioxide is recovered using a solution of 20-30% MEA, which reacts with CO_2 to form MEA-carbamate. The CO_2 is released upon heating the MEA-carbamate. MEA is currently used industrially for CO_2 capture because its low price and high adsorption capacity. [9] However,

large-scale CO_2 separation processes need to have lower energy requirements per mol of captured CO_2 than the current values obtained with MEA.

In general, amines react with acid gases to form salts, in the case of CO_2 they form soluble carbonate salts. Their reaction with CO_2 is reversible with temperature and heating the carbonate salt solution releases the adsorbed CO_2. Thus, CO_2 capture systems by amines are designed to create and later break amine salts.

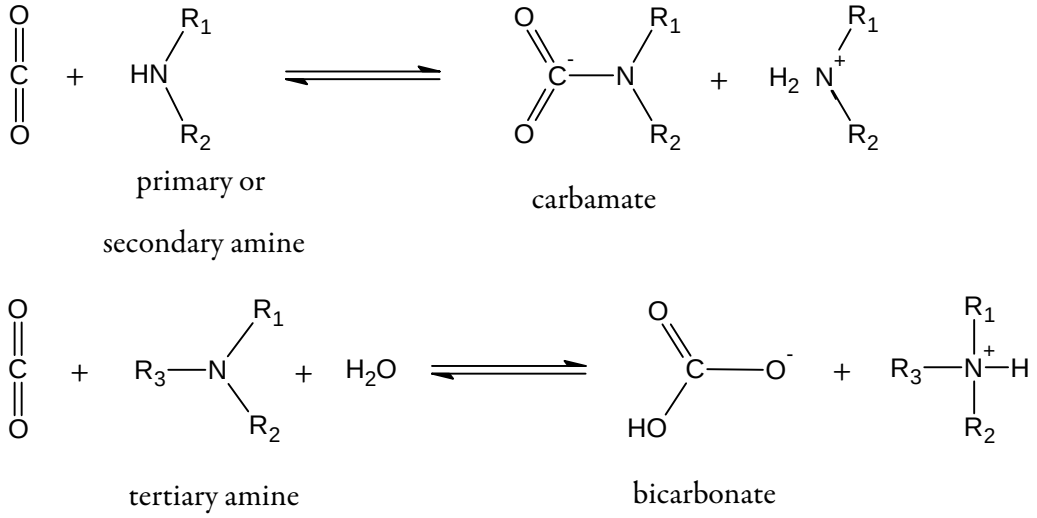

Figure 3.1. Reactions of aqueous amines with CO_2.

Whereas the reaction for primary, secondary and sterically hindered amines occurs via a zwitteron mechanism to form carbamates, tertiary amines react via a base catalyzed hydration of CO_2 that forms bicarbonate (seen in figure 3.1). The difference between mechanisms is caused by the absence of a hydrogen atom attached to the nitrogen atom in tertiary amines. Therefore, they have higher CO_2 loading capacity in per mole basis. [10]

Although the second mechanism in figure 3.1 occurs for all the amine kinds, the reaction rate is faster for the first one. Since both are competitive reactions, it is assumed that the main product is carbamate, except for some sterically hindered amines where bicarbonate formation might be dominant.

The main problem with the use of amines for CO_2 separation is that breaking the strong bond formed between CO_2 and the amine requires a large amount of energy, making the CO_2

release process energetically expensive. Therefore, a more efficient process, one in which the separating medium forms weaker bonds with the CO_2, is needed in order to implement a large-scale capture of CO_2 at an affordable cost.

Another common problem for amine absorbents is that, apart from CO_2, other acid gases might be present in the gas stream and react to form salts. If those salts are not broken with heat, they accumulate in the amine resulting in a loss of adsorbing capacity for the capture cycle. The stability of the amines in presence of common flue gas impurities, such as SO_2, NO_2, HCl, HF and O_2, is a major problem for three main reasons. (i) Fresh amines must be continually added due to the lost of CO_2 scrubbing capacity; (ii) the degradation products may rise a number of operating problems, such as: equipment corrosion, foaming and increased viscosity of the adsorbent; and (iii) volatile degradation products may be emitted in the gas exhaust increasing the environmental impact of the process. [11-13]

Viscosity is also a problem in solvents for gas capture, because the liquids have to be pumped through the absorption process. Therefore, amines have to be diluted in water to lower their viscosity to points where the gas-liquid contact equipments can operate without problem. The addition of water to the amines lowers their CO_2 capture capacity.

The research on amines has focused mainly on solving the problems of stability of the amines and improvements on the capture/stripping process. Different groups and companies have worked in the development of new amines with higher adsorption capacity, lower heat of adsorption, fast kinetics, and higher chemical stability. Freeman et al. [14] reduced the power loss during the regeneration by operating at higher temperatures (150°C), using piperazine (PZ) a thermally resistant solvent with high heat of CO_2 adsorption. Rochelle [15] reported lowering of the sensible heat losses from heating and cooling the recirculated solvent by using solvents with greater capacity, such as KS1 hindered amine. Bishnoi and Rochelle [16] used solvents with a faster rate of CO_2 adsorption, such as methyldiethanolamine with PZ, and observed an improved absorber performance with more dissolved CO_2. Jackson et al. [17] performed ab-initio studies of primary, secondary, sterically hindered primary amines and heterocycles and their carbamate derivatives in order to predict good capture solvents. They calculated the reaction energy and the equilibrium constant for the CO_2 capture reaction

scheme. They found that heterocycles have very good potential as capture solvents. Arstad and collaborators [18] used DFT to describe the molecular reactions relevant for CO_2 adsorption in aqueous NH3, MEA and DEA solutions.

In addition to studying state of the art amines, research has focused on improving the performance of the commonly used solvents, for instance the use of additives has reduced the oxidative degradation of MEA. [19] Likewise, amine blends, such as a mixed MEA/MDEA solution, have been reported to maximize the desirable quantities of the individual amines. Blend aim to retain much of the reactivity of primary or secondary amines at similar circulation rates while having low regeneration costs similar to those of tertiary amines. [10, 11, 20] Besides research on the amines, there are a number of research studies aimed at improving the capture/release process; for instance, modifications on the process configurations, such as absorber intercooling, stripper interheating and flashing systems, to reduce energetic requirements. [15]

Besides amines, it is possible to use aqueous ammonia as a CO_2 sorbent. This substance captures CO_2 by formation of stable salts, which are separated from the solvent stream by filtration or sedimentation. These salts can be used commercially as fertilizers; therefore no energy is required for solvent regeneration. This process is estimated to save 60% energy compared to absorption using MEA, the problem is that this is only an option until the level of demand for fertilizers is met. [21, 22]

Overall, state of the art amines improve some of the properties needed for the separation, but there is a trade-off in the others. Most of the proposed alternatives try to use these new amines in a mixture with conventional amines to get a synergetic effect for CO_2 capture. Moreover, hence studies on potential capture materials for CO_2 should not be based only on their greenhouse reduction potential. This it has been shown by life cycle analysis studies, amines used in CO_2 capture schemes have a high toxicity impact, mostly on freshwater. [13]

3.2. ZEOLITES

Zeolites are natural or synthetic hydrated aluminosilicate minerals, which form regular porous structures that can act as molecular sieves. They contain three-dimensional networks of

interconnecting channels or cages, which are commonly used to separate gas molecules. The latter are pore windows with a constricted aperture and the former have tubular diffusion paths. [23] There is a large variety of different zeolites, almost 200 different structural types have been accepted by the Structure Commission of the International Zeolite Association. [24] Zeolites are commonly used for the separation of compounds from product streams based on their large specific surface area, tunable acid-base properties and molecular sieving effect. Besides, zeolites may be modified to include a large variety of metal cations through a simple ion-exchange process. These modifications might lead to large changes in CO_2 sorption capacity, selectivity, and water tolerance.

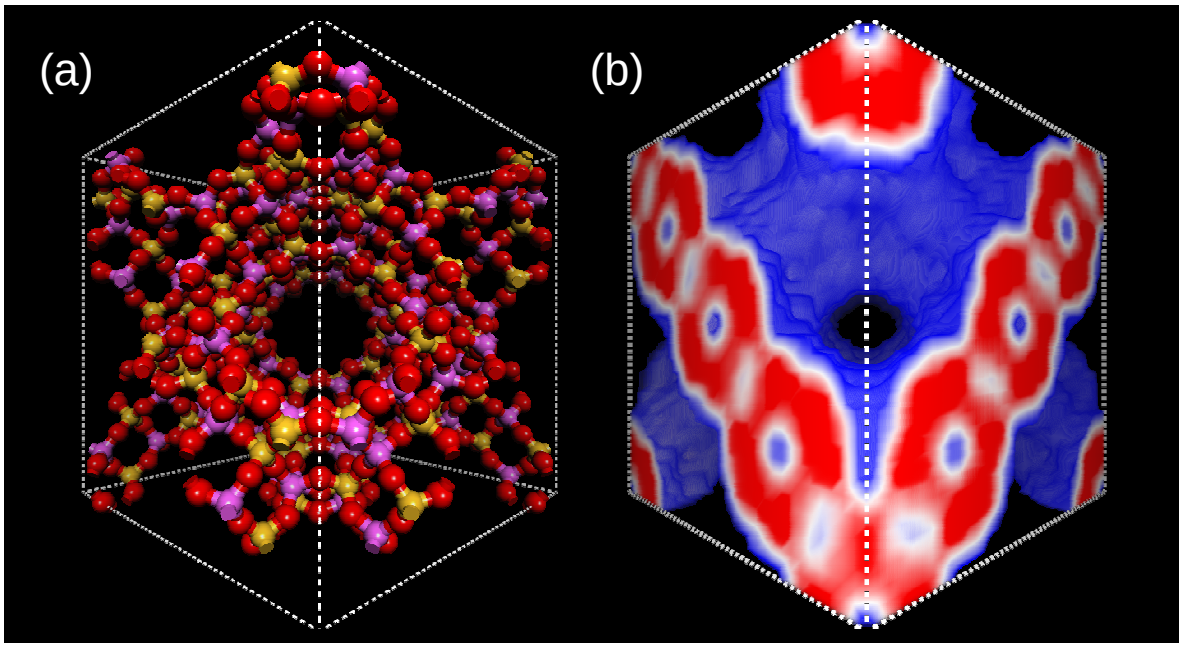

Figure 3.2. Representations of a unit cell of a FAU zeolite; (a) ball and stick model; (b) accessible volume (occupied volume is displayed in color, where red is the closest to the atom centers and blue the farthest).

Faujasite (FAU), a natural zeolite, and its synthetic forms, zeolites X and Y, are the most widely studied zeolites for CO_2 capture. The difference between zeolites X and Y is the silica to alumina (Si/Al) ratio on their framework. The former is for Si/Al between 2 and 3, while the latter is for Si/Al greater than 3, similar to the natural faujasite. [25] In Figure 3.2 is represented a model of zeolite X with balls and sticks, and a representation of the accessible volume of the same model.

Maurin et al. [26] using a combination of GCMC and experiments in dealuminated FAU observed a much higher increase in the isosteric heat of adsorption of CO_2 compared to CH_4, Ar and N_2, caused by the lateral interactions of CO_2 molecules among themselves. In a latter study, they observed that the addition of Li^+ and Na^+ cations in FAU increased the isosteric heat of adsorption of CO_2. The zeolite with Na^+ had a higher adsorption capacity and a more pronounced effect of adsorption to the temperature than the one with Li^+. [27] Zhang et al. [28] compared zeolite 13X to activated carbon and observed that the the CO_2 adsorption uptake of former at low pressures was much higher than the latter, however at pressures higher that 3 bar the zeolite saturated and the carbon adsorbed much more; making the zeolite more suitable for applications with low CO_2 concentration. Liu and Yang [29] using Gibbs ensemble MC studied supercritical CO_2 adsorption on NaA and NaX models. They found that the accessible pore volume is the main influencing factor in the absolute adsorption of zeolites with the same composition. Ghoufi et al. [30] combining GCMC and experiments showed that the large CO_2 selectivity on NaY is due to the different preferential sites of adsorption for CO_2 and CH_4. CO_2 mainly interacts with Na+ cations through electrostatic forces, while CH_4 has a more homogeneous distribution directed by van der Wals attractions. Cavenati et al. [31] studied the heats of adsorption for CH_4, CO_2 and N_2 on zeolite 13X and determined a preferential adsorption of CO_2 based on large differences in the heats of adsorption.

Besides faujasites, different kinds of zeolites and cation substitutions have been investigated for research on CO_2 capture. Searching for materials with high adsorption capacity, Zukal et al. [32] studied 6 high silica zeolites. The maximum capacity at 1.0 bar was obtained for TNU-1 and TM-5. They claimed that TM-5 is more suitable for CO_2 separation because it is more energetically homogeneous than TNU-9 and the energetic heterogeneity of TNU-9 makes removal of CO_2 from the channels more difficult. Krishna and van Baten [33] analyzed cage-type zeolites DDR, CHA, LTA and ERI for membrane separation of CO_2 from N_2, CH_4 or Ar. They found by using MD and GCMC that DDR and CHA yield the highest permeation selectivities CO_2 separation. They observed that in this kind of zeolites the window region has preponderance for CO_2 molecules. This hindered the intercage transport of CH_4, Ar or N_2, particularly in DDR, and consequently the CO_2 selectivity increased.

Leyssale et al. [34] using GCMC showed that the ITQ-1 zeolite is CO_2 selective for CO_2/CH_4 mixtures. This selectivity increased outside the Henry regime because of competitive adsorption. Harlick and Tezel [35] investigated the adsorption of CO_2/N_2 using 13 zeolites or zeolite based adsorbents, such as: 5A, 13X, NaY, NaY-10, H-Y-5. From the materials in the study, they claimed that the most promising adsorbents for CO_2 separation have low Si/Al ratio with cations in the structure and near linear CO_2 isotherms. Jia and Murad [36, 37] using Faujasite, MFI and Chabazite membranes studied the effect of pore structure, thermodynamic conditions and compositions on the permeation of CO_2/N_2 using MD. The authors found that for mixture components with similar sizes and adsorption characteristics (like O_2/N_2) small pore adsorbents are not suited for separations; however the separation of the mixture CO_2/N_2 is mainly governed by differences in adsorption, and this kind of mixtures can be separated efficiently by small pore adsorbents. In addition, they found that the mixture selectivity was higher than the ideal selectivity, because CO_2 was selectively adsorbed leaving little room for N_2. Although the latter component had a higher diffusion rate, the CO_2 selectivity increased because few N_2 molecules were adsorbed.

Moreover, the introduction of amine groups inside the pore framework has been attempted in order to increase the interactions between CO_2 and the zeolite. Bezerra et al. [38] studied the impregnation of two different amines, ethanolamine, and triethanolamine, on zeolite 13X. The impregnated zeolite suffered a detriment of the adsorption capacity for CO_2; the adsorbed amount on the impregnated zeolite was lower than on the pure one. However, at 348K, the adsorption in the impregnated amines increased compared to 298K and their uptake was comparable to the raw zeolite at 348 K. In a similar study, Chatti et al. [39] impregnated ethanolamine, ethylenediamine and isopropanolamine on zeolite 13X. They observed that the capacity of the amine-loaded zeolite was increased by ~25% for MEA and ~40% for IPA at 0.15 bar and 348K. In a different study, Y-type zeolite was modified by tetraethylenepentamine obtaining a large increase in the CO_2 adsorption capacity when low concentrations of water vapor were present in the gas stream. [40]

Since zeolites are crystalline and well-known structures, research of molecular simulations on CO_2 adsorption on zeolites has been extensive; this has led to the development of force fields

specific for the prediction of properties in zeolites. Garcia-Sanchez et al. [41] developed a force field for CO_2 specifically fitted to reproduce the adsorption properties of CO_2 in zeolites with different topologies and compositions. The authors claim that the force field is transferable to all possible Si/Al ratios with sodium as the extra framework cation. Previously, Plant et al. [42], using GCMC and MD in zeolites NaX and NaY, derived a force field specific for CO_2-Na^+ interactions from quantum chemical calculations.

The research on zeolites as CO_2 adsorbents has focused on understanding the mechanisms of separation of CO_2 from common flue gases and on finding the optimal conditions for CO_2 adsorptions on zeolites. Whereas the zeolites total capacity is limited by their pore volume, they allow the separation of low concentration sources of CO_2 with high uptakes at very low partial pressures. However, their small cavities also limit the introduction of CO_2 strong interacting species; diminishing the possibilities of designing tailor-made zeolites for CO_2 separation.

3.3. CARBONS

Carbons are obtained by the pyrolysis of organic materials rich in carbon, such as wood, lignite, coal, pitches and cokes, followed by activation of the chars obtained from them. The pyrolysis of any carbonaceous material in absence of air involves the decomposition of organic molecules, which finally become a solid porous carbon. These porous carbons contain predominantly macropores and practically inactive materials. An adsorbent with a highly developed porosity, and a correspondingly large surface area, is obtained by activating the carbonized material either by physical or chemical activation. The purity of the activated carbon produced, as well as its pore size distribution, is very much dependent on the starting material.

There are many different types of carbonaceous adsorbents such as: activated carbons, carbon molecular sieves, carbon nanotubes, nanobuds, and graphene. There are large differences among carbonaceous adsorbents in properties such as pore structure and active surface area. These unique characteristics are responsible for their adsorptive properties, which are exploited in many different liquid- and gas-phase applications. Carbons are predominantly

amorphous solids, except if a directing agent is used for their synthesis. Thus, they are described as graphitic or non-graphitic depending upon degree of crystallographic ordering. Graphitic carbons possess three-dimensional symmetry while non-graphitic carbons do not.

Porous carbons contain not only carbon, but also small amounts of oxygen, nitrogen, sulfur and hydrogen chemically bonded in the form of various functional groups, such as carbonyl, carboxyl and phenol groups. These functional groups might be derived from the raw material or they can be left from the activation process by the action of air or water vapor. These surface chemical properties play a significant role in adsorption. [43]

Carbons are more hydrophobic than other common adsorbents such as zeolites; however CO_2 uptake might still be reduced by competitive adsorption of water into the pores. Moreover, carbons usually have acidic character related to their oxygen containing surface groups. Therefore, capture of an acid gas such as CO_2 is favored upon modifying the carbon surface or controlling the porous network. Most research on carbonaceous adsorbents attempts to combine their natural characteristics, such as hydrophobicity and large pore volume and surface area, with designed synthesis: a controlled pore structure and task-specific surface chemistry. Silvestre-Albero et al. [44] employed carbon molecular sieve monoliths VR-5 and VR-93 to measure the adsorption of CO_2. They found that the amount adsorbed with both samples at high pressure exceeded the amount on commercial MAXSORB, a high surface area carbon adsorbent, and were comparable to the highest reported MOFs. They claimed that the appropriate selection of the preparation conditions allows the synthesis of carbon molecular sieves with a CO_2 adsorption capacity exceeding that of the best MOFs. MOFs are optimumized for a specific pressure range depending on their pore size, but the carbon molecular sieves behave successfully over a large pressure range. They observed that although the surface area is an indication of the adsorption capacity, the presence of a network of uniform and narrow micropores is a requirement for optimal packaging of CO_2 molecules at room temperature. Yong et al. [45] increased the CO_2 adsorption capacity at high temperatures of MAXSORB by functionalization with metal oxides. Martin et al. [46] found that the CO_2 capture capacity in a series of different activated carbons corresponded to a micropore volume filling process and was not limited to the adsorption surface. They claimed

that the micropore volume and average micropore width are the main controlling factors for CO_2 capture performance of carbons. Garcia et al. [47] used a design of experiments to study the response of CO_2 adsorption capacity to the changes in the CO_2 partial pressure, 1-3 bar, and the temperature, 15-65ºC, for a Nortit activated carbon. They found that the partial pressure, with a direct linear relationship with the capacity, was the most influential variable, while the temperature had a weaker inverse linear relationship. Radosz et al. [48] studied the selectivity of CO_2 over N_2 on activated carbon and charcoal and found moderate selectivities at low pressures, which decreased while increasing the pressure.

Since CO_2 is a weak acid, the introduction of bases onto the activated carbon is believed to favor their CO_2 capture performance. Basic nitrogen functionalities can be introduced through reaction with nitrogen containing reagents or activation with nitrogen containing precursors. Shafeeyan et al. [49] modified the surface activated carbon ammonia. Ammonia treatment increases the basicity of the carbon by introducing nitrogen functionalities to the carbon surface. They found that the decomposition of oxygen containing acidic groups and introduction of basic nitrogen functionalities on the carbon surface improved their adsorption ability. Bezerra et al. [38] impregnated carbons with MEA and TEA and observed a detriment of the textural properties. Although due to chemisorption at 348 K the capacities of the MEA impregnated carbon increased and reached values similar to those of the original support at 298 K.

Carbons, unlike zeolites, are complex porous materials. Hence, models of their structure are difficult to obtain. Carbons are usually modeled with the polydisperse ideal slit-pore model. Polydisperse ideal pore models the adsorption in a number of independent ideal pores with a range of sizes added together to give the total amount adsorbed in the material. The simplest geometries used are slits and cylinders. Slit pores are commonly used to reproduce graphitic surfaces and cylinders represent carbon nanotubes, Figure 3.3 shows sample models for the ideal graphitic pore and a single wall nanotube.

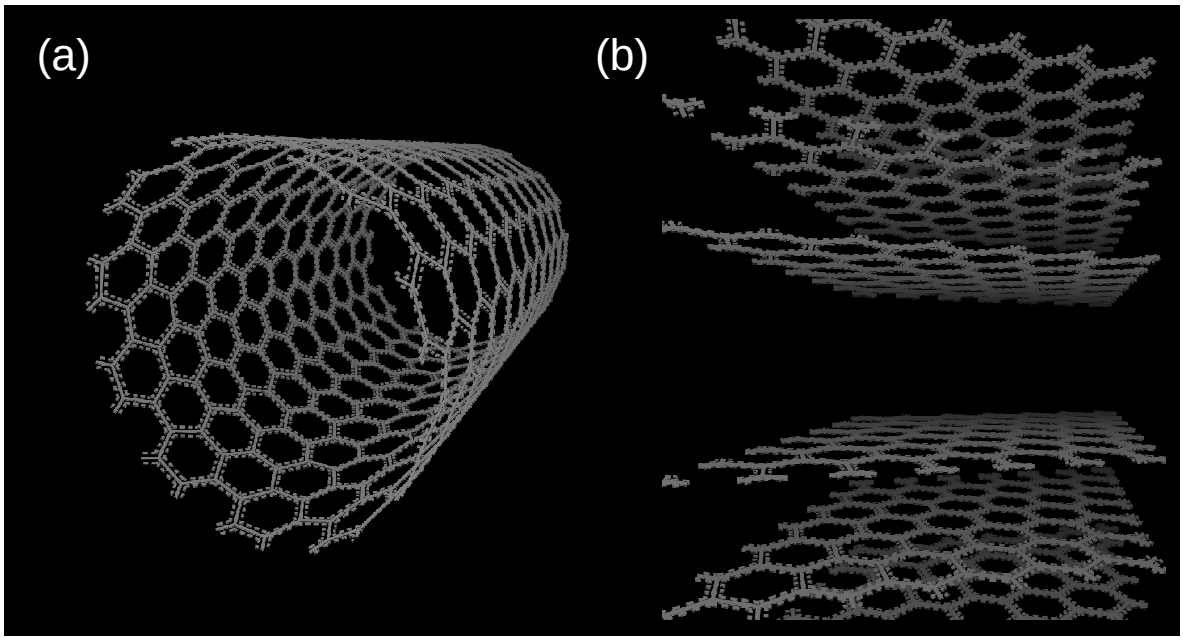

Figure 3.3. Models of a single walled carbon nanotube (a) and a stack of graphite sheets (b).

The problem with the polydisperse ideal model is the uniformity of individual pores and the independence of these pores. [50] Real materials have geometric and energetic non-uniformities that result in phenomena that the ideal pore model cannot capture. Tenney and Lastoskie [51] investigated CO_2 adsorption in slit pores with underlying graphitic structure and several variations of chemical heterogeneity, pore width and surface functional group orientation. They found that adsorption generally increased with increasing oxygen content. In addition, coal-like surfaces adsorbed CO_2 more strongly than planar homogeneous graphitic slit pores of comparable width. Huang et al. [52] simulated, using GCMC, CO_2/CH_4 separations in carbon nanotubes varying the diameters, the temperature and the pressure. The CO_2 adsorption in the nanotubes increased dramatically with an increase of the diameter, whereas the absolute amount of CH_4 adsorbed changed little with the pore size. For diameters less than 1.1 nm, the temperature and pressure have little effect on the adsorption behavior of the mixture. Palmer et al. [53] emulated using molecular simulations the separation of CO_2/CH_4 mixtures, using four types of microporous carbons, slit-pores, single walled carbon nanotube, an amorphous carbon and a carbon replica of zeolite Y. They found for the ideal models that at low pressure the pore size and morphology are the key variables for

an optimal adsorption and selectivity because they maximize the extent of confinement and do not restrict severely the degrees of freedom of CO_2.

The application of porous carbons for CO_2 is limited to higher CO_2 concentrations than zeolites, because in general the uptakes of the former are much lower at low CO_2 partial pressures. However, the hydrophobicity of the carbons makes them a convenient choice for industrial use in flue gases exhausts. Moreover, their larger pore volume, compared to zeolites, allows a better functionalization of their pores. This allows more flexibility to design an adsorbent selective for CO_2 separation. Carbons represent a challenge for molecular simulations due to their complex nature. Although there are simple models that can adequately predict the adsorption isotherms and can predict different operating conditions, they are limited in their assessments of changes in the adsorbent structure.

3.4. BUILDING BLOCK SOLIDS

Using a combination of rigid metal and/or organic based building blocks a broad array of metal organic frameworks (MOFs), zeolite imidazolate frameworks (ZIFs) and microporous organic polymers (MOPs) have been synthesized. By choosing appropriate building blocks, solids with designed shapes and functionalities can be tailor-made to provide optimal interaction with CO_2 molecules.

3.4.1. Metal Organic Frameworks

Metal organic frameworks, sometimes referred to as coordination polymers, are metal ions linked by organic bridging forming a porous structure. The organic linker molecules are typically rigid and contain 2 or 3 functional groups symmetrically arranged at the ends of the molecules. MOFs are easy to synthesize, highly porous, thermally stable and can be made in large quantities from low-cost ingredients. Besides, they can be designed for a specific pore size and functionalized for a specific application. The models of two different MOF structures are shown in Figure 3.4.

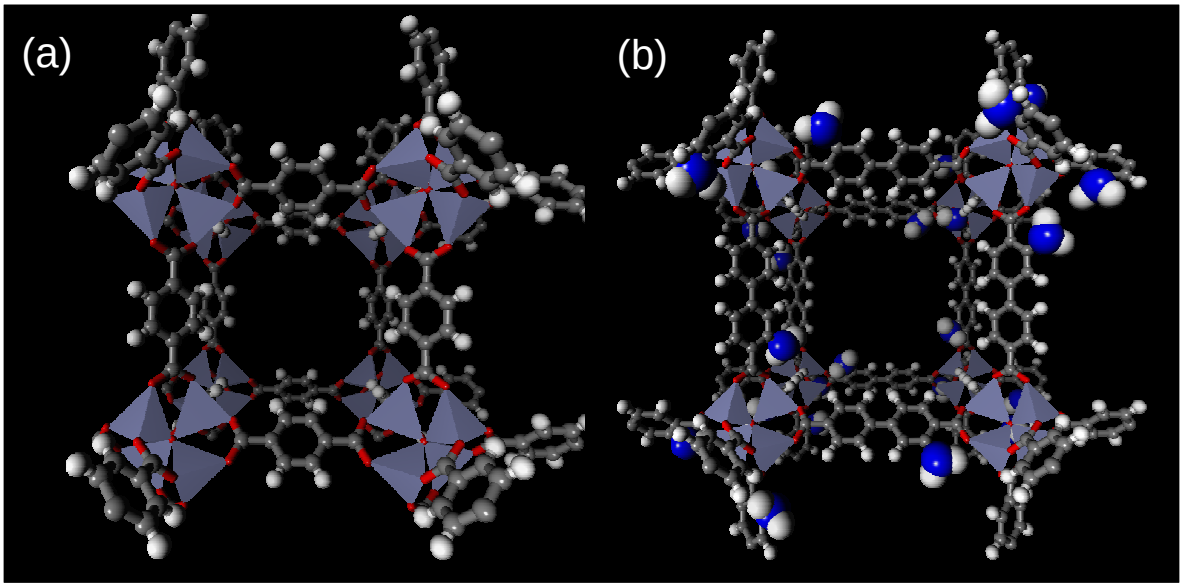

Figure 3.4. MOF-5 framework (a) and IRMOF-10 with NH_2 group at benzene position 2 (b).

By varying systematically the polyfunctional ligands in MOFs, it is possible to maximize the surface area and achieve tailored dimensions of cages and channels. This has resulted in the discovery of about 1000 different MOF structures. [54] Not all of them have stable open structures with sufficiently large pores for commercial applications and some of them are unstable upon removal of the solvent from the pores. Furthermore, there are flexible MOFs that open at a certain pressure, allowing gas molecules to enter their pores.[55] At first, these materials appear to be good candidates for separations when comparing single gas isotherms, the problem is that in mixtures if one component opens the framework all the other components might enter the structure, therefore the selectivity is not as high as considered from the single gas isotherms only.

The first study on MOFs as capture materials were triggered by the discovery of Li et al. [56] in 1998 of an unusually high CO_2 capacity of MOF-2 at 1 atm and -78ºC. Since then, different research groups have focused on finding frameworks with the highest CO_2 adsorption; the peak gravimetric adsorption for CO_2 has been reported in frameworks with high surface area and pore diameter greater than 15A. [55] For instance, Llewelyn et al. [57] observed that MIL frameworks, mil-101 and MIL-100, posses large CO_2 adsorption capacities and high enthalpies of adsorption. Peng et al. [58] using GCMC simulations determined the

selectivity and adsorption capacity of UMCM-1 and UMCM-2 and found materials with large capacities at high pressure, although their selectivities for CO_2 in N_2 and CH_4 are low. They suggest that the materials can be used as storage media.

Research groups have also investigated the use of different organic linkers and metal sites attempting to enhance the framework interactions with CO_2. Comotti et al. [59] found that the electrostatic interactions between CO_2 and Al(OH)(1,4-naphthalene dicarboxylate) provided enhanced capture capacity. CO_2 is excluded from entering the 0.30 nm pores but the interactions with the hydroxyl groups in the 0.77 nm diameter channels gives CO_2 a preferred adsorption over N_2. Dietzel et al. [60] systematically studied the influence of the identity of the metal center on the capture of CO_2 in a series of isostructural networks. The use of Mg as the open metal site had more than double CO_2 uptake than any other metal studied in the series. The authors claim that a coordination mode for CO_2 with the increased ionic character of the Mg_2^+-O interaction accounted for the high adsorption capacity. Salles et al. [61] studied the effects of the organic linker and pore size topology on CO_2 capture. They found that the effects of the surface are and free volume become evident only at high pressures while at low pressures electrostatic interactions might be more significant for high CO_2 uptakes. An et al. [62] synthesized cobalt adenine bio-MOFs and found large capacities at atmospheric pressure. Moreover, they estimated a large CO_2 selectivity over N_2. They claimed that the high capture was due to each cavity in bio-MOF-11 being densely populated with basic amino and pyrimidine groups, which have been reported to have one of the highest CO_2 interaction energy among MOF nitrogen-containing linker molecules. Couck et al. [63] functionalized MIL-53 with amine and observed that the separation factor for CO_2/CH_4 had a 12-fold increase. The incorporated amino groups reduced the number of surface apolar sites resulting in negligible CH_4 adsorption below 2 bar. Farha et al. [64] using a carborane based network with three different preparation conditions produced materials with three different porosities and crystallinity. The authors observed that the morphology of the samples significantly affected CO_2 adsorption. Nagakawa [65] found that the presence of amino groups and exposed metal sites enhanced the selectivity for CO_2 adsorption over N_2 and O_2. Arstad et al. [18] prepared three different MOFs with, and without, amine functionalities inside the pores. At low partial pressure, the highest CO_2 uptakes were obtained with the

functionalized MOFs. The enthalpy of adsorption greatly increased in the functionalized materials. However, they found no evidence of formation of carbonic acid or carbamate due to the separation between amine moieties. Panda et al. [66] synthesized ZTF-1 a three-dimensional amino functionalized framework that has both free tetrazole nitrogen and free -NH_2 functionalities, which have strong interactions with CO_2. They obtained large CO_2 adsorption uptakes at atmospheric pressure. Also, they determined by GCMC that the high capacity at low pressures is caused by the narrow pores and the exposed amine functionality and free tetrazole nitrogen.

In MOFs, computational methods have been used to identify the structure motifs that better suit for carbon capture, reducing material synthesis to only the most promising candidates. Several systematic computational studies investigate the effects of different factors on CO_2 adsorption on MOFs. [67] Yang et al. [68] using GCMC studied the separation of CO_2/H_2 mixtures in three different pairs of MOFs with and without catenation. They found a larger selectivity in the catenated MOFs due to the increased electrostatic interactions. Yazadin et al. [69] using molecular simulations in Cu-BTC predicted that the presence of water molecules increased the CO_2 uptake and selectivity respect to N_2 and CH_4. The water molecules increased the CO_2 adsorption by coordinating to open metal sites in the framework. The simulation predictions were confirmed experimentally by the authors. Babarao et al. [70, 71] studied by GCMC CO_2/CH_4 and CO_2/N_2 mixtures in rho-ZMOF and encountered large CO_2 selectivities due to the electrostatic interaction of CO_2 with the Na^+ ions and the framework. They also found that adding trace amounts of water decreased the selectivity by one order of magnitude. Yang et al. [72] used a combination of experimental measurements and molecular modeling for the adsorption of CO_2/CH_4 on UiO-66(Zr) found that each molecule adsorbs preferentially in two different porosities of the material. They observed that the CO_2 molecule enhances the mobility of the CH_4 molecule decreasing the selectivity of the material. Salles et al. [73] showed using molecular simulations that amine functionalization of IRMOF, increases the heat of adsorption for CO_2. However, functionalization decreases the total capacity due to a lowering of the free volume and the surface area.

3.4.2. Zeolitic Imidazole Frameworks

Zeolitic Imidazole Frameworks constitute a subclasss of MOFs that can adopt zeolite structure types based on the replacement of tetrahedral atoms in the zeolite, such as Si and Al, by transition metal ions, such as Zn and Co, and replacement of the bridging oxygens by imidazolates and benzimidazolates. [74]

There is an increasing interest in the research of ZIFs as potential CO_2 adsorbents, because in contrast to many MOFs, ZIFs have high thermal and chemical stability. Moreover, ZIFs have shown large CO_2 capacities and can separate CO_2 from mixtures with CH_4 and O2. Besides, some ZIFs, such as ZIF-69, have shown high affinity for CO_2 at low pressures. [75] Liu et al. [76] using MD and GCMC developed a force field for this latter material. The authors found that the small pores in those frameworks provided preferential adsorption sites for CO_2.

3.4.3. Microporous organic polymers

Microporous organic polymers are comprised predominantly of light non-metallic elements, such as H, B, C, and O, linked by strong covalent bonds. In general, all organic polymers have certain degree of free volume or porosity. However, only if they organic polymers are composed of rigid molecular linkers they become microporous materials in the dry state. These linkers give the polymers the degree of molecular rigidity necessary to obtain permanent microporosity. The main advantage of MOPs is the diverse kind of materials that can be synthesized. Moreover, there are different polymer post-modification processes that can be applied to introduce MOPs with specific chemical functionalities. [77]

Research on MOPs for CO_2 capture is encouraged by their low density, large surface area and chemical and thermal stability. In general, MOPs are chemically stable; however, some materials with large porosities, such as organic frameworks based on buroxine, have been reported to degrade by exposure to air. [77] Satyapal et al. [78] studied the CO_2 adsorption behavior of a framework of polymethylmethacrylate with PEI functionalization, a material used for CO_2 removal in space shuttle applications. They found that the sorbent is capable of removing low concentrations of CO_2 at room temperature and pressure. The material showed no loss in performance over hundreds of adsorption/desorption cycles. Furukawa and Yaghi

[79] measured the CO_2 capacity of 7 different organic frameworks. They found that COF-102 and COF-103, materials comprised of 3D structure with 1.2 nm pores, have very high CO_2 capture capacities, comparable to the most adsorbing MOFs. Dawson et al. [80] tested a range of MOPs for adsorption of CO_2 and found the highest uptake at 1 bar for the network containing triazole moieties. The authors found that the CO_2 uptake at 1 bar more closely related to the isosteric heat of adsorption than to the adsorbent's surface area. Martin et al. [81] studied a series of hypercrosslinked polymers for CO_2 capture. They claimed that the material was selective towards CO_2 and had a moderate heat of adsorption, which favored desorption.

The molecular blocks that can constitute different MOPs enable systematic studies to search for species with high affinity for CO_2. Choi et al. [82] using ab-initio calculations and GCMC simulations proposed 2 theoretical organic frameworks that have large CO_2 capacities, at high pressures (over 40 bar), much larger than the most adsorbing materials synthesized to date. Babarao et al. [83] by using GCMC simulations discovered a type of MOPs, covalente organic framework (COF) materials, with very large high pressure CO_2 capture. They proposed molecular based structure correlations that can predict the capacity of COFs for CO_2 capture.

In conclusion, building block solids (MOFs, ZIFs and MOPs) are a new kind of adsorbents with great flexibility to the type of functional groups that can include on their structure, which allows systematic designs based on molecular simulations. In comparison with zeolites, building block solids offer a much broader variety of chemical compositions, pore sizes, and surface areas. In contrast, because of organic functionalities, they are less thermally stable and might be less robust for large cyclic operations. Although research on this area has shown progress in synthesizing thermally and chemically stable adsorbents.

3.5. MESOPOROUS SILICA

The term mesoporous silica refers to a family of uniform porous materials first produced by Mobil Corporation. [84, 85] These porous materials are mesoporous silicates and aluminosilicates synthesized using liquid crystal templates. These materials are characterized by high surface areas, narrow pore-size distributions, large void inner volumes and the

possibility of fine-tuning their pore sizes during the synthesis. These remarkable features have attracted numerous research works using mesoporous silica, in particular as adsorbents in gas storage systems and as catalysts supports. [86-88]

The mesoporous materials reviewed in this section are characterized by amorphous walls with long-range ordering. This long-range ordering forms channels ordered in hexagonal (MCM-41, SBA-15), cubic (MCM-48), or laminar (MCM-50) arrays. In spite of their long-range order, their X-ray diffraction patterns consist only of a few diffraction lines at low angles.[54]

In general mesoporous materials, at moderate pressures, posses low adsorption capacities. Hence, there is scarce interest in using pure mesoporous silica for adsorption processes. Nonetheless, their modified or functionalized forms represent an attractive alternative for their application to adsorption. Organic moieties can be incorporated into the pores of silica adsorbents. For instance, amino groups can be grafted to the silica surface and selectively attract CO_2 molecules, as seen in Figure 3.5.

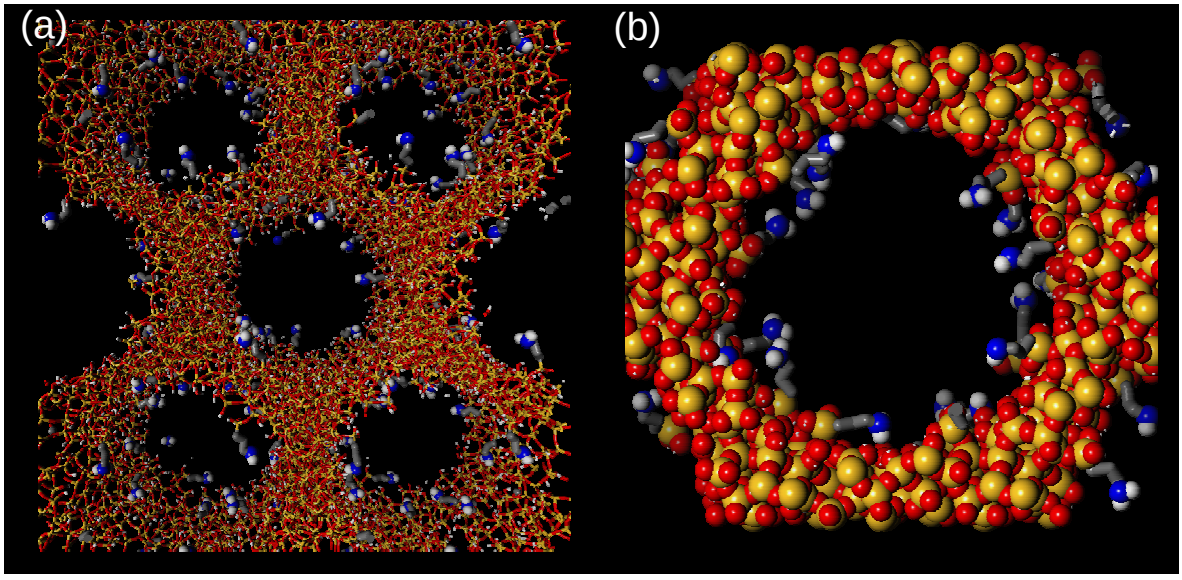

Figure 3.5. Aminopropyl functionalized MCM-41.

It is possible to functionalize mesoporous silica using the reaction of the surface silanol groups with organosilanes to form organic-inorganic hybrid materials. [89] There are two different main ways to link organic groups into silica surfaces: (i) co-condensation and (ii) postsynthesis silylation. In the former method, a fraction of the precursor of the mesoporous silica is

replaced by the organosilane, which is incorporated into the resulting mesoporous material. However, a fraction of the organosilane may get within the walls of the silica producing defects on the lattice. The latter method, postsynthesis, consists on modifying the inner surface of silica with an organic group. The most common way of postsynthesizing is the reaction of organosilanes with the silanol groups in the surface of the silica. As a result, the organic units lie on the surface when using this method, opposed to the co-condensation where they project into the pores. [90, 91] Amine moieties are the most commonly used functionalities added to the mesopores for CO_2 capture. The grafted amines attempt to emulate the traditional use of amines for CO_2 capture while avoiding the large energetic penalty of heating a diluted solution.

A very active area of research in recent years involves experimental studies on the use of postsynthesis amine functionalization of silica surfaces for CO_2 capture. In particular, a number of works have focused on understanding the interactions among CO_2, the functionalized chains and the silica surface. Specifically, 3-aminopropyltriethoxysilane (APTES) is commonly used as the coupling agent for the modification of silica surfaces in these studies. Leal et al. [92] studied the adsorption of CO_2 on silica gel grafted with APTES. They obtained a functionalization of up to 1.27 mmol amine/g and captured 0.6 mmol/g of CO_2 at 23ºC and 1 bar. Huang et al. [93] reported a silica xerogel functionalized with APTES capable of selectively adsorbing CO_2 and H_2S from natural gas streams: the material was completely regenerated by pressure or temperature swing under anhydrous conditions. Knowles et al. [94] observed reversible adsorption of CO_2 on silica gel 40 grafted with APTES, this uptake increased in the presence of water; however the desorption of CO_2 diminished. The authors claim that the extent of functionalization depends on the surface area, the porosity and the concentration of silanol groups on the substrate. Knöfel et al. [95, 96] used in situ FTIR spectroscopy and microcalorimetry to study the reactivity between carbon dioxide and amines functionalized on SBA-16. They proposed that chemisorption was the leading mechanism at low loadings and physisorption was more predominant at higher pressures. Serna-Guerrero et al. [97] grafted the triamine 2-[2-(3-trimethoxysilylpropyl amino) ethylamino] ethylamine on a pore-expanded MCM-41. They reported the presence of significant amounts of carbamate when the adsorption was done in the presence of water.

Bacsik et al. [98] functionalized SBA-1 with APTES using both co-condensation and postsynthesis. The postsynthesized material had a reduction of the pore volume of 81% after functionalization with 1.38 mmol amine/g, whereas the co-condensed material had an increase of 14%, due to the structural changes that resulted from the co-condensation. The authors reported a higher adsorption of CO_2 at 70ºC than at 20ºC for the postsynthesized material.

Although there are numerous experimental studies on the adsorption of CO_2 by amine-functionalized silica, simulation works on this field are still scarce. Chaffee [99] performed a visualization study of the possible grafting sites for aminopropyltrimethoxysilane (APTMS) on a mesoporous silica. The author calculated the geometric constraints for the amine grafting and the interactions that took place on the surface using molecular simulations. The APTMS chains were placed in an orderly fashion at the most energetically favorable grafting sites. Each APTMS molecule replaced two silanol groups on the surface. Schumacher et al. [100] simulated the adsorption of CO_2 on amine or phenyl groups functionalized by co-condensation on MCM-41. Using GCMC they reproduced the co-condensation by considering the organic group to be linked directly to a MCM-41 silicon atom. Using a similar approach, Williams et al.[101] functionalized MCM-41 with a series of different organic groups, studying the effect of different grafted groups on the capture of CO_2.

In summary, amine-functionalization increases the adsorption capabilities of mesoporous adsorbents. Nevertheless, it is important to the nature of the interactions with CO_2 in order to design adsorbents optimized for CO_2 selectivity. This is still subject of research since the grafted amines interact differently from the amines in solution. The potential of functionalized mesoporous silica as CO_2 separating adsorbents is large, since different functionalities can be added to these materials. The resulting materials possess good chemical and mechanical properties to be used in practical adsorption applications.

3.6. CONCLUSIONS

There are a large number of alternatives for the separation of GHGs; this number is expected to increase due to the continuous research on new classes of adsorbents. Among them, the

materials that successfully balance most effectively equipment cost and efficiency will become ready to be implemented.

The materials implemented in capture technologies may encounter severe conditions in system upsets or even during normal operations. Therefore, materials must be robust and resistant to thermal, chemical, and mechanical degradation.

In general adsorbents are a mid term alternative as capture materials for reduction of CO_2. Specially because as put by Ciferno et al. [102] *"It is neither realistic nor economical to try to substitute nonfossil sources of energy all at once, and the fact that new fossil-based power plants will be built in the future, at least within the 2050 time horizon of interest, cannot be ignored"*. The implementation of these technologies will help diminish the emissions caused by the combustion of fossil fuels, until a suitable substitute for power generation is found.

This review focused on materials for CO_2 capture, most of the available research in GHGs capture is focalized on this substance due to the large CO_2 emissions and the recent interest in limiting them. Nonetheless, the research on CO_2 capture has produced a large number of alternative adsorbents and adsorption technologies that are likely to be employed for capture of other GHGs.

In the following chapters, research on promising materials for adsorption and separation of GHGs will be presented. Different families of adsorbents are explored using molecular simulations and their performance as materials for GHG capture is discussed. Chapter 4 focuses on SF_6, a potent greenhouse gas, while chapters 5-6 relate to CO_2 adsorption.

REFERENCES

1. Metz B. *"Climate change 2007 mitigation of climate change : contribution of Working Group III to the Fourth Assessment Report of the Intergovernmental Panel on Climate Change"*. Cambridge; New York: Cambridge University Press; **2007**.

2. Abanades JC. *"The maximum capture efficiency of CO2 using a carbonation/calcination cycle of CaO/CaCO3"*. Chem Eng J. **2002**;90 (3).303-6.

3. Müller CR, Pacciani R, Bohn CD, Scott SA, Dennis JS. *"Investigation of the Enhanced Water Gas Shift Reaction Using Natural and Synthetic Sorbents for the Capture of CO2"*. Ind Eng Chem Res. **2009**;48 (23).10284-91.

4. Mosqueda HA, Vazquez C, Bosch P, Pfeiffer H. *"Chemical Sorption of Carbon Dioxide (CO2) on Lithium Oxide (Li2O)"*. Chem Mater. **2006**;18 (9).2307-10.

5. Kato M, Nakagawa K, Essaki K, Maezawa Y, Takeda S, Kogo R, et al. *"Novel CO2 Absorbents Using Lithium-Containing Oxide"*. Int J Appl Ceram Technol. **2005**;2 (6).467-75.

6. Meis NNAH, Bitter JH, de Jong KP. *"On the Influence and Role of Alkali Metals on Supported and Unsupported Activated Hydrotalcites for CO2 Sorption"*. Ind Eng Chem Res. **2010**;49 (17).8086-93.

7. Lee JM, Min YJ, Lee KB, Jeon SG, Na JG, Ryu HJ. *"Enhancement of CO2 Sorption Uptake on Hydrotalcite by Impregnation with K2CO3"*. Langmuir. **2010**;26 (24).18788-97.

8. Yong Z, Mata, Rodrigues AE. *"Adsorption of Carbon Dioxide onto Hydrotalcite-like Compounds (HTlcs) at High Temperatures"*. Ind Eng Chem Res. **2000**;40 (1).204-9.

9. Clark PD. *"Sulfur and Hydrogen Sulfide Recovery"*. Kirk-Othmer Encyclopedia of Chemical Technology: John Wiley & Sons, Inc.; **2000**. p.

10. Vaidya PD, Kenig EY. *"CO2-Alkanolamine Reaction Kinetics: A Review of Recent Studies"*. Chem Eng Technol. **2007**;30 (11).1467-74.

11. Rivera-Tinoco R, Bouallou C. *"Comparison of absorption rates and absorption capacity of ammonia solvents with MEA and MDEA aqueous blends for CO2 capture"*. Journal of Cleaner Production. **2010**;18 (9).875-80.

12. Thitakamol B, Veawab A. *"Foaming Behavior in CO2 Absorption Process Using Aqueous Solutions of Single and Blended Alkanolamines"*. Ind Eng Chem Res. **2007**;47 (1).216-25.

13. Veltman K, Singh B, Hertwich EG. *"Human and Environmental Impact Assessment of Postcombustion CO2 Capture Focusing on Emissions from Amine-Based Scrubbing Solvents to Air"*. Environ Sci Technol. **2010**;44 (4).1496-502.

14. Freeman SA, Dugas R, Van Wagener DH, Nguyen T, Rochelle GT. *"Carbon dioxide capture with concentrated, aqueous piperazine"*. International Journal of Greenhouse Gas Control. **2010**;4 (2).119-24.

15. Rochelle GT. *"Amine Scrubbing for CO2 Capture"*. Science. **2009**;325 (5948).1652-4.

16. Bishnoi S, Rochelle GT. *"Absorption of carbon dioxide in aqueous piperazine/methyldiethanolamine"*. AIChE J. **2002**;48 (12).2788-99.

17. Jackson P, Beste A, Attalla M. *"Insights into amine-based CO2 capture: an ab initio self-consistent reaction field investigation"*. Struct Chem. **2011**;22 (3).537-49.

18. Arstad B, Fjellvåg H, Kongshaug K, Swang O, Blom R. *"Amine functionalised metal organic frameworks (MOFs) as adsorbents for carbon dioxide"*. Adsorption. **2008**;14 (6).755-62.

19. Goff GS, Rochelle GT. *"Oxidation Inhibitors for Copper and Iron Catalyzed Degradation of Monoethanolamine in CO2 Capture Processes"*. Ind Eng Chem Res. **2005**;45 (8).2513-21.

20. Maneeintr K, Idem RO, Tontiwachwuthikul P, Wee AGH. *"Comparative Mass Transfer Performance Studies of CO2 Absorption into Aqueous Solutions of DEAB and MEA"*. Ind Eng Chem Res. **2010**;49 (6).2857-63.

21. Pellegrini G, Strube R, Manfrida G. *"Comparative study of chemical absorbents in postcombustion CO2 capture"*. Energy. **2010**;35 (2).851-7.

22. Yeh JT, Resnik KP, Rygle K, Pennline HW. *"Semi-batch absorption and regeneration studies for CO2 capture by aqueous ammonia"*. Fuel Process Technol. **2005**;86 (14-15).1533-46.

23. Hedin N, Chen L, Laaksonen A. *"Sorbents for CO2 capture from flue gas-aspects from materials and theoretical chemistry"*. Nanoscale. **2010**;2 (10).1819-41.

24. Baerlocher C, McCusker LB. Database of Zeolite Structures 1996 [07/07/2011]; Available from: http://www.iza-structure.org/databases/.

25. Rees LVC. *"Chapter 9. Ion exchange in zeolites"*. Annual Reports on the Progress of Chemistry, Section A: General Physical and Inorganic Chemistry. **1970**;67 191-212.

26. Maurin G, Bell R, Kuchta B, Poyet T, Llewellyn P. *"Adsorption of Non Polar and Quadrupolar Gases in Siliceous Faujasite: Molecular Simulations and Experiments"*. Adsorption. **2005**;11 (0).331-6.

27. Maurin G, Belmabkhout Y, Pirngruber G, Gaberova L, Llewellyn P. *"CO2 adsorption in LiY and NaY at high temperature: molecular simulations compared to experiments"*. Adsorption. **2007**;13 (5).453-60.

28. Zhang Z, Zhang W, Chen X, Xia Q, Li Z. *"Adsorption of CO2 on Zeolite 13X and Activated Carbon with Higher Surface Area"*. Sep Sci Technol. **2010**;45 (5).710-9.

29. Liu S, Yang X. *"Gibbs ensemble Monte Carlo simulation of supercritical CO2 adsorption on NaA and NaX zeolites"*. J Chem Phys. **2006**;124 (24).244705.

30. Ghoufi A, Gaberova L, Rouquerol J, Vincent D, Llewellyn PL, Maurin G. *"Adsorption of CO2, CH4 and their binary mixture in Faujasite NaY: A combination of molecular simulations with gravimetry-manometry and microcalorimetry measurements"*. Micropor Mesopor Mat. **2009**;119 (1-3).117-28.

31. Cavenati S, Grande CA, Rodrigues AE. *"Adsorption Equilibrium of Methane, Carbon Dioxide, and Nitrogen on Zeolite 13X at High Pressures"*. J Chem Eng Data. **2004**;49 (4).1095-101.

32. Zukal A, Mayerová J, Kubů M. *"Adsorption of Carbon Dioxide on High-Silica Zeolites with Different Framework Topology"*. Top Catal. **2010**;53 (19).1361-6.

33. Krishna R, van Baten JM. *"Using molecular simulations for screening of zeolites for separation of CO2/CH4 mixtures"*. Chem Eng J. **2007**;133 (1-3).121-31.

34. Leyssale J-M, Papadopoulos GK, Theodorou DN. *"Sorption Thermodynamics of CO2, CH4, and Their Mixtures in the ITQ-1 Zeolite as Revealed by Molecular Simulations"*. J Phys Chem B. **2006**;110 (45).22742-53.

35. Harlick PJE, Tezel FH. *"An experimental adsorbent screening study for CO2 removal from N2"*. Micropor Mesopor Mat. **2004**;76 (1-3).71-9.

36. Jia W, Murad S. *"Molecular dynamics simulations of gas separations using faujasite-journal article zeolite membranes"*. J Chem Phys. **2004**;120 (10).4877-85.

37. Jia W, Murad S. *"Separation of gas mixtures using a range of zeolite membranes: A molecular-dynamics study"*. J Chem Phys. **2005**;122 (23).234708.

38. Bezerra D, Oliveira R, Vieira R, Cavalcante C, Azevedo D. *"Adsorption of CO2 on nitrogen-enriched activated carbon and zeolite 13X"*. Adsorption. **2011**;17 (1).235-46.

39. Chatti R, Bansiwal AK, Thote JA, Kumar V, Jadhav P, Lokhande SK, et al. *"Amine loaded zeolites for carbon dioxide capture: Amine loading and adsorption studies"*. Micropor Mesopor Mat. **2009**;121 (1-3).84-9.

40. Su F, Lu C, Kuo S-C, Zeng W. *"Adsorption of CO2 on Amine-Functionalized Y-Type Zeolites"*. Energy Fuels. **2010**;24 (2).1441-8.

41. García-Sánchez A, Ania CO, Parra JB, Dubbeldam D, Vlugt TJH, Krishna R, et al. *"Transferable Force Field for Carbon Dioxide Adsorption in Zeolites"*. J Phys Chem C. **2009**;113 (20).8814-20.

42. Plant DF, Maurin G, Deroche I, Llewellyn PL. *"Investigation of CO2 adsorption in Faujasite systems: Grand Canonical Monte Carlo and molecular dynamics simulations based on a new derived Na+-CO2 force field"*. Micropor Mesopor Mat. **2007**;99 (1-2).70-8.

43. Henning K-D, von Kienle H. *"Carbon, 5. Activated Carbon"*. Ullmann's Encyclopedia of Industrial Chemistry: Wiley-VCH Verlag GmbH & Co. KGaA; **2000**. p.

44. Silvestre-Albero J, Wahby A, Sepulveda-Escribano A, Martinez-Escandell M, Kaneko K, Rodriguez-Reinoso F. *"Ultrahigh CO2 adsorption capacity on carbon molecular sieves at room temperature"*. Chem Commun. **2011**;47 (24).6840-2.

45. Yong Z, Mata VG, Rodrigues AE. *"Adsorption of Carbon Dioxide on Chemically Modified High Surface Area Carbon-Based Adsorbents at High Temperature"*. Adsorption. **2001**;7 (1).41-50.

46. Martín CF, Plaza MG, Pis JJ, Rubiera F, Pevida C, Centeno TA. *"On the limits of CO2 capture capacity of carbons"*. Sep Purif Technol. **2010**;74 (2).225-9.

47. García S, Gil MV, Martín CF, Pis JJ, Rubiera F, Pevida C. *"Breakthrough adsorption study of a commercial activated carbon for pre-combustion CO2 capture"*. Chem Eng J. **2011**;171 (2).549-56.

48. Radosz M, Hu X, Krutkramelis K, Shen Y. *"Flue-Gas Carbon Capture on Carbonaceous Sorbents: Toward a Low-Cost Multifunctional Carbon Filter for "Green" Energy Producers"*. Ind Eng Chem Res. **2008**;47 (10).3783-94.

49. Shafeeyan MS, Daud WMAW, Houshmand A, Shamiri A. *"A review on surface modification of activated carbon for carbon dioxide adsorption"*. J Anal Appl Pyrolysis. **2010**;89 (2).143-51.

50. Sweatman MB, Quirke N. *"Modelling gas mixture adsorption in active carbons"*. Mol Simul. **2005**;31 (9).667-81.

51. Tenney CM, Lastoskie CM. *"Molecular simulation of carbon dioxide adsorption chemically and structurally heterogeneous porous carbons"*. Environ Prog. **2006**;25 (4).343-54.

52. Huang L, Zhang L, Shao Q, Lu L, Lu X, Jiang S, et al. *"Simulations of Binary Mixture Adsorption of Carbon Dioxide and Methane in Carbon Nanotubes: Temperature, Pressure, and Pore Size Effects"*. J Phys Chem C. **2007**;111 (32).11912-20.

53. Palmer JC, Brennan JK, Hurley MM, Balboa A, Gubbins KE. *"Detailed structural models for activated carbons from molecular simulation"*. Carbon. **2009**;47 (12).2904-13.

54. Čejka J, Kubička D. *"Zeolites and Other Micro- and Mesoporous Molecular Sieves"*. Kirk-Othmer Encyclopedia of Chemical Technology: John Wiley & Sons, Inc.; **2000**. p.

55. D'Alessandro DM, Smit B, Long JR. *"Carbon Dioxide Capture: Prospects for New Materials"*. Angew Chem Int Ed. **2010**;49 (35).6058-82.

56. Li H, Eddaoudi M, Groy TL, Yaghi OM. *"Establishing Microporosity in Open Metal−Organic Frameworks: Gas Sorption Isotherms for Zn(BDC) (BDC = 1,4-Benzenedicarboxylate)"*. J Am Chem Soc. **1998**;120 (33).8571-2.

57. Llewellyn PL, Bourrelly S, Serre C, Vimont A, Daturi M, Hamon L, et al. *"High Uptakes of CO2 and CH4 in Mesoporous Metal ▪ Organic Frameworks MIL-100 and MIL-101"*. Langmuir. **2008**;24 (14).7245-50.

58. Peng X, Cheng X, Cao D. *"Computer simulations for the adsorption and separation of CO2/CH4/H2/N2 gases by UMCM-1 and UMCM-2 metal organic frameworks"*. J Mater Chem. **2011**;21 (30).11259-70.

59. Comotti A, Bracco S, Sozzani P, Horike S, Matsuda R, Chen J, et al. *"Nanochannels of Two Distinct Cross-Sections in a Porous Al-Based Coordination Polymer"*. J Am Chem Soc. **2008**;130 (41).13664-72.

60. Dietzel PDC, Besikiotis V, Blom R. *"Application of metal-organic frameworks with coordinatively unsaturated metal sites in storage and separation of methane and carbon dioxide"*. J Mater Chem. **2009**;19 (39).7362-70.

61. Salles F, Ghoufi A, Maurin G, Bell RG, Mellot-Draznieks C, Férey G. *"Molecular Dynamics Simulations of Breathing MOFs: Structural Transformations of MIL-53(Cr) upon Thermal Activation and CO2 Adsorption"*. Angew Chem Int Ed. **2008**;47 (44).8487-91.

62. An J, Geib SJ, Rosi NL. *"High and Selective CO2 Uptake in a Cobalt Adeninate Metal−Organic Framework Exhibiting Pyrimidine- and Amino-Decorated Pores"*. J Am Chem Soc. **2009**;132 (1).38-9.

63. Couck S, Denayer JFM, Baron GV, Rémy T, Gascon J, Kapteijn F. *"An Amine-Functionalized MIL-53 Metal−Organic Framework with Large Separation Power for CO2 and CH4"*. J Am Chem Soc. **2009**;131 (18).6326-7.

64. Farha OK, Spokoyny AM, Mulfort KL, Galli S, Hupp JT, Mirkin CA. *"Gas-Sorption Properties of Cobalt(II)−Carborane-Based Coordination Polymers as a Function of Morphology"*. Small. **2009**;5 (15).1727-31.

65. Nakagawa K, Tanaka D, Horike S, Shimomura S, Higuchi M, Kitagawa S. *"Enhanced selectivity of CO2 from a ternary gas mixture in an interdigitated porous framework"*. Chem Commun. **2010**;46 (24).4258-60.

66. Panda T, Pachfule P, Chen Y, Jiang J, Banerjee R. *"Amino functionalized zeolitic tetrazolate framework (ZTF) with high capacity for storage of carbon dioxide"*. Chem Commun. **2011**;47 (7).2011-3.

67. Düren T, Bae Y-S, Snurr RQ. *"Using molecular simulation to characterise metal-organic frameworks for adsorption applications"*. Chem Soc Rev. **2009**;38 (5).1237-47.

68. Yang Q, Xu Q, Liu B, Zhong C, Berend S. *"Molecular Simulation of CO2/H2 Mixture Separation in Metal-organic Frameworks: Effect of Catenation and Electrostatic Interactions"*. Chin J Chem Eng. **2009**;17 (5).781-90.

69. Yazaydın AOzr, Benin AI, Faheem SA, Jakubczak P, Low JJ, Willis RR, et al. *"Enhanced CO2 Adsorption in Metal-Organic Frameworks via Occupation of Open-Metal Sites by Coordinated Water Molecules"*. Chem Mater. **2009**;21 (8).1425-30.

70. Babarao R, Jiang J. *"Upgrade of natural gas in rho zeolite-like metal-organic framework and effect of water: a computational study"*. Energy & Environmental Science. **2009**;2 (10).1088-93.

71. Babarao R, Jiang J. *"Unprecedentedly High Selective Adsorption of Gas Mixtures in rho Zeolite-like Metal−Organic Framework: A Molecular Simulation Study"*. J Am Chem Soc. **2009**;131 (32).11417-25.

72. Yang Q, Wiersum AD, Jobic H, Guillerm V, Serre C, Llewellyn PL, et al. *"Understanding the Thermodynamic and Kinetic Behavior of the CO2/CH4 Gas Mixture within the Porous Zirconium*

Terephthalate UiO-66(Zr): A Joint Experimental and Modeling Approach". J Phys Chem C. **2011**;115 (28).13768-74.

73. Salles F, Jobic H, Ghoufi A, Llewellyn PL, Serre C, Bourrelly S, et al. *"Transport Diffusivity of CO2 in the Highly Flexible Metal–Organic Framework MIL-53(Cr)"*. Angew Chem Int Ed. **2009**;48 (44).8335-9.

74. D'Alessandro DM, McDonald T. *"Toward carbon dioxide capture using nanoporous materials"*. Pure Appl Chem. **2011**;83 (1).57-66.

75. Phan A, Doonan CJ, Uribe-Romo FJ, Knobler CB, O'Keeffe M, Yaghi OM. *"Synthesis, Structure, and Carbon Dioxide Capture Properties of Zeolitic Imidazolate Frameworks"*. Acc Chem Res. **2009**;43 (1).58-67.

76. Liu D, Zheng C, Yang Q, Zhong C. *"Understanding the Adsorption and Diffusion of Carbon Dioxide in Zeolitic Imidazolate Frameworks: A Molecular Simulation Study"*. J Phys Chem C. **2009**;113 (12).5004-9.

77. Jiang J-X, Cooper A. *"Microporous Organic Polymers: Design, Synthesis, and Function Functional Metal-Organic Frameworks: Gas Storage, Separation and Catalysis"*. Springer Berlin / Heidelberg; **2010**. p. 1-33.

78. Satyapal S, Filburn T, Trela J, Strange J. *"Performance and Properties of a Solid Amine Sorbent for Carbon Dioxide Removal in Space Life Support Applications"*. Energy Fuels. **2001**;15 (2).250-5.

79. Furukawa H, Yaghi OM. *"Storage of Hydrogen, Methane, and Carbon Dioxide in Highly Porous Covalent Organic Frameworks for Clean Energy Applications"*. J Am Chem Soc. **2009**;131 (25).8875-83.

80. Dawson R, Adams DJ, Cooper AI. *"Chemical tuning of CO2 sorption in robust nanoporous organic polymers"*. Chemical Science. **2011**;2 (6).1173-7.

81. Martin CF, Stockel E, Clowes R, Adams DJ, Cooper AI, Pis JJ, et al. *"Hypercrosslinked organic polymer networks as potential adsorbents for pre-combustion CO2 capture"*. J Mater Chem. **2011**;21 (14).5475-83.

82. Choi YJ, Choi JH, Choi KM, Kang JK. *"Covalent organic frameworks for extremely high reversible CO2 uptake capacity: a theoretical approach"*. J Mater Chem. **2011**;21 (4).1073-8.

83. Babarao R, Jiang J. *"Exceptionally high CO2 storage in covalent-organic frameworks: Atomistic simulation study"*. Energy & Environmental Science. **2008**;1 (1).139-43.

84. Beck JS, Vartuli JC, Roth WJ, Leonowicz ME, Kresge CT, Schmitt KD, et al. *"A new family of mesoporous molecular sieves prepared with liquid crystal templates"*. J Am Chem Soc. **1992**;114 (27).10834-43.

85. Kresge CT, Leonowicz ME, Roth WJ, Vartuli JC, Beck JS. *"Ordered mesoporous molecular sieves synthesized by a liquid-crystal template mechanism"*. Nature. **1992**;359 (6397).710-2.

86. Liu B, Wang W, Zhang X. *"A hybrid cylindrical model for characterization of MCM-41 by density functional theory"*. Phys Chem Chem Phys. **2004**;6 (15).3985-90.

87. Maddox MW, Sowers SL, Gubbins KE. *"Molecular simulation of binary mixture adsorption in buckytubes and MCM-41"*. Adsorption. **1996**;2 (1).23-32.

88. Yun J-H, Düren T, Keil FJ, Seaton NA. *"Adsorption of Methane, Ethane, and Their Binary Mixtures on MCM-41: Experimental Evaluation of Methods for the Prediction of Adsorption Equilibrium"*. Langmuir. **2002**;18 (7).2693-701.

89. Hoffmann F, Cornelius M, Morell J, Fröba M. *"Silica-Based Mesoporous Organic–Inorganic Hybrid Materials"*. Angew Chem Int Ed. **2006**;45 (20).3216-51.

90. Fryxell GE. *"The synthesis of functional mesoporous materials"*. Inorg Chem Commun. **2006**;9 (11).1141-50.

91. Hoffmann F, Fröba M. *"Silica-Based Mesoporous Organic–Inorganic Hybrid Materials"*. In: Rurack K, Marínez-Máñez R, editors. The supramolecular chemistry of organic-inorganic hybrid materials: Wiley-VCH; **2006**. p. 5924-48.

92. Leal O, Bolívar C, Ovalles C, García JJ, Espidel Y. *"Reversible adsorption of carbon dioxide on amine surface-bonded silica gel"*. Inorg Chim Acta. **1995**;240 (1-2).183-9.

93. Huang HY, Yang RT, Chinn D, Munson CL. *"Amine-Grafted MCM-48 and Silica Xerogel as Superior Sorbents for Acidic Gas Removal from Natural Gas"*. Ind Eng Chem Res. **2002**;42 (12).2427-33.

94. Knowles GP, Graham JV, Delaney SW, Chaffee AL. *"Aminopropyl-functionalized mesoporous silicas as CO2 adsorbents"*. Fuel Process Technol. **2005**;86 (14-15).1435-48.

95. Knöfel C, Descarpentries J, Benzaouia A, Zelenák V, Mornet S, Llewellyn PL, et al. *"Functionalised micro-/mesoporous silica for the adsorption of carbon dioxide"*. Micropor Mesopor Mat. **2007**;99 (1-2).79-85.

96. Knöfel C, Martin Cl, Hornebecq V, Llewellyn PL. *"Study of Carbon Dioxide Adsorption on Mesoporous Aminopropylsilane-Functionalized Silica and Titania Combining Microcalorimetry and in Situ Infrared Spectroscopy"*. J Phys Chem C. **2009**;113 (52).21726-34.

97. Serna-Guerrero R, Belmabkhout Y, Sayari A. *"Modeling CO2 adsorption on amine-functionalized mesoporous silica: 1. A semi-empirical equilibrium model"*. Chem Eng J. **2010**;161 (1-2).173-81.

98. Bacsik Z, Atluri R, Garcia-Bennett AE, Hedin N. *"Temperature-Induced Uptake of CO2 and Formation of Carbamates in Mesocaged Silica Modified with n-Propylamines"*. Langmuir. **2010**;26 (12).10013-24.

99. Chaffee AL. *"Molecular modeling of HMS hybrid materials for CO2 adsorption"*. Fuel Process Technol. **2005**;86 (14-15).1473-86.

100. Schumacher C, Gonzalez J, Pérez-Mendoza M, Wright PA, Seaton NA. *"Design of Hybrid Organic/Inorganic Adsorbents Based on Periodic Mesoporous Silica"*. Ind Eng Chem Res. **2006**;45 (16).5586-97.

101. Williams JJ, Wiersum AD, Seaton NA, Düren T. *"Effect of Surface Group Functionalization on the CO2/N2 Separation Properties of MCM-41: A Grand-Canonical Monte Carlo Simulation Study"*. J Phys Chem C. **2010**;114 (43).18538-47.

102. Ciferno JP, Marano JJ, Munson RK. *"Technology Integration Challenges"*. Chemical Engineering Progress. **2011**;107 (8).34-44.

Chapter IV

Separation of Sulfur Hexafluoride*

"Nature never undertakes any change unless her interests are served by an increase in entropy."

Max Planck

Emissions of carbon dioxide represent in terms of concentration the majority of the anthropogenic GHG generation. In addition, CO_2 is emitted in large point sources; this makes the design of a large-scale capture scheme of CO_2 the most cost effective way to reduce GHGs. However, apart from CO_2, various manufacturing processes release extremely potent and almost permanent GHGs. These gases, mainly perfluorocarbons and sulfur hexafluoride, are emitted from a broad range of industrial sources and very few natural sources. They are typically emitted in smaller quantities than CO_2; however, there is a pressing need for a strict control of their emissions because they are potent greenhouse gases with extremely long lifetimes.

Sulfur hexafluoride is a non-toxic and non-flammable gas. It is mainly used in gas insulated substations and related equipment in electrical transmission and distribution systems because

*** The results discussed in this chapter were published in "Optimization of the separation of sulfur hexafluoride and nitrogen by selective adsorption using Monte Carlo simulations". AIChE Journal, 57: 962–974. (2011)**

its arc quenching properties and high dielectric strength. In spite of these unique properties, SF_6 is a very potent greenhouse gas (GHG), it has a global warming potential 22000 larger than carbon dioxide's and an estimated atmospheric lifetime of 3200 years. [1, 2] Hence, given their long lasting effects, SF_6 emissions have to be reduced to a minimum.

However, the combination of the arc quenching properties, dielectric strength, and non-toxicity of SF_6 has prevented from finding a suitable substitute gas for insulation of electrical equipment. [3-5] As a result of not finding a suitable SF6 replacement, there have been numerous efforts to reduce the emissions of the facilities using SF_6. [6, 7] The main sources of SF_6 emissions are leakage and release of the gas during maintenance and refill of electric equipment. Therefore, one of the preferred options to diminish SF_6 emissions is mixing it with other gases to reduce the overall amount of SF_6 used. Nitrogen is the preferred gas for use in these mixtures, for two main reasons: first, mixtures of SF_6 and N_2 with a low concentration of SF_6 maintain high dielectric strength, similar to those of pure SF_6; second, nitrogen is a cheap gas naturally present in the atmosphere, which makes the overall process cheaper and environmentally friendlier. [8, 9] However, a mixture of sulfur hexafluoride and nitrogen increases the difficulty of recovering and recycling the SF_6 during the maintenance or reclaiming of older equipment. The presence of N_2 in the gas mixtures makes the separation by liquefaction an unpractical process, since an excessive amount of energy would be wasted in cooling down and pressurizing the mixture to the point of condensation; hence, an alternative process able to effectively separate SF_6 and N_2 is required.

The ideal material for SF_6 separation would be able to separate an inlet stream containing SF_6 and N_2 into two separate streams, the first with almost pure SF_6 (the objective of the recovery) and the second with concentrated nitrogen (to avoid emissions of SF_6). For illustration purposes, a simple scheme of this ideal arrangement is shown in Figure 4.1.

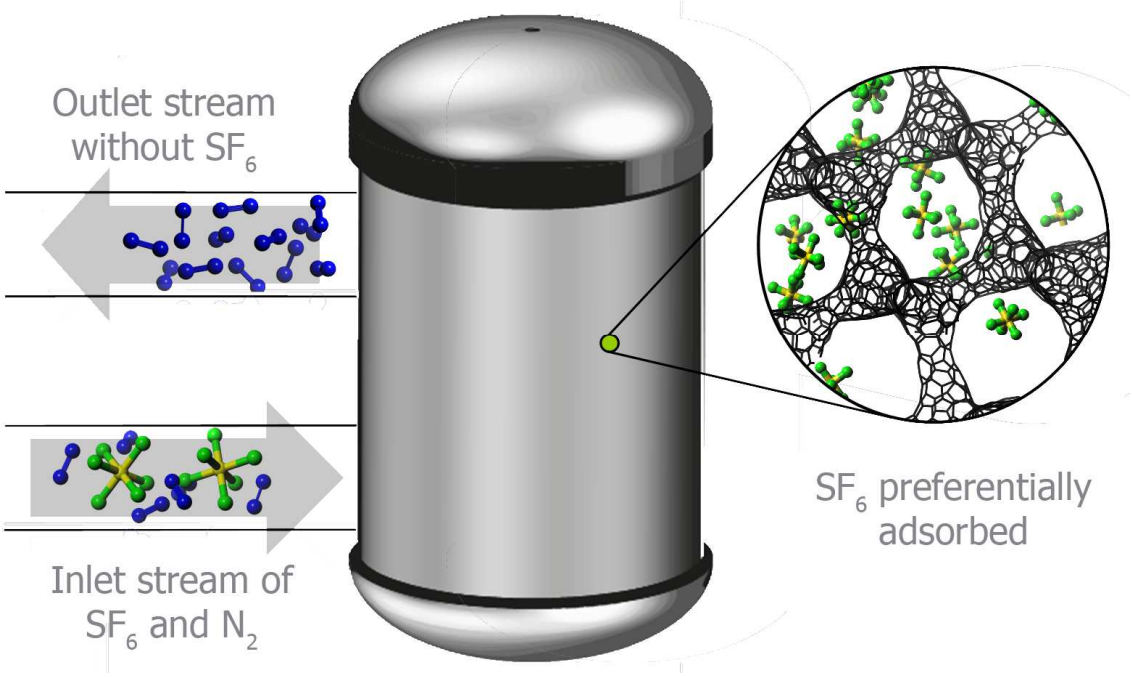

Figure 4.1. Scheme of an ideal system for the separation of SF_6 and N_2.

4.1. PREVIOUS WORKS ON SF_6/N_2 SEPARATION

In the previous chapter, a review of adsorbents focusing on CO_2 separation and capture was presented. The research published on separation of SF_6 is comparatively small, and the adsorbents studied fall into the same categories presented in the preceding chapter. However, for SF_6 most works deal more with the application of existing traditional adsorbents for the separation purposes than on the design of a tailor-made adsorbent for selective separation. In this section we present a review of different materials that have been used for separations of SF_6 from other gases and report the main findings of the works related to separating mixtures of SF_6/N_2.

Previous research dealing with the separation of SF_6/N_2 mixtures, are experimental studies using adsorbents or membranes that achieve separation either by molecularly sieving the N_2 or by preferentially adsorbing the SF_6 at low pressures. For instance, Toyoda et al. [10] used the molecular sieving effect of a Ca-A type zeolite with an effective diameter of 0.5 nm to adsorb N_2 but not SF_6. Yamamoto and co-workers [9] proposed a system of polyimide membranes and analyzed the influence of different operating variables, such as the gas feeding pressure

and the membrane temperature, on the gaseous mixture separation. Murase et al. [11] selectively adsorbed SF_6 from a mixture with nitrogen by using a Na-X type zeolite with a nominal pore diameter of 1.0 nm. They proposed that the filter, besides separating, could be used as a temporary storage medium. Shiojiri et al. [12] separated F-gases from gaseous mixtures containing N_2 by making use of the differences in surface diffusion, using a porous Vycor glass membrane. Inami et al. [8] studied the theoretical limit for SF_6/N_2 separation by liquefaction, and found that the liquid SF_6 recovery efficiency decreased greatly at higher N_2 content. The authors discussed that for SF_6 contents below 10%, even at a temperature below -50 °C, the SF_6 recovery was almost zero. Dagan et al. [13] reported a carbon molecular sieve membrane for the separation of SF_6 from N_2. They claimed that the high flux and selectivity due to the large differences in molecular sizes of SF_6 (0.502 nm) and N_2 (0.306 nm) enabled the design of a single stage separation system with over 99% recovery.

More recently, a few works using non-traditional adsorbents have been published. Ridell et al. [14] used self-assembled metal organic capsules in water solution, which strongly binded and increased the solubility of SF_6. The authors claimed that the solution had no affinity for N_2, which, in principle, would enable separation of SF_6 from a mixture with N_2. Cha et al. [15] studied the separation of SF_6 from N_2 using gas hydrates formation. They found that SF_6 could be recovered forming solid hydrates enriched with SF_6; however, depending on the initial composition of the mixture, several cycles may be required for obtaining high purity SF_6. Wolińska-Grabczyk et al. [16] studied the permeation of SF_6 and N_2 mixtures in poly(4-methyl-1-pentene), a crystalline membrane with small diffusion rates for molecules larger than 0.4 nm. The authors reported selectivities similar to those obtained by Yamamoto et al. by using a single stage process, instead of a two-stage one.

This summary shows that, similarly to CO_2, different types of materials can be used to separate SF_6. Nevertheless, there are no studies on the optimal interaction topologies or compounds for the selective separation of SF_6; there has been no attempt to study systematically a number of adsorbents for the adsorption of mixtures of SF_6 and N_2. Since experimental studies are labor intensive and can only focus on a small number of alternatives,

here we use molecular simulations to explore a large number of possible adsorbents in a systematic manner.

4.2. MOLECULAR SIMULATIONS OF SF_6/N_2 SEPARATION

In this chapter, we used GCMC to study systematically the separation conditions of a SF_6 and N_2 mixture. To the best of our knowledge, there are no published works focusing on simulations of SF_6 and N_2 mixtures separation. The objective of this work was twofold:

(1) To use molecular simulations, with simple models for the fluid and the adsorbent, as a quick scan of the optimal conditions for the separation of SF_6 from N_2.

(2) To check the validity of the results obtained with simple models by using more realistic materials, aiming to find an optimized material to separate the mixture.

In the present work, a complementary view to the usual optimization process is given: we used molecular simulations to illustrate an optimization procedure for the separation of SF_6 and N_2 by modifying operating variables, mainly the bulk pressure and mixture composition, and atomistic level parameters, essentially the pore diameter, of the solid material. The final objective was to find the optimal pore diameter to achieve the separation by adsorption of SF_6 from a SF_6/N_2 stream.

It is shown how molecular simulations can be used as a tool to optimize and design separation processes by using their predictive capabilities in a fast and reliable manner. First, a simple model of MCM-41 was used. Its hexagonal array of monodisperse pores were considerered independent smooth cylinders with a unique pore size. This material was chosen for two main reasons: (i) a simple pore geometry with almost cylindrical pores (straightforward to be modeled with simple simulation force fields) and (ii) it can be synthesized with narrow tunable pore size distributions from the microporous to the mesoporous range. [17-19] Pore size tunability makes this kind of materials a good model for investigating fundamental features of adsorption such as the effects of pore size for a given geometry, and as a starting point to achieve a systematical optimization.

Furthermore, the ideal smooth cylindrical pore was chosen for its instructive value. Although a cylindrical pore is an overly simplistic model of real pores, it provides a useful estimate of the effects of confinement on selectivity. This sort of fundamental study may provide guidelines in choosing materials with the appropriate pore size for gas separation applications. [20] Throughout the first part of this chapter, we employed a simple smooth cylindrical pore that represents MCM-41. We used this model to find the optimal diameter for a maximum SF_6 selectivity. Then, in the second part of this chapter, simulations were later performed with more realistic materials, using atomistic models of zeolite-templated carbon materials (ZTC), chosen to assess the predictability of the results obtained with the cylindrical pore model for the optimal diameter.

4.3. SIMULATION MODELS OF SF_6 AND N_2 MOLECULES

Two different sets of models were used for both SF_6 and N_2. The first one consisted of simple 1-site LJ models, which represent the fluid molecules by spheres with van der Waals type attractive and repulsive interactions. This set of models was only used for the initial stage of the optimization procedure. Although predictions from these models are usually less accurate than those of more refined force fields, they require less computational resources and provide a first good approximation for the optimal separation conditions. This set of models was used to run a series of adsorption isotherms with a broad range of pore diameters and a small separation step between each diameter. The results obtained from the 1-site model were further refined by using a second set of models, in which, to obtain better predictions, more degrees of freedom were added to the molecular structure.

Several LJ parameters for 1-site SF_6 and N_2 models are available in the literature. [21, 22] Some of them have been adjusted to predict the vapor-liquid coexistence region, while others are more accurate for the estimation of transport properties. In this work, the parameters for the LJ potential for both molecules were obtained by adjusting the experimental vapor-liquid equilibrium densities using the reference term of the soft-SAFT EoS, which is a LJ spherical fluid. [23, 24] The advantage of using this procedure is that the soft-SAFT is very accurate for

these fluids, and in addition, it provides a straightforward relationship between the pressure and the chemical potential, needed for the adsorption isotherms.

In the multisite models, the SF_6 molecule is represented by different interacting sites. This model includes the flexibility of he molecules, thus the changes in intramolecular energy have to be taken into account in the energy calculations. The flexible force field proposed by Olivet and Vega [25] was used to represent SF_6. In this model, explicit interactions are only considered to occur among fluorine atoms, and the interactions involving sulfur atoms are neglected on the assumption that a modified fluorine-fluorine LJ potential incorporates any sulfur-sulfur or sulfur-fluorine interactions. To account for the flexibility of the molecule, this model uses six harmonic stretching terms for the S-F bonds and twelve harmonic bending terms for the F-S-F angular deformations. The values of the parameters for the flexible part of this potential are θ_0 = 90°, k_θ= 307.36 kJ/(mol rad), r_0=0.1565 nm and k_r= 693.48 kJ/mol. This force field was obtained by simultaneously fitting selected vapor-liquid equilibrium (VLE) and transport properties to experimental data and it has proven to give accurate results for transport properties of SF_6/N_2 mixtures. [26] The LJ parameters of this SF6 model are given in Table 4.1.

Table 4.1. Lennard-Jones Parameters for the simulated force fields.

Force Field	σ_{ii} (nm)	ε_{ii}/k_B (K)
1-site SF_6	0.4650	251.10
Multisite flexible SF_6 (six F)	0.2769	73.13
1-site N_2	0.3582	98.83
Multisite N_2 (2 N)	0.3310	93.98

The diatomic N_2 molecule was reproduced using the model proposed by Galassi and Tildesley. [27] This force field uses a rigid dumbbell representation of N_2 molecules, with a distance between the nitrogen atoms of 0.1089 nm, and the intermolecular interactions are quantified by a LJ potential. The parameters of this potential were obtained by fitting experimental VLE data. The LJ parameters of this model are given in Table 4.1.

4.4. OPTIMAL SEPARATION DIAMETER USING A CYLINDRICAL SMOOTH PORE

MCM-41 is synthesized using template assisted synthetic routes. The resulting material is made up of a hexagonal array of relatively straight cylindrical unidirectional and non-interconnected pores. It may reach exceptional porosities, up to 80%, making it an excellent potential adsorbent material to be used in gas storage systems, separation processes, and catalysis. [28-30] The pore diameter of MCM-41 can be tuned within the mesoporous range (2.0-10.0 nm). Moreover by controlling the synthesis conditions, recent techniques have allowed the synthesis of silica materials in the pore range 1.0-2.0 nm. [19, 31, 32] In this chapter, MCM-41 is considered as a cylindrical smooth pore that can be obtained with diameters ranging from 1.0 – 4.0 nm.

4.4.1. MCM-41 model

MCM-41 is represented by a simple cylindrical model using the potential form given by Tjatjopoulos. [33] This model, given by Equation 4.1, assumes that the regular hexagonal surface of MCM-41 can be represented by a cylindrical homogeneous surface, in which the interaction sites are continuously distributed on a sequence of concentric surfaces that compose the pore wall.

$$U_{wall}(r,R) = \pi^2 \rho_s \varepsilon_{sf} \left[\frac{63}{32}\left[\frac{r}{\sigma_{SF}}\left(2-\frac{r}{R}\right)\right]^{-10} F\left[-\frac{9}{2};-\frac{9}{2};1;\left(1-\frac{r}{R}\right)^2\right] - 3\left[\frac{r}{\sigma_{SF}}\left(2-\frac{r}{R}\right)\right]^{-4} F\left[-\frac{3}{2};-\frac{3}{2};1;\left(1-\frac{r}{R}\right)^2\right] \right] \quad (4.1)$$

The variables R and r represent, respectively, the effective radius of the cylindrical pore and the distance between the interaction points of the fluid and the wall. The function *F[]* denotes the hypergeometric series. ρ_s is the effective surface density of the oxygen atoms of the pore wall (the silica atoms are considered embedded by the potential of the oxygen atoms). The values for the solid parameters used in this work were taken from Ravikovitch et al., ρ_S = 15.3 nm-2, ε_S/k_B = 193.1 K and σ_S = 0.2725 nm. [34]

Previous works have reported using this potential for representing the adsorption isotherms on MCM-41 obtaining good predictions of the adsorption isotherms as compared to experimental systems. [34-39]

The simple surface potential of Tjatjopoulos et al. is considered an appropriate choice to show the suitability of molecular simulations for process design. The use of this potential for the solid surface avoids additional complexity in the simulated system and saves computational time.

4.4.2. Simulation details for the smooth pore model

The simulations were performed using GCMC simulations. Details on the GCMC simulation procedure are given in chapter 2, retaining here just the details concerning the implementation for the particular system of interest and the different parameters used in the simulations:

- A simulation cell consisting of a cylinder with a diameter ranging from 1.0 to 4.0 nm and a fixed length of 10.0 nm.
- A cutoff radius of at least 6 times the collision diameter of the fluid molecules (σ_{LJ}). [40]
- $1.5x10^5$ MC steps for equilibrating the system and $2.0x10^6$ MC steps for data collection.
- An equal a priori probability to displace, insert or remove a molecule in each simulation step.
- Periodic boundary conditions in the *z*-direction.

The parameters ε_{ij} and σ_{ij} were calculated from their homoatomic pairs according to the Lorentz Berthelot combining rules.

The chemical potential was related to the pressure and the composition in the reservoir by the soft-SAFT EoS, fitted to simulation data. For consistency, we fitted the VLE diagrams of each model using the soft-SAFT equation, obtaining slightly different parameters depending on the models; these tuned parameters were used to calculate the chemical potential at different

pressures. Although we have used soft-SAFT for this purpose, any other accurate equation of state for these two fluids could be used to relate the pressure to the chemical potential. The soft-SAFT parameters (the LJ parameters and the chain length m) obtained by fitting the VLE data for the different models are reported in Table 4.2.

Table 4.2. The soft-SAFT parameters of the models used for the fugacity calculations.

Force Field	σ(nm)	ε/k_B(K)	m
1-site SF_6	0.4650	251.10	1.000
Multisite flexible SF_6	0.3918	200.40	1.654
1-site N_2	0.3582	98.83	1.000
Multisite N_2	0.3193	84.84	1.419

The simulation conditions were chosen to mimic the experimental conditions at which this separation takes place. For the thermodynamic conditions, we used the following values:

- The compositions for the fluid in the reservoir comprised a series of values from pure SF_6 to pure N_2, in terms of SF_6 mole fractions 0.00, 0.10, 0.25, 0.50, 0.75, 0.90 and 1.00.
- The pressure in the reservoir ranged from 50 to 2000 kPa, we chose this maximum value of pressure, close to the saturation pressure of pure SF_6, in order to compare the advantages of using adsorption over conventional liquefaction.
- The temperature of the reservoir was fixed at 300 K to simulate adsorption at room temperature.

4.4.3. Simulation results using the ideal pore model

We present next the most relevant results divided in two parts: first, the separation of SF_6 from N_2 using MCM-41 considering 1-site models for the fluid and a wide range of pore diameters, pressures, and compositions. Second, the separation of the same mixture in the same material at the optimal conditions found in the first case, but considering multisite models for the fluids.

- Separation considering one-site models for the fluids:

We present next the adsorption isotherms and the selectivity of MCM-41 for SF_6 and N_2, modeled as 1-site LJ spheres, using a range of pore diameters from 1.0 nm to 4.0 nm.

The excess adsorption isotherms for SF_6 at different pore sizes and compositions of the reservoir are shown in Figure 4.2. The plots show the change in the adsorption behavior going from a diluted gas mixture, 0.1 mole fraction of SF_6 to pure SF_6. Since we are interested on comparing the feasibility of separating the SF_6/N_2 mixture, the isotherms are shown in terms of the total pressure instead of SF_6 partial pressure.

Two important characteristics of the adsorption behavior can be extracted from the SF_6 adsorption isotherms. (i) First, there is an inflection point at a pore diameter of 2.0 nm: the effect of the composition on the adsorption of SF_6 behaves differently above and below this size. For pore diameters smaller than 2.0 nm, i.e. micropores, the amount of SF_6 adsorbed is a weak function of the composition. Even for low SF_6 mole fractions, its behavior is similar to pure SF_6. For mesopores, the fluid-solid interactions weaken when the loading increases and more molecules are forced to remain in the center of the pore, where the attraction due to the walls is smaller. [41] (ii) The second characteristic is that at 2000 kPa, for all the diameters studied, the adsorbent with pure SF_6 saturates, see Figure 4.2 at X_{SF6}=1.00. Hence, the point of maximum adsorption, which is an indication of the capacity of the solid material, is reached at relatively low pressures.

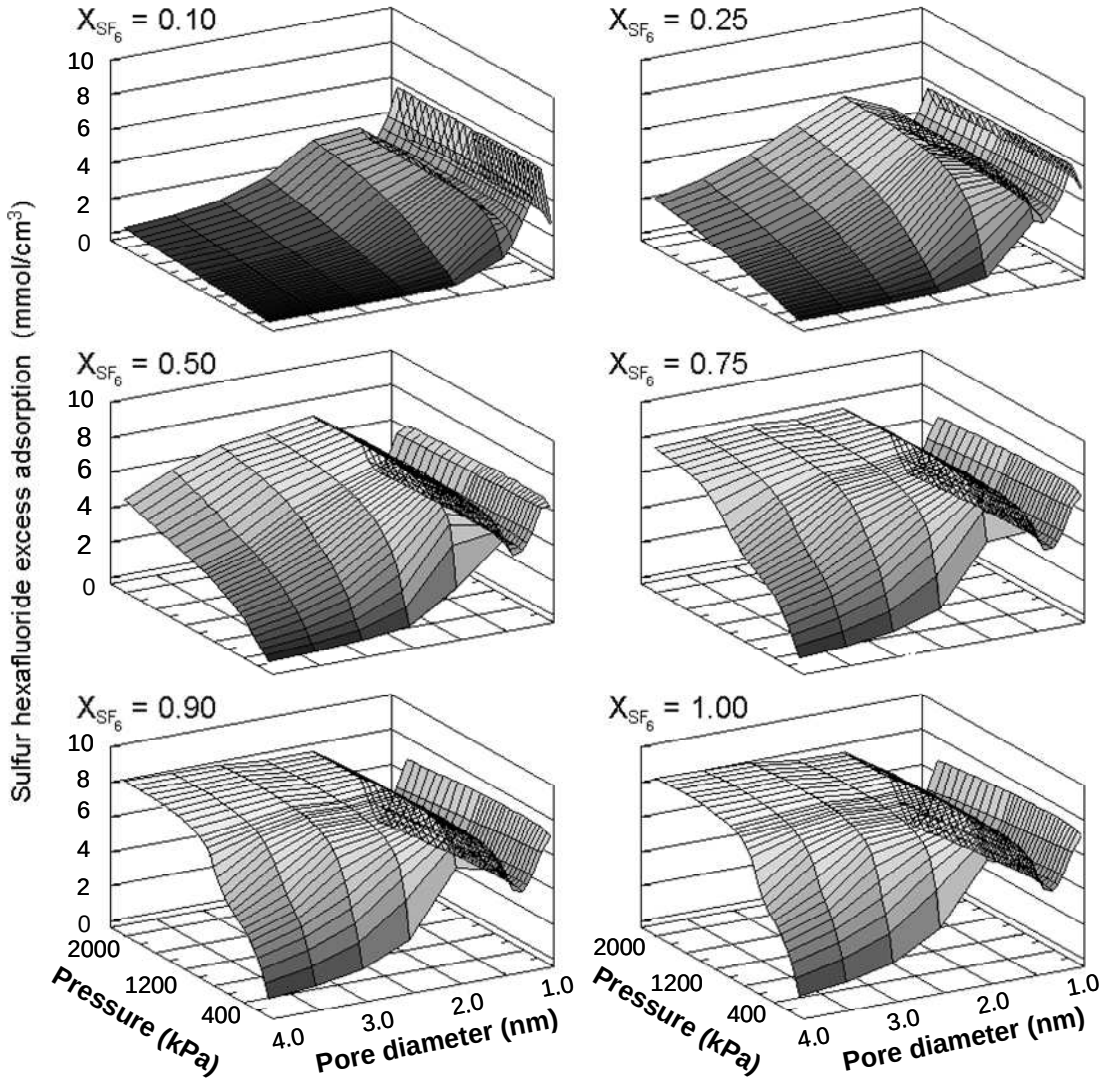

Figure 4.2. SF_6 excess adsorption isotherms for mixtures of SF_6 and N_2 using a 1-site model. See text for details.

The 1-site model for SF_6 predicts that the fluid-wall interactions are very strong and the pores fill up quickly. This is seen for SF_6 mole fractions above 0.75, at high contents of SF_6, the systems behave almost as if they were pure SF_6. This is a typical behavior for the larger molecule during adsorption of binary mixtures; at the lowest relative pressures, the larger molecule is strongly attracted to the wall and saturates the pore faster than the smaller one. [42, 43]

Since we are working with binary systems, it is important to understand not only the adsorption isotherms of SF_6, but also those of N_2. The excess adsorption isotherms for N_2 at different pore sizes and initial bulk compositions are depicted in Figure 4.3. The adsorption isotherms of N_2 show a strong influence of the composition on the adsorbed amount, this might be due to the SF_6 molecules being more attracted towards the wall and blocking the space for N_2 adsorption.

For mesopores, the adsorption of N_2 is very low for the pressure range analyzed, even for pure N_2. In general, for pure N_2, the uptake increases with decreasing pore diameter.

For a pore size of 1.0 nm, N_2 is strongly adsorbed, due to the confinement, when the mole fraction of SF_6 is small. Once SF_6 concentration starts to increase, the adsorbed amount of N_2 diminishes abruptly. This sudden decline of N_2 adsorption is due to the larger SF_6 molecule entering the pore occupying almost all the free space, obstructing the N_2 adsorption.

The general decrease of N_2 adsorption with increasing content of SF_6 is weaker for larger pore diameters, e.g. for a diameter of 4.0 nm the adsorbed amount of N_2 with 0.25 mole fraction of SF_6 is higher than it is for pure N_2. This might be because the adsorbed SF_6 molecules near the solid wall facilitate the adsorption of N_2.

A local adsorption minima is observed for the isotherms with presence of SF_6 for a diameter of 1.1 nm. This effect is not observed for pure N_2, meaning that SF_6 obstructs the adsorption of N_2 molecules.

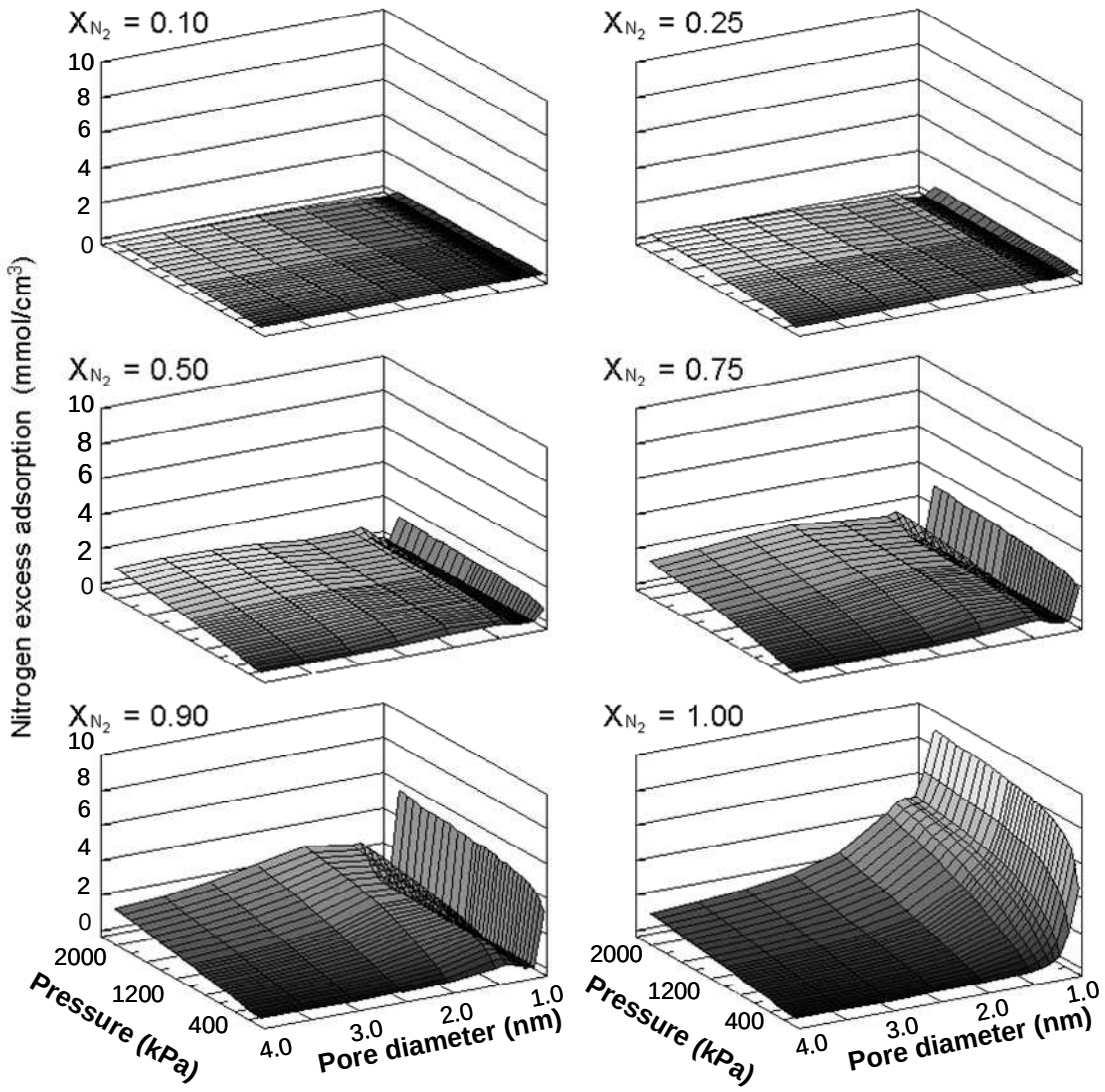

Figure 4.3. N_2 excess adsorption isotherms for mixtures of SF_6 and N_2 using a 1-site model. See text for details.

One of the advantages of using molecular simulations for generating adsorption isotherms is the additional microscopic information provided by them.

It is possible to take snapshots of specific configurations after equilibration of the simulation and explain the observed minimum observed at 1.1 nm. Figure 4.4 shows the SF_6 and N_2 molecules inside the cylindrical pore for different pore diameters. The snapshot in Figure 4.4b shows that the exclusion of N_2 in the 1.1 nm pore is due to optimal occupancy of the SF_6 molecules, they accommodated in an alternating fashion leaving almost no free

volume for the adsorption of N_2. At smaller pore diameters (see Figure 4.4a), SF_6 molecules are forced to accommodate in a straight line and N_2 molecules have enough room to adsorb around them. For pore diameters larger than 1.1 nm (see Figures 4.4c-d), SF_6 molecules are distributed in a similar alternating way, however the larger pore sizes have enough free space to allow the adsorption of N_2.

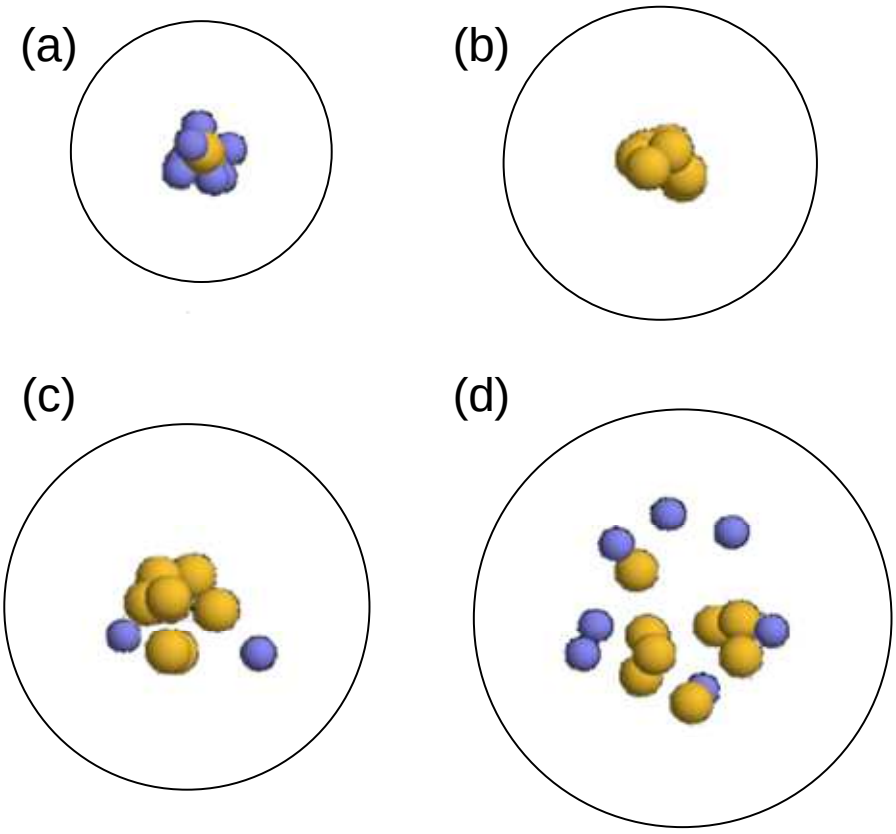

Figure 4.4. Snapshots of adsorbed SF_6 and N_2 at different pore sizes for mixtures with a molar fraction of SF_6 of 0.10. Pore diameters (a) 1.0 nm, (b) 1.1 nm, (c) 1.2 nm, and (d) 1.3 nm. SF_6 is represented in yellow and N_2 is represented in blue.

For a pore diameter of 1.1 nm the space available and the distribution of the SF_6 molecules is such that the N_2 is almost completely excluded from the pore. This counterintuitive pore size exclusion of the smaller molecule allows an adsorbent to capture the larger size molecule while leaving out the smaller one. The first report of this phenomena was predicted by Sommers et al. [44] for two spherical particles of different sizes in slit pores. This effect is more pronounced due to the LJ spheres used for the fluid force fields, because

spheres are invariant to rotations the smaller molecule is not able to fit in the small vacancies unless the whole sphere fits in the voids.

Furthermore, Figure 4.3 shows that for SF_6 mole fractions above 50% the amount of N_2 adsorbed is very small, thus, as pointed out by Inami et al. [8], it is a simple task to separate an enriched mixture of SF_6 with N_2; they claimed that an enriched SF_6/N_2 mixture could be separated by compressing and cooling the gas. The advantage of using adsorption over liquefaction is that the difficulty of recovering SF_6 from diluted mixtures is overcome, once the proper diameter for effective separation is found.

At higher pressures, N_2 starts to adsorb in the pore and begins to displace SF_6, compared to the adsorption of pure SF_6. This effect of competitive adsorption has been observed in other binary mixtures, such as mixtures of CO_2 and N_2 in MOFs, where CO_2 is preferentially adsorbed at low pressures but it is displaced by N_2 at higher pressures. [45] For instance, for a SF_6 mole fraction of 0.1, the amount of SF_6 adsorbed at a pore diameter of 1.5 nm reaches a plateau before 1000 kPa and further increasing the pressure only increases the adsorbed amount of N_2. This competitive behavior is due to the non-ideal behavior of SF_6 at higher pressures, as at these conditions the fugacity of SF_6 starts to deviate from the ideal behavior, while N_2 acts almost as an ideal gas. The fugacity of SF_6 does not increase as steeply with pressure as it does for N_2. For GCMC simulations, this means that it is increasingly easier to adsorb N_2 molecules because the acceptance rule for the creation of new molecules directly depends on the fugacity. [46] The main effect of this competitive behavior is that the SF_6 selectivity decreases with pressure.

The selectivity in a mixture is defined as the preference of one substance over the others to stay in a given phase. For separation processes, it is desirable to have a high selectivity of the substance to be separated. In adsorption, the selectivity is referred to the adsorbed phase. For instance, for a mixture of SF_6 and N_2 in a given adsorbent the SF_6 selectivity is defined as:

$$S_{SF_6-N_2} = \frac{x_{SF_6} / x_{N_2}}{y_{SF_6} / y_{N_2}} \quad (4.2)$$

S_{SF6-N2} is the selectivity of SF_6 over N_2; x_{SF6} and x_{N2} are the mole fractions of the two components on the adsorbent surface; y_{SF6} and y_{N2} are the corresponding mole fractions in the bulk. Values of S_{SF6-N2} larger than one mean that SF_6 is preferentially adsorbed over N_2. It has been stated previously that simulations are useful for estimating the general trend of the selectivity, but its value cannot be accurately assessed solely from molecular simulations, since small deviations in the number of molecules might result in large changes in selectivity. [47]

Since there is a complete exclusion of the N_2 molecules for a pore diameter of 1.1 nm, S_{SF6-N2} tends to infinity. In addition, the adsorption capacity for that pore diameter is among the highest for the pressure range analyzed. Two of the most important characteristics for evaluating an adsorbent for separation are selectivity and capacity. Therefore, from this initial exploration, the material with a pore diameter of 1.1 nm seems to be an ideal adsorbent for separating mixtures of SF_6 and N_2. Moreover, we have further investigated this "super selectivity" using refined force fields for the fluids, which take into account details of the molecular structure of the fluid molecules. The results of these new simulations are presented in the next subsection.

- Separation considering multisite models for the fluids:

Once a throughout study with the optimal conditions for separation was completed with simple models, additional simulations using multisite models were carried out to confirm the results and to test the reliability of 1-site models for process optimization. Given the results obtained for the 1-site model, the pore diameters close to 1.1 nm are examined in detail.

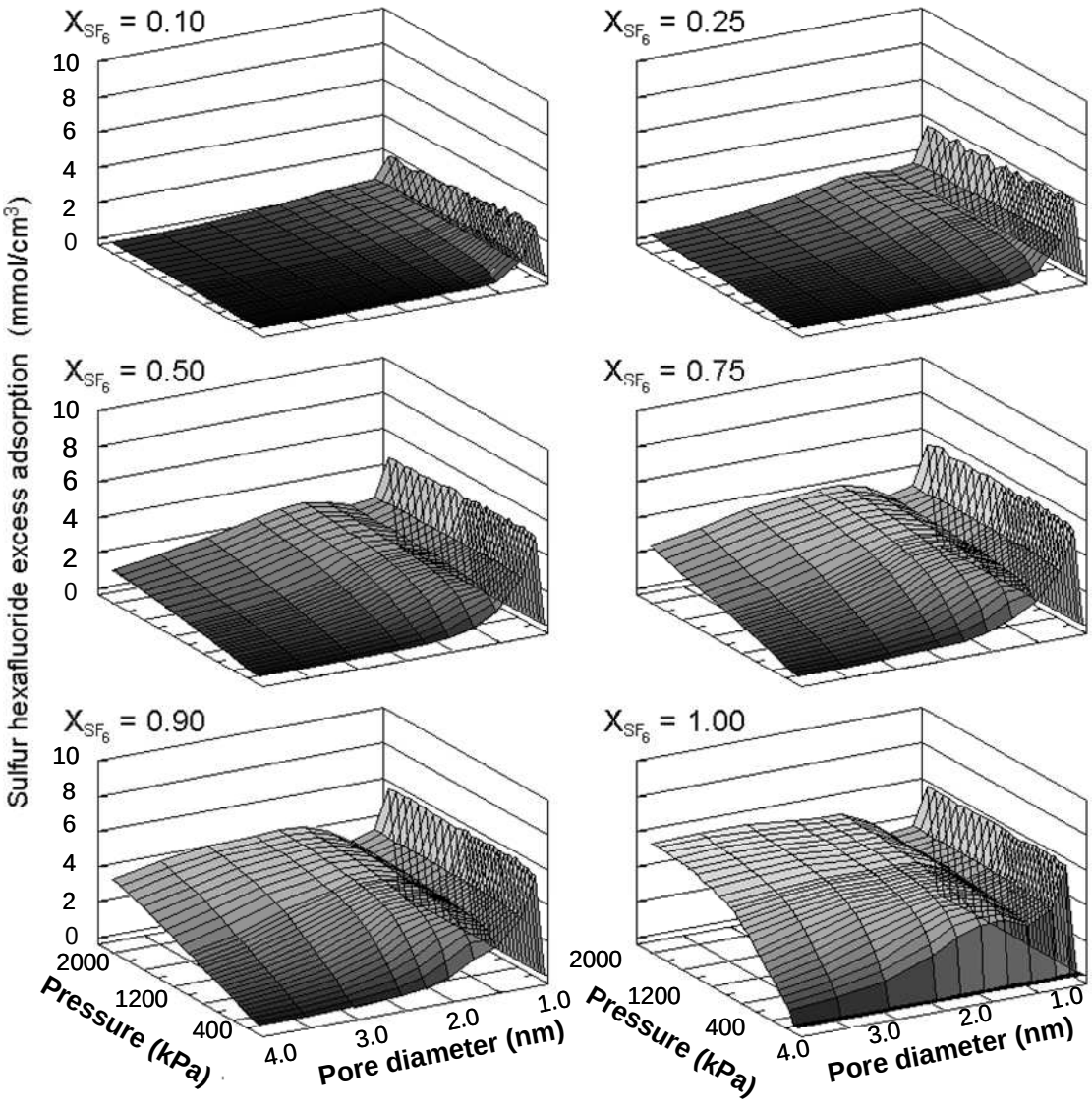

Figure 4.5. SF_6 excess adsorption isotherms for mixtures of SF_6 and N_2 using multisite models for the fluids. See text for details.

The aforementioned multisite models have additional degrees of freedom with respect to the 1-site models. The former can change orientation and, in the case of flexible models, their bonds and angles can vibrate. Although SF_6, a highly symmetric molecule, can be accurately represented by a spherical model, N_2 is a linear molecule; several works in the literature discuss the problems in interpretation and predictions resulting of using a spherical model for a linear molecule. [48, 49] The change of a spherical model to a linear one, has a significant effect on the adsorption behavior of pure components, specially at

pore diameters where the adsorption begins its transition from monolayer to multilayer. [48] In the previous section the 1-site models predicted an optimal adsorption diameter of 1.1 nm, which lies within this transition range. [50] It is important to confirm these results by using atomistic fluid models. It is expected that the results differ from those obtained with the 1-site spherical LJ models mainly because of the nature of N_2, but also because of the additional details introduced for the SF_6 molecule.

The adsorbed amount of SF_6 predicted by the multisite models is depicted in Figure 4.5. The most noticeable characteristic of these plots, compared to Figure 4.2, is the lack of adsorption of SF_6 at 1.0 nm; SF_6 molecules of the multisite model cannot access to the 1.0 nm pores. This behavior was also observed in the 1-site models for a pore diameter of 0.95 nm (not plotted).

The maximum capacity, for the pressure range studied, is reached for a pore diameter of 2.0 nm, as observed for the 1-site model; however, the total SF_6 uptake is different, it is smaller for the multisite than for the 1-site model, specially at low SF_6 mole fractions. In addition, the slope of the SF_6 uptake as a function of pressure is another important difference between the two sets. The 1-site model has a steeper slope than the multisite one, due to the differences in the geometry of the molecules.

As expected, the largest differences with the spherical model are observed for the N_2 isotherms using the multisite model depicted in Figure 4.6. The adsorption of N_2 molecules with the multisite model is not affected by the presence of SF_6 molecules as strongly as it was for the 1-site model. Therefore, the decrease in the adsorption of N_2 in presence of SF_6 is less pronounced. Additional insights into this effect can be inferred by looking at the equilibrated configurations, shown on Figure 4.7.

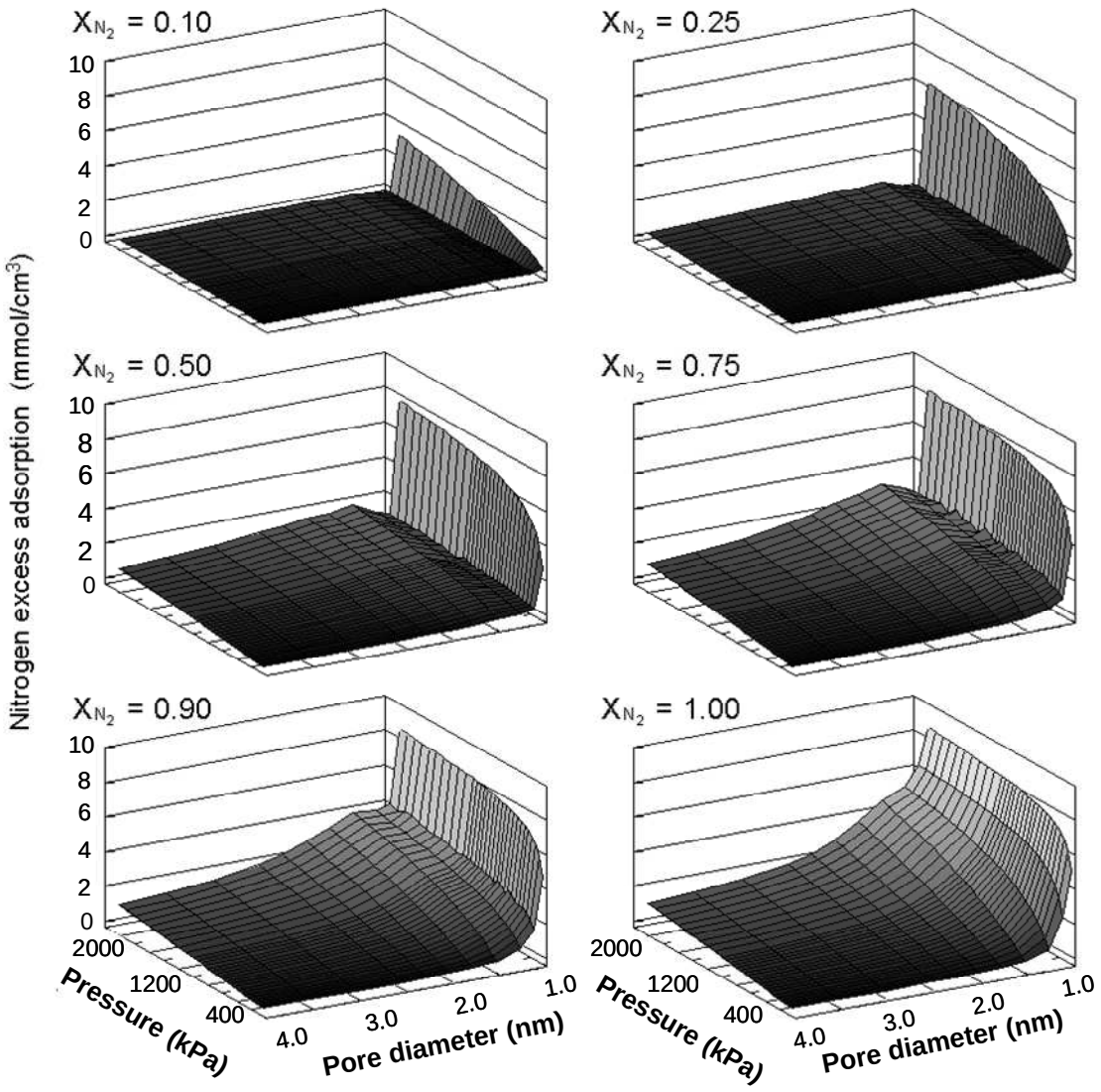

Figure 4.6. N_2 excess adsorption isotherms for mixtures of SF_6 and N_2 using multisite models for the fluids.

In the 1.0 nm pore, only N_2 molecules can get inside the pore and SF_6 molecules are excluded, as seen in Figure 4.7a. Figure 4.7b shows the local minimum for the adsorption of N_2 observed at 1.1 nm; at this diameter SF_6 molecules block a large portion of the free volume for the adsorption of N_2, although in this case N_2 molecules can rotate and accommodate to find free space in the narrow pore.

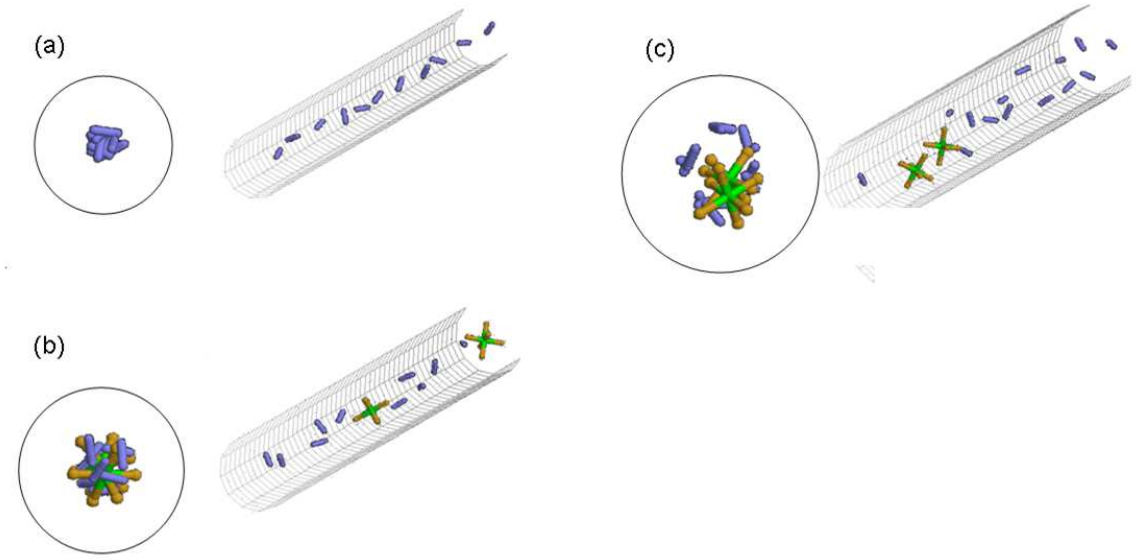

Figure 4.7. Snapshots of adsorbed SF_6 and N_2 at different pore sizes with a molar fraction of SF_6 of 0.10. Pore diameters (a) 1.0 nm and (b) 1.1 nm. N_2 is represented in blue while SF_6 is represented in yellow (the F atoms) and green (the bonds between atoms).

The competitive adsorption of N_2 at higher pressures is more marked for the multisite models than for the LJ models, partially because the amount of adsorbed SF_6 is lower in this case. Also due to the linear N_2 molecules fitting near the pore wall.

Unlike the spherical models, there is no complete exclusion effect for the multisite models. Hence, the selectivity plots in Figure 4.8 show changes for the pore diameter and the operating conditions as well. The local minimum observed in the N_2 adsorption for a pore diameter of 1.1 nm (for molar fractions of N_2 below 0.75) is also reflected in Figure 4.8; the maximum selectivity is reached at this point of minimum N_2 adsorption. This optimum selectivity occurs at a pore size where SF_6 blocks the free space for the adsorption of N_2, enhancing the separation of their molecules. This effect diminishes with pressure, because higher pressures favor the competition between SF_6 and N_2 and the packing of the molecules increases, creating more accessible space. [51] Furthermore, a local adsorption minimum for SF_6 is found at 1.5 nm, which is reflected in the selectivity plot as the minimum in selectivity. This selectivity minimum is the point where the transition from a single to multiple layers of SF_6 starts.

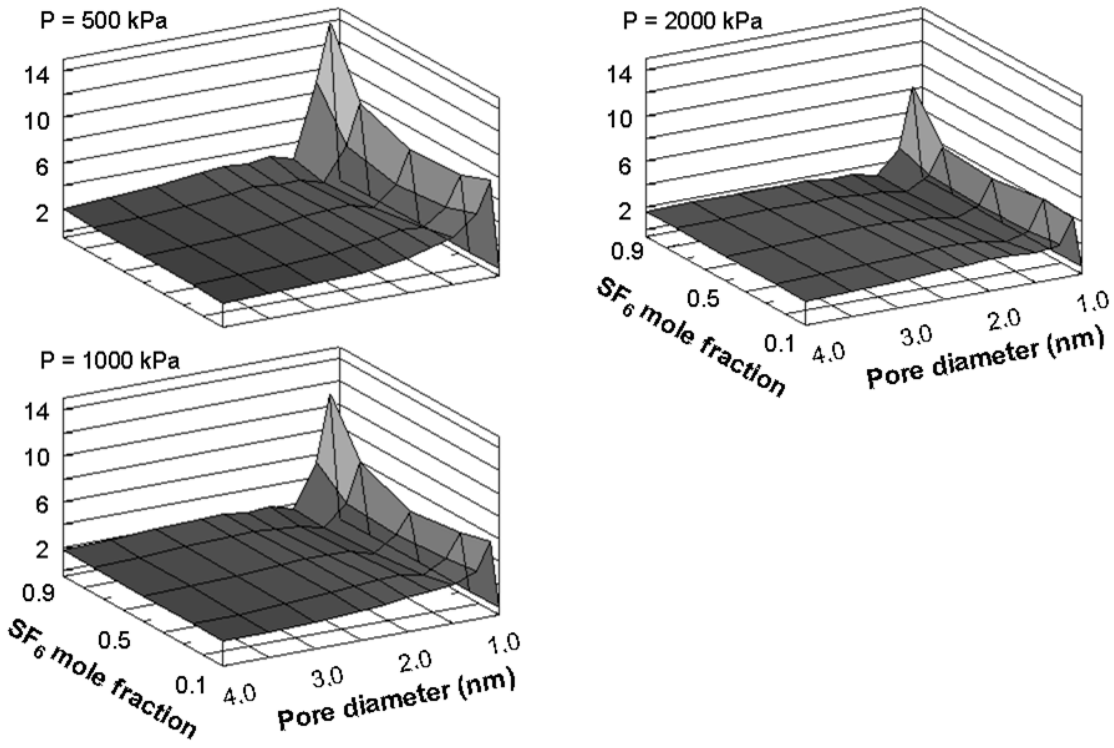

Figure 4.8. Selectivity of SF_6 over N_2 using multisite models.

It is also worth noting that the decrease of the selectivity with pressure for all compositionsis due to competitive adsorption. At low pressures, see Figure 4.8 at P = 500 kPa, the material is more selective towards SF_6 than at higher pressures, because competitive adsorption with N_2.

The selectivity plots follow the trend predicted by the theoretical analysis in a one-dimensional system performed by Talbot. [42] The larger molecule is attracted in a stronger manner to the solid material. For pressures below the iso-selective point, the composition has a strong influence on the selectivity; contrarily, approaching the isoselective point, increasing the pressure reduces the differences among the different compositions.

Similarly to the 1-site model, the selectivity is independent of pore size and composition for mesopores, because of the large free volume available for both molecules to adsorb. This independency of selectivity with pressure has been observed for other solid adsorbents with

large pore sizes and high volumetric capacity, such as mixtures of CH_4/H_2 in non-interpenetrated MOFs. [41, 52]

4.5. OPTIMAL SEPARATION DIAMETER USING ATOMISTIC MODELS[1]

Although the values for the adsorption isotherms should be different from those of the silica cylindrical model, ordered materials with almost cylindrical structures, such as zeolites, should follow the general trend observed with the ideal cylindrical pore.

As a final step in this study, once the optimal conditions for separation were found with the simple models, and these conditions corroborated with the refined force fields for the fluid, we evaluated the performance of a realistic material with a pore diameter similar to the optimal diameter found in the previous section. For this purpose, we have used two different solid materials with different shapes and similar pore sizes: (1) FAU-ZTC, which has a sharp pore size distribution located around 1.1-1.2 nm, and (2) EMT-ZTC, which has a bimodal and wider pore size distribution around 0.8-1.1 nm. [53, 54] Snapshots of both structures are presented in Figure 4.9 while details on the materials can be found in the original references. [53, 54]

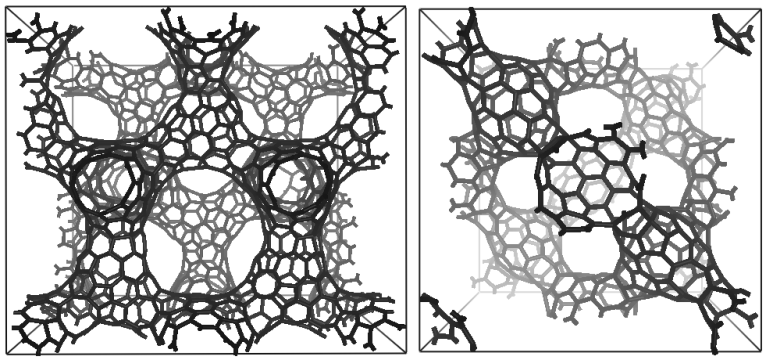

Figure 4.9. Models of the atomistic structures: EMT-ZTC (left) and FAU-ZTC (right).

[1] **The templated carbon models were provided by Thomas Roussel and were developed as part of his research at the Centre de Recherche en Matière Condensée et Nanosciences at Marseille, France.**

ZTCs are porous carbons with a well-tailored microporous structure obtained by using the template carbonization method employing a zeolite as the template. [55, 56] The pores and walls of the zeolite become the walls and pores of the carbon replica. Therefore, the carbon structures obtained by this method have very high surface areas and periodic ordered structures. [57] We have chosen these templated materials in the second part of this work as a possible material for the separation of SF_6 and N_2 because, in addition to having the appropriate pore diameter, these carbon materials have good stability at high temperatures and low affinity for water. [58] Besides, the high mechanical properties of ZTCs make them suitable to work at high pressures. [59] These characteristics offer unique advantages over inorganic molecular sieves and make the applications of such materials very attractive. In this chapter, we simulated the adsorption on the pores of hexagonal (EMT) and cubic (FAU-Y) zeolite-templated carbons, which have an average pore size close to 1.1nm. [54]

4.5.1. Zeolite templated carbons model

Recent synthesis techniques have allowed the design of carbon materials with a controlled pore size distribution. One of such techniques is the templating method using inorganic microporous hosts, such as zeolites, which leads to highly ordered microporous carbons (zeolite templated carbons). [56, 60-64] These new materials offer several desirable characteristics to achieve industrial separations of GHGs, such as high porosity, large specific surface areas, tunable shape, narrow pore size distributions, hydrophobic surface chemistry, stiffness, and robustness of their skeleton. [65-67]

As the focus of this chapter is in the application of ZTCs to CO_2 adsorption, rather than in the development of a molecular model for the materials, the details of the development of the ZTC models are not included in this thesis. The methodology to numerically synthesize these model materials, and the structural and mechanical characteristics of both models used for this work can be found in the literature. [53, 54]

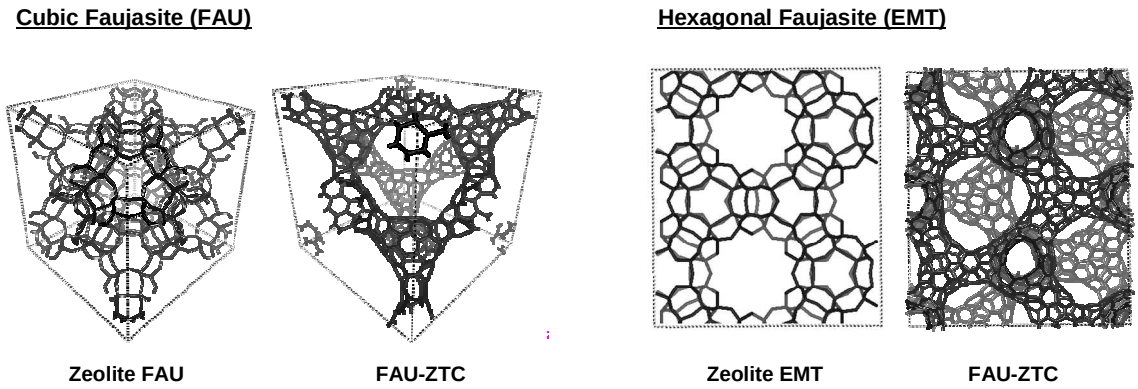

Figure 4.10. Atomistic nanostructures from GCMC simulations of ideal ZTCs: (left to right) one unit cell of the FAU zeolite used as a template; its carbon replica FAU-ZTC at equilibrium; two unit cells of the EMT zeolite used as a template; its carbon replica EMT-ZTC at equilibrium.

The carbon replica models of the cubic faujasite Y (FAU-ZTC) and of the hexagonal one (EMT-ZTC) are represented in Figure 4.10, along with their host templates. This figure illustrates how the ZTCs are negative templates of their respective zeolites. FAU-ZTC can be seen as a set of tetrahedrally interconnected single-walled nanotubes, with a unit cell length of 2.49 nm. Conversely, the EMT-ZTC structure can be considered as a pillared bundle of single-walled undulated nanotubes, hexagonally interconnected. The dimensions of its orthorhombic unit cell are a = 1.74 nm, b = 3.01 nm and c = 28.35 nm.

These atomistic represent two ordered microporous carbon replicas of siliceous forms of faujasite zeolite (cubic Y-FAU and hexagonal EMT). The models for ZTC were proposed by Roussel el al. [53, 54]

4.5.2. Simulation details for the carbon replicas

The simulations of the ZTCs were run at the same thermodynamic conditions than the MCM-41 simulations, except that only two selected representative condition for the mixture were simulated for the mixture composition: an bulk equimolar mixture of SF_6/N_2, and a mixture with low contents of SF_6 (0.1 mole fraction), as well as both pure fluids.

The ZTC structures were assumed rigid and the parameters for the carbon atoms in the ZTC were taken to be those customarily used to describe the carbon atoms of graphene sheets (Steele parameters), ε_C = 28.0 K and σ_C = 0.34 nm. [68]

The GCMC simulations were performed on a periodic box containing a unit cell of cubic FAU-ZTC (2.485 nm) and for a hexagonal EMT-ZTC (corresponding to two hexagonal orthorhombic unit cells in x,y directions: a = 3.4772 nm, b = 3.0114 nm, and c = 2.8346 nm). The systems were equilibrated for 1.0×10^6 Monte Carlo steps and 4.0×10^6 Monte Carlo steps were further performed for averaging purposes. The cut-off radius was taken to be less than half the simulation box length.

4.5.3. Simulation results for the carbon replicas

The adsorption isotherms of SF_6 and N_2 on ZTC materials, as a function of the partial pressure of each substance, are depicted in Figure 4.11. It can be observed in the figure how N_2 is displaced by SF_6 during the adsorption on both EMT-ZTC (Figure 4.11a) and FAU-ZTC (Figure 4.11b). The adsorption isotherms for pure SF_6 are almost identical to the isotherms of SF_6 in the mixture, whereas for N_2 the adsorption uptake of the pure fluid is much higher than when SF_6 is present.

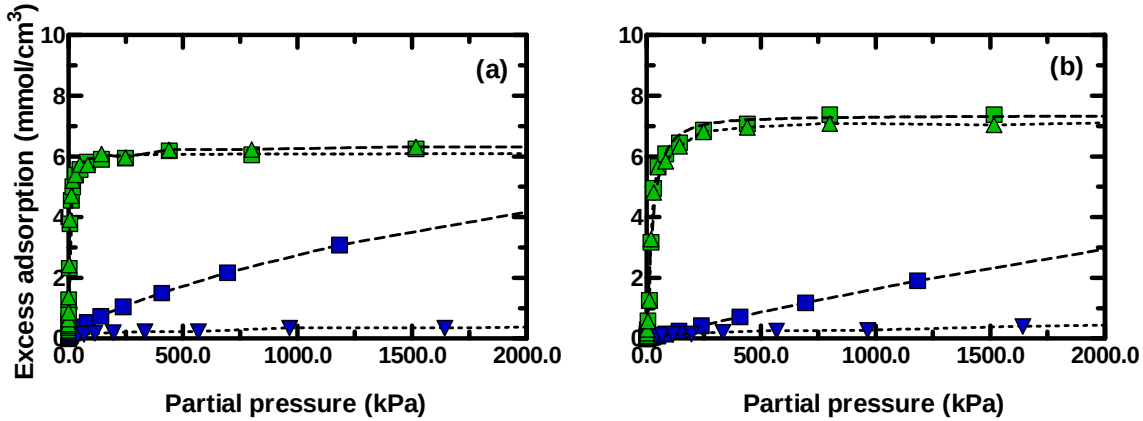

Figure 4.11. Adsorption isotherms on EMT-ZTC (a) and FAU-ZTC (b) as function of the partial pressure of each fluid of pure SF_6 (green squares), pure N_2 (blue squares), and SF_6 and N_2 in a mixture with 0.1 molar fraction of SF_6 (green and blue triangles, respectively).

The amount of SF_6 adsorbed on FAU-ZTC, which has a sharp pore size distribution at the desired pore size, is higher than for EMT-ZTC, and the opposite behavior is observed for N_2. This indicates an excellent efficiency for the separation on FAU-ZTC, as confirmed by the selectivity plots depicted in Figure 4.12. For pressures between 100-1000 kPa on FAU-ZTC optimal separation efficiency is achieved, with selectivity values around 130, much higher than any other previously reported material for this mixture separation. The behavior of FAU-ZTC in Figure 4.12 shows that the maximum selectivity is reached at intermediate pressures, opposed to other materials like EMT-ZTC where the optimum selectivity is reached at very low pressures. This selectivity trend in FAU-ZTC is due the exclusion effect discussed in the previous section, which is more marked at pressures where SF_6 is starting to saturate the pore. For application in separation processes, it is a desirable characteristic because the maximum selectivity might be close to the actual operating pressure.

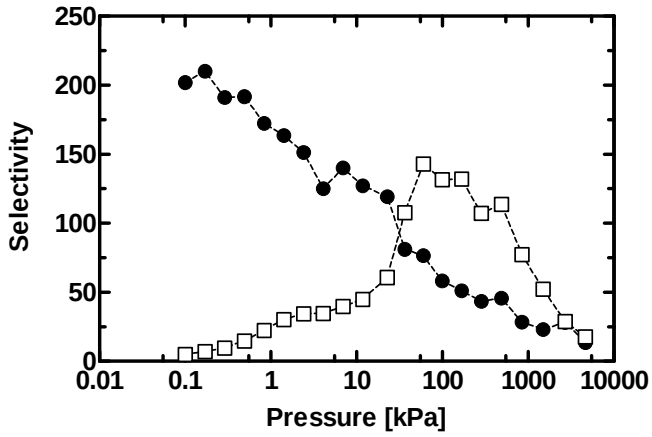

Figure 4.12. Selectivity of SF_6 over N_2 on EMT-ZTC (circles) and FAU-ZTC (squares) for a bulk equimolar mixture.

The slope of the adsorption isotherms is steeper for EMT-ZTC; this means that the solid-fluid interactions are stronger in this material. This is reflected in the selectivity, which decreases with increasing pressure for EMT-ZTC, while for FAU-ZTC the selectivity first increases until a certain pressure, and then it begins to decrease with pressure; at this point, the total capacity for SF_6 adsorption has been reached and the competitive adsorption of N_2 begins to displace some SF_6.

The predictions of the optimal diameter show that FAU-ZTC is an excellent technical option for separating SF_6/N_2 mixtures. This can be seen by comparing the values of the selectivity for FAU-ZTC (and even EMT-ZTC) to the ones reported in the literature. Experimentally, a selectivity of 12.8 was seen on Vycor glass [12], for inlet compositions of 0.10 mole fraction of SF_6 on a Ca-A zeolite a selectivity of 28.5 was obtained [10], likewise a selectivity of 44.3 was observed on a Na-X type zeolite [11]. Interestingly, the best adsorbent material in terms of selectivity, found in the literature (Na-X zeolite) has an average pore size of 1.0 nm. This confirms the results of our simulations, with the cylindrical model, for the optimal pore diameter. It is important to note that the values reported in the literature are equivalent to a dynamical separation process, whereas the values reported here are equivalent to a fixed value at a certain composition. We reported the values of our simulations for a molar fraction of SF_6 of 0.5 to take into account this difference. At low SF_6 concentration in the bulk, the selectivity is even greater.

Given the comparison with the other materials for SF_6/N_2 separations, the carbon replicas show very promising capabilities for separating SF_6/N_2 mixtures from a practical point of view, specially FAU-ZTC. The mechanical properties of ZTC would allow the separation using a device able to separate and store SF_6 for recovery and reutilization, such as the one portrayed by Murase et al. for separating SF_6 using zeolites [11].

4.6. CONCLUSIONS

This study illustrates how molecular simulations can be used to guide the selection for the optimal conditions for separations of mixtures by adsorption, and how an optimal material can be found following this procedure. The methodology has been applied to separate, by adsorption, sulfur hexafluoride (SF_6) from nitrogen (N_2), a mixture of key interest for electrical applications, whose separation is needed to avoid atmospheric emissions of SF_6, a very potent greenhouse gas.

We have first studied the influence of composition, pressure and pore diameter on the adsorption and separation of SF_6 and N_2 mixtures in MCM-41 by using GCMC molecular

simulation as a way to optimize the separation process. Results show that the maximum selectivity by adsorption is obtained for a cylindrical pore diameter of 1.1 nm; where sulfur hexafluoride molecules block the empty volume of the pore and prevent nitrogen from being adsorbed. The importance of using molecular simulation to find the optimum value is clearly shown by the narrow range of pore diameters with high selectivities; in addition, simulations help to visualize the distribution and orientation of the molecules at the molecular level. Furthermore, the simulation results showed that the selectivity is only slightly dependent of the pore diameter and the mixture composition for pore diameters larger than 2.0 nm due to the large free volume available for the two components.

Further simulations with more refined force fields for the fluids, including geometrical information and flexibility of the molecules, mainly corroborate the optimal conditions for separation obtained with the simple models.

Once the optimal pore diameter for separation in the simple MCM-41 model material was found, additional simulations were performed in ordered materials with almost cylindrical structures, such as zeolite carbon replicas. GCMC simulation results show very high selectivities for FAU-ZTC and EMT, being the selectivity higher for FAU-ZTC, a material with a narrow pore size distribution located around 1.1 nm. Selectivities found for this material are approximately four times higher than the best material for separation of SF_6/N_2 published in the open literature, for the working pressure range employed industrially. Given the mechanical properties of these carbon replicas, these materials show a great potential for applications in recovering SF_6 from SF_6/N_2 mixtures present in gas-insulated equipment.

REFERENCES

1. *"Kyoto Protocol to the United Nations Framework Convention on Climate Change"*. Review of European Community & International Environmental Law. **1998**;7 (2).214-7.

2. Ravishankara AR, Solomon S, Turnipseed AA, Warren RF. *"Atmospheric Lifetimes of Long-Lived Halogenated Species"*. Science. **1993**;259 (5092).194-9.

3. Hikita M, Ohtsuka S, Okabe S, Kaneko S. *"Insulation Characteristics of Gas Mixtures including Perfluorocarbon Gas"*. Dielectrics and Electrical Insulation, IEEE Transactions on. **2008**;15 (4).1015-22.

4. Katagiri H, Kasuya H, Mizoguchi H, Yanabu S. *"Investigation of the Performance of CF3 Gas as a Possible Substitute for SF6"*. Dielectrics and Electrical Insulation, IEEE Transactions on. **2008**;15 (5).1424-9.

5. Taniguchi S, Okabe S, Takahashi T, Shindo T. *"Discharge Characteristics of 5 m Long Air Gap under Foggy Conditions with Lightning Shielding of Transmission Line"*. Dielectrics and Electrical Insulation, IEEE Transactions on. **2008**;15 (4).1031-7.

6. Etter M, Koch H, editors. Sulfur hexafluoride SF6. Power and Energy Society General Meeting - Conversion and Delivery of Electrical Energy in the 21st Century, 2008 IEEE; 2008.

7. Olthoff JK, Christophorou LG, editors. A brief history of gaseous dielectrics research at NIST. Electrical Insulation and Dielectric Phenomena, 2001 Annual Report Conference on; 2001.

8. Inami K, Maeda Y, Habuchi Y, Yoshimura M, Hamano S, Hama H. *"Problems of the application of N2/SF6 mixtures to gas-insulated bus"*. Electrical Engineering in Japan. **2001**;137 (4).25-31.

9. Yamamoto O, Takuma T, Kinouchi M. *"Recovery of SF6 from N2/SF6 gas mixtures by using a polymer membrane"*. Electrical Insulation Magazine, IEEE. **2002**;18 (3).32-7.

10. Toyoda M, Murase H, Imai T, Naotsuka H, Kobayashi A, Takano K, et al. *"SF6 reclaimer from SF6/N2 mixtures by gas separation with molecular sieving effect"*. Power Delivery, IEEE Transactions on. **2003**;18 (2).442-8.

11. Murase H, Imai T, Inohara T, Toyoda M. *"Use of zeolite filter in portable equipment for recovering SF6 in SF6/N2 mixtures"*. Dielectrics and Electrical Insulation, IEEE Transactions on. **2004**;11 (1).166-73.

12. Shiojiri K, Yanagisawa Y, Yamasaki A, Kiyono F. *"Separation of F-gases (HFC-134a and SF6) from gaseous mixtures with nitrogen by surface diffusion through a porous Vycor glass membrane"*. J Membr Sci. **2006**;282 (1-2).442-9.

13. Dagan G, Agam G, Krakov V, Kaplan L, editors. Carbon Membrane Separator for Elimination of SF6 emissions from Gas-Insulated Electrical Utilities. 1st International Conference on SF6 and the Environment; 2000; San Diego, California.

14. Riddell IA, Smulders MMJ, Clegg JK, Nitschke JR. *"Encapsulation, storage and controlled release of sulfur hexafluoride from a metal-organic capsule"*. Chem Commun. **2011**;47 (1).457-9.

15. Cha I, Lee S, Lee JD, Lee G-w, Seo Y. *"Separation of SF6 from Gas Mixtures Using Gas Hydrate Formation"*. Environ Sci Technol. **2010**;44 (16).6117-22.

16. Wolińska-Grabczyk A, Jankowski A, Sekuła R, Kruczek B. *"Separation of SF6 from Binary Mixtures with N2 Using Commercial Poly(4-Methyl-1-Pentene) Films"*. Sep Sci Technol. **2011**;46 (8).1231-40.

17. Bhattacharyya S, Lelong G, Saboungi ML. *"Recent progress in the synthesis and selected applications of MCM-41: a short review"*. J Exp Nanosci. **2006**;1 (3).375 - 95.

18. Brady R, Woonton B, Gee ML, O'Connor AJ. *"Hierarchical mesoporous silica materials for separation of functional food ingredients -- A review"*. Innovative Food Science & Emerging Technologies. **2008**;9 (2).243-8.

19. Zhou Y, Antonietti M. *"Preparation of Highly Ordered Monolithic Super-Microporous Lamellar Silica with a Room-Temperature Ionic Liquid as Template via the Nanocasting Technique"*. Adv Mater. **2003**;15 (17).1452-5.

20. Mohanty S, Davis HT, McCormick AV. *"Shape selective adsorption in cylindrical pores"*. Chem Eng Sci. **2000**;55 (17).3377-83.

21. Aziz RA, Slaman MJ, Taylor WL, Hurly JJ. *"An improved intermolecular potential for sulfur hexafluoride"*. J Chem Phys. **1991**;94 (2).1034-8.

22. Neimark AV, Ravikovitch PI, Grün M, Schüth F, Unger KK. *"Pore Size Analysis of MCM-41 Type Adsorbents by Means of Nitrogen and Argon Adsorption"*. J Colloid Interface Sci. **1998**;207 (1).159-69.

23. Blas FJ, Vega LF. *"Thermodynamic behaviour of homonuclear and heteronuclear Lennard-Jones chains with association sites from simulation and theory"*. Mol Phys. **1997**;92 (1).135 - 50.

24. Pàmies JC, Vega LF. *"Vapor-Liquid Equilibria and Critical Behavior of Heavy n-Alkanes Using Transferable Parameters from the Soft-SAFT Equation of State"*. Ind Eng Chem Res. **2001**;40 (11).2532-43.

25. Olivet A, Vega LF. *"Optimized molecular force field for sulfur hexafluoride simulations"*. J Chem Phys. **2007**;126 (14).144502-11.

26. Olivet A, Vega LF. *"Predictions of Transport Properties in Gaseous Mixtures of Sulfur Hexafluoride and Nitrogen"*. J Phys Chem C. **2007**;111 (43).16013-20.

27. Galassi G, Tildesley DJ. *"Phase Diagrams of Diatomic Molecules Using the Gibbs Ensemble Monte Carlo Method"*. Mol Simul. **1994**;13 (1).11 - 24.

28. Liu B, Wang W, Zhang X. *"A hybrid cylindrical model for characterization of MCM-41 by density functional theory"*. Phys Chem Chem Phys. **2004**;6 (15).3985-90.

29. Maddox MW, Sowers SL, Gubbins KE. *"Molecular simulation of binary mixture adsorption in buckytubes and MCM-41"*. Adsorption. **1996**;2 (1).23-32.

30. Yun J-H, Duren T, Keil FJ, Seaton NA. *"Adsorption of Methane, Ethane, and Their Binary Mixtures on MCM-41: Experimental Evaluation of Methods for the Prediction of Adsorption Equilibrium"*. Langmuir. **2002**;18 (7).2693-701.

31. Kremer SPB, Kirschhock CEA, Aerts A, Aerts CA, Houthoofd KJ, Grobet PJ, et al. *"Zeotile-2: A microporous analogue of MCM-48"*. Solid State Sci. **2005**;7 (7).861-7.

32. Wu S, Song K, Guan J, Kan Q. *"Synthesis and characterization of super-microporous material with enhanced hydrothermal stability"*. Bull Mater Sci. **2011**;34 (4).979-83.

33. Tjatjopoulos GJ, Feke DL, Mann JA. *"Molecule-micropore interaction potentials"*. J Phys Chem. **1988**;92 (13).4006-7.

34. Ravikovitch PI, Vishnyakov A, Neimark AV. *"Density functional theories and molecular simulations of adsorption and phase transitions in nanopores"*. Phys Rev E. **2001**;64 (1).011602.

35. Cao D, Shen Z, Chen J, Zhang X. *"Experiment, molecular simulation and density functional theory for investigation of fluid confined in MCM-41"*. Microporous Mesoporous Mater. **2004**;67 (2-3).159-66.

36. Herdes C, Santos MA, Abelló S, Medina F, Vega LF. *"Search for a reliable methodology for PSD determination based on a combined molecular simulation-regularization-experimental approach: The case of PHTS materials"*. Appl Surf Sci. **2005**;252 (3).538-47.

37. Herdes C, Santos MA, Medina F, Vega LF. *"Pore Size Distribution Analysis of Selected Hexagonal Mesoporous Silicas by Grand Canonical Monte Carlo Simulations"*. Langmuir. **2005**;21 (19).8733-42.

38. Neimark AV, Ravikovitch PI, Vishnyakov A. *"Adsorption hysteresis in nanopores"*. Phys Rev E. **2000**;62 (2).R1493.

39. Ravikovitch PI, Haller GL, Neimark AV. *"Density functional theory model for calculating pore size distributions: pore structure of nanoporous catalysts"*. Adv Colloid Interface Sci. **1998**;76-77 203-26.

40. Duque D, Vega LF. *"Some issues on the calculation of interfacial properties by molecular simulation"*. The Journal of Chemical Physics. **2004**;121 (17).8611-7.

41. Gallo M, Glossman-Mitnik D. *"Fuel Gas Storage and Separations by Metal-Organic Frameworks: Simulated Adsorption Isotherms for H2 and CH4 and Their Equimolar Mixture"*. J Phys Chem C. **2009**;113 (16).6634-42.

42. Talbot J. *"Analysis of adsorption selectivity in a one-dimensional model system"*. AIChE J. **1997**;43 (10).2471-8.

43. Jiang J, Sandler SI. *"Monte Carlo Simulation of O2 and N2 Mixture Adsorption in Nanoporous Carbon (C168 Schwarzite)"*. Langmuir. **2003**;19 (14).5936-41.

44. Somers SA, McCormick AV, Davis HT. *"Superselectivity and solvation forces of a two component fluid adsorbed in slit micropores"*. J Chem Phys. **1993**;99 (12).9890-8.

45. Yang Q, Xue C, Zhong C, Chen J-F. *"Molecular simulation of separation of CO2 from flue gases in CU-BTC metal-organic framework"*. AIChE J. **2007**;53 (11).2832-40.

46. Heyden A, Düren T, J. Keil F. *"Study of molecular shape and non-ideality effects on mixture adsorption isotherms of small molecules in carbon nanotubes: A grand canonical Monte Carlo simulation study"*. Chem Eng Sci. **2002**;57 (13).2439-48.

47. Babarao R, Hu Z, Jiang J, Chempath S, Sandler SI. *"Storage and Separation of CO2 and CH4 in Silicalite, C168 Schwarzite, and IRMOF-1: A Comparative Study from Monte Carlo Simulation"*. Langmuir. **2006**;23 (2).659-66.

48. Bhatia SK, Tran K, Nguyen TX, Nicholson D. *"High-Pressure Adsorption Capacity and Structure of CO2 in Carbon Slit Pores: Theory and Simulation"*. Langmuir. **2004**;20 (22).9612-20.

49. Do DD, Do HD. *"Adsorption of Quadrupolar, Diatomic Nitrogen onto Graphitized Thermal Carbon Black and in Slit-shaped Carbon Pores. Effects of Surface Mediation"*. Adsorption Science and Technology. **2005**;23 267-88.

50. Lobo RF. *"Chemistry: The promise of emptiness"*. Nature. **2006**;443 (7113).757-8.

51. Gallo M, Nenoff TM, Mitchell MC. *"Selectivities for binary mixtures of hydrogen/methane and hydrogen/carbon dioxide in silicalite and ETS-10 by Grand Canonical Monte Carlo techniques"*. Fluid Phase Equilib. **2006**;247 (1-2).135-42.

52. Liu B, Yang Q, Xue C, Zhong C, Chen B, Smit B. *"Enhanced Adsorption Selectivity of Hydrogen/Methane Mixtures in Metalic-Organic Frameworks with Interpenetration: A Molecular Simulation Study"*. J Phys Chem C. **2008**;112 (26).9854-60.

53. Roussel T, Didion A, Pellenq RJM, Gadiou R, Bichara C, Vix-Guterl C. *"Experimental and Atomistic Simulation Study of the Structural and Adsorption Properties of Faujasite Zeolite−Templated Nanostructured Carbon Materials†"*. J Phys Chem C. **2007**;111 (43).15863-76.

54. Roussel T, Bichara C, Gubbins KE, Pellenq RJM. *"Hydrogen storage enhanced in Li-doped carbon replica of zeolites: A possible route to achieve fuel cell demand"*. J Chem Phys. **2009**;130 (17).174717-6.

55. Matsuoka K, Yamagishi Y, Yamazaki T, Setoyama N, Tomita A, Kyotani T. *"Extremely high microporosity and sharp pore size distribution of a large surface area carbon prepared in the nanochannels of zeolite Y"*. Carbon. **2005**;43 (4).876-9.

56. Kyotani T, Nagai T, Inoue S, Tomita A. *"Formation of New Type of Porous Carbon by Carbonization in Zeolite Nanochannels"*. Chem Mater. **1997**;9 (2).609-15.

57. Gaslain FOM, Parmentier J, Valtchev VP, Patarin J. *"First zeolite carbon replica with a well resolved X-ray diffraction pattern"*. Chemical Communications. **2006** (9).991-3.

58. Pellenq R, Roussel T, Puibasset J. *"Molecular simulations of water in hydrophobic microporous solids"*. Adsorption. **2008**;14 (4).733-42.

59. Hou P-X, Orikasa H, Itoi H, Nishihara H, Kyotani T. *"Densification of ordered microporous carbons and controlling their micropore size by hot-pressing"*. Carbon. **2007**;45 (10).2011-6.

60. Kyotani T. *"Control of pore structure in carbon"*. Carbon. **2000**;38 (2).269-86.

61. Ma Z, Kyotani T, Liu Z, Terasaki O, Tomita A. *"Very High Surface Area Microporous Carbon with a Three-Dimensional Nano-Array Structure: Synthesis and Its Molecular Structure"*. Chemistry of Materials. **2001**;13 (12).4413-5.

62. Ma Z, Kyotani T, Tomita A. *"Preparation of a high surface area microporous carbon having the structural regularity of Y zeolite"*. Chemical Communications. **2000** (23).2365-6.

63. Ryoo R, Joo SH, Jun S. *"Synthesis of Highly Ordered Carbon Molecular Sieves via Template-Mediated Structural Transformation"*. J Phys Chem B. **1999**;103 (37).7743-6.

64. Ryoo R, Joo SH, Kruk M, Jaroniec M. *"Ordered Mesoporous Carbons"*. Adv Mater. **2001**;13 (9).677-81.

65. Roussel T, Pellenq RJM, Bienfait M, Vix-Guterl C, Gadiou R, Béguin F, et al. *"Thermodynamic and Neutron Scattering Study of Hydrogen Adsorption in Two Mesoporous Ordered Carbons"*. Langmuir. **2006**;22 (10).4614-9.

66. Vix-Guterl C, Boulard S, eacute, verine, Parmentier J, Werckmann J, et al. *"Formation of Ordered Mesoporous Carbon Material from a Silica Template by a One-Step Chemical Vapour Infiltration Process"*. Chem Lett. **2002**;31 (10).1062-3.

67. Vix-Guterl C, Saadallah S, Vidal L, Reda M, Parmentier J, Patarin J. *"Template synthesis of a new type of ordered carbon structure from pitch"*. J Mater Chem. **2003**;13 (10).2535-9.

68. Kuznetsova A, J. T. Yates J, Simonyan VV, Johnson JK, Huffman CB, Smalley RE. *"Optimization of Xe adsorption kinetics in single walled carbon nanotubes"*. J Chem Phys. **2001**;115 (14).6691-8.

Chapter V

Carbon Dioxide Capture on Microporous Carbons*

"What happens if a big asteroid hits Earth? Judging from realistic simulations involving a sledgehammer and a common laboratory frog, we can assume it will be pretty bad."

Dave Barry

In view of the promising separation characteristics of ZTCs for separating SF_6 and N_2 presented in the previous chapter, the feasibility of using these materials for CO_2 capture was assessed by using a combined approach of simulations and experiments[1]. The presence of a microporous network on ZTCs makes them attractive materials for their use as adsorbents in separation of gases. Moreover, the intrinsic properties of carbons such as their hydrophobicity and high chemical and thermal resistance are desirable properties for CO_2 separation applications. These characteristics allow ZTCs to withstand high temperatures and pressures, which in principle makes them ideal materials for removing GHGs from steam gas. [1]

The reduction of CO_2 emissions from industrial gases requires the separation and purification from a mixture of gases and vapors. Processes to separate CO_2 from those mixtures are energy intensive; therefore, to be economically viable, an ideal CO_2 adsorbent should have high capacity and strong interactions with CO_2. [2] The high capacity and good mechanical

*** The results discussed in this chapter were published in "Microporous carbon adsorbents with high CO_2 capacities for industrial applications". Phys. Chem. Chem. Phys., 13: 16063-16070. (2011)**

[1] The experimental results presented in this chapter were carried out at the Institut de Science des Matériaux de Mulhouse by Camelia Matei Ghimbeu, Julien Parmentier, Roger Gadiou and Cathie Vix-Guterl.

properties of ZTCs make them interesting candidates for industrial CO_2 capture. The two ZTC atomistic structures used in this study have shown promising hydrogen adsorption capacities at high pressure for the bare structures, which can be enhanced by lithium functionalization. [3, 4]

In this chapter, insight of the ZTCs nanostructure is obtained by using CO_2 as a probe of their microporosity. In addition, the performances of ZTCs at 273 K and 298 K are compared to several inorganic (zeolites and mesoporous silicas) and organic (activated carbons, COFs and MOFs) adsorbents reported in the literature.

5.1. EXPERIMENTAL ZTCs

Two different ZTCs, a Na-Y faujasite carbon replica (FAU-ZTC) and a carbon replica of the hexagonal EMT zeolite (EMT-ZTC) were synthesized and characterized. The adsorption isotherms for nitrogen and carbon dioxide were measured volumetrically using a bench-scale adsorption/desorption apparatus. The details of the experimental synthesis and characterization procedures can be found elsewhere. [5] In essence, ZTCs can be defined as "negative-zeolites"; they are obtained as the result of filling the pores of a zeolite with a carbon precursor, consolidating the carbon structure inside the pore by carbonizing the precursor and finally removing the zeolite framework.

5.2. MOLECULAR MODELS OF ZTCs

The atomistic carbon structures of EMT and FAU-Y zeolite carbon replicas were generated by GCMC simulations.[2] The full details of the models can be found in the original references. [5-7] These structures are generated as the fully consolidated and perfectly filled solution of the carbon impregnation inside the zeolite pores. Although the model resembles the experimental material, and several key features are recovered, with the additional benefit of providing physical insight into the adsorption behaviour, one should bear in mind that this is a quite simple and ideal model; hence, some features and defects of the experimental material

[2] **The templated carbon models were provided by Thomas Roussel and were developed as part of his doctoral dissertation at the Centre de Recherche en Matière Condensée et Nanosciences at Marseille, France.**

do not show up into the model. It is expected that the experimental materials deviate from this ideal structure mainly due to diffusion problems of the precursor during the synthesis and/or to a collapse of the consolidated structure during calcination. However, future improvements in the synthesis techniques are expected to produce materials with a lower number of defects and thus closer to the models used in this work.

The micropore volumes of the models EMT-ZTC and FAU-ZTC are 0.48 and 0.78 cm^3/g respectively, whereas for the experimental ones are 1.45 and 1.47 cm^3/g. These differences in the micropore volume are attributed to the presence of larger micropores like edges or vacancies, absent in the perfect crystal models. This latter point is supported by comparing the pore size distribution of the models with the experimental ones. [8]

5.3. SIMULATION METHODOLOGY

The CO_2 simulated adsorption isotherms of the models were computed using the GCMC method. The interactions between CO_2 molecules were modeled using the TraPPE potential. [9] This potential treats carbon dioxide as a rigid molecule with 3 interaction sites. It describes the intermolecular interactions through pairwise-additive LJ 12–6 potential for the repulsive and dispersive terms, and coulombic potential for the first-order electrostatic contributions. As the molecules are taken to be rigid, with a C–O bond length of 0.116 nm and an O–C–O angle of 180°, there are no intramolecular interactions.

Moreover, N_2 molecules were also modeled using the TraPPE model. This force field uses a rigid dumbbell representation of N_2 molecules, with a distance between the nitrogen atoms of 0.11 nm, and the intermolecular interactions are quantified by a LJ potential. This model includes point charges in the nitrogen atoms and one point charge in the center of mass to maintain charge neutrality.

The ZTC structures were assumed rigid. The parameters for the carbon atoms in the ZTC were taken to be those customarily used to describe the adsorption on graphene sheets. [10] The LJ and coulombic parameters employed in the simulations are listed in Table 5.1. The interactions between unlike atoms were computed according to the Lorentz–Berthelot combining rules.

Table 5.1. TraPPE and Steele LJ and point charge parameters for CO_2, N_2 and carbon (ZTCs).

	ε_{ii}/k_B (K)	σ_{ii} (nm)	q_i (e)
C (in CO_2)	10	0.280	+0.70
O (in CO_2)	79.0	0.305	-0.35
C (ZTCs)	28.0	0.340	0.0
	36.0[3]	0.340	0.0
N (in N_2)	36.0	0.331	-0.482
COM[4] (in N_2)	0.0	0.0	0.964

Details on the GCMC simulation procedure are given in chapter 2, retaining here just the details concerning the implementation for the particular system of interest and the different parameters used in the simulations:

- The probabilities of displacement, rotation, creation, and deletion were set to 0.2, 0.2, 0.3 and 0.3, respectively.
- The system was equilibrated for 3.5×10^7 Monte Carlo steps, after which data were collected for 1.4×10^7 MC steps.
- The cutoff radius for the LJ interactions was set to less than half (0.499) the size of the shortest side of the unit cell.
- For statistical purposes, the size of the simulation box was adjusted, depending on the bulk pressure, in order to have at least 40 molecules inside the simulation cell for averaging purposes.
- Periodic boundary conditions were applied in the *x*, *y* and *z* dimensions.
- The solid adsorbent was considered rigid; the potential energies between fluid molecules and the solid atoms were tabulated on a three-dimensional grid with the purpose of saving

[3] **Using a scaling factor of 1.134 to account for the curvature.**

[4] **Center of mass of the nitrogen molecule**

computational time, during the simulations the fluid–solid potential energy at any position in the adsorbent was determined by grid linear interpolation. [11]

- Electrostatic interactions were treated using the Ewald summation method. [12]
- The fugacity was calculated by using the soft-SAFT EoS. [13]

5.4. CO_2 ADSORPTION ON EMT-ZTC

The simulated adsorption isotherm on EMT-ZTC compared to the corresponding experimental data is presented in Figure 5.1. The simulations overestimate the experimental data at low pressures ($<10^{-1}$ bar). This difference might be due to two different effects: first, the diffusion of CO_2 into the internal cages (small micropores <0.6 nm) is very slow and the experimental convergence criterion might not allow enough time for CO_2 to penetrate the whole material. Second, the internal cages might be kinetically inaccessible [14] for the CO_2 molecules in the experiments while the simulation method inserts molecules at random accessible spaces in the structure without considering any kinetic path.

Furthermore, since ZTC models are limited to a bulk of perfect structures with small micropores (<1.1 nm), they saturate at pressures slightly above 1.5 bar, and the total amount adsorbed is underestimated in the simulations. Therefore, the total capacity of this model material is reached between 1 and 3 bar. The additional amount adsorbed by the experimental material above this pressure range is due to the filling of larger micropores and mesopores (cavities and edges) present in the real material, which are not present in the ideal model structures.

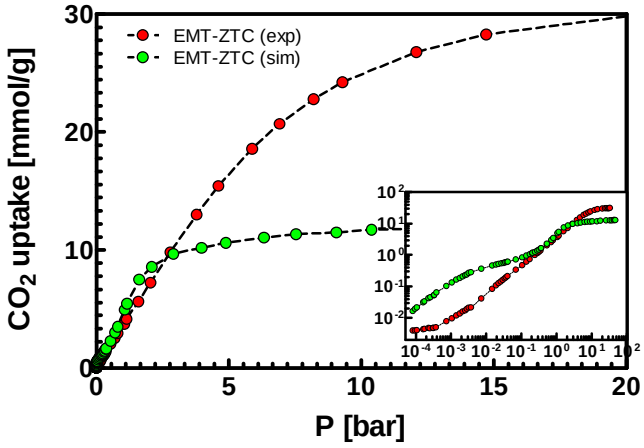

Figure 5.1. CO_2 adsorption isotherms at 273 K in EMT-ZTC for the experiments (red) and simulations (green). Inset: log-log representation.

A visual understanding of the adsorption behavior of CO_2 molecules in these materials was obtained by representing in Figure 5.2 the distribution of the accepted insertions of CO_2 molecules on the EMT-ZTC model during the simulations at different pressures. At low pressure, CO_2 molecules are mainly adsorbed inside the pillars of the carbon skeleton. At higher pressure (above 10^{-2}), it can be observed that CO_2 molecules start to adsorb in the larger pores. This pressure range corresponds to the point of mismatch between experimental and simulation results (also shown in Figure 5.2). The presence of CO_2 inside the pillars at very low pressures is an indication that this particular section of the model might be the main difference between the isotherms.

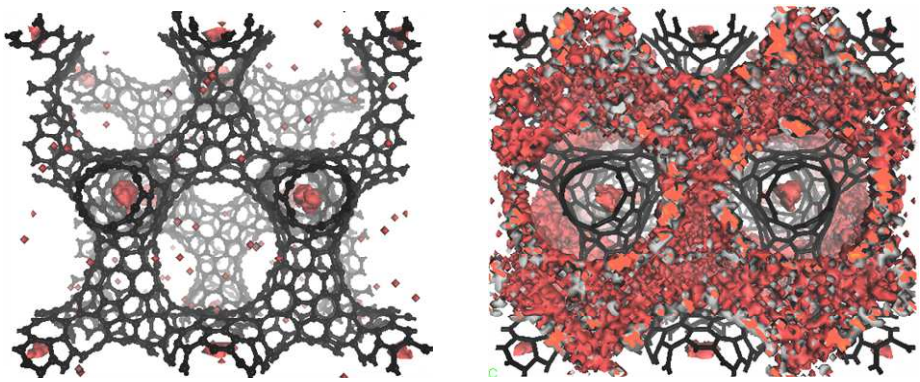

Figure 5.2. Distributions of the successfully inserted CO_2 molecules folded in two unit cells of EMT-ZTC at 10^{-3} bar (left) and 10^{-1} bar (right).

This latter hypothesis can be assessed by simulating EMT-ZTC with non-accessible cages. The region inside the cages is made non-accessible by excluding it from the possible attempted adsorption sites and correcting the acceptance rules. [15] The corrected simulated adsorption isotherm is in excellent agreement with the experimental results (depicted in Figure 5.3), supporting the claim about the non-accessibility of the pillars in the experimental material, and suggesting a new criterion to identify on the adsorption isotherm the presence of the tubular carbon nanostructure.

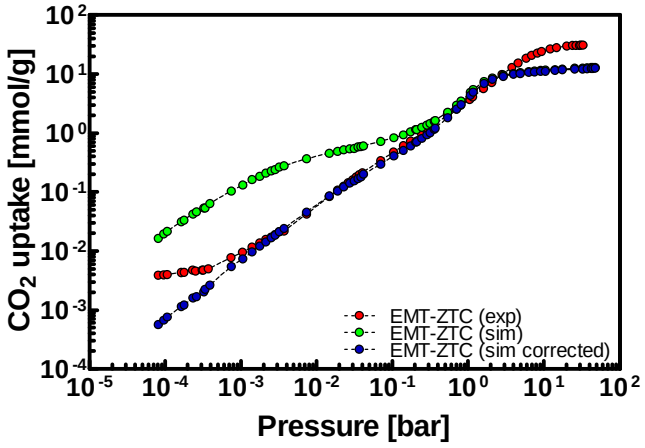

Figure 5.3. Experimental (green symbols) and simulated (red symbols) CO_2 adsorption isotherms at 273K for EMT-ZTC; the simulations for the refined models are reported in blue symbols. See text for details.

5.5. CO_2 ADSORPTION ON FAU-ZTC

Although, the FAU-ZTC model has internal cages similar to EMT-ZTC, in the former material the cages are not accessible due to their small size, while in the latter they are not accessible experimentally due to slow diffusion or defects in the structure. This is seen in a representation of the distribution of CO_2 molecules on the FAU-ZTC model during the simulations at different pressures, shown in Figure 5.4. As seen in the snapshots in Figure 5.4, the internal cages in FAU-ZTC do not participate in the adsorption process.

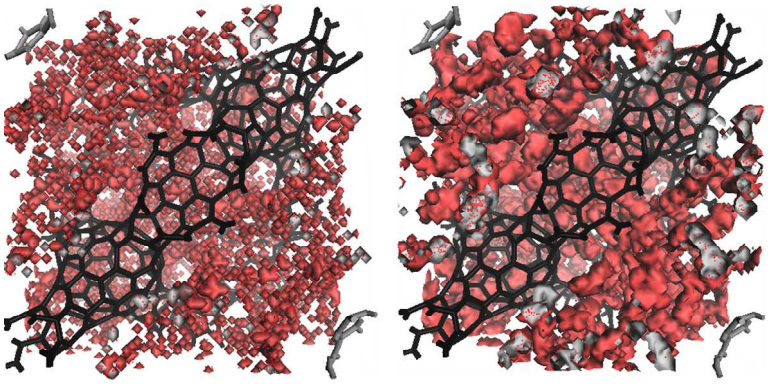

Figure 5.4. Distributions of the successfully inserted CO_2 molecules folded in one unit cell of FAU-ZTC at 10^{-2} bar (left) and 1 bar (right).

The experimental and simulated CO_2 adsorption isotherms for FAU-ZTC at 273 K are shown in Figure 5.5. For the entire pressure range, the simulated isotherm greatly underestimates the experimental one. A possible explanation for this large difference is that the extreme curvature of FAU-ZTC was not taken into account in the simulations. The parameters used to describe carbon–CO_2 interactions were adjusted for a flat graphene layer optimized for the interaction of adsorbates with graphitized carbon black; it has been demonstrated that these parameters do not accurately reproduce curved carbon surfaces. [14]

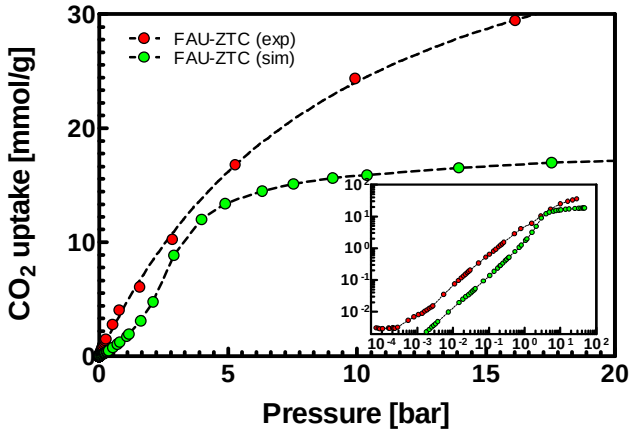

Figure 5.5. CO_2 adsorption isotherms at 273 K in FAU-ZTC for the experiments (red) and simulations (green). Inset: log-log scale plot of the isotherms.

The carbon atoms in FAU-ZTC must adopt an intermediate hybridization between sp^2 and sp^3 due to the imposed curved structure. The degree of hybridization depends on the

curvature of the material: a low curvature leads to hybridizations close to pure sp^2, while a high curvature leads to hybridizations towards sp^3. The curvature changes the carbon polarizability and implies higher dispersion energy for the bended carbon atoms. Therefore, not taking into account the curvature of FAU-ZTC might be responsible for the initial underestimation in the adsorption isotherm.

Although, apparently this argument can be applied for both structures, it was previously shown in the original reference for the generation of the models that the mean curvature of FAU-ZTC is much more extreme than for EMT-ZTC. [16] Here, the main details of the original thesis are included for consistency. They defined a parameter, called local curvature parameter (LCP), in the following manner: the angle θ_{ij} (or LCP) formed between the two vectors, r_i and r_j, normal to the planes (k^1_i, i, k^2_i) and (k^1_j, j, k^2_j); where i and j, are each pair of first neighbour carbon atoms and k^1_i, k^2_i, k^1_j and k^2_j are the other two first neighbours of i and j respectively (see schematic drawn in Figure 5.6). The data depicted in Figure 5.6 was taken from Figure 105 in Thomas Roussel's thesis. [16]

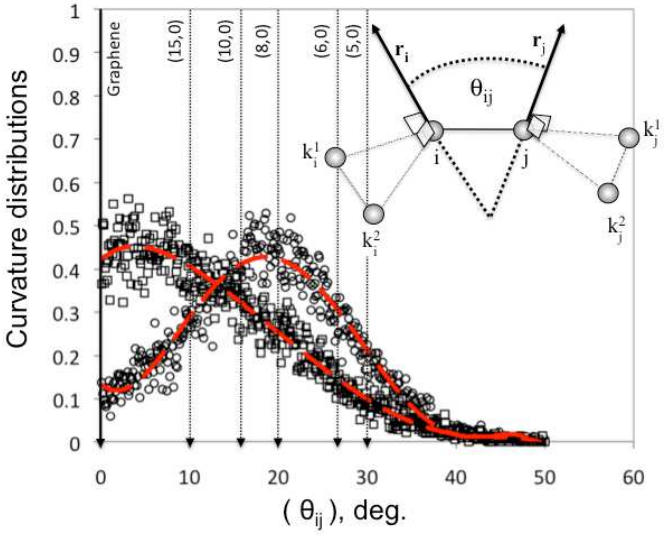

Figure 5.6. Local Curvature Parameter (LCP) distributions for EMT-ZTC (squares), FAU-ZTC (circles), graphene sheet (solid line arrows at θ_{ij} = 0°), and several SWNTs (dashed line arrows) with different chiral indices (n, 0) were n = 15, 10, 8, 6, 5. Schematic plot of the calculation of the LCP (ϑ_{ij}) for one pair of first neighbor carbon atoms, i and j, and their corresponding first neighbors k^1_i, k^2_i, k^1_j and k^1_j. See text for further explanation.

Roussel related θ_{ij} to the local curvature, calculating the LCP normalized distributions for zig-zag (n, 0) single-walled carbon nanotubes, with several chiral indices (n = 15, 10, 8, 6 and 5 and their corresponding diameters 1.17, 0.78, 0.63, 0.47, 0.39 nm). These distributions are discrete Dirac-like functions, and are represented by arrows in Figure 5.6. The LCP distributions exhibit large differences between both materials, as shown in Figure 5.6.

It is seen from Figure 5.6 that EMT-ZTC has a mean LCP smaller than a1.17 nm diameter nanotube (15,0). Hence, its structure is mostly flat, as would be a graphene sheet with a null LCP (θ_{ij} = 0). In contrast, FAU-ZTC shows an extreme local curvature, with a mean LCP corresponding to a 0.65 nm diameter nanotube. Therefore, although the parameters for graphite can reproduce the behavior of EMT-ZTC, the use of a modified well-depth potential for FAU-ZTC has to be considered.

To address the aforementioned limitations we have performed another set of simulations for FAU-ZTC. A different value for the carbon well depth was used to take into account the high curvature of FAU-ZTC. The solid–fluid interaction for the well depth was increased by a factor of 1.134 (ε_{Csolid} = 36.0 K). [17, 18] The corrected isotherm for FAU-ZTC (Figure 5.7) shows a much better agreement with the experimental results than the previously discussed isotherms using Steele parameters. Even though no perfect agreement with the experiment is obtained for this model, it captures the main features of the real material to open further studies involving CO_2 in gas mixtures using simulations as a guide. In addition, a more refined model could be developed by considering the magnitude of the charge redistribution in the carbon wall due to the curvature of FAU-ZTC; however, the development or refinement of models for ZTCs are out of the scope of the current thesis.

The underestimation in the amount adsorbed that remains after considering the curvature can be attributed to the fact that we have simulated a bulk of perfect ZTCs without heterospecies that slightly modify their adsorption properties, including modifications of the slope of the isotherm.

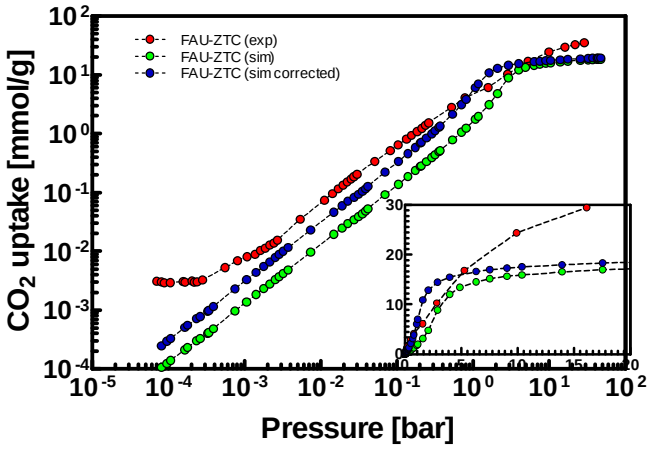

Figure 5.7. Log-log adsorption isotherms for CO_2 at 273K on FAU-ZTC experimental (red) and simulated considering the Steele parameters (green) and the parameters modified to consider the curvature (blue). Inset: linear scale plot of the isotherms. See text for details.

We should bear in mind that the objective of the simulations presented here is not to obtain quantitative agreement with the experimental data, neither replacing them, but to give additional insight into the simulation process and to be used as a guide to the experiments, provided they capture the main features of the experimental isotherms.

5.6. NITROGEN ADSORPTION ISOTHERMS

We present here the N_2 adsorption isotherms at 77K. The simulations with N_2 aim to prove the hypotheses for CO_2 adsorption on ZTCs discussed on the two previous sections. The use of a different probe gas aims to provide more information on the structure of these materials, in particular, on the effect of the extreme curvature in the case of FAU-ZTC, and on the presence of non-accessible pillars for EMT-ZTC. The results of the N_2 adsorption isotherms at 77K are shown in Figure 5.8.

The conclusions obtained from N_2 adsorption data are not directly extendable to the case of CO_2, given that the coverage of N_2 varies much more quickly. Moreover, it has been pointed out by previous studies that carbon materials with narrow microporosity cannot be characterized adequately by N_2 at 77K due to diffusion problems. [19] Experimentally, a very high uptake of N_2 is achieved at low pressure (i.e. ~1 mmol/g at $P < 10^{-5}$ bar); hence, it is not possible to differentiate data for supermicropores. In order to distinguish different sizes of

micropores present in the material, it is necessary to collect data with nitrogen at higher temperature or by using other probe molecules.

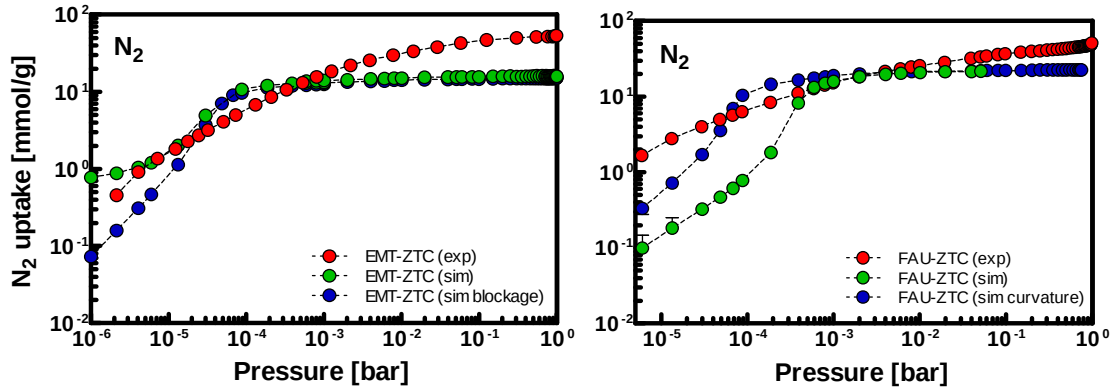

Figure 5.8. Adsorption isotherms for N_2 in EMT-ZTC (left) and FAU-ZTC (right) for experimental results (red), simulated isotherms (green) and corrected simulated isotherms using the two different bias (blue). See text for details.

In both materials, the experimental and simulated curves behave similarly in the limited range of data available for comparison using N_2 at 77 K. The contrast of the adsorption isotherms of N_2 at 77K and CO_2 at 273K for EMT-ZTC is shown in Figure 5.9, while Figure 5.10 shows the comparison for FAU-ZTC.

In Figure 5.9, we again consider only the effect of the accessibility of the cages formed by the carbon pillars and the analysis is split up in two regions. (1) First, above 10^{-4} bar for N_2 and 1 bar for CO_2: it is seen a change in the slope of the simulated adsorption isotherms due to the microporosity being filled out. This results in the compression of the simulated fluid, while experimentally the materials can still adsorb more molecules in their larger pores. Therefore, the model made only of carbon micropores saturates coverages of about 10 mmol/g. (2) Second, low relative pressures, *i.e.* [10^{-6} :2x10^{-5}] bar in the case of nitrogen and [10^{-1} :1] bar for CO_2. It was shown that in this range of pressure, the inclusion of CO_2 in the cages leads to an overestimation of the uptake, and their exclusion correctly predicts the slope of the adsorption isotherm at 273K. It is interesting to observe the opposite behavior in the case of N_2 at 77K. Indeed, if N_2 can access to the pillared cages, the simulated isotherm is then in perfect agreement with the experiment in this low-pressure range. This new insight of the EMT-

ZTCs microstructure reinforces the first assumption, and the criterion to identify the presence of a tubular pillared structure.

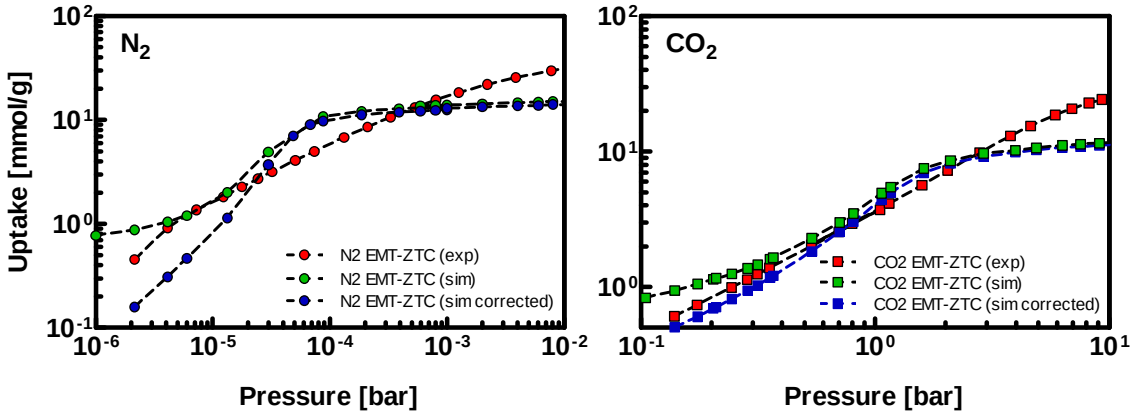

Figure 5.9. Adsorption isotherms for FAU-ZTC for N_2 at 77K (left) and CO_2 at 273K (right).

Another major point that can be extracted from the nitrogen data is that it is possible to characterize and distinguish the presence of different small micropores very close in size using two different probes at different thermodynamic conditions. This is specially important in the case of multimodal microporous materials with complex textural properties.

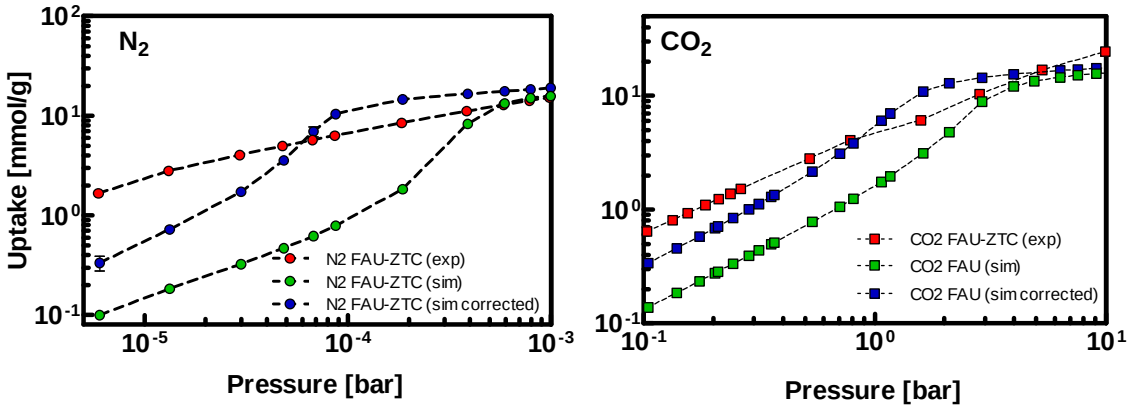

Figure 5.10. Adsorption isotherms for FAU-ZTC for N_2 at 77K (left) and CO_2 at 273K (right).

In the case of FAU-ZTCs, the experimental adsorption values are higher than the simulated ones for both probe molecules (N_2 and CO_2), even if curvature effects are included in the simulations. In this latter case, we observe a crossover at ~$6x10^{-5}$ bar for nitrogen, and ~0.8 bar for carbon dioxide. These crossovers correspond to an inflection point in the simulated

isotherms, meaning that the fluid starts to compress because of the limited accessible volume in the models, whereas the real material contains larger pores. We observe the same behaviour without taking into account curvature effects, and reach the same uptake at pressures of 10^{-3} bar and 6 bar, respectively, for nitrogen and carbon dioxide. This confirms that the curvature effect drastically affects the amount adsorbed. However, other effects are missing in the models. For instance, smaller pores due to eventual collapsed microstructures, hetero-species present from the organic precursors, or the presence of localized partial charges on the carbon structure would adjust better the slope of the experimental isotherm at very low coverage. These aspects have to be considered for further improvements of the model.

5.7. APPLICATION OF ZTCs FOR CO_2 CAPTURE APPLICATIONS

The potential application of ZTCs as CO_2 adsorbents is underlined by comparing them to other common adsorbents. The adsorption isotherms of ZTCs compared to different adsorbents at 298K (zeolites: 13-X; [20] COF-103; [21] MOFs: IRMOF-1, MOF-177, [22] MIL-101; [23] MCM-41 [24] and microporous carbons: [25] Maxsorb 'Kansai Netsu Kagaku Co.' and Norit 'R1 Extra, Norit Co.') are depicted in Figure 5.11a. In the range of 5–15 bar FAU-ZTC has the highest CO_2 uptake at 298 K. The adsorption at this pressure range is important because CO_2 is commonly found in mixtures at low partial pressures. Furthermore, FAU-ZTC is among the materials that have the highest total capacities reported experimentally, being surpassed only by MOF-177 and COF-103 materials. Note that theoretically, there are other more promising candidates available for CO_2 capture (i.e. COF-105, COF-108 [26, 27] and IRMOF-10 [28]).

While MOFs have low thermal stability, some of the unique properties of carbonaceous materials, such as their hardness, abrasion resistance and hydrophobicity, make them a preferred choice for industrial adsorbents. [29] The hydrophobicity of carbon materials is a very important characteristic to avoid quick saturation of the adsorbent under moist conditions. Usually, in industrial operation the flue gas is cooled before being emitted to the atmosphere. In this process water condenses, and latent heat can be recovered for district heating or other processes. The utilization of this energy is desirable; however, in some

processes the wet bulb temperature is too high for heat recovery. [30, 31] Thus, due temperature limitations, the flue gas can contain water. In Figure 5.11b, the adsorption isotherms of CO_2 at 273 K in ZTCs, are compared to different carbon materials taken from the literature (Norit R1 Extra, bituminous coal-based carbon BPL, Maxsorb, A10 fiber and an Activated carbon from Osaka Gas Co.). [25] Among them, Maxsorb is regarded as the most adsorbing carbon material with the highest CO_2 capacity. Interestingly, EMT-ZTC has the same capacity and a higher adsorption uptake up to 20 bar, and FAU-ZTC has a higher adsorption uptake for the entire pressure range. Both ZTCs adsorb 20% more than Maxsorb at 10 bar. This is important for the use of these adsorbents in a Pressure Swing Adsorption (PSA) application (i.e. series at the regeneration 1.0 bar and production 10.0 bar).

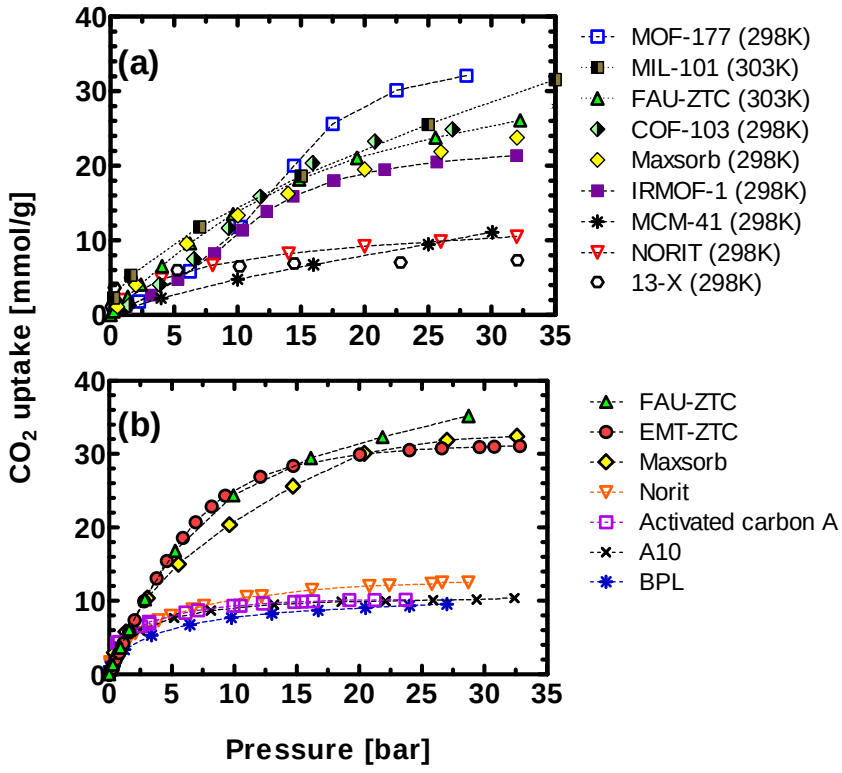

Figure 5.11. Comparison of ZTC performances versus other commonly used materials for CO_2 adsorption. (a) Experimental CO_2 adsorption isotherms at different temperatures (in parenthesis) for different porous materials; (b) CO_2 adsorption isotherms at 273K for different carbon materials. See text for details and references.

However, it is important to consider that the materials synthesized experimentally resembled more closely to the negative template of zeolites provided by the models, the capacity of the adsorption isotherms shown in Figure 5.11 would decrease. The CO_2 adsorption capacity for FAU-ZTC and EMT-ZTC models are 19.2 and 12.5 mmol g^{-1}, respectively. Although these values are closer to the reported values of most carbon materials, the value for FAU-ZTC is among the highest reported for carbon adsorbents. This means that the potential for CO_2 capture of the materials currently synthesized is higher than what would be expected from the perfect negative templates of the parent zeolites.

Consequently, zeolite templated carbons fulfill all the requirements aforementioned and highlight their potential application for CO_2 capture and separation. Research on these materials is currently being conducted and additional works addressing the potential of ZTCs for CO_2 capture have been published. [32, 33]

5.8. CONCLUSIONS

Monte Carlo molecular simulations were used to reproduce the CO_2 adsorption isotherms of two already-known molecular model structures. From the differences found between experiments and simulations, two different scenarios are proposed based on their different morphologies. First, FAU-ZTC showed an extremely high average curvature calculated from its local curvature; this was not observed for EMT-ZTC, which has a more planar structure. With the former material, the empirical Steele potential leads to an apparent inaccurate prediction of the solid–fluid interactions, underestimating the polarizability of curved sp^2 carbons. By accounting empirically for this latter effect a better agreement in the simulated adsorption isotherms was found. However, even accounting for the curvature of the material there is a mismatch between the experimental and simulated adsorption isotherms. Thus, the FAU-ZTC model requires further refinements, for instance considering the presence of hetero-species from the organic precursors, the presence of localized partial charges on the carbon structure or a larger pore size distribution due to the existence of voids and vacancies among the different crystallites. It is expected that the inclusion of those effects will increase the agreement of the FAU-ZTC model with the experimental results.

Second, in the case of the EMT-ZTC model, an overestimated amount of adsorbed CO_2 at very low pressure was found. It was possible to remove completely the discrepancy at low pressures by blocking the pillared structures in this carbon model. Experimentally, the pore blocking might be caused either by defects inside the cages or by slow diffusion of CO_2 in very small micropores. Interestingly, this study shows that adsorption isotherms of CO_2 at room temperature allow the size differentiation between narrow-micropores, as an interesting complementary probe to nitrogen molecules to characterize the textural properties of ZTCs.

Moreover, comparative CO_2 adsorption data on two ZTCs is reported. These two ZTCs compare favorably with the most CO_2 adsorbing organic frameworks at room temperature, and furthermore FAU-ZTC is shown to have the highest reported CO_2 adsorption capacity for carbonaceous materials. In the light of mitigation of CO_2 emissions, ZTCs are presented as promising capture materials under hostile environments, because of their extreme stiffness and stability.

REFERENCES

1. Ducrot-Boisgontier C, Parmentier J, Faour A, Patarin Jl, Pirngruber GD. *"FAU-Type Zeolite Nanocasted Carbon Replicas for CO2 Adsorption and Hydrogen Purification"*. Energy & Fuels. **2010**;24 (6).3595-602.

2. Yang RT. *"Gas separation by adsorption processes"*. Singapore; River Edge, N.J.: World Scientific; **1997**.

3. Nishihara H, Hou P-X, Li L-X, Ito M, Uchiyama M, Kaburagi T, et al. *"High-Pressure Hydrogen Storage in Zeolite-Templated Carbon"*. J Phys Chem C. **2009**;113 (8).3189-96.

4. Roussel T, Bichara C, Gubbins KE, Pellenq RJM. *"Hydrogen storage enhanced in Li-doped carbon replica of zeolites: A possible route to achieve fuel cell demand"*. J Chem Phys. **2009**;130 (17).174717-6.

5. Builes S, Roussel T, Ghimbeu CM, Parmentier J, Gadiou R, Vix-Guterl C, et al. *"Microporous carbon adsorbents with high CO2 capacities for industrial applications"*. Phys Chem Chem Phys. **2011**;13 (35).16063-70.

6. Nishihara H, Yang Q-H, Hou P-X, Unno M, Yamauchi S, Saito R, et al. *"A possible buckybowl-like structure of zeolite templated carbon"*. Carbon. **2009**;47 (5).1220-30.

7. Gaslain FOM, Parmentier J, Valtchev VP, Patarin J. *"First zeolite carbon replica with a well resolved X-ray diffraction pattern"*. Chem Commun. **2006** (9).991-3.

8. Lenosky T, Gonze X, Teter M, Elser V. *"Energetics of negatively curved graphitic carbon"*. Nature. **1992**;355 (6358).333-5.

9. Potoff JJ, Siepmann JI. *"Vapor-liquid equilibria of mixtures containing alkanes, carbon dioxide, and nitrogen"*. AIChE J. **2001**;47 (7).1676-82.

10. Kuznetsova A, J. T. Yates J, Simonyan VV, Johnson JK, Huffman CB, Smalley RE. *"Optimization of Xe adsorption kinetics in single walled carbon nanotubes"*. J Chem Phys. **2001**;115 (14).6691-8.

11. Roussel T, Bichara C, Pellenq RJM. *"Selenium and Carbon Nanostructures in the Pores of AlPO4-5"*. Adsorption. **2005**;11 (0).709-14.

12. Frenkel D, Smit B. *"Understanding molecular simulation: from algorithms to applications"*. San Diego: Academic Press; **2002**.

13. Blas FJ, Vega LF. *"Thermodynamic behaviour of homonuclear and heteronuclear Lennard-Jones chains with association sites from simulation and theory"*. Mol Phys. **1997**;92 135-50.

14. Jagiello J, Thommes M. *"Comparison of DFT characterization methods based on N2, Ar, CO2, and H2 adsorption applied to carbons with various pore size distributions"*. Carbon. **2004**;42 (7).1227-32.

15. Snurr RQ, Bell AT, Theodorou DN. *"Prediction of adsorption of aromatic hydrocarbons in silicalite from grand canonical Monte Carlo simulations with biased insertions"*. J Phys Chem. **1993**;97 (51).13742-52.

16. Roussel T. *Simulation Numerique de Repliques de Zeolithes en Carbone : Structures et Proprietes d'adsorption en vue d'une Application au Stockage d'hydrogene*. Marseille: Université de la Méditerranée Aix-Marseille II; 2007.

17. Klauda JB, Jiang J, Sandler SI. *"An ab Initio Study on the Effect of Carbon Surface Curvature and Ring Structure on N2(O2)−Carbon Intermolecular Potentials"*. J Phys Chem B. **2004**;108 (28).9842-51.

18. Nguyen TX, Cohaut N, Bae J-S, Bhatia SK. *"New Method for Atomistic Modeling of the Microstructure of Activated Carbons Using Hybrid Reverse Monte Carlo Simulation"*. Langmuir. **2008**;24 (15).7912-22.

19. Lozano-Castelló D, Cazorla-Amorós D, Linares-Solano A. *"Usefulness of CO2 adsorption at 273 K for the characterization of porous carbons"*. Carbon. **2004**;42 (7).1233-42.

20. Cavenati S, Grande CA, Rodrigues AE. *"Adsorption Equilibrium of Methane, Carbon Dioxide, and Nitrogen on Zeolite 13X at High Pressures"*. J Chem Eng Data. **2004**;49 (4).1095-101.

21. Furukawa H, Yaghi OM. *"Storage of Hydrogen, Methane, and Carbon Dioxide in Highly Porous Covalent Organic Frameworks for Clean Energy Applications"*. J Am Chem Soc. **2009**;131 (25).8875-83.

22. Millward AR, Yaghi OM. *"Metal−Organic Frameworks with Exceptionally High Capacity for Storage of Carbon Dioxide at Room Temperature"*. J Am Chem Soc. **2005**;127 (51).17998-9.

23. Llewellyn PL, Bourrelly S, Serre C, Vimont A, Daturi M, Hamon L, et al. *"High Uptakes of CO2 and CH4 in Mesoporous Metal ▪ Organic Frameworks MIL-100 and MIL-101"*. Langmuir. **2008**;24 (14).7245-50.

24. He, Seaton NA. *"Heats of Adsorption and Adsorption Heterogeneity for Methane, Ethane, and Carbon Dioxide in MCM-41"*. Langmuir. **2005**;22 (3).1150-5.

25. Himeno S, Komatsu T, Fujita S. *"High-Pressure Adsorption Equilibria of Methane and Carbon Dioxide on Several Activated Carbons"*. J Chem Eng Data. **2005**;50 (2).369-76.

26. Babarao R, Jiang J. *"Exceptionally high CO2 storage in covalent-organic frameworks: Atomistic simulation study"*. Energy & Environmental Science. **2008**;1 (1).139-43.

27. Lan J, Cao D, Wang W, Smit B. *"Doping of Alkali, Alkaline-Earth, and Transition Metals in Covalent-Organic Frameworks for Enhancing CO2 Capture by First-Principles Calculations and Molecular Simulations"*. ACS Nano. **2010**;4 (7).4225-37.

28. Babarao R, Jiang J. *"Molecular Screening of Metal−Organic Frameworks for CO2 Storage"*. Langmuir. **2008**;24 (12).6270-8.

29. Ho Y-S. *"Selection of optimum sorption isotherm"*. Carbon. **2004**;42 (10).2115-6.

30. Aresta M. *"Carbon Dioxide Recovery and Utilization"*. Aresta M, editor: Kluwer Publication; **2003**.

31. Kröber H, Teipel U. *"Micronization of Organic Substances by Supercritical Fluid Processes"*. Chem Eng Technol. **2004**;27 (5).510-4.

32. Youn H-K, Kim J, Chandrasekar G, Jin H, Ahn W-S. *"High pressure carbon dioxide adsorption on nanoporous carbons prepared by Zeolite Y templating"*. Materials Letters. **2011**;65 (12).1772-4.

33. Zhou J, Li W, Zhuo SP. *"CO2 Adsorption Performance of N-Doped Ordered Microporous Carbons Templated from Zeolite HY"*. Advanced Materials Research. **2011**;284-286 2102-5.

Chapter VI

Functionalized Silica for Carbon Dioxide Capture*

"Build for your team a feeling of oneness, of dependence on one another and of strength to be derived by unity."

Vince Lombardi

Organic-inorganic hybrid materials are an emerging kind of materials with promising characteristics for the separation of gas mixtures by adsorption. These materials are molecular composites with organic and inorganic components. Thanks to new molecular approaches, it is possible to tailor-make new functional hybrid materials with enhanced properties for specific applications. For instance, it is possible to use the desirable characteristics of amines for CO_2 capture (see chapter 3 for details), while avoiding the energetic penalty and the loss of amines due to degradation by introducing the amine functionalities into an adsorbent with a large surface area.[1] The idea behind the use of hybrid materials for CO_2 capture is to introduce an organic group that interacts strongly with CO_2 on an inorganic matrix decreasing (i) the energy requirements for desorbing the CO_2 and (ii) the equipment corrosion due to the presence of the amines inside the adsorbent.

Porous silica can be used as a support media of organic molecules such as amines. Merging the inherent sorptive behavior of porous solids with amines offers a route to favor physisorption over chemisorption, thus reducing the energy cost of regeneration against the CO_2 capture

*** The results discussed in this chapter were published in "Understanding CO2 capture in Amine-Functionalized MCM-41 by Molecular Simulation". J. Phys. Chem. C, 116, 4, 3017–3024. (2012)**

with conventional amines. One way to functionalize these materials is to use the reaction of silanol groups in the silica with organosilanes to form organic-inorganic hybrid materials.[2] The basic structure of organosilanes is $R_nSi(OR)_{4-n}$, where R can be an alkyl, aryl, or organofunctional group. The silanol groups can react with one of the OR groups in the organosilane according to the following reaction.

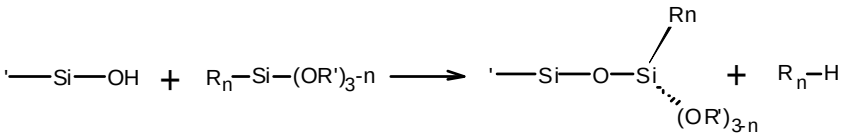

Mainly, there are two different ways to link amino moieties into silica surfaces: (i) co-condensation and (ii) postsynthesis silanation. In the former method, a fraction of the precursor of the mesoporous silica is replaced by aminosilane, which is incorporated into the resulting mesoporous material. However, a fraction of the aminosilane may get within the walls of the silica, creating defects on the lattice. The postsynthesis consists of modifying the inner surface of silica with an organic group that covalently bonds to the nonbridging oxygens. As a result, the organic units lay on the surface, opposed to the co-condensation, where they project into the pores.[3, 4] One of the most common postsynthesis methods is the reaction of organosilanes with the silanol groups in the silica surface.

The main differences obtained in the resulting functionalized materials by using the aforementioned methods are: (i) in the co-condensation method, only the tail of the organic groups project through the surface, that is, the R_n fraction of the original organosilane, whereas in a postfunctionalized material the entire organosilane remains on the surface. The silica in the silane is bonded directly to one nonbridging oxygen that was previously on the surface of the support, that is, a group similar to $R_nSi(OR)_{3-n}$ remains on the surface. (ii) The crystal structure remains unmodified with the post-functionalization approach, while the co-condensation can change the lattice structure of the functionalized product. Figure 6.1 illustrates the differences on the size over the surface obtained from the same precursor for the two different methods.

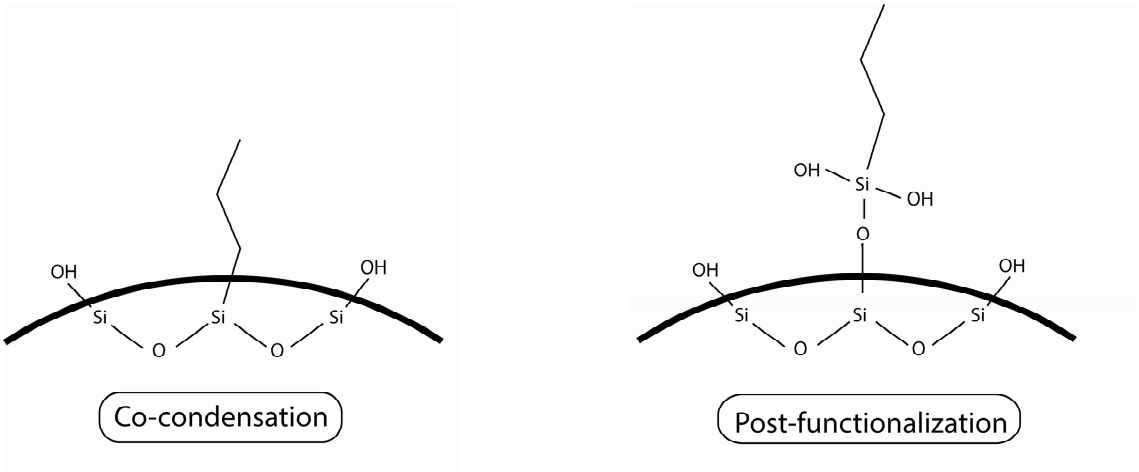

Figure 6.1. Illustration of the differences between co-condensation and post-functionalization for a sample propylthriethoxysilane molecule.

In this chapter, the different interactions of the grafted chains during the adsorption of CO_2 using silica models functionalized via postsynthesis methods with alkoxysilanes were studied. In order to consider post-functionalized silanes, the entire branched molecule was considered as the functional group covalently bonded to the surface. This implies the simulation of branched molecules, which were allowed to move constrained by a branched point. Since this kind of systems are challenging from a simulation point of view, we developed an efficient methodology to build the models of silica surfaces post-grafted with aminosilane groups. Moreover, in contrast to previous simulations studies which overlooked the chemisorbed CO_2 in amine-functionalized silica, we took into account both the chemisorbed and physisorbed CO_2 by explicitly considering the carbamate formation of the CO_2-amine reaction. Using this methodology, adsorption isotherms for different degrees of surface functionalization were studied comparing them with available experimental data for validation. The methodologies presented in this chapter produce simulated adsorption isotherms directly comparable to experimental data. Hence, making it possible to obtain a better insight of the sorption mechanism in amine-functionalized silica materials.

6.1. PREVIOUS WORK ON AMINE-FUNCTIONALIZED SILICA

Experimental studies on the use of postsynthesis amine functionalization of silica surfaces for CO_2 capture have become an active area of research in recent years (see review on chapter 3). Numerous works on this field have focused on understanding the interactions among CO_2, the functionalized chains and the silica surface. [5-11] The common findings of these experimental studies are: (i) the presence of water increases the reaction of CO_2 and the amines, increasing the adsorption but also decreasing the desorption. (ii) The chemisorption occurs mainly at low pressures and the CO_2 captured at higher pressures is physisorbed.

Although there are numerous experimental studies on the adsorption of CO_2 by amine-functionalized silica, the interactions and effects of amines on amorphous surfaces are not yet completely understood. Additional insight into this process, on the molecular level, can be gained by the use of molecular simulations. However, simulation works on this field are still scarce, and none of them, to our knowledge, has focused on the specific effect of postsynthesis functionalized chains on the adsorption of CO_2. Moreover, previous molecular simulation studies with amines and CO_2 have not considered the effect of the chemically captured CO_2. Taking into account the main effects of the sorption of CO_2 on hybrid materials will enable to optimize the conditions for CO_2 capture in this kind of materials. Hence, the purpose of this work is to give some insight into the effect of postsynthesis-functionalized chains on the adsorption of CO_2.

Previous simulations studies on CO_2 capture on amine-functionalized materials have not consideted the effect of chemisorption on the adsorption; these studies have assumed all the CO_2 to be physisorbed in the system. For instance, Chaffe [12] using molecular simulations, calculated the geometric constraints and the interactions that take place on the surface of APTMS grafted on mesoporous silica. The APTMS chains were placed in an orderly fashion at the most energetically favorable grafting sites; however, no studies of adsorption were performed. Schumacher et al. [13] calculated the adsorption of CO_2 on MCM-41 functionalized with amine or phenyl groups. The grafting of the molecules on the model MCM-41 emulated the experimental co-condensation by considering the organic groups to

be linked directly to a silicon atom in the MCM-41. Williams et al.[14] studied a series of different organic groups functionalized on MCM-41, studying their different CO_2 capture capacities. In this latter study, the authors used the same unit cell for the support and the functionalized material. Although they claimed that the simulations emulated conditions similar to those of post-functionalization, they only took into account in the simulations the organic part of the chains, not considering the silanes part, this type of grafting resembles more closely the obtained by co-condensation. The limited number of published jobs on molecular simulations of grafted amines has not yet fully considered adsorption of CO_2 on post-functionalized organosilanes. Moreover, previous works have considered that all the CO_2 captured by the grafted amines was adsorbed by physisorption only. In the following sections we will show (i) the development of a methodology for the simulation of postfunctionalized silica materials and (ii) the incorporation into the GCMC method of a mean of simulating the contribution of chemisorption into the adsorption isotherms of postfuncionalized materials.

6.2. SOLID ADSORBENT MODELS

The first step to reproduce the functionalized silica is to build a realistic model that can represent the experimental solid material. Then, on the basis of that model, it is possible to tether the aminosilanes to the surface silanols to obtain the organic-inorganic materials.

6.2.1. Silica xerogel

Atomistic models of silica gel were built following the works of MacElroy and Raghavan. [15, 16] Silica gels, such as aero- and xero- gels are composed of a random network of spherical particles. [17] Hence, they can be modeled as a randomly arranged rigid matrix of solid spheres. The full details on the silica gel model can be found elsewhere. [15, 16]

The general procedure used for creating the silica gel models is as follows:

1) Initially a hard-sphere model is used to fill a cubic box. The radius of the spheres is initially obtained from the desired surface area and the dimensions of the box are adjusted to the

desired porosity (the number of spheres has to be fixed). The spheres are placed at random positions until they fit in the simulation cell. After this initial model is built, the spheres are interconnected using Lennard-Jones interactions for the spheres, and minimizing the energy by allowing them to move. The interconnected spheres are then used as the basis for the atomistic model. These hard spheres are later replaced by amorphous silica spheres to reproduce the silica gel.

2) The silica spheres are built using a realistic model for amorphous silica. First, the initial amorphous silica blocks were taken from the Materials Studio structures database. [18] Then, silica spheres are carved out from this amorphous silica model. A sphere is cut from the amorphous silica model with a radius equal to the radius of the hard spheres and a random central point inside the silica block. The silica atoms within this radius are kept, and all the oxygen atoms in the system bonded to these silica atoms are also included in the silica sphere. Nonbridging oxygens in the surface of the sphere are obtained by cutting the periodic silica structure in such manner. Then, all the nonbridging oxygen atoms are connected to hydrogen atoms to form surface hydroxyl groups. The final structure generated by this procedure provides a sufficiently realistic model of amorphous silica, particularly of its hydroxylated surface.

3) Finally, the hard spheres are replaced by the spheres carved from amorphous silica, obtaining the silica gel model.

4) The surface area and the pore volume of the generated model are determined using the method proposed by Düren et al. [19] The resulting values are compared to the desired surface area and pore volume, if they are outside the desired tolerance the procedure is repeated adjusting the radius of the hard-spheres.

In Figure 6.2 a graphic representation of the generation procedure at each different step is shown, each of the steps is described briefly next to a series of snapshots created during the construction of a sample model.

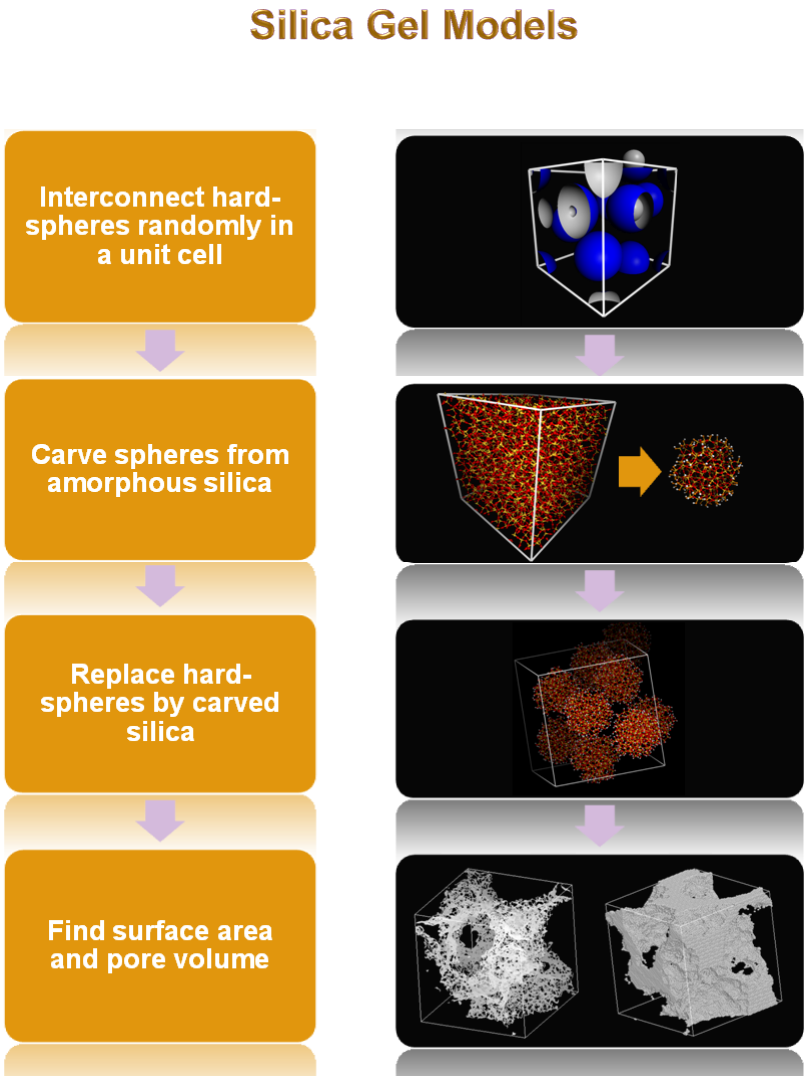

Figure 6.2. Illustration of the protocol followed for the generation of the silica gel models.

The aforementioned steps are repeated until the model obtained by replacing the carved silica is satisfactory (using as convergence criteria the surface area and the pore volume). Figure 6.3 depicts a flowchart of this generation procedure.

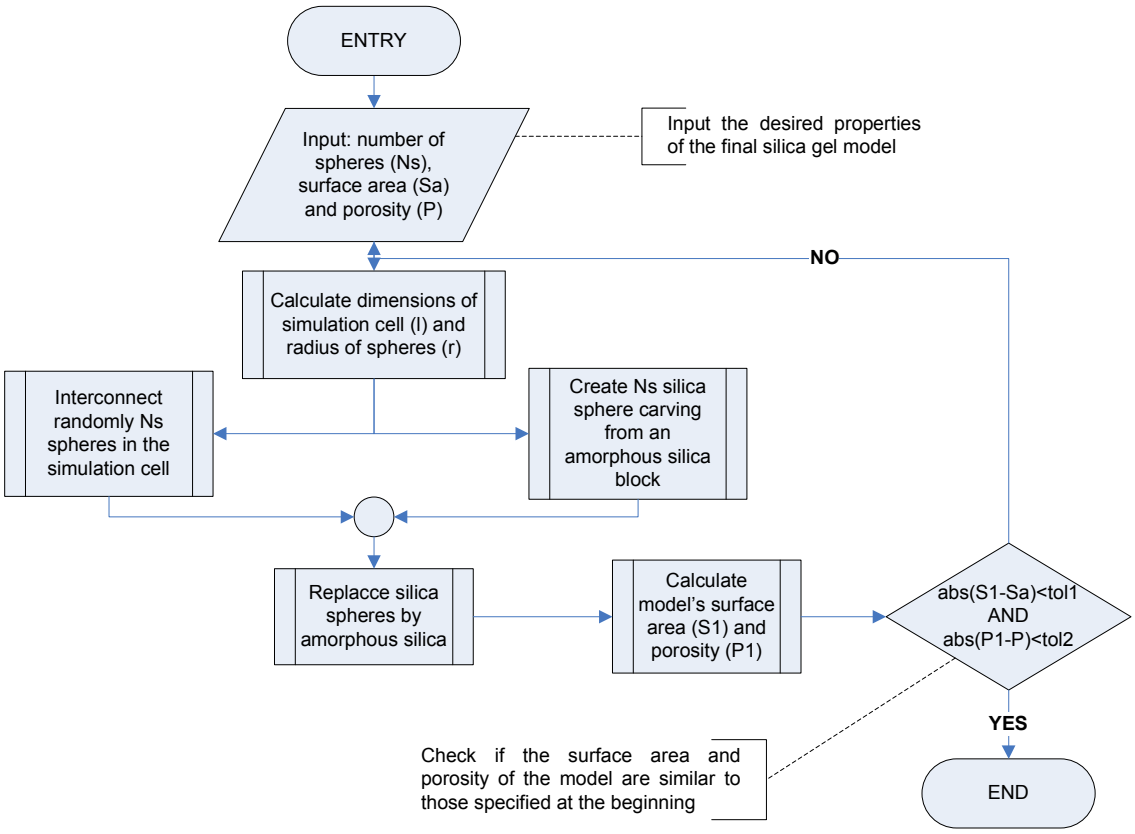

Figure 6.3. Representation of the method used to generate the silica gels.

For the initial code development and understanding of the basic interactions between the chains and the adsorbed materials a model of silica xerogel with a BET surface area of 907 m^2/g, a pore volume of 0.21 cm^3/g and 4.86 surface OHs/nm^2 was generated. The xerogel model was created using 4 interconnected silica spheres with a radius of 1.8 nm in a cubic unite cell of 5.7 nm length. We used this model because silica xerogels are materials with high surface area and high concentration of surface silanol groups. A snapshot of this model xerogel is depicted in Figure 6.4.

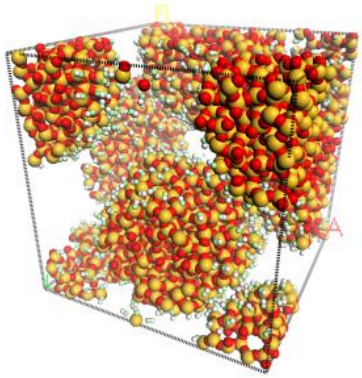

Figure 6.4. Model silica xerogel used for the simulations of functionalization. Color key: Si: yellow; bridging O: red; nonbridging O: green; H: white. The silanol groups are displayed as balls and sticks, and the internal silica are represented as van der Waals spheres.

6.2.2. MCM-41 model

The atomistic models of MCM-41 are generated following the work of Pellenq et al.[20] The full details of the generation of the model can be found elsewhere. [20, 21] Unlike in chapter 4 where we used a cylindrical surface model of MCM-41, in this chapter we are interested in the amorphous silica surface of MCM-41. For this reason, the ideal cylindrical pore model cannot be used to represent MCM-41; an atomistic pore model is used to reproduce the hydroxylated surface of mesoporous silica.

MCM-41 consists of a hexagonal array of straight cylindrical unidirectional and non-interconnected pores with amorphous walls. The model of this mesoporous adsorbent is generated by carving out a hexagonal array of cylindrical pores in a 6.42 x 4.28 x 4.28 nm^3 model of amorphous silica, this structure was extracted from the database available in the Materials Studio software package. [18] The silica atoms outside the volume of the carved cylinder are kept, and all also the oxygen atoms bonded to these silica atoms are included in the silica model. The procedure of forming the surface silanol groups is analog to the one explained in the previous section for the silica gel. The resulting model was subjected to geometry optimization using the universal force field[22] in Materials Studio.

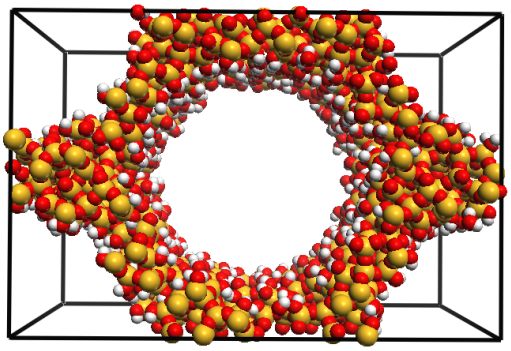

Figure 6.5. MCM-41 used for the simulations of functionalization. Color key: Si: yellow; bridging O: red; H: white.

A model of MCM-41 with a BET surface area of 983.4 m^2/g, a pore volume of 0.61 cm^3/g and 5.6 surface OHs/nm^2 was generated by carving cylinders with a radius of 16.5 nm. The obtained model is depicted in Figure 6.5. These properties are similar to those usually found in the literature for this material. MCM-41 was chosen as the model structure because our goal is to relate the simulations performed with the model to some of the data available and most of the published data for amino functionalized adsorbents for CO_2 capture employ MCM-41.

6.3. FUNCTIONALIZATION OF SILICA SURFACES

The first approach to model the functionalization of silica surfaces is to simplify the chemistry of the reactions for the organic-inorganic hybrids. Experimentally the silanol groups in the surface of the silica react with siloxanes from the organic chain; in addition to binding to the surface the chains can also form bonds among themselves. In this work we simplified the problem by considering that (i) all the functionalized chains are covalently tethered to the surface and (ii) no bond is formed between neighboring chains. Even if polymerization is possible, the main phenomenon is still the grafting to the surface, and hence this assumption should not have a great influence on the final adsorption results.

The functionalized model consists of the solid silica with a number of surface silanol groups replaced by organic groups. For simplicity, we consider that the molecules react with the

surface in a monodentate manner and that the other two alkoxy moieties hydrolyze forming two silanols. A sample scheme of APTES in the surface of the silica as considered by the simulations is depicted in Figure 6.6.

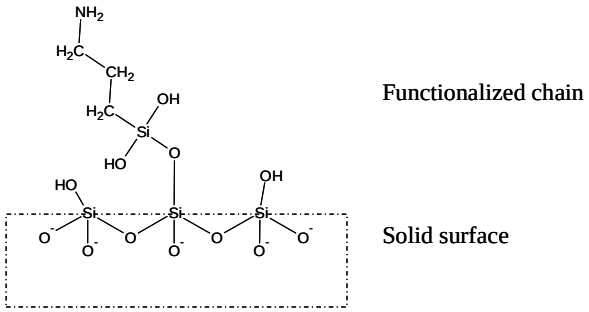

Figure 6.6. Functionalized chain from the coupling agent APTES and the silica surface (as considered by the model used in this work).

Although the silica material can be modeled as a rigid structure, according to the experimental behavior of the system, the surface groups should move during the simulations of adsorption of CO_2. Therefore, the simulations of adsorption require a method capable of regrowing branched chains efficiently; the different torsion and bending angles in the surface groups are handled using a coupled-decoupled configurational bias (CDCB) algorithm. [23] Additionally, we use pregenerated Gaussian distributions for increasing the acceptance rates of the probabilities of generating the bending and torsion angles for the grafted molecules, these biased distributions are corrected in the acceptance rules. [24] The expressions and the parameters for the calculation of the energy of the surface group are described in detail in the next section.

The method proposed here is different to the one used previously by other authors for the simulations of co-condensation. [13, 14] In the simulations of co-condensation, the the dimensions of the unit cell were modified and the silanol groups were replaced by the R_n fraction of the silanes. The surface groups were introduced to the silica model by randomly replacing selected silanols by the functional groups. Then, an energy minimization routine was performed by swapping the surface groups to different possible grafting sites for a predefined number of steps.

In our approach we use a systematic approach for the functionalization of the surface. For all the possible substitution sites in the silica (i.e., the surface silanols), we calculate the Rosenbluth factor (W_i) for the first and second beads of the organic chain that replaces the silanol (Equation 6.2). We consider as the first atom in our chains the oxygen atom bonded to the surface silica and as the second atom the silicon bonded to the organic chain (see Figure 6.6). The position of the first bead for each chain is selected according to the probability P_{chain} given by Equation 6.2. This approach is similar to the experimental postsynthesis because the molecules are not grafted to the surface unless they have enough available pore space.

$$Wi = \frac{\exp(-\beta U_k)}{\sum_{j=1}^{N_{pos}} \exp(-\beta U_j)} \tag{6.1}$$

$$P_{chain} = W_1 * W_2 \tag{6.2}$$

where U_k is the intramolecular energy of the bead i replacing the hydroxyl group k; and N_{pos} is the number of remaining, non-substituted, surface silanols in the silica. Using Equation 6.1 for selecting the grafting point means that the lowest energy position among all the possible surface silanols is preferentially chosen. However to avoid bias against certain positions, all the accessible sites should have a non-null probability of being chosen. . For illustration purposes a schematic drawing of the grafting of silica xerogel with APTES is shown in Figure 6.7.

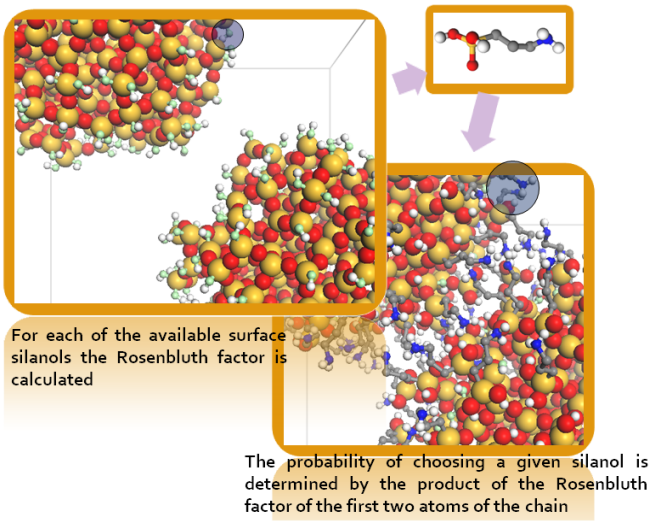

Figure 6.7. Schematic snapshots of the grafting procedure on a sample silica xerogel using APTES.

Once the location of the grafted ends for all chains has been selected we start to grow the remaining beads by using the CDCB algorithm. The chains are grown sequentially bead by bead. The next chain is not started until the preceding one has been grown entirely. If at some point it is not possible to continue the chain growth, then one chain is selected at random from the already grown chains or the currently grown chain. The grafting point for this random chain is changed to a different position, using Equation 6.2 on the remaining surface silanols. The loop continues until all surface groups have been successfully grown. This grafting scheme is similar to the approach followed by Chaffee[12], where the most favorable position for grafting a full chain was chosen unless there was an overlap among previously grown chains. However, in our case, the method is implemented in an automated and extendable approach. The basic flowchart of the implemented functionalization algorithm is depicted in Figure 6.8.

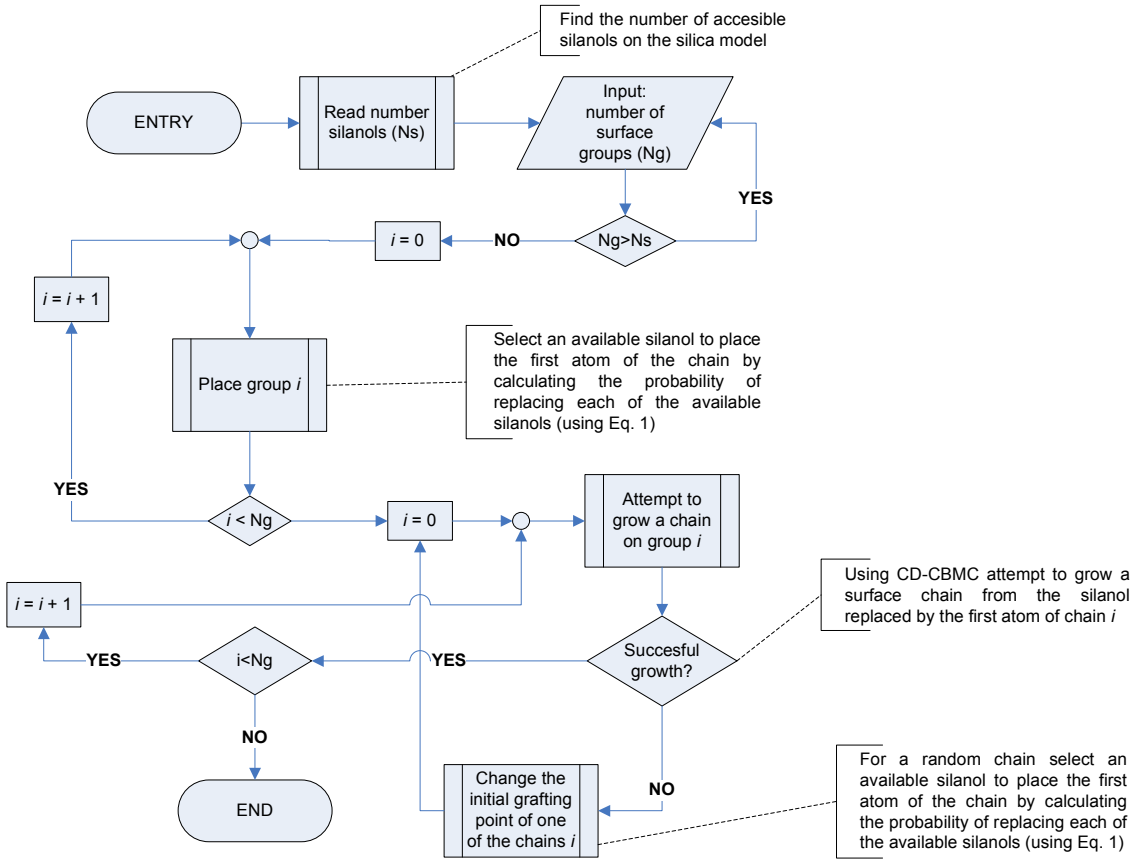

Figure 6.8. Flowchart of the algorithm for grafting the surface groups.

Following the preceding approach, the maximum loading of the surface groups is limited by the number of available silanol groups in the surface, the length, and shape of the grafted chain and the geometry of the surface

6.4. SIMULATION METHODOLOGY

The CO_2 adsorption process in the functionalized silica models is simulated using GCMC.

- The soft-SAFT equation of state is used to relate the pressure of the bulk fluid to the chemical potential of the adsorbate and the temperature of the system. [25, 26]
- The adsorption isotherms are calculated by simulating the average number of CO_2 molecules at different sets of bulk pressures at constant temperature and volume. For each value of pressure in the isotherm, 1.0×10^7 MC steps are used for equilibration and 1.4×10^7 MC steps for data collection.
- The fluid molecules undergo GCMC trials: insertion, deletion, and translation/rotation. As the surface chains have one end fixed to the solid silica, the grafted chains have a fixed amount of molecules; and they are subjected to regrowing trials only. The positions of the different atoms of the chain are recalculated during the chains regrowth using the CDCB method with pregenerated Gaussians for the bending angles and torsional potentials.[22, 23]
- The simulation cell is periodic in three dimensions. The insertion and deletion of fluid molecules is restricted to the open pore space, using a cavity bias, to avoid CO_2 molecules being adsorbed inside the silica skeleton. [27]
- The intermolecular interactions are calculated through pairwise-additive Lennard-Jones (LJ) 12-6 potentials for the repulsive and dispersive terms, and Coulombic potentials for the first-order electrostatic contributions. [28] The interactions between LJ points are computed according to the Lorentz–Berthelot combining rules. The cutoff radius for the LJ interactions is at least six times the collision diameter of the fluid molecules (~1.8 nm). [29]

- The standard Ewald technique is employed for calculating the Coulombic potential. [28] The values of the Ewald parameters are chosen to achieve relative errors of $<10^{-5}$ in the Coulombic energy calculations.

The expression for the calculation of the energy during each trial is given by Equation 6.3.

$$U = \sum_i \sum_{j>i} 4\varepsilon_{ij}\left[\left(\frac{\sigma_{ij}}{r_{ij}}\right)^{12} - \left(\frac{\sigma_{ij}}{r_{ij}}\right)^{6}\right] + \sum_i \sum_{j>i} \frac{q_i q_j}{4\pi\varepsilon_0 r_{ij}} + \sum \frac{k_i^{angle}}{2}\left(\theta_i - \theta_i^{eq}\right)^2 + \sum U^{tors} \tag{6.3}$$

where r_{ij} is the distance between points i and j; ε_{ij} and σ_{ij} are the LJ parameters; q_i is the point charge of i; ε_0 is the vacuum permittivity; k_i^{angle}, θ_i and θ_i^{eq} are the bending constant, the bending angle and the equilibrium bending angle respectively; U_{tors} is the energy associated with the torsion of the molecules. It can be described by one of two different sets of cosine series.

$$U^{tors} = C_1\left(1+\cos(\phi)\right) + C_2\left(1-\cos(2\phi)\right) + C_3\left(1+\cos(3\phi)\right) \tag{6.4}$$

$$U^{tors} = C_0 + \sum_{i=1}^{6} C_i \cos(i\phi) \tag{6.5}$$

ϕ is the current dihedral angle and C_i are constant parameters.

The interactions of the CO_2 molecules were modeled using the TraPPE potential[30]. This potential treats carbon dioxide as a rigid molecule with 3 interaction sites. CO_2 molecules are taken to be rigid, with a C-O bond length of 0.116 nm and an O-C-O angle of 180°. The Lennard-Jones parameters for the solid silica atoms in the xerogel were obtained from the works of MacElroy in amorphous silica.[15, 31] While the parameters for MCM-41 were obtained from previous simulations on the adsorption of CO_2 on mesoporous silica.[13, 32] For both materials, silica gel and MCM-41, the effective potentials employed consider the LJ interactions of the silicon atoms embedded by the oxygen potential. However, due to the distinct geometry of the structures different values for the LJ well depth are commonly used for simulating these silica surfaces. The point charges for the solid material were calculated by

Brodka et al. from semiempirical calculations for silica clusters; [33] and they have been used previously to simulate the adsorption of CO_2 on mesoporous silica. [13] The parameters for the intermolecular interactions of the fluid and the solid molecules are given in Table 6.1.

Table 6.1. Parameters for the non-bonded interactions for the amorphous silica and carbon dioxide.

Site	σ (nm)	ε/k_B (K)	q (e)	ref
		Silica		
Si	0	0	-0.5	[31, 33]
$O_{bridging}$	0.2708	228.4 /185.0[1]	0.0	[31, 33]
$O_{nonbridging}$	0.3000	228.4 / 185.0[1]	-0.7	[31, 33]
H	0	0	-0.7	[31, 33]
		CO_2		
C	0.2785	29.999	0.6645	[34]
O	0.3064	82.997	-0.33225	[34]
		N_2		
N	0.331	36.0	-0.482	[30]
COM[2]	0.0	0.0	0.964	[30]

The parameters for the siloxane part of the organic chains are taken from the MM2 force field for siloxane compounds. [35] The parameters for the rest of the organic surface groups are taken from the TraPPE force field. The hydrogens bonded to carbon atoms are not explicitly considered in the models; their interactions are embedded in the potential of the carbon atoms. The charges in the surface chains have to be adjusted to maintain electrical neutrality in the simulation cell. The parameters for the intramolecular energy of the functionalized groups are listed in Tables 6.2-6.5.

The non-bonded parameters for the grafted APTES of chains are included in Table 6.2.

[1] **Values of the LJ well depth for the silica xerogel / MCM-41 respectively**

[2] **Center of mass of the N_2 molecule**

Table 6.2. Parameters for the non-bonded interactions for the aminosilane.

Site	σ (nm)	ε/k_B (K)	q (e)	ref
	Amino propyl chains			
[O]-Si	0.28	55.0	-0.4	[36]
[Si]	0.58	0.5	0.16	[37]
Si[O]-H	0.302	93.0	-0.675	[38]
SiO-[H]	0.0	0.0	0.46	[38]
Si[CH_2]CH_2	0.395	46.0	0.1	[37]
CH_2[CH_2]CH_2	0.395	46.0	0.1	[37]
CH_2[CH_2]NH_2	0.395	46.0	0.28	[39]
[N]H_2	0.334	111.0	-0.867	[39]
HN-[H]	0.0	0.0	0.3685	[39]

The bonded parameters for the functionalized chains are presented in Tables 6.3-6.5.

Table 6.3. Bond lengths for the grafted chains.

Bond	r_0 (nm)	ref
	Amino propyl	
O-Si	0.16	[40] / [41]
Si-O(H)	0.16	[42]
Si-CH_2	0.191	[41]
O-H	0.0945	[38]
CH_2-CH_2	0.154	[37]
CH_2-N(H_2)	0.1448	[39]
N-H	0.101	[39]

Table 6.4. Equilibrium bond angles and force constants for the grafted chains.

Bonds	θ_i^{eq} (deg)	k_i^{angle}/k_b (K/rad^2)[3]	ref
	Amino propyl		
O-Si-O	109.47	151106.3	[43]
O-Si-CH_2	108.5	25340.0	[44]
Si-O-H	114.9	----	[40]

[3] **Bond angles with no k_i^{angle} value are rigid.**

Bonds	θ_i^{eq} (deg)	k_i^{angle}/k_b (K/rad^2)[4]	ref
	Amino propyl		
Si-CH_2-CH_2	110.0	96223.2	[41]
CH_2-CH_2-CH_2	114.0	62500.0	[37]
CH_2-CH_2-N	109.5	56600.0	[39]
CH_2-N-H	112.9	62500.0	[39]
H-N-H	106.4	43910.0	[39]

Table 6.5. Torsional parameters for the grafted chains.

Equation 6.4

Torsion group	C_1/k_b (K)	C_2/k_b (K)	C_3/k_b (K)	ref
O-Si-O-H	0	0	163.56	[38]
CH_2-Si-O-H	0	0	163.56	[38]
O-Si-CH_2-CH_2	0	0	84.03	[44]

Equation 6.5

Torsion group	C_0/k_b (K)	C_1/k_b (K)	C_2/k_b (K)	C_3/k_b (K)
CH_2-CH_2-CH_2-N	438	481	150	-115
CH_2-CH_2-N-H	190.0	47.8	105	-105
	C_4/k_b (K)	C_5/k_b (K)	C_6/k_b (K)	ref
CH_2-CH_2-CH_2-N	-0.57	0.08	-0.01	[39]
CH_2-CH_2-N-H	0	0	0	[39]

According to experimental isosteric heat of adsorption and IR data, physisorption is the leading mechanism of adsorption of CO_2 in silica surfaces functionalized with monoamines, except at low pressures.[9, 11] During the simulation runs, all of the interactions are assumed to be strictly physical; that is, the chemical reaction between carbon dioxide and the amines to form carbamates is explicitly not considered; The relevance of this assumption in the simulated adsorption isotherms and the way to overcome this limitation will be addressed in the following section.

[4] **Bond angles with no k_i^{angle} value are rigid.**

6.5. ADSORPTION OF CO_2 ON SILICA GEL

Four different functionalized models were generated, by replacing 0.25, 0.5, 1.0 and 1.5 OHs/nm^2, calculated with respect to the surface areas of the silica support in terms of volume. Usually the values for the number of amines per area are calculated taking into account the surface area in terms of gram. However, for a straightforward comparison with the surface silanols of the support, in this section this quantity is calculated in terms of volume.

Subsequently we will refer to the different degrees of substitution as: (i) G0, for the silica support; (ii) G1, for the material functionalized with 0.25 OHs/nm^2 (0.36 mmol APTES/g) ; (iii) G2, for the silica with 0.5 OHs/nm^2 (0.69 mmol APTES/g); (iv) G3, for the silica with 1.0 OHs/nm^2 (1.28 mmol APTES/g) and (v) G4, for the silica with 1.5 OHs/nm^2 (1.78 mmol APTES/g).

The experimental loading of APTES on porous silica ranges from 0.95-2.5 mmol/g. [5, 6, 45] Using the algorithm discussed in the previous section it is possible to functionalize up to 2.3 mmol amines/g or 2.0 molecules APTES/nm^2 on the support G0, which has 4.6 OHs/nm^2. This means that only 43% of the available surface groups of the model xerogel can be functionalized. Although the functionalization procedure does not consider a bidentate mechanism, less than half of the surface silanols can be functionalized. This limitation is caused by esteric effects, where the base of the APTES chains hinder the grafting of their neighbor silanols. Knowles et al[7] grafted 1.8 mmol amine/g for a mesoporous silica with a surface area of 909 m^2/g, similar to our model. Therefore, although we can functionalize up to higher loadings (2.2mmol) we have used 1.78 mmol APTES/g, G4, as the model material for high loading of grafted chains for comparative purposes.

Figure 6.9 depicts a plot of the number of MC cycles needed to obtain a given grafting density, each MC cycle is an attempt to change the grafting point of one of the molecules. The points represent the molecules as they are tethered during the simulation (each different position in the ordinates corresponds to a different chain normalized in terms of mmol/g) and the continuous line is the total number of molecules grafted until that point. From this plot, it is possible to obtain the upper limit (geometrically and energetically) for the functionalization

of the silica gel model. For the model silica gel the upper limit for monodentated grafted octyltriethoxysilane molecule is around 2.3 mmol/g.

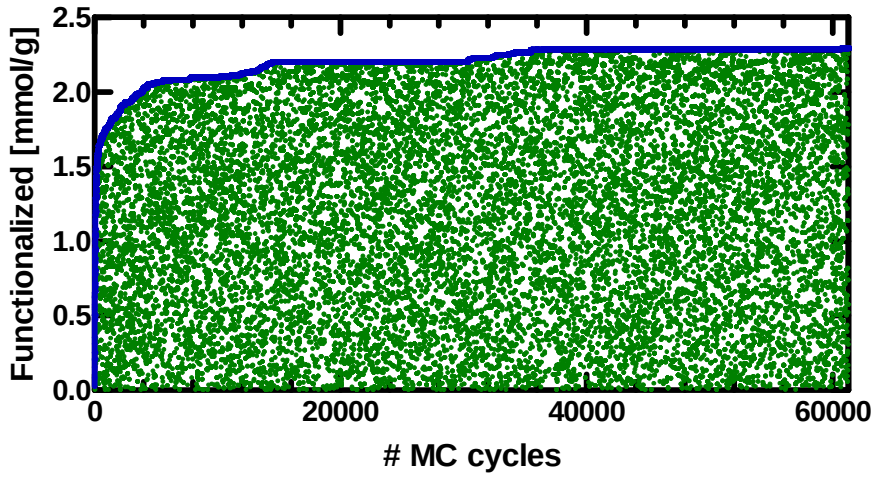

Figure 6.9. Degree of functionalization as a function of the number of computational cycles required for the grafting simulation.

Although the aim of functionalization is to increase the adsorption capabilities of the silica, two important adsorption properties, the surface area and the pore volume, decrease when the material is functionalized. Figure 6.10 shows the relationship of these properties with the degree of functionalization of the model xerogel. The main disadvantage of functionalizing adsorbents is that the grafted chains may occupy parts of the pore space that had high fluid-solid interactions. In order to increase the capture capabilities of the material, this drawback has to be compensated by increased interactions between the fluid and the surface groups. It is seen in Figure 6.10 that even if the interactions CO_2-amine are greatly increased there should be an optimum amine loading where a maximum CO_2 capture capacity is reached.

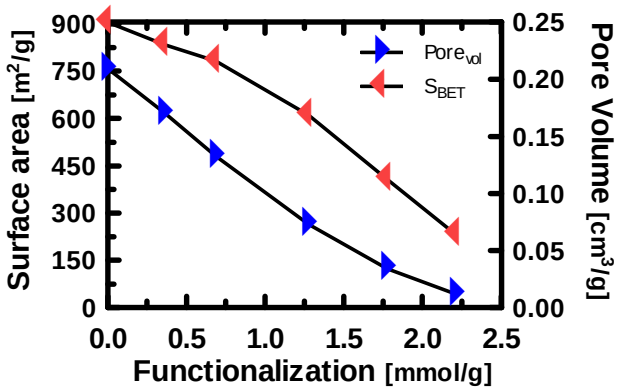

Figure 6.10. Surface area and pore volume as functions of the degree of functionalization. Symbols represent simulation results while the lines are a guide to the eyes.

Adsorption isotherms are a useful tool to characterize the substract and the functionalized materials. Moreover, CO_2 isotherms allow differentiating the capture potential of the different materials for a range of pressures. Figure 6.11 depicts the CO_2 adsorption isotherms at 298K of the model silica xerogel, for the substrate and the functionalized materials. The isotherms are given in terms of surface area to ease the comparison among adsorbents with different surface area. The behavior at low pressures, Figure 6.11b, is similar to what has been observed experimentally; the functionalized materials adsorb strongly at first, then, at higher pressures, the silica support adsorbs more CO_2 than the functionalized material. As shown in Figure 6.11 the capacity of the latter materials decreases with the degree of functionalization, therefore their CO_2 adsorption capacity decreases as well.

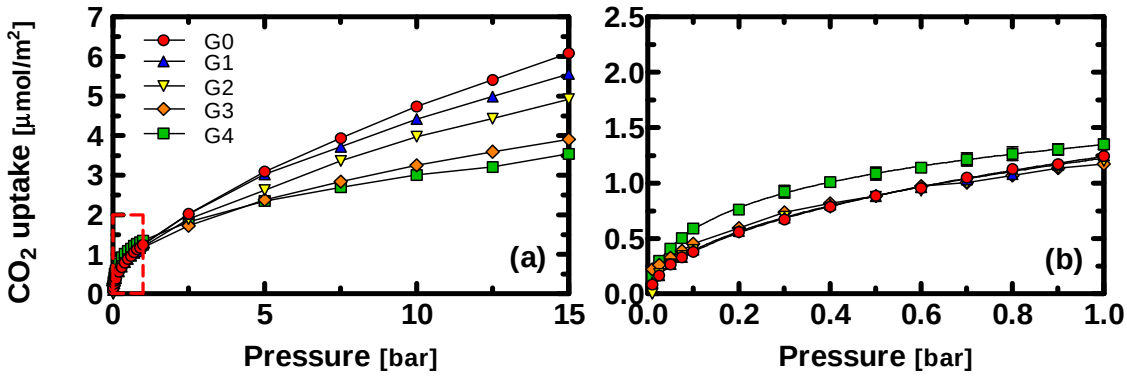

Figure 6.11. Adsorption isotherms at 298 K of CO_2 on silica xerogel functionalized with different amounts of APTES at high pressure (a) and at pressures lower than 1 bar (b).

The initial slope for the CO_2 uptake on G4 is much lower than the slope observed experimentally for amine-functionalized silica.[5, 6] This behavior is expected because in these simulations the reaction of CO_2 with the amines is not explicitly considered. This effect can be included in a new set of configurations without changing the type of potential used (i.e., LJ and Coulombic) assuming that the chemical reaction occurs at very low pressures. Experimental studies have shown by IR spectrometry that the reaction CO_2-amines occurs mainly at low pressures and most of the CO_2 captured afterwards is by means of physisorption.[9, 11]

Therefore, the effects of chemisorption on the adsorption isotherms can be taken into account in the GCMC simulations by including a fixed amount of CO_2 molecules chemically bonded to the chains. Primary amines in the grafted chains react with CO_2 forming a carbamate and a protonated base; i.e., two different monoamine chains are required for capturing a single CO_2 molecule. These molecules represent the amount of CO_2 fixed by chemical reaction; their inclusion in the system takes into account the occupancy and the interactions of the chemisorbed CO_2 on the adsorption isotherms. Instead of grafting only amine chains during the functionalization, a predefined number of chains including the carbamates and the protonated amines are also tethered to the solid.

The non-bonded parameters for the three different types of chains are included in Table 6.6. The first part of the chains, the silane section, remains unmodified by the chemical reaction (their charges are slightly modified in each case to achieve charge neutrality in the system) and the main differences are seen around the nitrogen atom of the chains.

The bonded parameters for the functionalized chains are presented in Tables 6.7-6.9. The values for the carbamate base and protonated base use the same parameters than the aminosilane chains unless it is explicitly stated otherwise.

Table 6.6. Parameters for the non-bonded interactions for the aminosilane.

Site	σ (nm)	ε/k_B (K)	q (e)	ref
Amino propyl chains				
[O]-Si	0.28	55.0	-0.4	[36]
[Si]	0.58	0.5	0.16	[37]
Si[O]-H	0.302	93.0	-0.675	[38]
SiO-[H]	0.0	0.0	0.46	[38]
Si[CH_2]CH_2	0.395	46.0	0.1	[37]
CH_2[CH_2]CH_2	0.395	46.0	0.1	[37]
CH_2[CH_2]NH_2	0.395	46.0	0.28	[39]
CH_2[N]H	0.334	111.0	-0.93	[39, 46]
N-[H]	0.0	0.0	0.37	[39]
N[C]O2	0.356	35.3	1.15	[46]
C-[O]	0.303	60.4	-0.86	[46]
Protonated amino propyl chains				
[O]-Si	0.28	55.0	-0.4	[36]
[Si]	0.58	0.5	0.187	[37]
Si[O]-H	0.302	93.0	-0.675	[38]
SiO-[H]	0.0	0.0	0.46	[38]
Si[CH_2]CH_2	0.395	46.0	0.2	[37, 46]
CH_2[CH_2]CH_2	0.395	46.0	0.21	[37, 46]
CH_2[CH_2]NH_3	0.395	46.0	0.25	[39, 46]
CH_2[N]H_3	0.334	111.0	-0.39	[39, 46]
NH_2-[H]	0.0	0.0	0.351	[39, 46]

Table 6.7. Bond lengths for the carbamate and protonated amines[5].

Bond	r_0 (nm)	ref
Amine carbamate		
C-O	0.1254	[46]
N-C	0.1474	[46]
Protonated amine		
C-N	0.1524	[46]
N-H	0.1026	[46]

[5] **The parameters not specified are the same as for the AMPTES chains in Tables 3-5**

Table 6.8. Equilibrium bond angles and force constants for the grafted chains.

Bonds	θ_i^{eq} (deg)	k_i^{angle}/k_b (K/rad^2)[6]	ref
	Amine carbamate		
H-N-CH_2	111.68	44312.7	[46]
O-C$^-$-O	131.0	85604.1	[46]
O-C$^-$-N	114.5	95675.2	[46]
CH_2-N-C$^-$	117.2	77748.6	[46]
H-N-C$^-$	110.4	41694.2	[46]
	Protonated amine		
CH2-CH2-N	111.56	77345.8	[46]
H-N-CH2	111.79	44312.7	[46]
H-N-H	107.04	39377.9	[46]

Table 6.9. Torsional parameters for the grafted chains**.**

Equation 6.4

Torsion group	C_1/k_b (K)	C_2/k_b (K)	C_3/k_b (K)	ref
Si-CH_2-CH_2-CH_2	355.03	-68.19	791.32	[37]
Si-CH_2-CH_2-CH_2	355.03	-68.19	791.32	[37]

Equation 6.5

Torsion group	C_0/k_b (K)	C_1/k_b (K)	C_2/k_b (K)	C_3/k_b (K)
CH_2-CH_2-N-C$^-$	1466.0	-2188.0	1381	-890
CH_2-N-C$^-$-O	1585	-163	-629	0
	C_4/k_b (K)	C_5/k_b (K)	C_6/k_b (K)	ref
CH_2-CH_2-N-C$^-$	329	-137	52.6	[39, 46]
CH_2-N-C$^-$-O	0	0	0	[39, 46]

Figure 6.12 shows an illustrative sketch of the modified grafting scheme, instead of grafting initially only APTES chains two additional types of chains can be grafted, carbamates and protonated amines. The total amount and the proportion of each kind of molecule are given by the desired grafting density and the chemisorbed data obtained from the experimental data at very low pressures.

[6] **Bond angles with no k_i^{angle} value are rigid.**

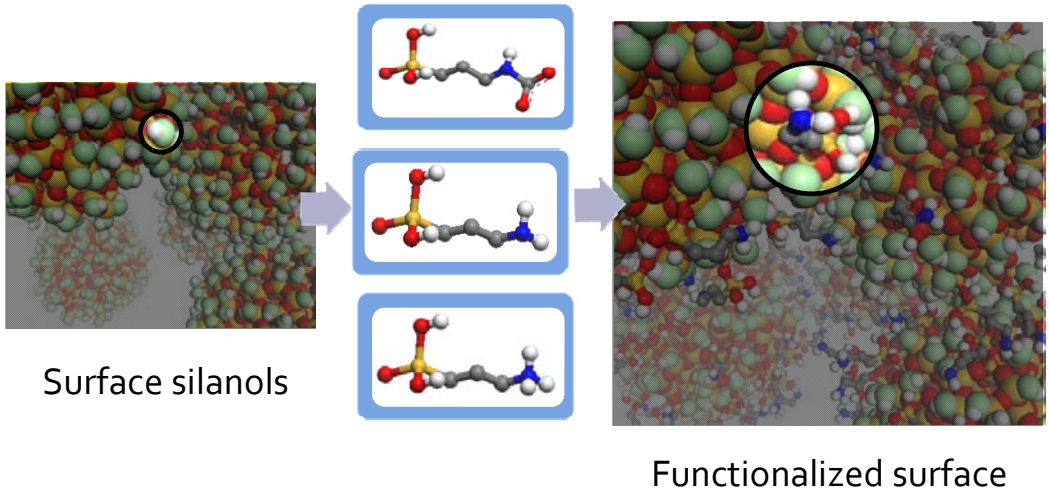

Figure 6.12. Modified scheme replacing silanol groups that allows considering the chemisorbed CO_2 in the simulations.

The inclusion of carbamates in the simulation considers that at very low pressures CO_2 reacts with the amine chains forming carbamate species and that any further increase in the pressure has no effect on the reaction. The inter- and intramolecular interactions in the system are modified due to the inclusion of the carbamates and the protonated amines. The simulation parameters employed in the simulations with these additional grafted chains are shown in tables 6.6-6.9.

This method can be easily implemented and takes into account both chemisorbed and physisorbed CO_2 simplifying the comparison of experimental isotherms with simulation results. The former value has to be determined initially from experimental data, given that in grafted amines the reaction ratio is lower than the actual stoichometric ratio. For the xerogel model the amount of CO_2 was fixed using a ratio of 1 mol of CO_2 for every 10 mols of NH_2, which was obtained from the data of Knofel et al.[9] at 0.05 bar. In Figure 6.13 are presented the adsorption isotherms considering both chemisorbed and physisorbed CO_2.

The initial uptake of the isotherms for the functionalized materials, in Figure 6.13, is mostly due to the contribution of the chemical reaction. During the simulations, CO_2 does not form further carbamates with the amines, hence the rest of the isotherm corresponds to additional physisorbed CO_2. This behavior is similar to the observed by Knofel et al. for SBA-16, where

the support adsorbs less in terms of surface area, below 1 bar. Then, at 1 bar the uptake is higher for the functionalized material but the slope is lower than that of the support. In addition, at high pressures the functionalized materials adsorb less than the support in terms of surface area. [8, 9] This higher capacity is probably the result of the more heterogeneous surface of the functionalized material compared to the support.

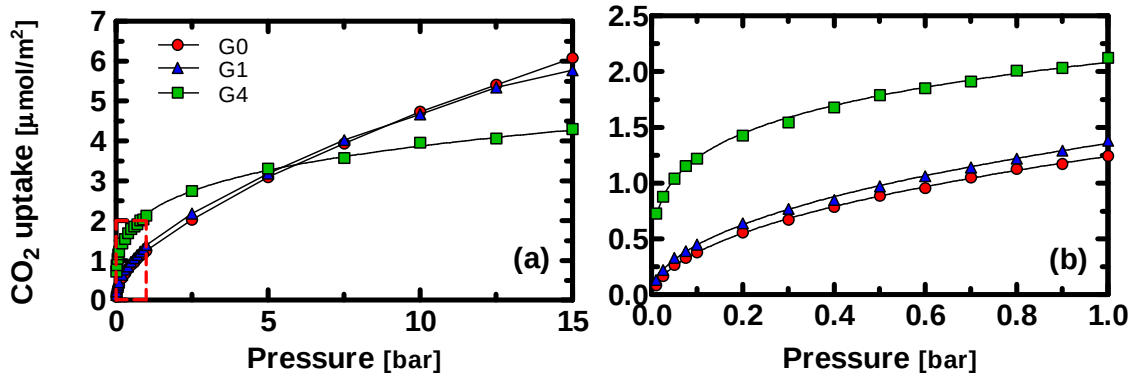

Figure 6.13. Adsorption isotherms at 298 K of CO_2 on silica xerogel functionalized with different amounts of APTES at high pressure corrected for considering the chemisorbed CO_2 (a) and at pressures lower than 1 bar (b). Symbols as in Figure 6.11.

The crossover between the isotherms in Figure 6.13 represents the pressure at which the functionalized material and the support have equal uptake. Thus, if a particular capture application operates at partial pressures below this point the functionalized material is preferred to the support. However, if the application operates at higher pressures the functionalized material captures less CO_2 than the support. For example, the crossover pressure of G4 and G0 is approximately 5 bar, then for applications at 1 bar G4 is a preferred choice over G0 for adsorbing CO_2.

Although the isotherms in Figure 6.13 represent more closely the behavior observed experimentally, the importance of the plots in Figure 6.11 should not be underestimated. They represent the CO_2 physisorbed in the xerogel. Therefore, molecular simulations can serve as a guide of the CO_2 amount that can be desorbed easily for carbon capture applications. This quantity cannot be differentiated in the experimental isotherms. Hence, the

simulations provide an easy way to compare the changes in physisorbed CO_2 and isolate the effect of chemisorption on the adsorption isotherms of functionalized materials.

Grafting the chains on silica has two diametrically opposed effects on the CO_2 adsorption: (i) an increased interaction with the fluid, which increases the number of favorable sites of adsorption and (ii) a reduction of some of the favorable adsorption sites of the support due to the volume occupied by the chains. At higher pressures the support adsorbs more CO_2 than the functionalized material. This is due to the effect of the functionalization on the surface area and pore volume, as seen in Figure 6.10. As a result, the capacity of the material and some of the fluid-fluid interactions are reduced as well. Thus, the functionalized materials have lower capacities than their original supports. This is of special relevance for materials with low pore volume, where functionalization implies the loss of most of their adsorption capacity. This effect can be seen in the density profiles of the distance of the CO_2 molecules to their closest atom in the silica surface, shown in Figure 6.14; for clarity only data for G0, G1, and G4 are plotted.

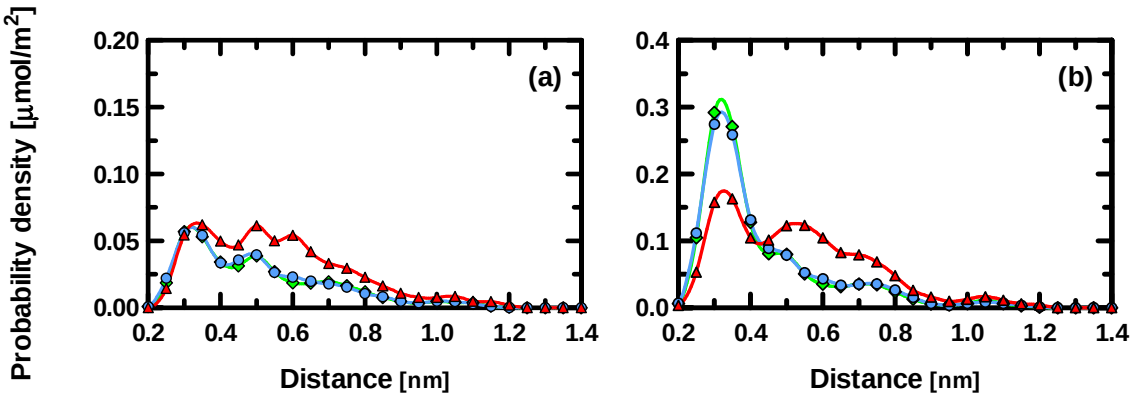

Figure 6.14. Density profiles of the distance of the carbon atom (C) in CO_2 to the closest atom in the silica surface at 298 K for 0.1 bar (a) and 1.0 bar (b).

In the density profiles in Figure 6.14 the distance of the carbon atom of the CO_2 molecules to the nearest atom in the silica surface during the GCMC simulations was calculated. This distance was plotted as a probability density normalized with respect to the number of CO_2 molecules per unit area of the adsorbent.

The density profiles explain why at higher pressure G4 physisorbs less CO_2 than the other adsorbents. The amine chains pull the CO_2 away from the solid, since steric effects do not allow chains to adsorb near the surface. The first peak in Figure 6.14 for G4 is smaller than that for G0 and G1; this means that because CO_2 cannot approach the silica surface this adsorption has to be compensated by the amines. The second and third peaks of G4 correspond to this enhanced adsorption; CO_2 is adsorbed further away from the solid silica as a result of the increased interactions with the chains. Because of the decrease in the volume caused by the grafting, at some point, the effect of the first peak for the support surpasses the effect of the second and third one for the functionalized material. At this point, the functionalized material adsorbs less CO_2 than the support or the materials functionalized to a lower degree.

It is also important to study the behavior of the grafted APTES chains in the surface during the adsorption of CO_2. We calculated the distribution of the angle between the oxygen atom grafted to the surface, the silica atom of the chain and the nitrogen atom ($\theta_{O\text{-}Si\text{-}N}$, see configuration III in Figure 6.15) for each chain during the simulation of CO_2 adsorption. This angle is an approximate value of the angle formed between the chains and the surface. Although the surface is irregular, $\theta_{O\text{-}Si\text{-}N}$ provides a local tendency of the chains. The angle distributions for G1, G2 and G4 at 0.1, 1.0 and 20.0 bar are shown in Figure 6.15.

An angle of $\theta_{O\text{-}Si\text{-}N}$=90º is defined as the position where the chains are parallel to the surface and $\theta_{O\text{-}Si\text{-}N}$ =180º as having perpendicular chains. In the distribution plots two main peaks exist, the first for the parallel position, around 90º, and the second one for the perpendicular position, closer to 130º than to 180º due to geometrical constraints.

In general, the distribution of the chains is a strong function of the degree of functionalization. Also, the increase of pressure decreases the number of chains parallel to the surface. The distribution for G1 is bimodal positively skewed. This means that the grafted chains tend to bend parallel to the surface. For this material the presence of CO_2 changes the distribution of the chains. First, at low pressure the chains distribute preferentially parallel to the surface. With increasing pressure, CO_2 molecules get closer to the surface, as seen in

Figure 6.14a the distance is similar as the obtained for G0. This means that some of the chains that lay over the surface change their position to a more perpendicular one to allow the adsorption of CO_2. When the amount of CO_2 molecules increases, this position is no longer favorable and the chains bend toward the surface to let more CO_2 get close to the surface.

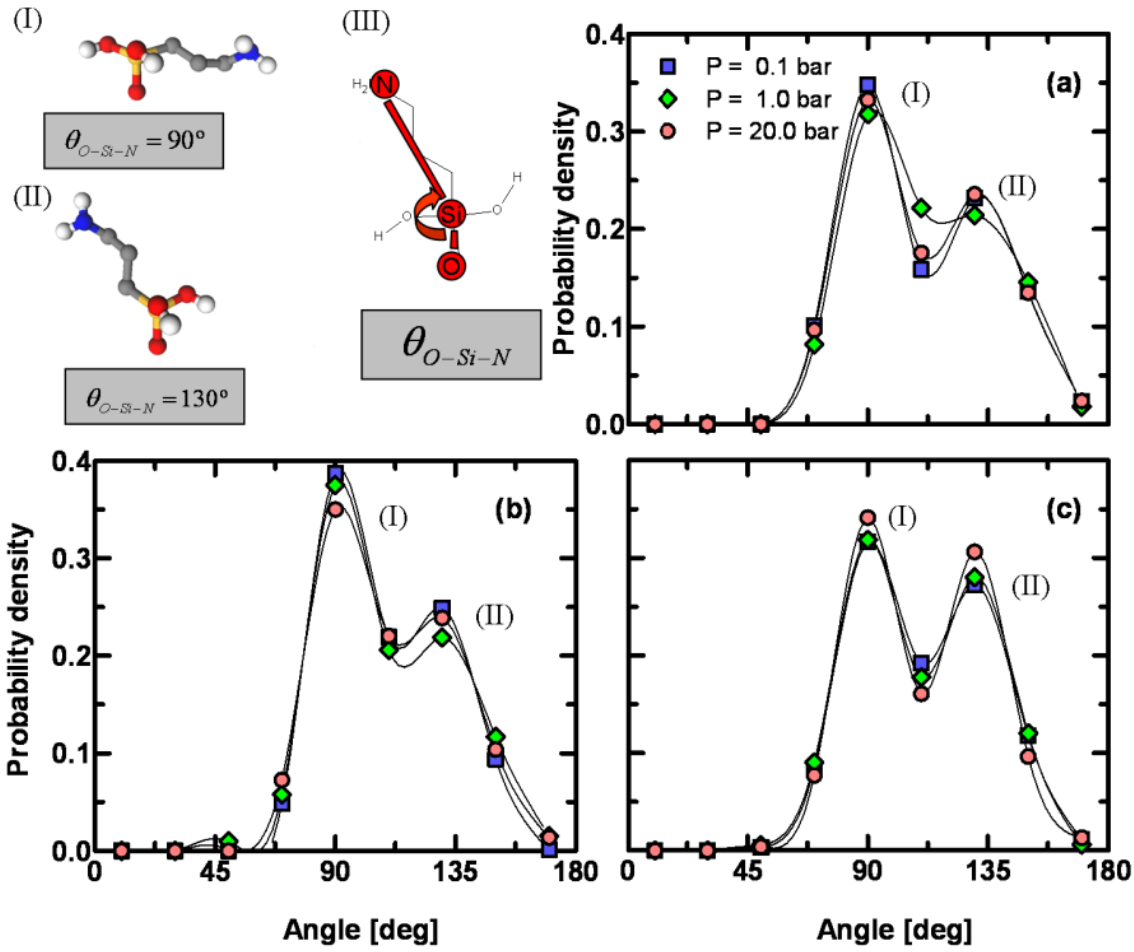

Figure 6.15. Density profiles of the angle θO-Si-N in the grafted APTES: G1 (a), G2 (b) and G4 (c) at different pressures. (Top left) Sketch of the angles for molecules parallel to the surface (I) and with an angle of 130º (II); and an explanation of how the angle is defined (III).

For G2 the distribution is similar to the one for G1. Figure 6.15b is also bimodal but its first peak and the middle point are higher than for Figure 6.15a. This is because the large number of ungrafted silanols on the surface attract the amino moieties on the chains, increasing the number of chains that preferentially bend parallel to the surface. This number is larger than for G1 due to the increased number of hydroxyl groups in the base of each grafted chain; the

chains bend toward the base of each other. These results are different for the material with the highest amine loading, G4. Although for this material the hydroxyl density is higher, the available pore space for bending the chains decreases and the chains are forced to remain in perpendicular configurations. The distribution is similar to a bimodal symmetric, specially at higher pressures. These findings are similar to those observed by Dacquin et al. [47] for octyl chains functionalized on MCM-41 by co-condensation. However, the intermediate degree of functionalization where additional silanol groups at the base of the post-functionalized silane increase the amount of parallel surface groups (corresponding to G2 in this work) was not observed for their linear co-condensation functionalized chains.

Overall, silica xerogel functionalized amines shows promising CO_2 capture at low pressures. The low cost of silica gel makes it an ideal silica material for functionalization. However, most fundamental research studies on functionalization employ regular mesoporous structures, such as MCM-41. Therefore, simulations of adsorption on MCM-41 are presented in the following section for validation of the simulation methodology and comparison with experimental data.

6.6. ADSORPTION OF CO_2 ON MCM-41

The validation of the functionalization methodology requires the use of a set of data of CO_2 adsorption isotherms for different degrees of functionalization and a large range of pressures. For this purpose, we employed the experimental data of Schumacher et al. [13, 32] as a reference. They functionalized MCM-41 using different amounts of APTES obtaining two materials with an estimated 9.6 and 16.9% of surface groups in the solid. We created two different models by functionalizing 9 and 17% APTES respect to the model MCM-41. Subsequently, the different degrees of substitution are referred to as: (i) M0, for the silica support; (ii) M1, for the model with 9% APTES; and (iii) M2, for the silica with 17% APTES.

The first step before applying the proposed method for functionalization is to validate the M0 model. The model should be able to predict accurately experimental adsorption isotherms. The simulated adsorption isotherms of N_2 at 77 K and CO_2 at 263 K were compared with the

experimental data of Schumacher et al. The comparison of the simulated and experimental N_2 isotherms is shown in Figure 6.16a. The agreement for N_2 at low pressures is excellent, validating M0 as an adequate representation of the experimental MCM-41. This agreement at low pressures indicates that the preferred adsorption sites that are first occupied by the adsorbed molecules are accurately represented by the model. At higher pressures two main differences between the simulated and experimental data are observed, first the pressure at which the pore filling occurs is lower in the simulation, and second the capacity of the experimental material is larger than that of the model. The point where the pore filling occurs is very sensitive to the pore size, whereas the capacity is given by the accessible volume. These underestimations in the simulated results for the N_2 isotherms might be caused by a slightly smaller pore size in the model than in the experimental material. The isotherms for CO_2 at 263 K are shown in Figure 6.16b. A good agreement between the experimental and simulated results over the whole pressure range is obtained. This clearly demonstrates that the employed M0 model is a sufficiently realistic representation of the experimental MCM-41.

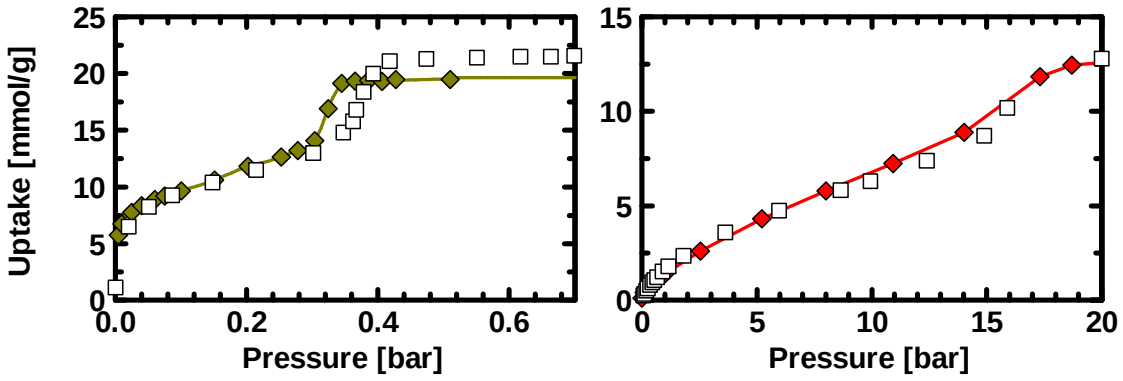

Figure 6.16. Experimental (line) and simulated (symbols) adsorption isotherms of nitrogen at 77 K (top) and carbon dioxide at 263 K (bottom) on MCM-41.

Having validated the MCM-41 model, the functionalization methodology has to be corroborated by comparing the results on functionalized silica. In this section, experimental results on APTES postfunctionalized on MCM-41 are compared to their corresponding models. CO_2 adsorption isotherms at 263 K of MCM-41 for the substrate and the functionalized materials are depicted in Figure 6.17. The behavior at high pressures, shows

good agreement between the experimental and simulated results. Because the force fields employed in the simulations only account for physical interactions; the good agreement with the experiments indicates that physisorption is the leading mechanism at high pressures.

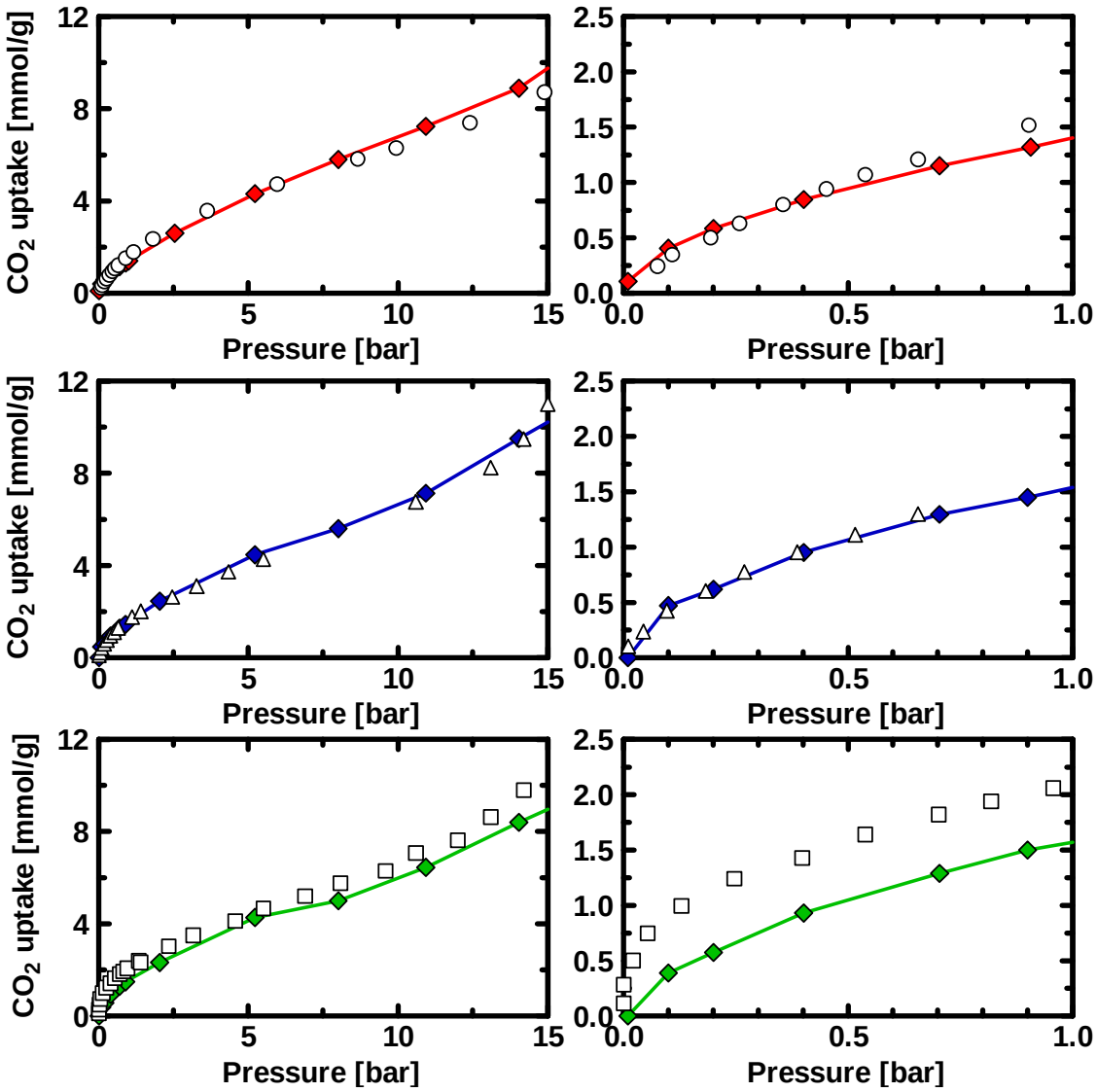

Figure 6.17. Experimental (symbols) and simulated (line) adsorption isotherms at 263 K of CO_2 on M0 (circles), M1 (triangles) and M2 (squares) at high pressure (left) and at pressures lower than 1 bar (right).

On the other hand, at low pressures, the experimental data have a higher uptake than the simulated functionalized materials, specially M2. As seen in the previous section, this difference is due to not considering the carbamate formation of CO_2 and amines. The largest mismatch between simulated and experimental results is expected to occur at low pressures,

since CO_2 reacts with the amines mainly at low pressures and most of the CO_2 captured afterwards is by means of physisorption.

Similarly to the silica xerogel, the simulations considering the carbamates in the initial isotherms have to be included in order to capture the low pressure behavior. In this set of simulations, the amount of carbamates was fixed using the experimental data of Schumacher et al.[13] at 0.05 bar as basis for each material. The resulting adsorption isotherms considering the chemisorbed amount are presented in Figure 6.18.

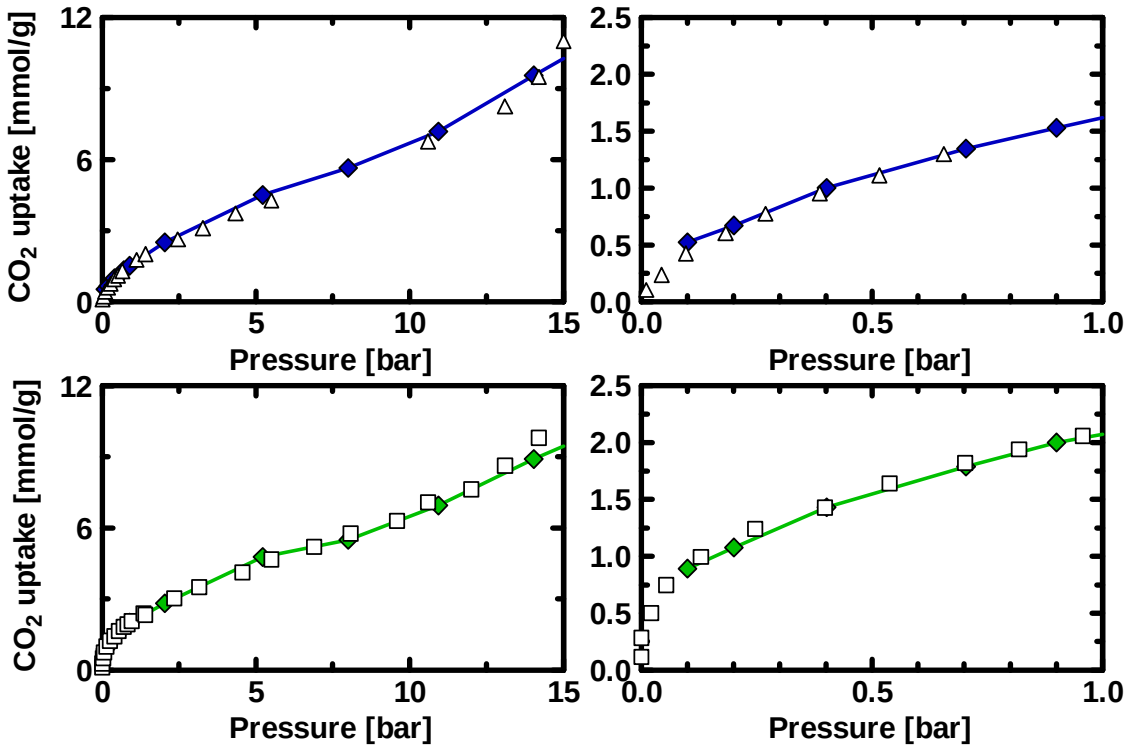

Figure 6.18. Experimental (symbols) and simulated (line) adsorption isotherms at 263 K considering the chemisorption in the simulated results. Symbols as in Figure 6.17.

The simulated plots for M1 and M2 in Figure 6.18 start at pressures above 0.05 bar. Since this point was chosen as the basis for the chemisorbed CO_2 molecules, simulated isotherms below this pressure would have to be adjusted by considering a lower number of carbamates in the initial grafting. Therefore, in Figure 6.18 to avoid misleading the reader we included only simulation values for M1 and M2 above 0.05 bar.

Figure 6.18 shows that that the inclusion of the carbamate species corrects the simulated isotherms at low pressures. For M1 and M2 an excellent agreement between the Moreover, a better agreement for the isotherms at higher pressures is obtained. The simulated carbamates allow for a quick and accurate prediction of the capture capabilities of an amine-functionalized material. Therefore, molecular simulations serve as a guide of the CO_2 amount that can be desorbed easily for carbon capture applications. Simulations provide an easy way to compare the changes in physisorbed CO_2 and isolate the effect of chemisorption on the adsorption isotherms of functionalized materials.

The density profiles of CO_2 allow a more clear understanding of the effect of functionalization on the captured CO_2. In those density profiles it is possible to differentiate the chemisorbed and physisorbed CO_2 analyzing their influence at different pressures. For the density profiles shown in Figure 6.19, we calculated the distance of the carbon atom of the CO_2 molecules to the nearest atom in the silica surface during the GCMC simulations with and without considering the chemisorbed species. This distance was plotted as a probability density of the adsorbed CO_2 molecules on MCM-41.

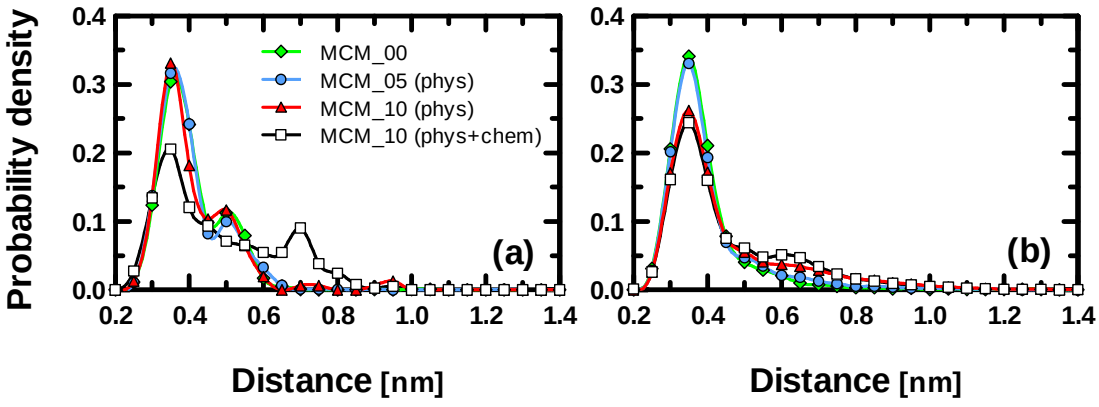

Figure 6.19. Density profiles of the distance of the carbon atom (C) in CO_2 to the closest atom in the silica surface at 263 K for 0.1 bar (a) and 5.0 bar (b) for M0 (diamonds), physisorbed CO_2 on M1 (circles), physisorbed CO_2 on M2 (triangles) and physisorbed CO_2 and the carbamates on M2 (squares).

The density profiles explain why at higher coverage M2 physisorbs less CO_2 than the other adsorbents. The amine chains pull the CO_2 away from the solid, as steric effects do not allow the chains to adsorb in some regions with high fluid-solid interactions.

At low pressures, Figure 6.19a, the physisorbed CO_2 in the three surfaces is similar. At low coverage the CO_2 molecules adsorb close to the surface for the three surfaces, and low coverage implies that this proximity is not prevented by the grafted molecules. However, when the CO_2 coverage increases a change in the molecules physisorbed close to the surface is observed. The first peak in Figure 6.19b for M2 is smaller than for M0 and M1, because CO_2 cannot approach the silica surface the adsorption has to be compensated by the interactions with the amines. The second peak of the physisorbed M2 corresponds to this enhanced adsorption; CO_2 is adsorbed further away from the solid silica as a result of the increased interactions with the chains.

If the chemisorbed CO_2 is considered in the density profiles; at low pressures, where a large fraction of the captured CO_2 is chemisorbed, a decrease in the probability of the molecules adsorbed close to the surface is observed. Moreover, a peak at 0.7 nm is present, which corresponds to the carbamates bonded to the grafted chains. At higher pressure the proportion of chemisorbed CO_2 is small and the influence in the overall CO_2 probability is lower. However, a small peak close to 0.6 nm is seen, which indicates the carbamate molecules and physisorbed CO_2 molecules interacting with the tail of the grafted chains.

The excellent capability of M2 to capture CO_2 is a promising characteristic for its use in separation of CO_2 from low concentration streams, such as those produced in post-combustion applications. However, besides a large CO_2 adsorption capacity the material has to be able to separate CO_2 from a mixture with other gases. N_2 is the main component in a typical post-combustion gas, with a smaller fraction of CO_2, O_2 and non-condensed H_2O. We simulated the separation of CO_2 from a mixture with N_2 in order to asses the capabilities of M2 to separate post-combustion gases. A diluted mixture of 0.1 mol of CO_2 on 0.9 mols of N_2 were used to reproduce the capture conditions present in the flue gases. Figure 6.20 shows the adsorption isotherms of N_2 and CO_2 from this mixture at 298K for M0 and M2 as function of the total pressure.

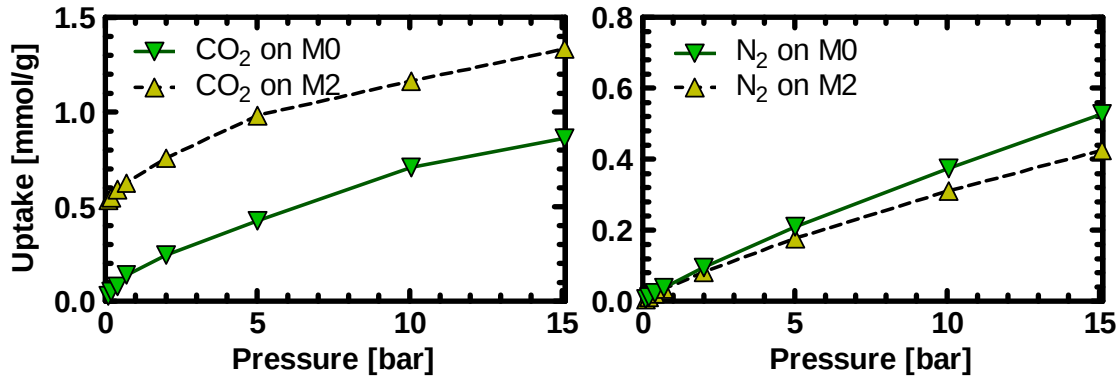

Figure 6.20. Adsorption isotherms in terms of the total pressure for the mixture of 0.1 mol CO_2 and 0.9 of N_2 at 298K. Adsorption of CO_2 (left) and N_2 (right) on M2 (upward triangles) and M0 (downward triangles).

The trend of adsorption on M0 is very similar for N_2 and CO_2, increasing the pressure has an almost linear effect on the uptake. However, for M2 the chemisorbed CO_2 changes the behavior at low pressures and adsorbs much more CO_2 while the nitrogen adsorption is not affected by chemical reactions with the amines. If we exclude the chemisorbed CO_2 and only take into account the physisorbed CO_2 on M2 a very similar trend to M0 is observed. This behavior is better seen by plotting the selectivity of adsorbing CO_2 over N_2 in the mixture, in Figure 6.21 we plotted the CO_2 selectivity for M0 and M2. In this case we added the selectivity for M2 considering only the physisorbed CO_2.

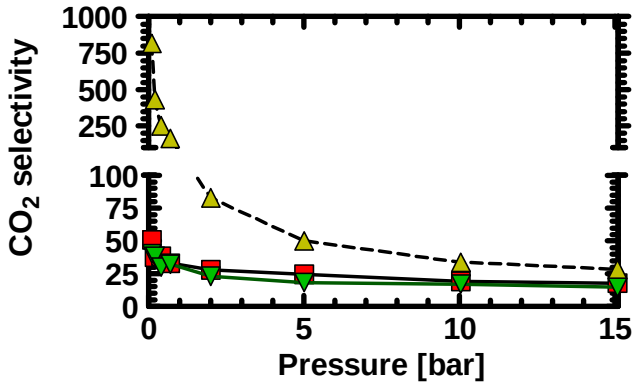

Figure 6.21. Selectivity of CO_2 over N_2 on the mixture of 0.1 CO_2/ 0.9 N_2 at 298K. M2 with chemisorption (upward triangles) , M2 without chemisorption (squares) and M0 (downward triangles).

For pressures below 2 bar M2 has much higher selectivity for CO_2. Therefore, for applications with very low concentration of CO_2 this material has a promising separation potential. However, from the physisorption only plots it is seen that the selectivity of the material is very similar to those of CO_2. Thus, in order to reach a high selectivity of CO_2 using functionalized materials the CO_2 desorption would need an increase in temperature besides decreasing the applied pressure. Moreover, if the presence of a contaminant decreases the reaction of CO_2 with the amines the lower limit for the selectivity is similar to the selectivity of the raw MCM-41.

The future implementation of functionalized materials would require the use of organic chains with a higher proportion of amino groups to increase the capture of CO_2 while compensating for the decrease in the pore volume and surface area due to functionalization.

6.7. CONCLUSIONS

A new simulation method for the design of postsynthesis functionalized silica was developed. The procedure is based on replacing the surface silanols by organosilanes using molecular simulations. The grafting sites are chosen using energy-bias calculations on the surface silanols. Results from this new method give comparable results to those obtained experimentally for grafted aminosilanes into silica materials.

Furthermore, a new method for considering the chemisorbed CO_2 was presented. The inclusion of carbamates and protonated amines in the grafted chains allow taking into account the energetics of the chemically sorbed CO_2 and their effects on the adsorption isotherms. This enables molecular simulations to be used for the prediction of systems with chemisorbed species without requiring major modifications of the simulation algorithms.

The overall results show that molecular simulations can serve as a guide to quantify the CO_2 amount that can be desorbed easily for carbon capture application, emphasizing the importance of this approach for the optimization of selected materials. In particular, the isotherms indicate that although chemisorption is an important part of this process at low pressures, physisorption plays an important role in the capture of CO_2 in these materials.

Because simulations consider only the absorbed CO_2, they can serve as a guide to the experiments and help to determine the fraction of physisorbed CO_2 in the system. Functionalization increases the interactions of the CO_2 molecules with the surface, whereas it decreases the available space for adsorption of CO_2; the overall efficiency of the improved adsorption lies on the availability of adsorption space versus stronger interactions.

Regarding the structure of the anchored molecules, chains tend to bend parallel to the surface, attracted by the surface silanols. This tendency is modified by the presence of adsorbed molecules, which can change the distribution of the molecules towards an intermediate position tilted by the physisorbed molecules.

Functionalized materials can greatly enhance the CO_2 selectivity of silica materials especially for applications with low partial pressure of CO_2. However, the enhanced sorption is the result of combined chemical and physical interactions and the secondary reactions in the presence of contaminants might decrease the adsorption capabilities of the material.

REFERENCES

1. Sayari A, Belmabkhout Y. *"Stabilization of Amine-Containing CO2 Adsorbents: Dramatic Effect of Water Vapor"*. J Am Chem Soc. **2010**;132 (18).6312-4.

2. Hoffmann F, Cornelius M, Morell J, Fröba M. *"Silica-Based Mesoporous Organic–Inorganic Hybrid Materials"*. Angew Chem Int Ed. **2006**;45 (20).3216-51.

3. Fryxell GE. *"The synthesis of functional mesoporous materials"*. Inorg Chem Commun. **2006**;9 (11).1141-50.

4. Hoffmann F, Fröba M. *"Silica-Based Mesoporous Organic–Inorganic Hybrid Materials"*. In: Rurack K, Marínez-Máñez R, editors. The supramolecular chemistry of organic-inorganic hybrid materials: Wiley-VCH; **2006**. p. 5924-48.

5. Leal O, Bolívar C, Ovalles C, García JJ, Espidel Y. *"Reversible adsorption of carbon dioxide on amine surface-bonded silica gel"*. Inorg Chim Acta. **1995**;240 (1-2).183-9.

6. Huang HY, Yang RT, Chinn D, Munson CL. *"Amine-Grafted MCM-48 and Silica Xerogel as Superior Sorbents for Acidic Gas Removal from Natural Gas"*. Ind Eng Chem Res. **2002**;42 (12).2427-33.

7. Knowles GP, Graham JV, Delaney SW, Chaffee AL. *"Aminopropyl-functionalized mesoporous silicas as CO2 adsorbents"*. Fuel Process Technol. **2005**;86 (14-15).1435-48.

8. Knöfel C, Descarpentries J, Benzaouia A, Zelenák V, Mornet S, Llewellyn PL, et al. *"Functionalised micro-/mesoporous silica for the adsorption of carbon dioxide"*. Micropor Mesopor Mat. **2007**;99 (1-2).79-85.

9. Knöfel C, Martin Cl, Hornebecq V, Llewellyn PL. *"Study of Carbon Dioxide Adsorption on Mesoporous Aminopropylsilane-Functionalized Silica and Titania Combining Microcalorimetry and in Situ Infrared Spectroscopy"*. J Phys Chem C. **2009**;113 (52).21726-34.

10. Serna-Guerrero R, Belmabkhout Y, Sayari A. *"Modeling CO2 adsorption on amine-functionalized mesoporous silica: 1. A semi-empirical equilibrium model"*. Chem Eng J. **2010**;161 (1-2).173-81.

11. Bacsik Z, Atluri R, Garcia-Bennett AE, Hedin N. *"Temperature-Induced Uptake of CO2 and Formation of Carbamates in Mesocaged Silica Modified with n-Propylamines"*. Langmuir. **2010**;26 (12).10013-24.

12. Chaffee AL. *"Molecular modeling of HMS hybrid materials for CO2 adsorption"*. Fuel Process Technol. **2005**;86 (14-15).1473-86.

13. Schumacher C, Gonzalez J, Pérez-Mendoza M, Wright PA, Seaton NA. *"Design of Hybrid Organic/Inorganic Adsorbents Based on Periodic Mesoporous Silica"*. Ind Eng Chem Res. **2006**;45 (16).5586-97.

14. Williams JJ, Wiersum AD, Seaton NA, Düren T. *"Effect of Surface Group Functionalization on the CO2/N2 Separation Properties of MCM-41: A Grand-Canonical Monte Carlo Simulation Study"*. J Phys Chem C. **2010**;114 (43).18538-47.

15. MacElroy JMD, Raghavan K. *"Adsorption and diffusion of a Lennard-Jones vapor in microporous silica"*. J Chem Phys. **1990**;93 (3).2068-79.

16. MacElroy JMD, Raghavan K. *"Transport of an adsorbing vapour in a model silica system"*. J Chem Soc, Faraday Trans. **1991**;87 (13).1971-87.

17. Gavalda S, Gubbins KE, Hanzawa Y, Kaneko K, Thomson KT. *"Nitrogen Adsorption in Carbon Aerogels: A Molecular Simulation Study"*. Langmuir. **2002**;18 (6).2141-51.

18. Accelrys Software Inc. Materials Studio, Release 5.5. San Diego: Accelrys Software Inc.2010.

19. Düren T, Millange F, Férey G, Walton KS, Snurr RQ. *"Calculating Geometric Surface Areas as a Characterization Tool for Metal−Organic Frameworks"*. J Phys Chem C. **2007**;111 (42).15350-6.

20. Ho LN, Perez Pellitero J, Porcheron F, Pellenq RJM. *"Enhanced CO2 Solubility in Hybrid MCM-41: Molecular Simulations and Experiments"*. Langmuir. **2011**;27 (13).8187-97.

21. Coasne B. *"Grand canonical Monte Carlo simulation of argon adsorption at the surface of silica nanopores: Effect of pore size, pore morphology, and surface roughness"*. J Chem Phys. **2004**;120 (6).2913.

22. Rappe AK, Casewit CJ, Colwell KS, Goddard WA, Skiff WM. *"UFF, a full periodic table force field for molecular mechanics and molecular dynamics simulations"*. J Am Chem Soc. **1992**;114 (25).10024-35.

23. Martin MG, Siepmann JI. *"Novel Configurational-Bias Monte Carlo Method for Branched Molecules. Transferable Potentials for Phase Equilibria. 2. United-Atom Description of Branched Alkanes"*. J Phys Chem B. **1999**;103 (21).4508-17.

24. Martin MG, Frischknecht AL. *"Using arbitrary trial distributions to improve intramolecular sampling in configurational-bias Monte Carlo"*. Mol Phys. **2006**;104 (15).2439 - 56.

25. Blas FJ, Vega LF. *"Thermodynamic behaviour of homonuclear and heteronuclear Lennard-Jones chains with association sites from simulation and theory"*. Mol Phys. **1997**;92 135-50.

26. Builes S, Roussel T, Vega LF. *"Optimization of the separation of sulfur hexafluoride and nitrogen by selective adsorption using monte carlo simulations"*. AIChE J. **2011**;57 (4).962-74.

27. Snurr RQ, Bell AT, Theodorou DN. *"Prediction of adsorption of aromatic hydrocarbons in silicalite from grand canonical Monte Carlo simulations with biased insertions"*. J Phys Chem. **1993**;97 (51).13742-52.

28. Frenkel D, Smit B. *"Understanding molecular simulation: from algorithms to applications"*. San Diego: Academic Press; **2002**.

29. Duque D, Vega LF. *"Some issues on the calculation of interfacial properties by molecular simulation"*. J Chem Phys. **2004**;121 (17).8611-7.

30. Potoff JJ, Siepmann JI. *"Vapor-liquid equilibria of mixtures containing alkanes, carbon dioxide, and nitrogen"*. AIChE J. **2001**;47 (7).1676-82.

31. MacElroy JMD. *"Molecular simulation of the kinetic selectivity of a model silica system"*. Mol Phys. **2002**;100 (14).2369 - 76.

32. Schumacher C, Gonzalez J, Wright PA, Seaton NA. *"Generation of Atomistic Models of Periodic Mesoporous Silica by Kinetic Monte Carlo Simulation of the Synthesis of the Material"*. J Phys Chem B. **2005**;110 (1).319-33.

33. Brodka A, Zerda TW. *"Properties of liquid acetone in silica pores: Molecular dynamics simulation"*. J Chem Phys. **1996**;104 (16).6319-26.

34. Harris JG, Yung KH. *"Carbon Dioxide's Liquid-Vapor Coexistence Curve And Critical Properties as Predicted by a Simple Molecular Model"*. J Phys Chem. **1995**;99 (31).12021-4.

35. Frierson MR, Allinger NL. *"Molecular mechanics (MM2) calculations on siloxanes"*. J Phys Org Chem. **1989**;2 (7).573-9.

36. Stubbs JM, Potoff JJ, Siepmann JI. *"Transferable Potentials for Phase Equilibria. 6. United-Atom Description for Ethers, Glycols, Ketones, and Aldehydes"*. J Phys Chem B. **2004**;108 (45).17596-605.

37. Martin MG, Siepmann JI. *"Transferable Potentials for Phase Equilibria. 1. United-Atom Description of n-Alkanes"*. J Phys Chem B. **1998**;102 (14).2569-77.

38. Chen B, Potoff JJ, Siepmann JI. *"Monte Carlo Calculations for Alcohols and Their Mixtures with Alkanes. Transferable Potentials for Phase Equilibria. 5. United-Atom Description of Primary, Secondary, and Tertiary Alcohols"*. J Phys Chem B. **2001**;105 (15).3093-104.

39. Wick CD, Stubbs JM, Rai N, Siepmann JI. *"Transferable Potentials for Phase Equilibria. 7. Primary, Secondary, and Tertiary Amines, Nitroalkanes and Nitrobenzene, Nitriles, Amides, Pyridine, and Pyrimidine"*. J Phys Chem B. **2005**;109 (40).18974-82.

40. Zhuravlev ND, Siepmann JI, Schure MR. *"Surface Coverages of Bonded-Phase Ligands on Silica: A Computational Study"*. Anal Chem. **2001**;73 (16).4006-11.

41. Zhang L, Jiang S. *"Molecular simulation study of nanoscale friction for alkyl monolayers on Si(111)"*. J Chem Phys. **2002**;117 (4).1804-11.

42. Lopes PEM, Murashov V, Tazi M, Demchuk E, MacKerell AD. *"Development of an Empirical Force Field for Silica. Application to the Quartz−Water Interface"*. J Phys Chem B. **2006**;110 (6).2782-92.

43. Ionescu TC, Qi F, McCabe C, Striolo A, Kieffer J, Cummings PT. *"Evaluation of Force Fields for Molecular Simulation of Polyhedral Oligomeric Silsesquioxanes"*. J Phys Chem B. **2006**;110 (6).2502-10.

44. Stimson LM, Wilson MR. *"Molecular dynamics simulations of side chain liquid crystal polymer molecules in isotropic and liquid-crystalline melts"*. J Chem Phys. **2005**;123 (3).034908-10.

45. Zelenak V, Halamova D, Gaberova L, Bloch E, Llewellyn P. *"Amine-modified SBA-12 mesoporous silica for carbon dioxide capture: Effect of amine basicity on sorption properties"*. Micropor Mesopor Mat. **2008**;116 (1-3).358-64.

46. Gutowski KE, Maginn EJ. *"Amine-Functionalized Task-Specific Ionic Liquids: A Mechanistic Explanation for the Dramatic Increase in Viscosity upon Complexation with CO2 from Molecular Simulation"*. J Am Chem Soc. **2008**;130 (44).14690-704.

47. Dacquin J-P, Cross HE, Brown DR, Düren T, Williams JJ, Lee AF, et al. *"Interdependent lateral interactions, hydrophobicity and acid strength and their influence on the catalytic activity of nanoporous sulfonic acid silicas"*. Green Chem. **2010**;12 (8).1383-91.

Chapter VII

Conclusions and Future Work

"… all arguments concerning existence are founded on the relation of cause and effect; that our knowledge of that relation is derived entirely from experience; and all our experimental conclusions proceed upon the supposition that the future will be conformable to the past. .... Without the influence of custom, we should be entirely ignorant of every matter of fact beyond what is immediately present to the memory and senses."

David Hume (An Enquiry Concerning Human Understanding)

A large number of materials capable of separating and capturing GHGs exist, and thanks to new synthesis techniques their number is likely to keep increasing. In this dissertation we evaluated a series of basic separation characteristics of potential candidates for adsorption and separation of GHGs.

The capture and separation of two very different greenhouse gases, SF_6 and CO_2, were studied using molecular simulations; different materials were proposed and analyzed as alternatives for the reduction of emissions of greenhouse gases.

First, a general analysis of the influence of different variables, such as composition, pressure, and pore diameter, on the adsorption of SF_6 and N_2 on solid adsorbents was performed. The

maximum selectivity by adsorption for this mixture for all the composition range is obtained for a cylindrical pore diameter of 1.1 nm. At this particular pore size, sulfur hexafluoride molecules block the empty volume of the pore and prevent nitrogen from being adsorbed. Once this optimal pore diameter was found, additional simulations were performed in zeolite carbon replicas FAU-ZTC and EMT-ZTC, ordered materials with almost cylindrical structures and a narrow pore size distribution located around 1.1 nm. Simulation results show very high selectivities for EMT-ZTC and FAU-ZTC, being the selectivity higher for FAU-ZTC. Selectivities found for this latter material are approximately four times higher than the best material for separation published in the open literature. Given the mechanical properties of these carbon replicas, these materials show a great potential for applications in recovering SF_6 from SF_6/N_2 mixtures present in gas-insulated equipment. Further experimental work is required for validating the separation conditions in the actual carbon replicas.

The performance of the two carbon replicas was evaluated using molecular simulations and experiments. These two ZTCs compare favorably with the most CO_2 adsorbing organic frameworks at room temperature, and FAU-ZTC is shown to have the highest reported CO_2 adsorption capacity for carbonaceous materials. In the light of mitigation of CO_2 emissions, ZTCs are promising materials under hostile environments, because of their extreme stiffness and stability. Moreover, from the differences found between experiments and simulations, two different scenarios are proposed based on the different morphologies of the two ZTCs studied. First based on the local curvature of the atoms on FAU-ZTC an extremely high curvature was found; this was not observed for EMT-ZTC, which has a more planar structure. With the former material, the empirical Steele potential leads to an apparent inaccurate prediction of the solid–fluid interactions, underestimating the polarizability of curved sp2 carbons. By accounting empirically for this latter effect a better agreement in the simulated adsorption isotherms was found. However, even accounting for the curvature of the material there is a mismatch between the experimental and simulated adsorption isotherms. Thus, the FAU-ZTC model requires further refinements, for instance refined simulations might include the presence of hetero-species from the organic precursors, the presence of localized partial charges on the carbon structure or a larger pore size distribution including the presence of voids and vacancies among the different crystallites. It is expected that the

inclusion of those effects will increase the agreement of the FAU-ZTC model with the experimental results.

Contrarily, in the case of the EMT-ZTC model, an overestimated amount of adsorbed CO_2 at very low pressure was found; at higher pressures the model captured most of the main adsorption properties of the real material. By blocking inside of the pillared structures in this carbon model it was possible to remove completely the discrepancy at low pressures. Experimentally, the pore blocking might be caused either by defects inside the cages or by slow CO_2 diffusion in those very small micropores. Interestingly, this study shows that adsorption isotherms of CO_2 at room temperature allow the size differentiation between narrow-micropores, making them an interesting complementary probe to nitrogen molecules for characterizing the textural properties of ZTCs.

In addition, a completely different kind of materials was evaluated for the adsorption of CO_2, hybrid organic-inorganic materials. These materials are tailored to benefit from the strong interactions of CO_2 and amines supported over the resistant an inert surface of inorganic porous materials. A new simulation method for the design of post-synthesis functionalized silica was developed. The procedure is based on replacing the surface silanols by organosilanes using molecular simulations. The grafting sites are chosen using energy-bias calculations on the surface silanols. Results from this new method give comparable results to those obtained experimentally for grafted aminosilanes into silica materials.

Furthermore, a new method for considering the chemisorbed CO_2 was presented. The inclusion of carbamates and protonated amines in the grafted chains allow taking into account the energetics of the chemically sorbed CO_2 and their effects on the adsorption isotherms. This enables molecular simulations to be used for the prediction of systems with chemisorbed species without requiring major modifications of the simulation algorithms. The overall results show that molecular simulations can serve as a guide to quantify the CO_2 amount that can be desorbed easily for carbon capture application, emphasizing the importance of this approach for the optimization of selected materials. The overall results show that molecular simulations can serve as a guide to quantify the CO_2 amount that can be desorbed easily for

carbon capture application, emphasizing the importance of this approach for the optimization of selected materials

Functionalized materials can greatly enhance the CO_2 selectivity of silica materials especially for applications with low partial pressure of CO_2. However, the enhanced sorption is the result of combined chemical and physical interactions and the secondary reactions in the presence of contaminants might decrease the adsorption capabilities of the material.

Future work with the developed methodologies for functionalized amines will attempt to explore and optimize the density and types of amines required to separate CO_2 contained in a different mixtures. Another further research topic is to study the effect of different fluid species that can change the nature of the amines and/or the reaction of the CO_2-amines, such as SO_2 and H_2O, on the adsorption isotherms.

In summary in this dissertation, we have evaluated from a fundamental point of view using molecular simulations the technical capabilities of different materials for the adsorption and separation of two different GHGs. It is important to consider that different options of adsorbents or other means to capture CO_2 might be technically feasible. However, clear goals and energetic evaluations have to be considered to evaluate further research and funding efforts aimed towards finding the most viable alternatives for capturing GHGs.

It is necessary to consider that advanced capture technologies might require different operating temperatures or pressures than those present in the plant emitting the GHGs; those different conditions present a challenge for the system integration, which might outweigh the gains obtained by the use of the advanced technology. In general, the benefits of implementing a particular separation technology have to compensate any negative consequences of operating the separation process out of the normal range of pressures and temperatures for the process.

The future implementation of the different novel materials for separation of GHGs has to be decided early, before major investments on new generation plants are undertaken. The search for a perfect capture material for each GHG might be far from over, but we need to compromise among the existing alternatives by implementing a methodology for evaluating the most viable solutions. Moreover, the option of waiting for a better solution must be

considered as an alternative that competes with the others in the search of the optimal action. Hence, the consequences of our actions and inactions should be clearly evaluated for a better decision making in the capture of greenhouse gases.

References

"Kyoto Protocol to the United Nations Framework Convention on Climate Change". Review of European Community & International Environmental Law. **1998**;7 (2).214-7.

Accelrys Software Inc. Materials Studio, Release 5.5. San Diego: Accelrys Software Inc.2010.

Allen MP, Tildesley DJ. *"Computer Simulation of Liquids"*: Clarendon Press; **1987**.

An J, Geib SJ, Rosi NL. *"High and Selective CO2 Uptake in a Cobalt Adeninate Metal−Organic Framework Exhibiting Pyrimidine- and Amino-Decorated Pores"*. J Am Chem Soc. **2009**;132 (1).38-9.

Aresta M. *"Carbon Dioxide Recovery and Utilization"*. Aresta M, editor: Kluwer Publication; **2003**.

Arstad B, Fjellvåg H, Kongshaug K, Swang O, Blom R. *"Amine functionalised metal organic frameworks (MOFs) as adsorbents for carbon dioxide"*. Adsorption. **2008**;14 (6).755-62.

Aziz RA, Slaman MJ, Taylor WL, Hurly JJ. *"An improved intermolecular potential for sulfur hexafluoride"*. J Chem Phys. **1991**;94 (2).1034-8.

Babarao R, Hu Z, Jiang J, Chempath S, Sandler SI. *"Storage and Separation of CO2 and CH4 in Silicalite, C168 Schwarzite, and IRMOF-1: A Comparative Study from Monte Carlo Simulation"*. Langmuir. **2006**;23 (2).659-66.

Babarao R, Jiang J. *"Exceptionally high CO2 storage in covalent-organic frameworks: Atomistic simulation study"*. Energy & Environmental Science. **2008**;1 (1).139-43.

Babarao R, Jiang J. *"Unprecedentedly High Selective Adsorption of Gas Mixtures in rho Zeolite-like Metal−Organic Framework: A Molecular Simulation Study"*. J Am Chem Soc. **2009**;131 (32).11417-25.

Babarao R, Jiang J. *"Upgrade of natural gas in rho zeolite-like metal-organic framework and effect of water: a computational study"*. Energy & Environmental Science. **2009**;2 (10).1088-93.

Bacsik Z, Atluri R, Garcia-Bennett AE, Hedin N. *"Temperature-Induced Uptake of CO2 and Formation of Carbamates in Mesocaged Silica Modified with n-Propylamines"*. Langmuir. **2010**;26 (12).10013-24.

Baerlocher C, McCusker LB. Database of Zeolite Structures 1996 [07/07/2011]; Available from: http://www.iza-structure.org/databases/.

Beck JS, Vartuli JC, Roth WJ, Leonowicz ME, Kresge CT, Schmitt KD, et al. *"A new family of mesoporous molecular sieves prepared with liquid crystal templates"*. J Am Chem Soc. **1992**;114 (27).10834-43.

Bezerra D, Oliveira R, Vieira R, Cavalcante C, Azevedo D. *"Adsorption of CO2 on nitrogen-enriched activated carbon and zeolite 13X"*. Adsorption. **2011**;17 (1).235-46.

Bhatia SK, Tran K, Nguyen TX, Nicholson D. *"High-pressure adsorption capacity and structure of CO2 in carbon slit pores: Theory and simulation"*. Langmuir. **2004**;20 (22).9612-20.

Bhattacharyya S, Lelong G, Saboungi M-L. *"Recent progress in the synthesis and selected applications of MCM-41: a short review"*. J Exp Nanosci. **2006**;1 (3).375 - 95.

Bishnoi S, Rochelle GT. *"Absorption of carbon dioxide in aqueous piperazine/methyldiethanolamine"*. AIChE J. **2002**;48 (12).2788-99.

Blas FJ, Vega LF. *"Thermodynamic behaviour of homonuclear and heteronuclear Lennard-Jones chains with association sites from simulation and theory"*. Mol Phys. **1997**;92 135-50.

Brady R, Woonton B, Gee ML, O'Connor AJ. *"Hierarchical mesoporous silica materials for separation of functional food ingredients -- A review"*. Innovative Food Science & Emerging Technologies. **2008**;9 (2).243-8.

Brodka A, Zerda TW. *"Properties of liquid acetone in silica pores: Molecular dynamics simulation"*. J Chem Phys. **1996**;104 (16).6319-26.

Builes S, Roussel T, Ghimbeu CM, Parmentier J, Gadiou R, Vix-Guterl C, et al. *"Microporous carbon adsorbents with high CO2 capacities for industrial applications"*. Phys Chem Chem Phys. **2011**;13 (35).16063-70.

Builes S, Roussel T, Vega LF. *"Optimization of the separation of sulfur hexafluoride and nitrogen by selective adsorption using monte carlo simulations"*. AIChE J. **2011**;57 (4).962-74.

Cao D, Shen Z, Chen J, Zhang X. *"Experiment, molecular simulation and density functional theory for investigation of fluid confined in MCM-41"*. Micropor Mesopor Mat. **2004**;67 (2-3).159-66.

Cavenati S, Grande CA, Rodrigues AE. *"Adsorption Equilibrium of Methane, Carbon Dioxide, and Nitrogen on Zeolite 13X at High Pressures"*. J Chem Eng Data. **2004**;49 (4).1095-101.

Čejka J, Kubička D. *"Zeolites and Other Micro- and Mesoporous Molecular Sieves"*. Kirk-Othmer Encyclopedia of Chemical Technology: John Wiley & Sons, Inc.; **2000**. p.

Ciferno JP, Marano JJ, Munson RK. *"Technology Integration Challenges"*. Chem Eng Prog. **2011**;107 (8).33-44.

Clark PD. *"Sulfur and Hydrogen Sulfide Recovery"*. Kirk-Othmer Encyclopedia of Chemical Technology: John Wiley & Sons, Inc.; **2000**. p.

Coasne B, Pellenq RJ-M. *"Grand canonical Monte Carlo simulation of argon adsorption at the surface of silica nanopores: Effect of pore size, pore morphology, and surface roughness"*. J Chem Phys. **2004**;120 (6).2913-22.

Comotti A, Bracco S, Sozzani P, Horike S, Matsuda R, Chen J, et al. *"Nanochannels of Two Distinct Cross-Sections in a Porous Al-Based Coordination Polymer"*. J Am Chem Soc. **2008**;130 (41).13664-72.

Couck S, Denayer JFM, Baron GV, Rémy T, Gascon J, Kapteijn F. *"An Amine-Functionalized MIL-53 Metal−Organic Framework with Large Separation Power for CO2 and CH4"*. J Am Chem Soc. **2009**;131 (18).6326-7.

Cha I, Lee S, Lee JD, Lee G-w, Seo Y. *"Separation of SF6 from Gas Mixtures Using Gas Hydrate Formation"*. Environ Sci Technol. **2010**;44 (16).6117-22.

Chaffee AL. *"Molecular modeling of HMS hybrid materials for CO2 adsorption"*. Fuel Process Technol. **2005**;86 (14-15).1473-86.

Chatti R, Bansiwal AK, Thote JA, Kumar V, Jadhav P, Lokhande SK, et al. *"Amine loaded zeolites for carbon dioxide capture: Amine loading and adsorption studies"*. Micropor Mesopor Mat. **2009**;121 (1-3).84-9.

Chen B, Potoff JJ, Siepmann JI. *"Monte Carlo Calculations for Alcohols and Their Mixtures with Alkanes. Transferable Potentials for Phase Equilibria. 5. United-Atom Description of Primary, Secondary, and Tertiary Alcohols"*. J Phys Chem B. **2001**;105 (15).3093-104.

Choi YJ, Choi JH, Choi KM, Kang JK. *"Covalent organic frameworks for extremely high reversible CO2 uptake capacity: a theoretical approach"*. J Mater Chem. **2011**;21 (4).1073-8.

D'Alessandro DM, McDonald T. *"Toward carbon dioxide capture using nanoporous materials"*. Pure Appl Chem. **2011**;83 (1).57-66.

D'Alessandro DM, Smit B, Long JR. *"Carbon Dioxide Capture: Prospects for New Materials"*. Angew Chem Int Ed. **2010**;49 (35).6058-82.

Dabrowski A. *"Adsorption - from theory to practice"*. Adv Colloid Interface Sci. **2001**;93 (1-3).135-224.

Dacquin J-P, Cross HE, Brown DR, Düren T, Williams JJ, Lee AF, et al. *"Interdependent lateral interactions, hydrophobicity and acid strength and their influence on the catalytic activity of nanoporous sulfonic acid silicas"*. Green Chem. **2010**;12 (8).1383-91.

Dagan G, Agam G, Krakov V, Kaplan L, editors. Carbon Membrane Separator for Elimination of SF6 emissions from Gas-Insulated Electrical Utilities. 1st International Conference on SF6 and the Environment; 2000; San Diego, California.

Davies GM, Seaton NA. *"The effect of the choice of pore model on the characterization of the internal structure of microporous carbons using pore size distributions"*. Carbon. **1998**;36 (10).1473-90.

Dawson R, Adams DJ, Cooper AI. *"Chemical tuning of CO2 sorption in robust nanoporous organic polymers"*. Chemical Science. **2011**;2 (6).1173-7.

Dietzel PDC, Besikiotis V, Blom R. *"Application of metal-organic frameworks with coordinatively unsaturated metal sites in storage and separation of methane and carbon dioxide"*. J Mater Chem. **2009**;19 (39).7362-70.

Do DD, Do HD. *"Adsorption of Quadrupolar, Diatomic Nitrogen onto Graphitized Thermal Carbon Black and in Slit-shaped Carbon Pores. Effects of Surface Mediation"*. Adsorption Science and Technology. **2005**;23 267-88.

Do DD, Do HD. *"GCMC-surface area of carbonaceous materials with N2 and Ar adsorption as an alternative to the classical BET method"*. Carbon. **2005**;43 (10).2112-21.

Do DD, Nicholson D, Do HD. *"Effects of Adsorbent Deformation on the Adsorption of Gases in Slitlike Graphitic Pores: A Computer Simulation Study"*. J Phys Chem C. **2008**;112 (36).14075-89.

Do DD, Nicholson D, Fan C. *"Development of Equations for Differential and Integral Enthalpy Change of Adsorption for Simulation Studies"*. Langmuir. **2011**;27 (23).14290-9.

Ducrot-Boisgontier C, Parmentier J, Faour A, Patarin Jl, Pirngruber GD. *"FAU-Type Zeolite Nanocasted Carbon Replicas for CO2 Adsorption and Hydrogen Purification"*. Energy Fuels. **2010**;24 (6).3595-602.

Duque D, Vega LF. *"Some issues on the calculation of interfacial properties by molecular simulation"*. J Chem Phys. **2004**;121 (17).8611-7.

Düren T, Bae Y-S, Snurr RQ. *"Using molecular simulation to characterise metal-organic frameworks for adsorption applications"*. Chem Soc Rev. **2009**;38 (5).1237-47.

Düren T, Millange F, Férey G, Walton KS, Snurr RQ. *"Calculating Geometric Surface Areas as a Characterization Tool for Metal−Organic Frameworks"*. J Phys Chem C. **2007**;111 (42).15350-6.

Etter M, Koch H, editors. Sulfur hexafluoride SF6. Power and Energy Society General Meeting - Conversion and Delivery of Electrical Energy in the 21st Century, 2008 IEEE; 2008.

Everett DH. *"Manual of Symbols and Terminology for Physicochemical Quantities and Units: Appendix II: Definitions, terminology and symbols in colloid and surface chemistry - part 1: Colloid and surface chemistry."*. International Union of Pure and Applied Chemistry. **1972**;31 579-638.

Fairen-Jimenez D, Moggach SA, Wharmby MT, Wright PA, Parsons S, Düren T. *"Opening the Gate: Framework Flexibility in ZIF-8 Explored by Experiments and Simulations"*. J Am Chem Soc. **2011**;133 (23).8900-2.

Farha OK, Spokoyny AM, Mulfort KL, Galli S, Hupp JT, Mirkin CA. *"Gas-Sorption Properties of Cobalt(II)−Carborane-Based Coordination Polymers as a Function of Morphology"*. Small. **2009**;5 (15).1727-31.

Freeman SA, Dugas R, Van Wagener DH, Nguyen T, Rochelle GT. *"Carbon dioxide capture with concentrated, aqueous piperazine"*. International Journal of Greenhouse Gas Control. **2010**;4 (2).119-24.

Frenkel D, Mooij GCAM, Smit B. *"Novel scheme to study structural and thermal properties of continuously deformable molecules"*. J Phys: Condens Matter. **1992**;4 (12).3053.

Frenkel D, Smit B. *"Understanding molecular simulation: from algorithms to applications"*. San Diego: Academic Press; **2002**.

Frierson MR, Allinger NL. *"Molecular mechanics (MM2) calculations on siloxanes"*. J Phys Org Chem. **1989**;2 (7).573-9.

Fryxell GE. *"The synthesis of functional mesoporous materials"*. Inorg Chem Commun. **2006**;9 (11).1141-50.

Fuchs AH, Cheetham AK. *"Adsorption of Guest Molecules in Zeolitic Materials: Computational Aspects"*. J Phys Chem B. **2001**;105 (31).7375-83.

Furukawa H, Yaghi OM. *"Storage of Hydrogen, Methane, and Carbon Dioxide in Highly Porous Covalent Organic Frameworks for Clean Energy Applications"*. J Am Chem Soc. **2009**;131 (25).8875-83.

Galassi G, Tildesley DJ. *"Phase Diagrams of Diatomic Molecules Using the Gibbs Ensemble Monte Carlo Method"*. Mol Simul. **1994**;13 (1).11 - 24.

Gallo M, Glossman-Mitnik D. *"Fuel Gas Storage and Separations by Metal-Organic Frameworks: Simulated Adsorption Isotherms for H2 and CH4 and Their Equimolar Mixture"*. J Phys Chem C. **2009**;113 (16).6634-42.

Gallo M, Nenoff TM, Mitchell MC. *"Selectivities for binary mixtures of hydrogen/methane and hydrogen/carbon dioxide in silicalite and ETS-10 by Grand Canonical Monte Carlo techniques"*. Fluid Phase Equilib. **2006**;247 (1-2).135-42.

García-Sánchez A, Ania CO, Parra JB, Dubbeldam D, Vlugt TJH, Krishna R, et al. *"Transferable Force Field for Carbon Dioxide Adsorption in Zeolites"*. J Phys Chem C. **2009**;113 (20).8814-20.

García S, Gil MV, Martín CF, Pis JJ, Rubiera F, Pevida C. *"Breakthrough adsorption study of a commercial activated carbon for pre-combustion CO2 capture"*. Chem Eng J. **2011**;171 (2).549-56.

Gaslain FOM, Parmentier J, Valtchev VP, Patarin J. *"First zeolite carbon replica with a well resolved X-ray diffraction pattern"*. Chem Commun. **2006** (9).991-3.

Gavalda S, Gubbins KE, Hanzawa Y, Kaneko K, Thomson KT. *"Nitrogen Adsorption in Carbon Aerogels: A Molecular Simulation Study"*. Langmuir. **2002**;18 (6).2141-51.

Ghoufi A, Gaberova L, Rouquerol J, Vincent D, Llewellyn PL, Maurin G. *"Adsorption of CO2, CH4 and their binary mixture in Faujasite NaY: A combination of molecular simulations with gravimetry-manometry and microcalorimetry measurements"*. Micropor Mesopor Mat. **2009**;119 (1-3).117-28.

Goff GS, Rochelle GT. *"Oxidation Inhibitors for Copper and Iron Catalyzed Degradation of Monoethanolamine in CO2 Capture Processes"*. Ind Eng Chem Res. **2005**;45 (8).2513-21.

Goj A, Sholl DS, Akten ED, Kohen D. *"Atomistic Simulations of CO2 and N2 Adsorption in Silica Zeolites: The Impact of Pore Size and Shape"*. J Phys Chem B. **2002**;106 (33).8367-75.

Gutowski KE, Maginn EJ. *"Amine-Functionalized Task-Specific Ionic Liquids: A Mechanistic Explanation for the Dramatic Increase in Viscosity upon Complexation with CO2 from Molecular Simulation"*. J Am Chem Soc. **2008**;130 (44).14690-704.

Harlick PJE, Tezel FH. *"An experimental adsorbent screening study for CO2 removal from N2"*. Micropor Mesopor Mat. **2004**;76 (1-3).71-9.

Harris JG, Yung KH. *"Carbon Dioxide's Liquid-Vapor Coexistence Curve And Critical Properties as Predicted by a Simple Molecular Model"*. J Phys Chem. **1995**;99 (31).12021-4.

He, Seaton NA. *"Heats of Adsorption and Adsorption Heterogeneity for Methane, Ethane, and Carbon Dioxide in MCM-41"*. Langmuir. **2005**;22 (3).1150-5.

Hedin N, Chen L, Laaksonen A. *"Sorbents for CO2 capture from flue gas-aspects from materials and theoretical chemistry"*. Nanoscale. **2010**;2 (10).1819-41.

Henning K-D, von Kienle H. *"Carbon, 5. Activated Carbon"*. Ullmann's Encyclopedia of Industrial Chemistry: Wiley-VCH Verlag GmbH & Co. KGaA; **2000**. p.

Herdes C, Santos MA, Abelló S, Medina F, Vega LF. *"Search for a reliable methodology for PSD determination based on a combined molecular simulation-regularization-experimental approach: The case of PHTS materials"*. Appl Surf Sci. **2005**;252 (3).538-47.

Herdes C, Santos MA, Medina F, Vega LF. *"Pore Size Distribution Analysis of Selected Hexagonal Mesoporous Silicas by Grand Canonical Monte Carlo Simulations"*. Langmuir. **2005**;21 (19).8733-42.

Heyden A, Düren T, J. Keil F. *"Study of molecular shape and non-ideality effects on mixture adsorption isotherms of small molecules in carbon nanotubes: A grand canonical Monte Carlo simulation study"*. Chem Eng Sci. **2002**;57 (13).2439-48.

Hikita M, Ohtsuka S, Okabe S, Kaneko S. *"Insulation Characteristics of Gas Mixtures including Perfluorocarbon Gas"*. Dielectrics and Electrical Insulation, IEEE Transactions on. **2008**;15 (4).1015-22.

Himeno S, Komatsu T, Fujita S. *"High-Pressure Adsorption Equilibria of Methane and Carbon Dioxide on Several Activated Carbons"*. J Chem Eng Data. **2005**;50 (2).369-76.

Ho LN, Perez Pellitero J, Porcheron F, Pellenq RJM. *"Enhanced CO2 Solubility in Hybrid MCM-41: Molecular Simulations and Experiments"*. Langmuir. **2011**;27 (13).8187-97.

Ho Y-S. *"Selection of optimum sorption isotherm"*. Carbon. **2004**;42 (10).2115-6.

Hoffmann F, Cornelius M, Morell J, Fröba M. *"Silica-Based Mesoporous Organic–Inorganic Hybrid Materials"*. Angew Chem Int Ed. **2006**;45 (20).3216-51.

Hoffmann F, Fröba M. *"Silica-Based Mesoporous Organic–Inorganic Hybrid Materials"*. In: Rurack K, Marínez-Máñez R, editors. The supramolecular chemistry of organic-inorganic hybrid materials: Wiley-VCH; **2006**. p. 5924-48.

Hou P-X, Orikasa H, Itoi H, Nishihara H, Kyotani T. *"Densification of ordered microporous carbons and controlling their micropore size by hot-pressing"*. Carbon. **2007**;45 (10).2011-6.

Huang HY, Yang RT, Chinn D, Munson CL. *"Amine-Grafted MCM-48 and Silica Xerogel as Superior Sorbents for Acidic Gas Removal from Natural Gas"*. Ind Eng Chem Res. **2002**;42 (12).2427-33.

Huang L, Zhang L, Shao Q, Lu L, Lu X, Jiang S, et al. *"Simulations of Binary Mixture Adsorption of Carbon Dioxide and Methane in Carbon Nanotubes: Temperature, Pressure, and Pore Size Effects"*. J Phys Chem C. **2007**;111 (32).11912-20.

Inami K, Maeda Y, Habuchi Y, Yoshimura M, Hamano S, Hama H. *"Problems of the application of N2/SF6 mixtures to gas-insulated bus"*. Electrical Engineering in Japan. **2001**;137 (4).25-31.

Ionescu TC, Qi F, McCabe C, Striolo A, Kieffer J, Cummings PT. *"Evaluation of Force Fields for Molecular Simulation of Polyhedral Oligomeric Silsesquioxanes"*. J Phys Chem B. **2006**;110 (6).2502-10.

Jackson P, Beste A, Attalla M. *"Insights into amine-based CO2 capture: an ab initio self-consistent reaction field investigation"*. Struct Chem. **2011**;22 (3).537-49.

Jagiello J, Thommes M. *"Comparison of DFT characterization methods based on N2, Ar, CO2, and H2 adsorption applied to carbons with various pore size distributions"*. Carbon. **2004**;42 (7).1227-32.

Jia W, Murad S. *"Molecular dynamics simulations of gas separations using faujasite-journal article zeolite membranes"*. J Chem Phys. **2004**;120 (10).4877-85.

Jia W, Murad S. *"Separation of gas mixtures using a range of zeolite membranes: A molecular-dynamics study"*. J Chem Phys. **2005**;122 (23).234708.

Jiang J-X, Cooper A. *"Microporous Organic Polymers: Design, Synthesis, and Function Functional Metal-Organic Frameworks: Gas Storage, Separation and Catalysis"*. Springer Berlin / Heidelberg; **2010**. p. 1-33.

Jiang J, Sandler SI. *"Monte Carlo Simulation of O2 and N2 Mixture Adsorption in Nanoporous Carbon (C168 Schwarzite)"*. Langmuir. **2003**;19 (14).5936-41.

Juan Carlos A. *"The maximum capture efficiency of CO2 using a carbonation/calcination cycle of CaO/CaCO3"*. Chem Eng J. **2002**;90 (3).303-6.

Katagiri H, Kasuya H, Mizoguchi H, Yanabu S. *"Investigation of the Performance of CF3 Gas as a Possible Substitute for SF6"*. Dielectrics and Electrical Insulation, IEEE Transactions on. **2008**;15 (5).1424-9.

Kato M, Nakagawa K, Essaki K, Maezawa Y, Takeda S, Kogo R, et al. *"Novel CO2 Absorbents Using Lithium-Containing Oxide"*. Int J Appl Ceram Technol. **2005**;2 (6).467-75.

Klauda JB, Jiang J, Sandler SI. *"An ab Initio Study on the Effect of Carbon Surface Curvature and Ring Structure on N2(O2)−Carbon Intermolecular Potentials"*. J Phys Chem B. **2004**;108 (28).9842-51.

Knöfel C, Descarpentries J, Benzaouia A, Zelenák V, Mornet S, Llewellyn PL, et al. *"Functionalised micro-/mesoporous silica for the adsorption of carbon dioxide"*. Micropor Mesopor Mat. **2007**;99 (1-2).79-85.

Knöfel C, Martin Cl, Hornebecq V, Llewellyn PL. *"Study of Carbon Dioxide Adsorption on Mesoporous Aminopropylsilane-Functionalized Silica and Titania Combining Microcalorimetry and in Situ Infrared Spectroscopy"*. J Phys Chem C. **2009**;113 (52).21726-34.

Knowles GP, Graham JV, Delaney SW, Chaffee AL. *"Aminopropyl-functionalized mesoporous silicas as CO2 adsorbents"*. Fuel Process Technol. **2005**;86 (14-15).1435-48.

Kremer SPB, Kirschhock CEA, Aerts A, Aerts CA, Houthoofd KJ, Grobet PJ, et al. *"Zeotile-2: A microporous analogue of MCM-48"*. Solid State Sci. **2005**;7 (7).861-7.

Kresge CT, Leonowicz ME, Roth WJ, Vartuli JC, Beck JS. *"Ordered mesoporous molecular sieves synthesized by a liquid-crystal template mechanism"*. Nature. **1992**;359 (6397).710-2.

Krishna R, van Baten JM. *"Using molecular simulations for screening of zeolites for separation of CO2/CH4 mixtures"*. Chem Eng J. **2007**;133 (1-3).121-31.

Kröber H, Teipel U. *"Micronization of Organic Substances by Supercritical Fluid Processes"*. Chem Eng Technol. **2004**;27 (5).510-4.

Kuznetsova A, J. T. Yates J, Simonyan VV, Johnson JK, Huffman CB, Smalley RE. *"Optimization of Xe adsorption kinetics in single walled carbon nanotubes"*. J Chem Phys. **2001**;115 (14).6691-8.

Kyotani T. *"Control of pore structure in carbon"*. Carbon. **2000**;38 (2).269-86.

Kyotani T, Nagai T, Inoue S, Tomita A. *"Formation of New Type of Porous Carbon by Carbonization in Zeolite Nanochannels"*. Chem Mater. **1997**;9 (2).609-15.

Lachet V, Boutin A, Tavitian B, H. Fuchs A. *"Grand canonical Monte Carlo simulations of adsorption of mixtures of xylene molecules in faujasite zeolites"*. Faraday Discuss. **1997**;106 307-23.

Lan J, Cao D, Wang W, Smit B. *"Doping of Alkali, Alkaline-Earth, and Transition Metals in Covalent-Organic Frameworks for Enhancing CO2 Capture by First-Principles Calculations and Molecular Simulations"*. ACS Nano. **2010**;4 (7).4225-37.

Leal O, Bolívar C, Ovalles C, García JJ, Espidel Y. *"Reversible adsorption of carbon dioxide on amine surface-bonded silica gel"*. Inorg Chim Acta. **1995**;240 (1-2).183-9.

Lee JM, Min YJ, Lee KB, Jeon SG, Na JG, Ryu HJ. *"Enhancement of CO2 Sorption Uptake on Hydrotalcite by Impregnation with K2CO3"*. Langmuir. **2010**;26 (24).18788-97.

Lenosky T, Gonze X, Teter M, Elser V. *"Energetics of negatively curved graphitic carbon"*. Nature. **1992**;355 (6358).333-5.

Leyssale J-M, Papadopoulos GK, Theodorou DN. *"Sorption Thermodynamics of CO2, CH4, and Their Mixtures in the ITQ-1 Zeolite as Revealed by Molecular Simulations"*. J Phys Chem B. **2006**;110 (45).22742-53.

Li H, Eddaoudi M, Groy TL, Yaghi OM. *"Establishing Microporosity in Open Metal–Organic Frameworks: Gas Sorption Isotherms for Zn(BDC) (BDC = 1,4-Benzenedicarboxylate)"*. J Am Chem Soc. **1998**;120 (33).8571-2.

Liu B, Wang W, Zhang X. *"A hybrid cylindrical model for characterization of MCM-41 by density functional theory"*. Phys Chem Chem Phys. **2004**;6 (15).3985-90.

Liu B, Yang Q, Xue C, Zhong C, Chen B, Smit B. *"Enhanced Adsorption Selectivity of Hydrogen/Methane Mixtures in Metalic-Organic Frameworks with Interpenetration: A Molecular Simulation Study"*. J Phys Chem C. **2008**;112 (26).9854-60.

Liu D, Zheng C, Yang Q, Zhong C. *"Understanding the Adsorption and Diffusion of Carbon Dioxide in Zeolitic Imidazolate Frameworks: A Molecular Simulation Study"*. J Phys Chem C. **2009**;113 (12).5004-9.

Liu S, Yang X. *"Gibbs ensemble Monte Carlo simulation of supercritical CO2 adsorption on NaA and NaX zeolites"*. J Chem Phys. **2006**;124 (24).244705.

Lobo RF. *"Chemistry: The promise of emptiness"*. Nature. **2006**;443 (7113).757-8.

Lopes PEM, Murashov V, Tazi M, Demchuk E, MacKerell AD. *"Development of an Empirical Force Field for Silica. Application to the Quartz−Water Interface"*. J Phys Chem B. **2006**;110 (6).2782-92.

Lozano-Castelló D, Cazorla-Amorós D, Linares-Solano A. *"Usefulness of CO2 adsorption at 273 K for the characterization of porous carbons"*. Carbon. **2004**;42 (7).1233-42.

Llewellyn PL, Bourrelly S, Serre C, Vimont A, Daturi M, Hamon L, et al. *"High Uptakes of CO2 and CH4 in Mesoporous Metal ▪ Organic Frameworks MIL-100 and MIL-101"*. Langmuir. **2008**;24 (14).7245-50.

Ma Z, Kyotani T, Tomita A. *"Synthesis methods for preparing microporous carbons with a structural regularity of zeolite Y"*. Carbon. **2002**;40 (13).2367-74.

MacElroy JMD. *"Molecular simulation of the kinetic selectivity of a model silica system"*. Mol Phys. **2002**;100 (14).2369 - 76.

MacElroy JMD, Raghavan K. *"Adsorption and diffusion of a Lennard-Jones vapor in microporous silica"*. J Chem Phys. **1990**;93 (3).2068-79.

MacElroy JMD, Raghavan K. *"Transport of an adsorbing vapour in a model silica system"*. J Chem Soc, Faraday Trans. **1991**;87 (13).1971-87.

Maddox MW, Sowers SL, Gubbins KE. *"Molecular simulation of binary mixture adsorption in buckytubes and MCM-41"*. Adsorption. **1996**;2 (1).23-32.

Maneeintr K, Idem RO, Tontiwachwuthikul P, Wee AGH. *"Comparative Mass Transfer Performance Studies of CO2 Absorption into Aqueous Solutions of DEAB and MEA"*. Ind Eng Chem Res. **2010**;49 (6).2857-63.

Martín CF, Plaza MG, Pis JJ, Rubiera F, Pevida C, Centeno TA. *"On the limits of CO2 capture capacity of carbons"*. Sep Purif Technol. **2010**;74 (2).225-9.

Martin CF, Stockel E, Clowes R, Adams DJ, Cooper AI, Pis JJ, et al. *"Hypercrosslinked organic polymer networks as potential adsorbents for pre-combustion CO2 capture"*. J Mater Chem. **2011**;21 (14).5475-83.

Martin MG, Frischknecht AL. *"Using arbitrary trial distributions to improve intramolecular sampling in configurational-bias Monte Carlo"*. Mol Phys. **2006**;104 (15).2439 - 56.

Martin MG, Siepmann JI. *"Transferable Potentials for Phase Equilibria. 1. United-Atom Description of n-Alkanes"*. J Phys Chem B. **1998**;102 (14).2569-77.

Martin MG, Siepmann JI. *"Novel Configurational-Bias Monte Carlo Method for Branched Molecules. Transferable Potentials for Phase Equilibria. 2. United-Atom Description of Branched Alkanes"*. J Phys Chem B. **1999**;103 (21).4508-17.

Matsuoka K, Yamagishi Y, Yamazaki T, Setoyama N, Tomita A, Kyotani T. *"Extremely high microporosity and sharp pore size distribution of a large surface area carbon prepared in the nanochannels of zeolite Y"*. Carbon. **2005**;43 (4).876-9.

Maurin G, Belmabkhout Y, Pirngruber G, Gaberova L, Llewellyn P. *"CO2 adsorption in LiY and NaY at high temperature: molecular simulations compared to experiments"*. Adsorption. **2007**;13 (5).453-60.

Maurin G, Bell R, Kuchta B, Poyet T, Llewellyn P. *"Adsorption of Non Polar and Quadrupolar Gases in Siliceous Faujasite: Molecular Simulations and Experiments"*. Adsorption. **2005**;11 (0).331-6.

Meis NNAH, Bitter JH, de Jong KP. *"On the Influence and Role of Alkali Metals on Supported and Unsupported Activated Hydrotalcites for CO2 Sorption"*. Ind Eng Chem Res. **2010**;49 (17).8086-93.

Metropolis N, Rosenbluth AW, Rosenbluth MN, Teller AH, Teller E. *"Equation of State Calculations by Fast Computing Machines"*. J Chem Phys. **1953**;21 (6).1087-92.

Metz B. *"Climate change 2007 mitigation of climate change : contribution of Working Group III to the Fourth Assessment Report of the Intergovernmental Panel on Climate Change"*. Cambridge; New York: Cambridge University Press; **2007**.

Millward AR, Yaghi OM. *"Metal−Organic Frameworks with Exceptionally High Capacity for Storage of Carbon Dioxide at Room Temperature"*. J Am Chem Soc. **2005**;127 (51).17998-9.

Mohanty S, Davis HT, McCormick AV. *"Shape selective adsorption in cylindrical pores"*. Chem Eng Sci. **2000**;55 (17).3377-83.

Mosqueda HA, Vazquez C, Bosch P, Pfeiffer H. *"Chemical Sorption of Carbon Dioxide (CO2) on Lithium Oxide (Li2O)"*. Chem Mater. **2006**;18 (9).2307-10.

Müller CR, Pacciani R, Bohn CD, Scott SA, Dennis JS. *"Investigation of the Enhanced Water Gas Shift Reaction Using Natural and Synthetic Sorbents for the Capture of CO2"*. Ind Eng Chem Res. **2009**;48 (23).10284-91.

Murase H, Imai T, Inohara T, Toyoda M. *"Use of zeolite filter in portable equipment for recovering SF6 in SF6/N2 mixtures"*. Dielectrics and Electrical Insulation, IEEE Transactions on. **2004**;11 (1).166-73.

Myers AL, Calles JA, Calleja G. *"Comparison of molecular simulation of adsorption with experiment"*. Adsorption. **1997**;3 (2).107-15.

Nakagawa K, Tanaka D, Horike S, Shimomura S, Higuchi M, Kitagawa S. *"Enhanced selectivity of CO2 from a ternary gas mixture in an interdigitated porous framework"*. Chem Commun. **2010**;46 (24).4258-60.

Neimark AV, Ravikovitch PI, Grün M, Schüth F, Unger KK. *"Pore Size Analysis of MCM-41 Type Adsorbents by Means of Nitrogen and Argon Adsorption"*. J Colloid Interface Sci. **1998**;207 (1).159-69.

Neimark AV, Ravikovitch PI, Vishnyakov A. *"Adsorption hysteresis in nanopores"*. Physical Review E. **2000**;62 (2).R1493.

Nguyen PTM, Do DD, Nicholson D. *"On The Cavitation and Pore Blocking in Cylindrical Pores with Simple Connectivity"*. J Phys Chem B. **2011**;115 (42).12160-72.

Nguyen TX, Cohaut N, Bae J-S, Bhatia SK. *"New Method for Atomistic Modeling of the Microstructure of Activated Carbons Using Hybrid Reverse Monte Carlo Simulation"*. Langmuir. **2008**;24 (15).7912-22.

Nishihara H, Hou P-X, Li L-X, Ito M, Uchiyama M, Kaburagi T, et al. *"High-Pressure Hydrogen Storage in Zeolite-Templated Carbon"*. J Phys Chem C. **2009**;113 (8).3189-96.

Nishihara H, Yang Q-H, Hou P-X, Unno M, Yamauchi S, Saito R, et al. *"A possible buckybowl-like structure of zeolite templated carbon"*. Carbon. **2009**;47 (5).1220-30.

Olivet A, Vega LF. *"Optimized molecular force field for sulfur hexafluoride simulations"*. J Chem Phys. **2007**;126 (14).144502-11.

Olivet A, Vega LF. *"Predictions of Transport Properties in Gaseous Mixtures of Sulfur Hexafluoride and Nitrogen"*. J Phys Chem C. **2007**;111 (43).16013-20.

Olthoff JK, Christophorou LG, editors. A brief history of gaseous dielectrics research at NIST. Electrical Insulation and Dielectric Phenomena, 2001 Annual Report Conference on; 2001.

Palmer JC, Brennan JK, Hurley MM, Balboa A, Gubbins KE. *"Detailed structural models for activated carbons from molecular simulation"*. Carbon. **2009**;47 (12).2904-13.

Pàmies JC, Vega LF. *"Vapor-Liquid Equilibria and Critical Behavior of Heavy n-Alkanes Using Transferable Parameters from the Soft-SAFT Equation of State"*. Ind Eng Chem Res. **2001**;40 (11).2532-43.

Panda T, Pachfule P, Chen Y, Jiang J, Banerjee R. *"Amino functionalized zeolitic tetrazolate framework (ZTF) with high capacity for storage of carbon dioxide"*. Chem Commun. **2011**;47 (7).2011-3.

Pantatosaki E, Papaioannou A, Stubos AK, Papadopoulos GK. *"Atomistic simulation of sorption in model pores with reduced spatial periodicity"*. Appl Surf Sci. **2007**;253 (13).5606-9.

Pellegrini G, Strube R, Manfrida G. *"Comparative study of chemical absorbents in postcombustion CO2 capture"*. Energy. **2010**;35 (2).851-7.

Pellenq R, Roussel T, Puibasset J. *"Molecular simulations of water in hydrophobic microporous solids"*. Adsorption. **2008**;14 (4).733-42.

Peng X, Cheng X, Cao D. *"Computer simulations for the adsorption and separation of CO2/CH4/H2/N2 gases by UMCM-1 and UMCM-2 metal organic frameworks"*. J Mater Chem. **2011**;21 (30).11259-70.

Phan A, Doonan CJ, Uribe-Romo FJ, Knobler CB, O'Keeffe M, Yaghi OM. *"Synthesis, Structure, and Carbon Dioxide Capture Properties of Zeolitic Imidazolate Frameworks"*. Acc Chem Res. **2009**;43 (1).58-67.

Plant DF, Maurin G, Deroche I, Llewellyn PL. *"Investigation of CO2 adsorption in Faujasite systems: Grand Canonical Monte Carlo and molecular dynamics simulations based on a new derived Na+-CO2 force field"*. Micropor Mesopor Mat. **2007**;99 (1-2).70-8.

Potoff JJ, Siepmann JI. *"Vapor-liquid equilibria of mixtures containing alkanes, carbon dioxide, and nitrogen"*. AIChE J. **2001**;47 (7).1676-82.

Radosz M, Hu X, Krutkramelis K, Shen Y. *"Flue-Gas Carbon Capture on Carbonaceous Sorbents: Toward a Low-Cost Multifunctional Carbon Filter for "Green" Energy Producers"*. Ind Eng Chem Res. **2008**;47 (10).3783-94.

Ralph TY. *"Sorbent Selection: Equilibrium Isotherms, Diffusion, Cyclic Processes, and Sorbent Selection Criteria"*. Adsorbents: Fundamentals and Applications; **2003**. p. 17-53.

Ravikovitch PI, Haller GL, Neimark AV. *"Density functional theory model for calculating pore size distributions: pore structure of nanoporous catalysts"*. Adv Colloid Interface Sci. **1998**;76-77 203-26.

Ravikovitch PI, Vishnyakov A, Neimark AV. *"Density functional theories and molecular simulations of adsorption and phase transitions in nanopores"*. Physical Review E. **2001**;64 (1).011602.

Ravishankara AR, Solomon S, Turnipseed AA, Warren RF. *"Atmospheric Lifetimes of Long-Lived Halogenated Species"*. Science. **1993**;259 (5092).194-9.

Rees LVC. *"Chapter 9. Ion exchange in zeolites"*. Annual Reports on the Progress of Chemistry, Section A: General Physical and Inorganic Chemistry. **1970**;67 191-212.

Riddell IA, Smulders MMJ, Clegg JK, Nitschke JR. *"Encapsulation, storage and controlled release of sulfur hexafluoride from a metal-organic capsule"*. Chem Commun. **2011**;47 (1).457-9.

Rivera-Tinoco R, Bouallou C. *"Comparison of absorption rates and absorption capacity of ammonia solvents with MEA and MDEA aqueous blends for CO2 capture"*. Journal of Cleaner Production. **2010**;18 (9).875-80.

Rochelle GT. *"Amine Scrubbing for CO2 Capture"*. Science. **2009**;325 (5948).1652-4.

Rossin A, Fairen-Jimenez D, Düren T, Giambastiani G, Peruzzini M, Vitillo JG. *"Hydrogen Uptake by {H[Mg(HCOO)3]⊃NHMe2}∞ and Determination of Its H2 Adsorption Sites through Monte Carlo Simulations"*. Langmuir. **2011**;27 (16).10124-31.

Roussel T, Bichara C, Gubbins KE, Pellenq RJM. *"Hydrogen storage enhanced in Li-doped carbon replica of zeolites: A possible route to achieve fuel cell demand"*. J Chem Phys. **2009**;130 (17).174717-6.

Roussel T, Bichara C, Pellenq RJM. *"Selenium and Carbon Nanostructures in the Pores of AlPO4-5"*. Adsorption. **2005**;11 (0).709-14.

Roussel T, Didion A, Pellenq RJM, Gadiou R, Bichara C, Vix-Guterl C. *"Experimental and Atomistic Simulation Study of the Structural and Adsorption Properties of Faujasite*

Zeolite−Templated Nanostructured Carbon Materials†". J Phys Chem C. **2007**;111 (43).15863-76.

Roussel T, Pellenq RJM, Bienfait M, Vix-Guterl C, Gadiou R, Béguin F, et al. *"Thermodynamic and Neutron Scattering Study of Hydrogen Adsorption in Two Mesoporous Ordered Carbons"*. Langmuir. **2006**;22 (10).4614-9.

Ryoo R, Joo SH, Jun S. *"Synthesis of Highly Ordered Carbon Molecular Sieves via Template-Mediated Structural Transformation"*. J Phys Chem B. **1999**;103 (37).7743-6.

Ryoo R, Joo SH, Kruk M, Jaroniec M. *"Ordered Mesoporous Carbons"*. Adv Mater. **2001**;13 (9).677-81.

Salles F, Ghoufi A, Maurin G, Bell RG, Mellot-Draznieks C, Férey G. *"Molecular Dynamics Simulations of Breathing MOFs: Structural Transformations of MIL-53(Cr) upon Thermal Activation and CO2 Adsorption"*. Angew Chem Int Ed. **2008**;47 (44).8487-91.

Salles F, Jobic H, Ghoufi A, Llewellyn PL, Serre C, Bourrelly S, et al. *"Transport Diffusivity of CO2 in the Highly Flexible Metal−Organic Framework MIL-53(Cr)"*. Angew Chem Int Ed. **2009**;48 (44).8335-9.

Satyapal S, Filburn T, Trela J, Strange J. *"Performance and Properties of a Solid Amine Sorbent for Carbon Dioxide Removal in Space Life Support Applications"*. Energy Fuels. **2001**;15 (2).250-5.

Sayari A, Belmabkhout Y. *"Stabilization of Amine-Containing CO2 Adsorbents: Dramatic Effect of Water Vapor"*. J Am Chem Soc. **2010**;132 (18).6312-4.

Schumacher C, Gonzalez J, Pérez-Mendoza M, Wright PA, Seaton NA. *"Design of Hybrid Organic/Inorganic Adsorbents Based on Periodic Mesoporous Silica"*. Ind Eng Chem Res. **2006**;45 (16).5586-97.

Schumacher C, Gonzalez J, Wright PA, Seaton NA. *"Generation of Atomistic Models of Periodic Mesoporous Silica by Kinetic Monte Carlo Simulation of the Synthesis of the Material"*. J Phys Chem B. **2005**;110 (1).319-33.

Serna-Guerrero R, Belmabkhout Y, Sayari A. *"Modeling CO2 adsorption on amine-functionalized mesoporous silica: 1. A semi-empirical equilibrium model"*. Chem Eng J. **2010**;161 (1-2).173-81.

Shafeeyan MS, Daud WMAW, Houshmand A, Shamiri A. *"A review on surface modification of activated carbon for carbon dioxide adsorption"*. J Anal Appl Pyrolysis. **2010**;89 (2).143-51.

Shiojiri K, Yanagisawa Y, Yamasaki A, Kiyono F. *"Separation of F-gases (HFC-134a and SF6) from gaseous mixtures with nitrogen by surface diffusion through a porous Vycor glass membrane"*. J Membr Sci. **2006**;282 (1-2).442-9.

Silvestre-Albero J, Wahby A, Sepulveda-Escribano A, Martinez-Escandell M, Kaneko K, Rodriguez-Reinoso F. *"Ultrahigh CO2 adsorption capacity on carbon molecular sieves at room temperature"*. Chem Commun. **2011**;47 (24).6840-2.

Snurr RQ, Bell AT, Theodorou DN. *"Prediction of adsorption of aromatic hydrocarbons in silicalite from grand canonical Monte Carlo simulations with biased insertions"*. J Phys Chem. **1993**;97 (51).13742-52.

Somers SA, McCormick AV, Davis HT. *"Superselectivity and solvation forces of a two component fluid adsorbed in slit micropores"*. J Chem Phys. **1993**;99 (12).9890-8.

Steele W. *"Molecular interactions for physical adsorption"*. Chem Rev. **1993**;93 (7).2355-78.

Stimson LM, Wilson MR. *"Molecular dynamics simulations of side chain liquid crystal polymer molecules in isotropic and liquid-crystalline melts"*. J Chem Phys. **2005**;123 (3).034908-10.

Stowe K. *"Introduction to Statistical Mechanics and Thermodynamics"*. 1 ed. New York: Wiley; **1983**.

Stubbs JM, Potoff JJ, Siepmann JI. *"Transferable Potentials for Phase Equilibria. 6. United-Atom Description for Ethers, Glycols, Ketones, and Aldehydes"*. J Phys Chem B. **2004**;108 (45).17596-605.

Su F, Lu C, Kuo S-C, Zeng W. *"Adsorption of CO2 on Amine-Functionalized Y-Type Zeolites"*. Energy Fuels. **2010**;24 (2).1441-8.

Sweatman MB, Quirke N. *"Modelling Gas Adsorption in Slit-Pores Using Monte Carlo Simulation"*. Mol Simul. **2001**;27 (5-6).295-321.

Sweatman MB, Quirke N. *"Modelling gas mixture adsorption in active carbons"*. Mol Simul. **2005**;31 (9).667-81.

Talbot J. *"Analysis of adsorption selectivity in a one-dimensional model system"*. AIChE J. **1997**;43 (10).2471-8.

Taniguchi S, Okabe S, Takahashi T, Shindo T. *"Discharge Characteristics of 5 m Long Air Gap under Foggy Conditions with Lightning Shielding of Transmission Line"*. Dielectrics and Electrical Insulation, IEEE Transactions on. **2008**;15 (4).1031-7.

Tenney CM, Lastoskie CM. *"Molecular simulation of carbon dioxide adsorption chemically and structurally heterogeneous porous carbons"*. Environ Prog. **2006**;25 (4).343-54.

Thitakamol B, Veawab A. *"Foaming Behavior in CO2 Absorption Process Using Aqueous Solutions of Single and Blended Alkanolamines"*. Ind Eng Chem Res. **2007**;47 (1).216-25.

Tjatjopoulos GJ, Feke DL, Mann JA. *"Molecule-micropore interaction potentials"*. J Phys Chem. **1988**;92 (13).4006-7.

Toyoda M, Murase H, Imai T, Naotsuka H, Kobayashi A, Takano K, et al. *"SF6 reclaimer from SF6/N2 mixtures by gas separation with molecular sieving effect"*. Power Delivery, IEEE Transactions on. **2003**;18 (2).442-8.

Truhlar DG, Brown FB, Schwenke DW, Steckler R, Garrett BC. *"Dynamics Calculations Based on Ab Initio Potential Energy Surfaces"*. In: Bartlett RJ, editor. Comparison of Ab Initio Quantum Chemistry with Experiment for Small Molecules. Dordrecht, Holland: Reidel Publishing Company; **1985**. p. 95-139.

Vaidya PD, Kenig EY. *"CO2-Alkanolamine Reaction Kinetics: A Review of Recent Studies"*. Chem Eng Technol. **2007**;30 (11).1467-74.

Veltman K, Singh B, Hertwich EG. *"Human and Environmental Impact Assessment of Postcombustion CO2 Capture Focusing on Emissions from Amine-Based Scrubbing Solvents to Air"*. Environ Sci Technol. **2010**;44 (4).1496-502.

Vix-Guterl C, Boulard S, eacute, verine, Parmentier J, Werckmann J, et al. *"Formation of Ordered Mesoporous Carbon Material from a Silica Template by a One-Step Chemical Vapour Infiltration Process"*. Chem Lett. **2002**;31 (10).1062-3.

Vix-Guterl C, Saadallah S, Vidal L, Reda M, Parmentier J, Patarin J. *"Template synthesis of a new type of ordered carbon structure from pitch"*. J Mater Chem. **2003**;13 (10).2535-9.

Wick CD, Stubbs JM, Rai N, Siepmann JI. *"Transferable Potentials for Phase Equilibria. 7. Primary, Secondary, and Tertiary Amines, Nitroalkanes and Nitrobenzene, Nitriles, Amides, Pyridine, and Pyrimidine"*. J Phys Chem B. **2005**;109 (40).18974-82.

Williams JJ, Wiersum AD, Seaton NA, Düren T. *"Effect of Surface Group Functionalization on the CO2/N2 Separation Properties of MCM-41: A Grand-Canonical Monte Carlo Simulation Study"*. J Phys Chem C. **2010**;114 (43).18538-47.

Wolińska-Grabczyk A, Jankowski A, Sekuła R, Kruczek B. *"Separation of SF6 from Binary Mixtures with N2 Using Commercial Poly(4-Methyl-1-Pentene) Films"*. Sep Sci Technol. **2011**;46 (8).1231-40.

Wongkoblap A, Do DD, Nicholson D. *"Explanation of the unusual peak of calorimetric heat in the adsorption of nitrogen, argon and methane on graphitized thermal carbon black"*. Phys Chem Chem Phys. **2008**;10 (8).1106-13.

Wu S, Song K, Guan J, Kan Q. *"Synthesis and characterization of super-microporous material with enhanced hydrothermal stability"*. Bull Mater Sci. **2011**;34 (4).979-83.

Yamamoto O, Takuma T, Kinouchi M. *"Recovery of SF6 from N2/SF6 gas mixtures by using a polymer membrane"*. Electrical Insulation Magazine, IEEE. **2002**;18 (3).32-7.

Yang Q, Wiersum AD, Jobic H, Guillerm V, Serre C, Llewellyn PL, et al. *"Understanding the Thermodynamic and Kinetic Behavior of the CO2/CH4 Gas Mixture within the Porous Zirconium Terephthalate UiO-66(Zr): A Joint Experimental and Modeling Approach"*. J Phys Chem C. **2011**;115 (28).13768-74.

Yang Q, Xu Q, Liu B, Zhong C, Berend S. *"Molecular Simulation of CO2/H2 Mixture Separation in Metal-organic Frameworks: Effect of Catenation and Electrostatic Interactions"*. Chin J Chem Eng. **2009**;17 (5).781-90.

Yang Q, Xue C, Zhong C, Chen J-F. *"Molecular simulation of separation of CO2 from flue gases in CU-BTC metal-organic framework"*. AIChE J. **2007**;53 (11).2832-40.

Yang RT. *"Gas separation by adsorption processes"*. Singapore; River Edge, N.J.: World Scientific; **1997**.

Yazaydın AOzr, Benin AI, Faheem SA, Jakubczak P, Low JJ, Willis RR, et al. *"Enhanced CO2 Adsorption in Metal-Organic Frameworks via Occupation of Open-Metal Sites by Coordinated Water Molecules"*. Chem Mater. **2009**;21 (8).1425-30.

Yeh JT, Resnik KP, Rygle K, Pennline HW. *"Semi-batch absorption and regeneration studies for CO2 capture by aqueous ammonia"*. Fuel Process Technol. **2005**;86 (14-15).1533-46.

Yong Z, Mata, Rodrigues AE. *"Adsorption of Carbon Dioxide onto Hydrotalcite-like Compounds (HTlcs) at High Temperatures"*. Ind Eng Chem Res. **2000**;40 (1).204-9.

Yong Z, Mata VG, Rodrigues AE. *"Adsorption of Carbon Dioxide on Chemically Modified High Surface Area Carbon-Based Adsorbents at High Temperature"*. Adsorption. **2001**;7 (1).41-50.

Youn H-K, Kim J, Chandrasekar G, Jin H, Ahn W-S. *"High pressure carbon dioxide adsorption on nanoporous carbons prepared by Zeolite Y templating"*. Mater Lett. **2011**;65 (12).1772-4.

Yun J-H, Düren T, Keil FJ, Seaton NA. *"Adsorption of Methane, Ethane, and Their Binary Mixtures on MCM-41: Experimental Evaluation of Methods for the Prediction of Adsorption Equilibrium"*. Langmuir. **2002**;18 (7).2693-701.

Zelenak V, Halamova D, Gaberova L, Bloch E, Llewellyn P. *"Amine-modified SBA-12 mesoporous silica for carbon dioxide capture: Effect of amine basicity on sorption properties"*. Micropor Mesopor Mat. **2008**;116 (1-3).358-64.

Zhang L, Jiang S. *"Molecular simulation study of nanoscale friction for alkyl monolayers on Si(111)"*. J Chem Phys. **2002**;117 (4).1804-11.

Zhang Z, Zhang W, Chen X, Xia Q, Li Z. *"Adsorption of CO2 on Zeolite 13X and Activated Carbon with Higher Surface Area"*. Sep Sci Technol. **2010**;45 (5).710-9.

Zhou J, Li W, Zhang Z, Xing W, Zhuo S. *"Carbon dioxide adsorption performance of N-doped zeolite Y templated carbons"*. RSC Advances. **2012**.

Zhou Y, Antonietti M. *"Preparation of Highly Ordered Monolithic Super-Microporous Lamellar Silica with a Room-Temperature Ionic Liquid as Template via the Nanocasting Technique"*. Adv Mater. **2003**;15 (17).1452-5.

Zhuravlev ND, Siepmann JI, Schure MR. *"Surface Coverages of Bonded-Phase Ligands on Silica: A Computational Study"*. Anal Chem. **2001**;73 (16).4006-11.

Zukal A, Mayerová J, Kubů M. *"Adsorption of Carbon Dioxide on High-Silica Zeolites with Different Framework Topology"*. Top Catal. **2010**;53 (19).1361-6.